# Spatiotemporal Variability in Groundwater–Surface Water Exchange Within a Perennial Stream: Alder Creek, Southwestern Ontario

by

Corey Michael Zanatta

A thesis

presented to the University of Waterloo

in fulfillment of the

thesis requirement for the degree of

Master of Science

in

Earth Sciences

Waterloo, Ontario, Canada, 2025

© Corey Michael Zanatta 2025

## Author's Declaration

I hereby declare that I am the sole author of this thesis. This is a true copy of the thesis, including any required final revisions, as accepted by my examiners.

I understand that my thesis may be made electronically available to the public.

# Abstract

Groundwater discharge plays a crucial role in sustaining streamflow within creeks and rivers year-round while also supporting the aquatic life that live in them. However, due to numerous external pressures such as increased groundwater usage, changes in land uses, and climate change, these water bodies are under increased strain, putting increased emphasis on the need to protect and preserve them. To do this requires an increased understanding of groundwater-surface water interactions, which are complex processes that are challenging to accurately identify and quantify.

This work seeks to strengthen understanding of these complex processes. This involved the application of numerous small-scale techniques related to temperature readings, infrared imaging and hydraulic gradients to locate zones of groundwater discharge during reconnaissance of a moderately sized watershed to identify suspected gaining reaches for further study. At these identified study sites, detailed studies were completed to verify the reconnaissance results, quantify the groundwater-surface water exchange and assess its seasonal and temporal variability. This was done through the application of a combination of techniques, which involved monitoring hydraulic gradients, estimating streambed hydraulic conductivities, using temperature profiles and Darcy's law to estimate groundwater fluxes, developing flow nets of study reaches, and performing differential stream gauging.

The reconnaissance proved effective at identifying signs of groundwater discharge throughout the watershed, based on clusters of cold streambed readings and infrared imaging differentiating groundwater discharge near and along the streambank from their surroundings based on temperature contrasts. The reconnaissance ultimately led to the identification of two sites exhibiting groundwater discharge conditions. At these study sites, groundwater discharge conditions were confirmed based on upward hydraulic gradients, upward Darcy fluxes and largely upward temperature profile fluxes, in depth follow up infrared imaging, and differential stream gauging identifying gaining conditions. Based on the point scale techniques of Darcy fluxes and temperature profile fluxes, groundwater-surface water exchange was found to exhibit similar spatial patterns with groundwater discharge appearing often highest in the areas of the study reaches where discharge was identified during the reconnaissance while signs of recharge were also found, highlighting the spatial variability along the reaches of study.

While effective at assessing spatial variability, these point measurement techniques were unable to accurately quantify groundwater discharge because they greatly underestimated the benchmark of differential stream gauging. This was attributed to the point measurement technique's ability to only account for the vertical component of groundwater discharge, which was found to be small, indicating a significant alternative source of groundwater discharge. Based on a lack of instrumentation immediately at the streambanks, and visible discharge at some streambank locations, the discrepancy was attributed to groundwater discharge near the streambanks. Flow nets were initially unsuccessful in accounting for this significant component of groundwater discharge, which was attributed to the inability to accurately represent the high hydraulic conductivities near the streambank because of limited field data. When applying a higher, but reasonable, hydraulic conductivity value, the estimates of discharge were much more in line with differential stream gauging estimates, suggesting a significant component of groundwater discharge entering near the streambank.

Groundwater-surface water exchange was also found to be influenced by temporal variability, as seen by the increase in groundwater discharge measured between the winter and summer using the point measurement techniques. Hydraulic conductivities were influenced by changes in water viscosity, while bi-weekly and continuous monitoring of vertical and horizontal hydraulic gradients indicated the presence of groundwater discharge conditions and showed variability with time. Continuous datasets provided even greater insight, including identifying seasonal trends and the reversal of hydraulic gradients in responses to extreme flow events. Continuous monitoring, though differential stream gauging, also indicated variability in groundwater-surface exchange over the overall gaining stream reach. These results highlight the importance of considering variability when assessing groundwater- surface water interactions. The findings of this study make clear the significant complexity that exists with regards to groundwater-surface water interactions, and the many challenges that must be considered in order to better comprehend these processes.

# Acknowledgements

First off, I would like to thank my supervisor Dr. David Rudolph. Your support and guidance were invaluable throughout my graduate studies. From encouraging my participation in conferences, to taking additional classes, to challenging me to critically examine my results, you pushed me out of my comfort zone in ways that helped me grow as both a student and a person. On a personal level, I always enjoyed our conversations, whether it was about books, sports and/or current events that provided a reprieve from research and school.

Secondly, I wanted to sincerely thank Dr. Andrew Wiebe. My success would not have been possible without your support throughout this research. You always were available to talk, offer feedback, and share ideas to help address challenges as they arose. You were at my side during the best and worst days in the field and your willingness to help was crucial to the success of this work.

I would also like to thank my other committee members, Dr. Walter Illman and Dr. Randy Stotler. Your valuable feedback and insights were extremely helpful in addressing a number of hurdles I faced over the course of my research. I greatly appreciated the time and thought you put into supporting my work.

Thank you to my colleagues in the Rudolph research group including Matthew White Pendleton, Oliver Conway-White, Haoyu Yin, Jiangyue (Joey) Ju, Jiaqi Weng, Brampton Dakin, and Aaron Vandenhoff who either provided valuable assistance in the field and/or thoughtful feedback on my research.

A big thanks to co-op students Anna Maziarz, Michaela Ali, Vance Smith, and Allison Yang who played a valuable role in the success of my field studies.

I would like to also thank Gary Flynn from the Ontario Ministry of the Environment, Conservation and Parks for his assistance in operating the UAV and sharing the data used in this study.

I'm also incredibly grateful to the Crumb, Jackson, and Mighton families for providing me with access to their properties in order to perform these studies as without their gracious permission none of this research would have been possible.

I'd also acknowledge my funders: Global Water Futures Observatories program (CFI-MSI Project No. 42687), Canada First Research Excellence Fund - Global Water Futures program (Transformative

Sensor Technologies and Smart Watersheds project, awarded to Claude Duguay), Natural Sciences and Engineering Research Council of Canada (NSERC; funding reference number 571298, awarded to W.A. Illman), and Ontario Ministry of the Environment, Conservation and Parks (Great Lakes Project Number 9801).

Lastly, to my family. While I often kept my research close to the vest, your support in encouraging me to follow my interests has been greatly appreciated.

Scripts were written with the help of AI tools (ChatGPT) to assist with plotting data.

# Table of Contents

Author's Declaration ..... ii

Abstract ..... iii

Acknowledgements ..... v

List of Figures ..... xi

List of Tables ..... xv

Chapter 1 Introduction ..... 1

1.1 Background ..... 1

1.2 Field Site ..... 2

1.3 Objectives ..... 2

1.4 Thesis Organization ..... 3

Chapter 2 Assessment of Field Monitoring Techniques for Identifying Groundwater Discharge in Streams ..... 4

2.1 Introduction ..... 4

2.2 Background ..... 6

2.3 Methodology ..... 9

2.3.1 Field Site ..... 9

2.3.2 Reconnaissance Surveys to detect Groundwater Discharge ..... 10

2.3.3 Instrumentation at Study Sites ..... 12

2.3.4 Detailed Infrared Imaging ..... 13

2.3.5 Single Well Response Tests ..... 13

2.3.6 Groundwater Flux Estimates using Darcy's Law ..... 14

2.3.7 Groundwater Flux Estimates using Streambed Temperature Profiling ..... 14

2.3.8 Presentation of Data ..... 17

2.3.9 Differential Stream Gauging ..... 17
2.4 Results and Discussion ..... 18
2.4.1 Reconnaissance Streambed Temperature Findings ..... 18
2.4.2 Reconnaissance Visual and Infrared Imaging Observations ..... 18
2.4.3 Reconnaissance Hydraulic Gradient Findings ..... 19
2.4.4 Site Specific Investigations ..... 20
2.4.5 Study Site Descriptions ..... 20
2.4.6 Handheld Infrared Imaging ..... 21
2.4.7 Aerial Infrared Imaging ..... 22
2.4.8 Vertical Hydraulic Gradients ..... 23
2.4.9 Darcy Groundwater Fluxes ..... 24
2.4.10 Temperature Profiling Groundwater Fluxes ..... 24
2.5 Conclusions ..... 27
2.6 Figures ..... 29
Chapter 3 Quantifying Groundwater-Surface Water Exchange Within a Stream Through Field Monitoring ..... 47
3.1 Introduction ..... 47
3.2 Methodology ..... 49
3.2.1 Field Site ..... 49
3.2.2 Study Sites ..... 50
3.2.3 Instrumentation at Study Sites ..... 51
3.2.4 Groundwater Flux Estimates using Streambed Temperature Profiling ..... 52
3.2.5 Hydraulic Head and Hydraulic Gradient Measurements ..... 53
3.2.6 Horizontal Hydraulic Conductivities ($K_h$) ..... 54

3.2.7 Vertical Hydraulic Conductivity ..... 55
3.2.8 Darcy's Groundwater Flux Estimates Assuming Isotropic Conditions ..... 55
3.2.9 Spatial Distribution Analysis ..... 55
3.2.10 Quantifying Groundwater-Surface Water Exchange using Point Measurement Fluxes ..... 56
3.2.11 Stream Gauging ..... 56
3.2.12 Flow Net ..... 57
3.3 Results ..... 58
3.3.1 Differential Stream Gauging ..... 58
3.3.2 Horizontal Hydraulic Conductivities ..... 58
3.3.3 Vertical Hydraulic Gradients ..... 59
3.3.4 Groundwater Flux and Discharge Estimates using Darcy's Law ..... 59
3.3.5 Groundwater Flux and Discharge Estimates using Streambed Temperature Profiling ..... 60
3.3.6 Groundwater Flux and Discharge Estimates assuming Anisotropy ..... 62
3.3.7 Groundwater Discharge using Flow Nets ..... 62
3.4 Discussion ..... 64
3.5 Conclusions ..... 71
3.6 Figures ..... 74
3.7 Tables ..... 91
Chapter 4 Assessing Temporal Variability in Groundwater-Surface Water Exchange Within a Stream Through Continuous Monitoring ..... 94
4.1 Introduction ..... 94
4.2 Methodology ..... 96
4.2.1 Field Site ..... 96
4.2.2 Study Sites ..... 97

4.2.3 Instrumentation at Study Sites ..... 97
4.2.4 Surface Water Level, Groundwater Level and Hydraulic Gradient Measurements ..... 98
4.2.5 Trend Analysis ..... 99
4.2.6 Stream Gauging ..... 99
4.3 Results ..... 100
4.3.1 Continuous Surface Water and Groundwater Levels ..... 100
4.3.2 Periodic Vertical Hydraulic Gradients ..... 101
4.3.3 Continuous Vertical Hydraulic Gradients ..... 101
4.3.4 Continuous Horizontal Hydraulic Gradients ..... 103
4.3.5 Continuous Differential Stream Gauging Estimates ..... 104
4.4 Discussion ..... 105
4.5 Conclusions ..... 107
4.6 Figures ..... 109
4.7 Tables ..... 124
Chapter 5 Final Conclusions and Recommendations ..... 128
5.1 Conclusions ..... 128
5.2 Recommendations ..... 130
References ..... 132
Data Availability Statement ..... 144
Appendix A Thiessen Polygons ..... 145
Appendix B Vertical Hydraulic Conductivity ..... 149
Appendix C Temperature Profiles ..... 153
Appendix D Hydraulic Gradient Error Calculations ..... 157
Appendix E Rating Curve Procedure ..... 159

# List of Figures

Figure 2.1: Alder Creek watershed. ..... 29
Figure 2.2: Surficial geology of the Alder Creek watershed. ..... 30
Figure 2.3: Temperature probes used during (a) reconnaissance and (b) temperature profiling. ..... 31
Figure 2.4: Temporary extractable drive point piezometer known as a Henry Sampler (MHE Products Ltd.) used during reconnaissance. ..... 32
Figure 2.5: Shape of temperature profiles for both groundwater discharge and groundwater recharge conditions in the winter and summer months. ..... 33
Figure 2.6: Map of streambed temperature data collected during reconnaissance, some areas of visual/infrared observations of groundwater discharge and identified study sites. ..... 34
Figure 2.7: Photos of the study reaches of interest (a) Site 1 and (b) Site 2. ..... 35
Figure 2.8: Map of piezometer installation locations and suspected areas of discharge based on reconnaissance findings at Site 1. ..... 36
Figure 2.9: Discharge conditions identified at Site 1 near riparian zone. (a) Visual and (b) infrared images collected during reconnaissance. Images confirming the presence of groundwater discharge in (c) winter and (d) summer. ..... 37
Figure 2.10: Discharge conditions identified at Site 1 near point bar. (a) Visual and (b) infrared images collected during reconnaissance. Images confirming the presence of groundwater discharge in (c) winter and (d) summer. ..... 38
Figure 2.11: Map of piezometer installation locations and suspected areas of discharge based on reconnaissance findings at Site 2. ..... 39
Figure 2.12: Discharge conditions identified at Site 2 through bank seepage near spring. (a) Visual and infrared images confirming the presence of groundwater discharge in (b) winter and (c) summer. ..... 40
Figure 2.13: Spring found just downstream of Site 2 during reconnaissance that discharges into Alder Creek. The main branch of the spring (a) is fed by two converging smaller branches (b) and (c) discharging from the base of trees. Infrared images of the spring captured the following summer (d, e and f) correspond to the above images (Image (b) taken during reconnaissance, (a) and (c) taken the following summer.). ..... 41
Figure 2.14: (a) Visual and (b) infrared snapshots of aerial UAV survey over Site 1, performed in the summer of 2024. ..... 42

Figure 2.15: Site 1 (a) vertical hydraulic gradients measured on February 23, 2024, (b) hydraulic conductivities measured in May 2024 and (c) vertical fluxes estimated using Darcy's law. ..... 43
Figure 2.16: Site 2 (a) vertical hydraulic gradients measured on February 8, 2024, (b) hydraulic conductivities measured in May 2024 and (c) vertical fluxes estimated using Darcy's law. ..... 44
Figure 2.17: Vertical flux estimates based on streambed temperature profiles for Site 1 in (a) winter 2024 and (b) summer 2024. ..... 45
Figure 2.18: Vertical flux estimates based on streambed temperature profiles for Site 2 in (a) winter 2024 and (b) summer 2024. ..... 46
Figure 3.1: Alder Creek watershed and study site locations. ..... 74
Figure 3.2: Surficial geology of the Alder Creek watershed. ..... 75
Figure 3.3: Photos of (a) Site 1 and (b) Site 2. ..... 76
Figure 3.4: Map of Site 1 and piezometer installations. 'BMP' indicates 'bank mini-piezometer.' ..... 77
Figure 3.5: Map of Site 2 and piezometer installations. 'BMP' indicates 'bank mini-piezometer.' ..... 78
Figure 3.6: Examples of Thiessen polygon approach applied at Site 1 for (a) Darcy fluxes and (b) temperature profile fluxes ..... 79
Figure 3.7: Examples of Thiessen polygon approach applied at Site 2 for (a) Darcy fluxes and (b) temperature profile fluxes ..... 80
Figure 3.8: Stream gauging locations at Site 1. ..... 81
Figure 3.9: Differential stream gauging estimates of net increase in streamflow due to groundwater discharge. The error bars show the combined error resulting from the individual measurements, assuming 5% error for both upstream and downstream streamflow measurements ..... 82
Figure 3.10: Site 1 (a) winter vertical hydraulic gradients, (b) horizontal hydraulic conductivities measured in May 2024, and (c) vertical fluxes estimated using Darcy's law. ..... 83
Figure 3.11: Site 1 (a) summer vertical hydraulic gradients, (b) horizontal hydraulic conductivities measured in May 2024, and (c) vertical fluxes estimated using Darcy's law. ..... 84
Figure 3.12: Site 2 (a) winter vertical hydraulic gradients, (b) horizontal hydraulic conductivities measured in May 2024, and (c) vertical fluxes estimated using Darcy's law. ..... 85
Figure 3.13: Site 2 (a) summer vertical hydraulic gradients, (b) horizontal hydraulic conductivities measured in May 2024, and (c) vertical fluxes estimated using Darcy's law. ..... 86
Figure 3.14: Vertical flux estimates based on streambed temperature profiles for Site 1 in (a) winter 2024 and (b) summer 2024. ..... 87

Figure 3.15: Vertical flux estimates based on streambed temperature profiles for Site 2 in (a) winter 2024 and (b) summer 2024. ..... 88
Figure 3.16: Groundwater flow net for Site 1 on August 20, 2024. ..... 89
Figure 3.17: Groundwater flow net for Site 2 on August 23, 2024. ..... 90
Figure 4.1: Alder Creek watershed and study site locations. ..... 109
Figure 4.2: Surficial geology of the Alder Creek watershed. ..... 110
Figure 4.3: Photos of (a) Site 1 and (b) Site 2. ..... 111
Figure 4.4: Map of piezometer installation locations at Site 1. ..... 112
Figure 4.5: Map of piezometer installation locations at Site 2. ..... 113
Figure 4.6: Stream gauging locations at Site 1. ..... 114
Figure 4.7: (a) Surface water levels measured at Site 1's piezometer 13, (b) streambank groundwater levels measured at Site 1's piezometer 14 and (c) surface water levels measured at the Huron Road Hydrometric Station from November 7, 2023, to November 7, 2024 (Government of Canada, 2025b). ..... 115
Figure 4.8: Historical surface water levels measured at the Huron Road Hydrometric Station between March 1, 2015, and March 1, 2018 (Government of Canada, 2025b). ..... 116
Figure 4.9: Continuous vertical hydraulic gradients (VHG) for Site 1 piezometers from November 7, 2023, to November 7, 2024 (data lost for piezometer 3 and 11 due to piezometer damage following storm event on July 17, 2024). Surface water levels at Piezometer 1 are shown in bottom panel. ..... 117
Figure 4.10: Continuous vertical hydraulic gradients (VHG) for Site 2 piezometers from December 1, 2023, to August 29, 2024. Surface water levels at Piezometer 15 are shown in bottom panel. ..... 118
Figure 4.11: Continuous horizontal hydraulic gradients (HHG) for Site 1 piezometers from November 7, 2023, to November 7, 2024 (data lost for piezometer 3 and 11 due to piezometer damage following storm event on July 17, 2024). Surface water levels at Piezometer 1 are shown in bottom panel. ..... 119
Figure 4.12: Continuous horizontal hydraulic gradients (HHG) for Site 2 piezometers from December 1, 2023, to August 29, 2024. Surface water levels at Piezometer 15 are shown in bottom panel. ..... 120
Figure 4.13: Streamflow rating curve for Site 1 upstream gauging station. ..... 121
Figure 4.14: Streamflow rating curve for Site 1 downstream gauging station. ..... 122
Figure 4.15: The (a) vertical hydraulic gradient measured at Piezometer 1, the (b) difference in streamflow measured through differential stream gauging where positive is assumed to be

groundwater discharge (L/s), and the (c) stream stage (m) data measured at Piezometer 1 from November 7, 2023, to May 29, 2024, at Site 1..... 123

# List of Tables

Table 3.1: Average vertical hydraulic gradient and vertical flux values from temperature profiling, determined from data collected at each streambed piezometer and resulting average vertical hydraulic conductivity. ..... 91
Table 3.2: Anisotropy ratios determined for both sites in the winter and summer using average horizontal hydraulic conductivity values determined from single well response test results and average vertical hydraulic conductivity values determined using temperature profiling related vertical flux estimates and vertical hydraulic gradient measurements applied to a rearranged form of Darcy's law. ..... 92
Table 3.3: Summary of groundwater discharge estimates. ..... 93
Table 4.1: Modified Mann Kendall trend test results for Site 1 vertical hydraulic gradients..... 124
Table 4.2: Modified Mann Kendall trend test results for Site 2 vertical hydraulic gradients..... 125
Table 4.3: Modified Mann Kendall trend test results for Site 1 horizontal hydraulic gradients. ..... 126
Table 4.4: Modified Mann Kendall trend test results for Site 2 horizontal hydraulic gradients. ..... 127

# Chapter 1
# Introduction

## 1.1 Background

The interactions between groundwater and surface water have historically been treated as unique components of the water cycle, and, as a result, have largely been investigated individually (Kalbus et al., 2006). However, over the past few decades the importance of understanding the interaction between groundwater and surface water has come to the forefront (Brodie et al., 2007). Due to the interconnected nature of groundwater and surface water, the contamination or development of one will ultimately impact the other (Winter, 1999). As the need for clean water continues to grow with increased demand, and as issues related to water quality and quantity become a greater concern due to factors such as climate change, understanding their interaction becomes increasingly important (Green et al. 2011; Taylor & Stefan, 2009).

Groundwater discharge is one type of groundwater-surface water interaction. This is the flow of groundwater into surface water under conditions where the hydraulic head in the vicinity of the surface water feature is higher than the surface water level, resulting in discharging conditions (Kalbus et al., 2006). Groundwater discharge is understood to have a major effect on the physical, chemical, and biological integrity of surface water features, playing a major role in maintaining baseflow in creeks and rivers, particularly during periods of low precipitation (Kendy & Bredehoeft, 2006). Areas exhibiting groundwater discharge conditions have also been found to provide suitable breeding environments for aquatic species such as trout, largely due to the stable nature of groundwater temperatures (Aldous & Gannett, 2021).

Groundwater discharge also influences surface water quality, conveying contaminants from a wide range of different anthropogenic practices. The contamination of groundwater can ultimately result in elevated levels of contaminants within surface water features (Harris, 1995). Contaminants from point and non-point sources such as landfills, fertilized agricultural fields or road networks where road salt is applied pose particular threats to surface water quality (Howard & Livingstone, 2000).

Identifying groundwater discharge and quantifying groundwater-surface water exchange is a significant challenge. This is largely due to the complexity of groundwater-surface water interactions, and the difficulty of identifying field techniques best suited to assess the specific spatial and temporal processes relevant to a specific study (Kalbus et al., 2006). While a wide range of different techniques

exist, they all have varying advantages and disadvantages that must be considered (Ma et al., 2024). To minimize the limitations of these techniques and to reduce the uncertainty in the results, a multiscale approach using numerous different techniques is recommended (Kalbus et al., 2006).

## 1.2 Field Site

For the current study, a small to moderately sized watershed known as the Alder Creek watershed was selected for investigation. The watershed located in southwestern Ontario is situated within the south-central portion of the Waterloo Moraine and covers a 79 $km^2$ section of the larger Grand River watershed. The watershed is adjacent to the cities of Kitchener and Waterloo, with a footprint in two municipal jurisdictions, the Region of Waterloo, and Oxford County. The main surface water feature within the watershed is Alder Creek (~15 km in length). Alder Creek flows into the Nith River, a tributary of the Grand River, which flows into Lake Erie.

Approximately 40% of Kitchener's water supply is drawn from aquifers within the Alder Creek watershed (Sousa et al., 2014; Matrix and SSPA, 2014; Wiebe et al., 2023). As water demands increase in response to significant population growth in this expanding urban center, groundwater extraction from this region will likely increase. In addition, through changing land uses and as weather patterns become increasingly unpredictable due to climate change, groundwater recharge rates are expected to change. As such, interest is growing regarding their effect on the Waterloo Moraine's aquifer system, from both a quantity and quality point of view including the potential impact they may have on baseflow to Alder Creek and the aquatic ecosystems within it.

## 1.3 Objectives

The main goal of this study is to identify and quantify groundwater-surface water exchange and assess its spatial and temporal variability using numerous techniques along a perennial stream within an urbanizing watershed in southern Ontario. The main objectives are to:

1) Employ and evaluate the utility of several small scale reconnaissance techniques such as streambed temperature readings, infrared imaging, and hydraulic gradient measurements to identify zones of groundwater discharge along a perennial stream.

2) Validate the reconnaissance findings by employing detailed infrared imaging to detect discharge regions, confirm, and quantify groundwater discharging conditions using Darcy's law and temperature profiling approaches, and perform differential stream gauging at stream reaches identified through the reconnaissance surveys to be potential areas of groundwater discharge.

3) Analyze the spatial variability of groundwater-surface water exchange along the identified stream reaches using high density point measurement flux techniques related to temperature profiling and Darcy's law.

4) Quantify groundwater-surface water exchange across selected stream reaches of study by applying temperature profiling, Darcy's law, flow nets and differential stream gauging techniques.

5) Assess the temporal variability of groundwater-surface water exchange through long term monitoring of surface water levels, groundwater levels, hydraulic gradients, and streamflow.

## 1.4 Thesis Organization

This thesis is composed of five chapters. Chapter 1 introduces the topic and the goal/objectives of this research. Chapter 2 focuses on the identification of stream reaches exhibiting groundwater discharge conditions through the application of reconnaissance-scale monitoring tools along Alder Creek. This is followed by the verification of the reconnaissance work through longer-term, site-specific studies by applying a variety of different techniques to quantify groundwater-surface water exchange. Chapter 3 focuses on developing a better understanding of the applicability of various multiscale techniques to quantify groundwater-surface water exchange and to assess its spatial variability. Chapter 4 assesses the influence of temporal variability on groundwater-surface water exchange using numerous continuous monitoring approaches and data sets. Chapter 5 provides final conclusions and recommendations for future work.

# Chapter 2
# Assessment of Field Monitoring Techniques for Identifying Groundwater Discharge in Streams

## 2.1 Introduction

Surface water features such as creeks and rivers are under increased strain due to a multitude of external pressures, including increased urbanization, extensive agricultural practices, and climate change. As a result, greater emphasis on water resource management is required to preserve water quality and quantity within our communities and in the rural landscape. A major factor to consider with regard to sustainably maintaining these surface water features is groundwater discharge, and the vital role it plays. Groundwater discharge is crucial in maintaining streamflow year-round, especially during periods of low precipitation where baseflow is the main component of streamflow. This consistent source of replenishment not only keeps streams flowing but also helps maintain the aquatic ecosystems which support aquatic fauna and flora populations. However, because of increasing, long-term groundwater extraction for domestic or commercial uses in certain areas, baseflow rates in stream systems near production water wells have been documented to be decreasing at local and regional scales (Barlow & Leake, 2012; Zipper et al., 2024), Furthermore, due to the anticipated impacts of climate change and the related unpredictability pertaining to annual precipitation and snowmelt timing and volume, less confidence can be placed in forecasting expected groundwater recharge, storage and subsequent discharge (Dubois et al., 2022; Green et al., 2011; Taylor et al., 2013).

Groundwater discharge also plays a significant role regarding surface water quality, as it transports nutrients and other solutes that are ultimately released to surface water features (Laursen & Seitzinger, 2005; Wallis et al., 2020). At low levels, these nutrients are beneficial to aquatic life by supporting, for example, biogeochemical processes within the hyporheic zone (Bardini et al., 2012). Higher concentrations of nutrient discharge can be detrimental, and act as a contaminant that harms the aquatic ecosystem (e.g., eutrophication) (Holman et al., 2008). As a result, it is becoming more important than ever to be able to identify areas of groundwater discharge (gaining stream reaches) within waterways, to better address water quantity and quality concerns. Through the identification of these areas, further studies can be appropriately targeted to better understand impacts from

groundwater extraction, and to quantify water quality, while assisting in the development of Best Management Practices (BMPs), such as mitigation strategies to address these concerns. In addition, the information gathered will be invaluable in supporting the next generation of integrated hydrogeologic modelling tools, that will be employed to assist in developing water management strategies at varying scales.

The identification of groundwater discharge is a challenging endeavor. This is largely due to the high spatial variability of flow and exchange rates between groundwater and surface water (Conant Jr., 2004), an issue only exacerbated by the significant heterogeneity of streams in glacial depositional settings. At the same time, while many techniques exist to identify groundwater discharge, they are highly variable both in type and scale of application, making it difficult to identify techniques that that are the most applicable to local site conditions (Kalbus et al., 2006).

The goal of the current study is to identify stream reaches exhibiting groundwater discharge conditions within a small to moderately sized watershed, using a novel reconnaissance approach, and to subsequently verify the presence of groundwater discharge conditions through the completion of detailed, longer-term studies of identified stream reaches of interest. To identify these groundwater discharge conditions, a reconnaissance survey that applied manual, small-scale measurement tools including handheld infrared cameras, temperature probes, and temporary extractable drive point piezometers was performed. These techniques are commonly employed at the reach scale in climates with noticeable seasonal contrasts in surface and groundwater temperatures. However, they have infrequently been applied to detect areas of groundwater discharge in reconnaissance-scale work over large areas (i.e. watershed scale), likely due to their spatial limitations. However, in watersheds with thick foliation, it is believed these techniques may be more applicable, especially as more commonly used techniques for regional scale reconnaissance (e.g., UAS, helicopters, DTS systems) face geographic and sensitivity limitations in such settings.

Gaining reaches identified through the reconnaissance surveys were then instrumented and studied using temperature profiling to estimate flux, measure hydraulic gradients and estimate hydraulic conductivities to determine Darcy fluxes, along with applying a differential stream gauging technique to verify the presence of groundwater discharge conditions. Information from these detailed investigations was then used to provide support to the proposed reconnaissance approach and provide insight into the utility of different groundwater discharge identification techniques.

## 2.2 Background

The observation of natural processes has been used as a guide to detect the presence of groundwater discharge, including through the identification of flora that thrive on groundwater (i.e. phreatophytes) (Rosenberry et al., 2000), the observation of aquatic fauna that prefer habitats and breeding areas related to groundwater discharge (i.e. trout) (Aldous & Gannett, 2021), and the identification and monitoring of icings in Arctic terrain (Crites et al., 2020; Glass et al., 2021). Practical, field-based techniques have also been used to identify and quantify groundwater discharge, including, for example, tools like seepage meters (Lee & Cherry, 1979), which are applicable for small scale measurements, as well as water chemical tracers such as $Radon^{222}$ (Cook et al., 2003; Kluge et al., 2007; Tecklenburg & Blume, 2017) that are applicable at larger scales.

Heat tracing via temperature monitoring is one of the more commonly used techniques for identifying groundwater discharge. Its value lies largely in the temperature contrast found between surface water and groundwater at certain times of year (Schmidt et al., 2007). Groundwater temperatures often remain relatively consistent year-round, while surface water temperatures can vary considerably. These conditions make the summer and winter months the optimum time of the year to perform temperature-related studies, as these are the seasons when surface water temperatures reach their highest and lowest temperatures respectively, resulting in the greatest contrast with groundwater.

A variety of different tools related to temperature monitoring have been developed and used to identify groundwater discharge over varying spatial scales. One of these tools is thermal infrared imaging (IR), which is a remote sensing technique performed using infrared cameras that can detect the natural thermal infrared radiation emitted by objects. Groundwater discharge from seeps and springs can, therefore, be identified based on the distinct temperature contrast that exists, particularly during the winter and summer months, between emergent groundwater and its surroundings, including surface water and streambank settings.

Large scale regional thermal infrared imaging of surface water features has been performed previously using satellites (Handcock et al., 2006), aircraft (Liu et al., 2016), and unmanned aerial systems (UAS) (Watts et al., 2023) to identify groundwater discharge conditions, including streambank seepage. However, due to the presence of tree canopies and vegetation growth along the banks of, and within, surface water features, aerial infrared imaging techniques have been found to be

limited in their ability to identify groundwater discharge conditions (Handcock et al., 2006). This is especially true in smaller, and often more complex, surface water features like creeks, where visibility for aerial infrared imaging is often limited, and the variability in morphology and hydrological conditions can limit its effectiveness (Handcock et al., 2006).

At a local scale, the use of ground based infrared imaging has proven useful, using handheld thermal infrared imaging cameras (Deitchman & Loheide, 2009; Moore et al., 2023; Schuetz & Weiler, 2011). This approach, while limited by how much work the operator puts into it, does allow for the identification of localized groundwater discharge features that may not be apparent in the more regional scale methods. However, like all infrared imaging techniques, it can only identify the groundwater discharge temperature contrast that reaches the streams surface, not within the water column or the streambed, highlighting the need for streambed temperature measurements to improve groundwater discharge identification.

Using streambed temperature as a tracer is another temperature-related technique that has been extensively used to better understand a wide range of hydrologic and hydrogeologic processes related to groundwater-surface water interactions. This approach has been used to identify surface water infiltration, groundwater discharge, and streambed hydraulic conductivities (Anibas et al., 2009; Conant Jr., 2004; Ghysels et al., 2021; Jensen & Engesgaard, 2011; Lapham, 1989; Lautz & Ribaudo, 2012; Schmidt et al., 2007). The theory behind using streambed temperatures to better understand groundwater-surface water interactions is based on the concept of heat transport and the relationship between its various mechanisms (i.e., advection and heat conduction) (Constantz, 2008; Stonestrom & Constantz, 2003). Based on the relationship between these mechanisms, and the exchange between the groundwater and surface water sources, the shape of the vertical temperature profile within the streambed will vary and can provide insight into the direction and magnitude of flow within the streambed sediments.

Temperature measurements have been made in a variety of different ways but often consist of a combination of continuous temperature data using in situ thermistors and dataloggers, as well as temporally discreet manual temperature measurements using temperature probes installed to desired depth(s) within the streambed (Anibas, 2011; Conant Jr., 2004; Jensen & Engesgaard, 2011; Schmidt et al., 2007). The depth and number of temperature measurements made within the streambed depend on the method employed and range from a singular depth below the streambed (Conant Jr., 2004;

Schmidt et al., 2007; Westberg, 2012) to several depths (Anibas et al., 2009; Ghysels et al., 2021; Hatch et al. 2006; Kurylyk et al., 2017; Lautz & Ribaudo, 2012; Schmidt et al., 2006). Streambed temperature monitoring can be conducted at a highly detailed spatial scale over small stream reaches (Conant Jr., 2004; Ghysels et al., 2021; Lautz & Ribaudo, 2012; Schmidt et al., 2007), or by sparse, spread-out temperature mapping studies (Anibas et al., 2011; Jensen & Engesgaard, 2011). Although approaches vary with regards to how temperature data are collected, various (1D) analytical models (Bredehoeft & Papadopoulos, 1965; Stallman, 1965) have been developed based on the concept of heat transport, to which temperature data (i.e. temperature profiles) can be utilized to determine the direction and magnitude of groundwater flux. These include steady-state (Anibas et al., 2011; Ghysels et al., 2021; Kurylyk et al., 2017; Schmidt et al., 2007) and transient (Hatch et al., 2006; Keery et al., 2007; Luce et al., 2013) conditions within streambed temperature profiles. A constraint of these techniques, however, is in their spatial limitations, as measurements at a point scale make it challenging to assess groundwater discharge in detail over longer reaches of a stream.

Another temperature monitoring technique which has been applied at larger spatial scales is the distributed temperature sensors (DTS) method (Briggs et al., 2012; Krause et al., 2012; Lowry et al., 2007; Selker et al., 2006). These devices work by sending a light pulse along an optical fiber deployed within a water feature and monitoring the return light signal. As the behavior of the incident light pulse is influenced by the temperature along the optical fiber, monitoring of the returning light signal can determine temperatures at a temperature resolution of 0.01°C, and a spatial resolution of approximately 1 m over a scale of several kilometres (Briggs et al., 2012; Selker et al., 2006). For example, this type of survey can provide a spatially continuous temperature dataset over long stream reach segments and can be used in identifying areas of groundwater discharge (Briggs et al., 2012; Lowry et al., 2007; Selker et al., 2006). However, several disadvantages exist regarding this technology. These include challenges measuring temperatures at the groundwater-surface water interface when laying the cable along cobbly or bedrock lined streambeds, the cost of these systems, installation difficulties in remote settings due to the need for a continuous power source, durability concerns of the fiber optic cable, as well as both a challenging calibration process and complex data analysis (Mohamed et al., 2021).

In addition to temperature monitoring techniques, other methods exist that can be used to identify the presence of groundwater discharge. Hydraulic head (h) and vertical hydraulic gradients ($\Delta h/\Delta l$) are point measurement techniques that can be used to identify the possible presence of groundwater

discharge conditions (Binley et al., 2013). Using piezometer installations within streams, the direction of groundwater flow can be determined based on the difference between surface and groundwater levels (Δh). Using the depth of the piezometer relative to the streambed surface (Δl), the vertical hydraulic gradient can be calculated, providing a magnitude to groundwater flow. However, groundwater discharge flux is also reliant on the hydraulic conductivity (K). This latter parameter can be estimated using single well response tests and anisotropy ratios. They can then be combined with the measured hydraulic gradient data to estimate local groundwater flux.

Differential stream gauging can also be applied to identify stream reaches exhibiting groundwater discharge (Becker et al., 2004; Cey et al., 1998; McCallum et al., 2012). The technique of differential stream gauging involves measuring streamflow upstream and downstream of the reach of interest under baseflow conditions, where groundwater can be assumed to be the only contributor to changes in streamflow (Kalbus et al., 2006). If streamflow increases over the reach of interest (i.e., gaining reach), groundwater discharge conditions are assumed to be present. For increased effectiveness when using this technique, no tributaries or other sources of inflow, such as artificial drainage features, should be present along the reach of study. Baseflow conditions can be expected during periods of low flow, when precipitation and overland flow have not occurred in the days leading up to and during stream gauging events, thus simplifying the analysis (Kalbus et al., 2006).

## 2.3 Methodology

### 2.3.1 Field Site

The field site for this research is the 79 $km^2$ Alder Creek watershed, located in the greater Grand River watershed of southwestern Ontario (Figure 2.1). Annual air temperatures in this area range from a minimum daily average of -10.2°C in January to a maximum daily average of 26.2°C in July, while average annual precipitation is approximately 900 mm per year (Government of Canada, 2025a). Average groundwater recharge rates within the watershed are approximately 320 mm per year (Matrix and SSPA, 2014; Wiebe et al., 2022). Alder Creek is a perennial stream, approximately 15 km in length from the headwaters to the confluence with the Nith River. In the upper to middle reaches of the watershed are numerous smaller, spring-fed tributaries. Alder Creek forms a tributary of the Grand River, which drains into Lake Erie (Figure 2.1).

The Alder Creek watershed has a heterogeneous surficial geology (Figure 2.2) because of its location within the south-central portion of the Waterloo Moraine. The Waterloo Moraine is a significant topographic relief feature, composed of numerous glacial till sheets deposited during the advance and retreat of glaciers in the region, and is interlayered with glaciofluvial sand and gravel deposits (Bajc et al., 2014; CH2MHILL and SSPA, 2003; Karrow, 1993; Martin & Frind, 1998). These sand and gravel deposits contain many of the major overburden aquifers that have provided the Regional Municipality of Waterloo (RMOW) with much of its municipal water supply for decades.

A significant component of the overall groundwater extracted by the RMOW is derived from the wellfields located within the Alder Creek watershed. These wellfields include the Mannheim West wellfield (Figure 2.2), which alone supplies approximately 40% of the total groundwater extracted from wellfields in the City of Kitchener, Ontario (Sousa et al., 2014; Matrix and SSPA, 2014; Wiebe et al., 2023). However, because of significant population growth in this urban area, the demand for water is expected to continue to increase, potentially resulting in increased groundwater usage. At the same time, changes in groundwater recharge rates are expected as land uses within the watershed change from historically agricultural, to increasingly urban (e.g., development of buildings, roads, etc.), while climate change results in more unpredictable weather patterns. Due to these changes, greater interest is arising with regards to how the increased strain being put on the groundwater supply within the Waterloo Moraine's aquifer system will affect baseflow to Alder Creek and the aquatic ecosystems that rely on it.

### 2.3.2 Reconnaissance Surveys to detect Groundwater Discharge

To identify reaches of the stream displaying groundwater discharge conditions, reconnaissance of the main channel of Alder Creek, and several of its tributaries was performed during the summer of 2023 (June & July) utilizing a series of field monitoring techniques. The summer season was selected to take advantage of the expected temperature contrasts between surface water and groundwater, during this time of year. Although surface water temperatures increase with increasing air temperatures, groundwater temperatures tend to remain relatively consistent year-round, producing a temperature contrast useful for identifying areas of groundwater discharge with thermal techniques.

Several hand-held tools were used to identify contrasting temperature conditions during the reconnaissance surveys. This included a subsurface temperature probe, which was a tool designed to measure temperatures in the streambed (Figure 2.3a). The device consists of a stainless steel YSI

Model 418 thermistor probe that was run through, and nearly completely encased within a 1.35 m long, 1.5 cm outer diameter pointed aluminum pipe. Near its base, the thermistor tip was exposed through a small hole in its protective aluminum casing. The thermistor probe cable that ran through the top of the pipe was connected to an Oakton® CPTEMP14 Temp-14 Thermistor Thermometer, which has an accuracy of ±0.2°C and a resolution of 0.1°C. The temperature probe was inserted periodically into the stream water column by operators wading or boating along the stream to measure stream water temperatures, and into the streambed at depths ranging from between 20 to 30 cm to measure subsurface temperatures. It was anticipated that at this depth, the influence of diurnal temperature oscillations (more prevalent at shallower depths) would be minimal, if not avoided altogether (Conant Jr., 2004). These readings were made along most of the main channel of Alder Creek, from the headwater region to the outlet. Potential groundwater discharge conditions were identified where the streambed temperatures were similar to expected groundwater temperatures of approximately 10°C.

Visual observations and infrared imaging were additional methods applied to identify groundwater discharge. Visual observation was a simplistic method applied that involved visually scanning streambanks for signs of dampness, or visible seepage, as well as identifying springs and spring fed tributaries discharging into the main channel of Alder Creek. While visual inspection is a valuable tool to identify groundwater discharge, infrared cameras provide significantly greater insight and confidence by detecting temperature contrasts that are imperceptible to the human eye. A FLIR® ThermaCAM P25 handheld infrared (IR) camera was used in the reconnaissance work to scan the surface water and the streambanks along Alder Creek, to identify areas displaying colder temperatures relative to the surroundings of the stream during the summer months. These were inferred to be areas of local groundwater discharge. Infrared imagery was also used to identify areas of cooler surface water temperatures relative to the surrounding surface water, specifically in shallow, calm settings where mixing was minimized, and contrasts were more visible. Locations where cold temperature anomalies were detected along the length of Alder Creek with infrared imaging were photographed with an optical camera, spatially mapped with GPS coordinates, and paired with the corresponding infrared images. Locations identified through infrared imagery were then further assessed using the temperature probe (Figure 2.3a), which allowed for the measurement of streambed temperatures (± 0.2°C) at desired depths, in addition to their ability to identify suspected areas of

groundwater discharge based on cold streambed temperatures that were not identifiable with the infrared imagery.

A temporary extractable drive point piezometer, known as a Henry Sampler (MHE Products Ltd.), was also used to measure vertical hydraulic gradients at a point measurement scale within the streambed of Alder Creek (Figure 2.4). This device is tapped into the streambed to the desired measurement depth, and through the removal of an internal rod that prevents sediments from entering the screened section at the bottom, groundwater can fill the steel drive-point device, permitting the measurement of the hydraulic head at that depth in the streambed. At locations where the hydraulic head in the stream bed exceeded the stream water level, based on measurements made from the top of the drive point casing using a small-diameter water tape, groundwater discharge conditions were inferred to exist. This device could, therefore, provide additional support to the temperature reconnaissance monitoring in identifying areas exhibiting groundwater discharge conditions.

The various data sets collected through the reconnaissance monitoring surveys were compiled and presented in maps of the Alder Creek watershed using the Geographic Information System (GIS) program ArcGIS® Pro (ESRI). Regions along the main channel of Alder Creek, where groundwater discharge conditions were interpreted to be occurring, were identified as potential sites for more detailed site investigation. In addition to the evidence of groundwater discharge, potential study sites were considered based on ease of access with regards to transporting and installing field instrumentation, and on landowner permission. Based on these considerations, two sites were selected for detailed investigation of groundwater-surface water interactions. All field data collected during the reconnaissance, and at the identified sites, can be found in Zanatta et al. (2025).

### 2.3.3 Instrumentation at Study Sites

At the two field sites identified for more detailed site investigation based on the reconnaissance surveys, conventional PVC piezometers (1” and 1 ½” ID) and mini-piezometers (1/4" ID) were installed in the streambed to measure hydraulic heads and conduct single-well response tests. The piezometers were installed at multiple locations across and along the study site stream reaches, with the goal of capturing heterogeneity in the stream bed. In the case of Site 1, 23 mini-piezometers and 4 conventional piezometers were installed in the streambed, while at Site 2, 16 mini-piezometers and 4 conventional piezometers were installed in the streambed. The conventional PVC piezometers were manually driven into the streambed with a pounding device, while the mini-piezometer installations

followed the procedure of Lee and Cherry (1979), which utilizes an extractable temporary drive casing. The installation processes assumed the natural collapse of streambed material around the piezometer screens, to seal them and reduce the risk of unwanted vertical flow. The midpoints of the piezometer screens were installed to depths ranging from 40 and 55 centimetre below the streambed. The screen length of the conventional piezometers was ~30 cm (slotted), while the screen length of the mini-piezometers was ~15 cm (perforated and Nitex® wrapped). To keep each mini-piezometer from being damaged or removed by the flowing stream water, the mini-piezometer tubing was threaded through a rubber stopper, which was clamped to a bolt fastened to a metal plate, with rocks stacked on the plate to stabilize it. All piezometers were developed after installation.

Following the installation and development of the piezometers and mini-piezometers, the instrument coordinates and elevations were surveyed using a Sokkia GCX3 GNSS receiver surveying device, a total station, and an automatic level. Manual surface water and groundwater level readings were recorded approximately biweekly for each piezometer. Using the relative water level difference between the groundwater and surface water, along with the known installation depths of the midpoint of the piezometer screen below the streambed, vertical hydraulic gradients were calculated to determine the direction of vertical groundwater flow.

### 2.3.4 Detailed Infrared Imaging

Building on the infrared imaging conducted during the reconnaissance surveys, more detailed infrared imaging was performed at the two study sites using a TOPDON TC005 thermal infrared (IR) imaging camera. This included infrared imaging of the streambanks at each site during both the winter (2024) and the following summer (2024), to verify the earlier reconnaissance work and to gain new insight into seasonal groundwater discharge conditions along the reach that may have been missed. In addition to the handheld infrared camera, the sites were further assessed by a drone-based infrared system, which utilized a DJI Matrice 300 UAV with a DJI H20T camera to provide both standard and infrared video/images that could be used to identify groundwater discharge from an aerial perspective. The aerial infrared surveys were completed in the summer of 2024.

### 2.3.5 Single Well Response Tests

To determine horizontal hydraulic conductivities ($K_h$) representative of the material around each piezometer screen, single well response tests were performed in May 2024. For the conventional

piezometers, the tests were completed by performing slug tests (rising and falling head protocols). The change in head over time due to the displacement of water was monitored at 1 second intervals using a Solinst LevelLogger®, which was installed just above the base of the piezometers. The head responses were monitored until water levels had recovered to near steady state conditions. For the mini-piezometers, falling head tests were performed. Air bubbles were first purged from the mini-piezometers, and an initial head was then measured using a ruler placed on the steel plate installed at the streambed. Then, using a Mityvac® handheld vacuum/pressure pump air was removed from the mini-piezometers, allowing for the head to rise above the initial static level. A video of the recovery was recorded after the vacuum was released, with the mini-piezometer held beside the ruler. During post processing, the videos were viewed in slow motion, and periodic readings of head along the ruler were recorded with their associated elapsed times until the head returned to its original pre-test level. To calculate the horizontal hydraulic conductivities, the Hvorslev (1951) approach was applied, while also incorporating the Butler (1996) recommendation of matching points within the interval of $h/h_0$ between 0.15 and 0.25 with a line of best fit.

### 2.3.6 Groundwater Flux Estimates using Darcy's Law

Using the hydraulic conductivity values acquired from the single well response tests and the measured vertical hydraulic gradients at each piezometer location, vertical flux estimates were calculated using Darcy's law. While a similar approach has been applied in previous studies (Binley et al., 2013; Cey et al., 1998; Käser et al., 2009), it is recognized that single well response tests on vertical well screens may provide estimates most representative of the horizontal hydraulic conductivity. As a result, the calculated vertical fluxes may be an overestimation if there was a directional anisotropy in hydraulic conductivity within the streambed, which may infer lower actual vertical hydraulic conductivities (Freeze and Cherry, 1979). Isotropic conditions were assumed for these estimates.

### 2.3.7 Groundwater Flux Estimates using Streambed Temperature Profiling

Streambed temperatures are commonly used as a tracer to estimate the direction and magnitude of groundwater flow, based on the relationship between advective heat transport of groundwater flow through the streambed and the conduction of heat that occurs through and between the solid and liquid phases of the streambed (Constantz, 2008). Vertical temperature profiles, developed under steady state conditions for an assumed homogeneous medium, can be fit to 1-D steady state analytical

solutions, such as that of Bredehoeft and Papadopulos (1965), to generate flux estimates deemed representative of the mean vertical flux over the length of the temperature profile (Irvine et al., 2016). In these cases, temperature profiles that are concave upward in shape exhibit groundwater recharge conditions, while those that are concave downward in shape exhibit groundwater discharge conditions (Figure 2.5) (Kurylyk et al., 2017).

To generate these flux estimates, temperature data were collected through manual measurements of the streambed over a multi-day period at both study sites in the winter and summer of 2024. At the first site, temperature data was collected over 3 days, between February 21 and 29, and over 3 days, between July 22 and 24. At the second site, temperature data were collected over 1 day on February 8, and over the 2-day period of July 25 and 26. Temperature profiles were initially measured near the piezometers and mini-piezometers on the first day of each study, with the remaining time spent focusing on the collection of temperature profiles in additional locations to improve spatial coverage. The time periods for the temperature profiling were selected to take advantage of when large temperature contrasts were anticipated to exist between groundwater and surface water.

Temperature data were collected by measuring discrete subsurface temperatures at seven streambed depths (0 cm, 10 cm, 20 cm, 25 cm, 30 cm, 40 cm, 50 cm), using a stainless-steel Digi-Sense® Penetration Thermistor probe. Due to the significant hammering required to collect data at these desired depths, these thermistor probes were encased within a more durable pointed steel pipe temperature probe that was 1.45 m long and had a 1.5 cm outer diameter (Figure 2.3b). The cable for the thermistor probe ran up the inside of the steel pipe where it would connect at the top to a Digi-Sense® 91428-05 Temp-14 Single-Input Thermistor Thermometer, with an accuracy of ±0.2°C and a resolution of 0.1°C. Temperature readings were made by progressively advancing the probe to the desired depth, beginning at 0 cm, and then waiting until the Digi-Sense® 91428-05 Temp-14 Single-Input Thermistor Thermometer produced a stable reading that held steady for at least 5 seconds. Once stable, the probe was manually driven to the next desired depth, and the process was repeated until a depth of 50 cm. A total of 7 temperature readings were collected at each profiling location. Data collected up to this depth was considered sufficient to develop temperature-depth profile curves necessary to quantify groundwater-surface water flux exchange. While these temperature probes were designed to be more rugged than the temperature probe used for the reconnaissance survey (Figure 2.3a), in order to allow for deeper temperature readings, several of them did break and had to be replaced over the course of this work.

In addition to the measurement of the manual temperature profiles, continuously recording thermistor devices were installed as vertical series of 6 to 7 thermistors, between the stream bed and a maximum depth of 50 cm. These continuously recording temperature profiles were installed along the thalweg of the stream at the study sites, where groundwater flow was presumed to be predominantly vertical. These recording thermistors permitted the monitoring of the diel variability of groundwater temperatures over the course of the winter and summer temperature profiling periods, in order to estimate the approximate depth with which steady state temperature conditions existed. At depths greater than 50 cm, the diel temperature signal was expected to be fully dampened, making monitoring at greater depths unnecessary (Kurylyk et al., 2019).

Temperatures were measured at dozens of locations along the streambed at each study site, to provide spatially distributed streambed temperature data across the reaches of interest. These measurements were made along relatively evenly spaced transects, with temperature profiles normally measured along the thalweg of the stream, as well as at locations to the left and right of the thalweg. These transects were also designed to coincide with the locations of the piezometer and mini-piezometer installations, to allow for correlation of the temperature profile fluxes to vertical hydraulic gradient and Darcy flux measurements.

Vertical groundwater fluxes were estimated by applying the spreadsheet solver "FLUX-LM", developed by Kurylyk et al. (2017), to the temperature data collected. This spreadsheet solver was based on the 1-D analytical solution of Shan & Bodvarsson (2004), an extension of the Bredehoeft and Papadopulos (1965) steady state solution. Using the temperature data, the associated depths of readings, and estimated thermal conductivity values representative of the sediment layer being studied, estimates of vertical groundwater flux can be made. The FLUX-LM tool initially determines the upper and lower boundary conditions based on field measured temperature-depth profile data. Using these defined boundary conditions, a theoretical temperature-depth profile was calculated for a given flux, followed by the calculation of the root mean square error (RMSE) between the actual measured temperature-depth profile and the newly generated theoretically calculated temperature-depth profile. FLUX-LM then solves for the optimal flux value for the actual measured-temperature depth profile, based on curve fitting for the lowest possible RMSE.

Four fundamental assumptions define this solution. These are: (1) heat transfer is restricted to one dimension (vertical), (2) the Darcy flux of each layer is constant and uniform, (3) temperature profiles

are at steady state, and (4) the soil properties are homogeneous within each layer. To address these assumptions, heat transfer was considered to be minimal in the non-vertical direction, while the stream, as the only local point of discharge, is assumed to have constant and uniform vertical fluxes through its streambed. In addition, only temperature data collected below the component of the temperature profile exhibiting transience was applied (diel temperature amplitude of less than 1°C) (Kurylyk et al., 2017), which for this work was identified to be temperature data collected from 10 cm and below, agreeing well with the recommendations of Anibas et al. (2011) and Ghysels et al. (2021). The geologic material of the streambed was deemed to be homogeneous, limiting the system to one layer. A thermal conductivity value of 2.2 W/(m °C) for 100% saturated sandy soil was obtained from the literature (Monteith & Unsworth, 2013), as it was comparable to what was found in the streambed at the study sites.

### 2.3.8 Presentation of Data

For spatial interpretation of the raw vertical hydraulic gradient, hydraulic conductivity, Darcy vertical flux, and temperature profile related vertical flux point measurement data over the entirety of the study reaches, the geostatistical method of ordinary kriging was applied. This method uses spatial autocorrelation among point measurements to predict values, resulting in continuous spatial maps. To visualize the relative spatial distribution of each unique dataset, a quantile distribution of the kriging datasets was used. The datasets were divided into five classes of equal size, based on the ranked order of values, allowing for the relative ranking of the datasets, which groups the data by their position within the larger dataset instead of with regards to their overall magnitude. The maps, therefore, display the data in zones that correspond to these quantile groups, providing a clear, relative understanding of spatial variation across the study reaches of interest. This ultimately allows for areas of high and low vertical hydraulic gradients, hydraulic conductivity, and flux to be identified with respect to each unique dataset, and, more importantly, provide a better understanding of how they relate to the zones of groundwater discharge identified in the reconnaissance.

### 2.3.9 Differential Stream Gauging

Stream gauging was performed up and downstream of the identified reaches of interest to confirm that the study reaches exhibited a net increase in streamflow, indicative of groundwater discharge occurring over the gauged reach. Streamflow data was collected during the late spring and summer months of 2024 and 2025, using a StreamPRO® acoustic doppler current profiler (ADCP). Stream

gauging was performed numerous times at or near baseflow conditions, because, under these conditions, it could be assumed that increases in streamflow were of groundwater origin only, and would not include other sources, such as precipitation, overland flow and tributaries.

## 2.4 Results and Discussion

### 2.4.1 Reconnaissance Streambed Temperature Findings

The reconnaissance survey covered nearly 20 km of Alder Creek, including a majority of the main walkable channel and approximately 25% of the watershed's total waterways, when accounting for its tributaries. Using the subsurface temperature probe, variability in streambed temperatures were found throughout the watershed, indicative of the spatial variability in groundwater-surface water exchange. Warmer streambed temperatures were most commonly found within the northern reaches of the watershed (Figure 2.6). However, the relatively cold streambed temperatures, deemed to be most representative of groundwater discharge conditions (approximately $\leq 10°C$), were measured most often in the southern reaches of the watershed (Figure 2.6). Cold streambed temperatures were also detected at or near the sources of the Trout Farm tributary and the Hallman Road tributary, known spring-fed tributaries feeding Alder Creek (Figure 2.6) (CH2MHILL and SSPA, 2003). The similarities in streambed temperature measured in the main channel to those that were measured at or near the springs lends support to the interpretation that cold temperature readings within the streambed are indicative of potential groundwater discharge locations.

### 2.4.2 Reconnaissance Visual and Infrared Imaging Observations

As presented in Figure 2.6, signs of possible groundwater discharge were encountered at various locations along the main channel of Alder Creek during the reconnaissance surveys while scanning the stream and its streambanks using visual observations and infrared imaging. The combined imagery, shown in Figure 2.6, provides examples of presumed points of groundwater discharge, illustrating the utility of this approach. Optical and infrared imaging evidence of groundwater discharge was observed at various local scales and in different vegetative settings; however, it was primarily recorded along the streambanks. While most points of groundwater discharge appeared to be occurring in natural settings, some were also related to the locations of agricultural tiles and urban drain outfalls. To confirm the presence of groundwater discharge conditions, the temperature probe

was inserted into the streambed/streambank at the groundwater discharge source to quantitatively measure the temperature and confirm that it was a relatively cold temperature, as would be expected of groundwater at this time of year.

The visual and infrared reconnaissance methods are limited to exposed streambank and stream edge settings, where groundwater discharge can be observed by eye and the infrared method can detect clear temperature contrasts. Both lines of evidence of groundwater discharge are generally difficult, if not impossible, to recognize beneath the surface of the stream, as they would be concealed by the surface water. This was where the streambed temperature readings obtained by inserting the temperature probe within the streambed discussed above, were of value. The combination of the infrared camera with the temperature probe provided valuable insight at the reconnaissance-scale when surveying for locations of groundwater discharge along a steam channel.

### 2.4.3 Reconnaissance Hydraulic Gradient Findings

The Henry sampler was found to be a largely impractical tool to measure hydraulic gradients due to a number of factors. This includes challenges pertaining to installing the device into the streambed, due to its frequently highly armoured nature, as the tool largely lacked the structural fortitude to be installed at a desirable depth without damaging the tool itself. Another challenge was the amount of time required to install the tool, wait for the groundwater levels to equilibrate within the pipe, and make measurements of the surface water level, groundwater level, and depth of installation below the streambed. Due to the sheer size of the watershed and the amount of time available to perform the study, it was decided it would be more effective to focus on the other techniques in order to increase the efficiency for identifying groundwater discharge conditions, emphasizing the value of the streambed temperatures measurements and visual observations/infrared imaging techniques. It is recommended that this tool be applied over shorter study reaches, or when time is less of a concern, and in streambeds where cobbles in the streambed are sparse and allow for easier installation of the tool. In the case of armoured streambed channels, the development of a more robust retractable drive point piezometer is recommended, as it would ease the installation of devices such as Henry samplers, ultimately increasing the efficiency of data collection.

### 2.4.4 Site Specific Investigations

Once the reconnaissance was completed, the data collected was assessed in ArcGIS (Figure 2.6) to identify areas of potential groundwater discharge for further study. Based on the reconnaissance findings, two stream reaches of interest where groundwater discharge conditions appeared to be present were identified as study sites for instrumentation, detailed study, and verification of the reconnaissance findings. These reaches are referred to as Site 1 and Site 2 in the text (Figure 2.6).

### 2.4.5 Study Site Descriptions

Site 1 is an approximately 110 m long reach located in the mid to lower region of the Alder Creek watershed, within the community of New Dundee, Ontario (Figures 2.6 and 2.7a). Manual streamflow measurements at the site ranged from 0.1 $m^3/s$ to 5.6 $m^3/s$. This stream reach is on average, 8 m wide and is located along a meander bend. The average depth of the stream during low flow conditions in summer is approximately 0.4 m but is up to 1 m in pools. The surficial geology of the streambed primarily consists of cobbles and gravel, although near the inner bank of the bend, the streambed is largely silt. Based on qualitative observations made during instrument installation at the site, along with streambed horizontal hydraulic conductivity estimates made through single well response tests, the working conceptual model developed indicates the presence of sand beneath the streambed interface. At this site, streambanks tend to rise sharply along much of the study reach, with trees, shrubs, and grasses present, while small sections of the reach exhibit more gradual slopes, with a greater presence of shrubs and grasses.

Site 2 is situated along a 40 m long reach, located near the bottom of the Alder Creek watershed and approximately 3 km downstream of Site 1 (Figures 2.6 and 2.7b). Manual streamflow measurements were found to have ranged from 0.3 $m^3/s$ to 4.2 $m^3/s$ at the site. This reach of stream is about 8.5 m wide and relatively straight. The average depth during low flow conditions in summer is approximately 0.6 m, with a maximum depth of 0.7 m. The surficial geology of the streambed is made up of fewer cobbles and gravels relative to Site 1, with an increased presence of sand. While a portion of the streambed near the western streambank, is largely composed of fine-grained materials. Like Site 1, the working conceptual model developed, based on qualitative observations and streambed horizontal hydraulic conductivity estimates, indicates sandy material beneath the streambed interface. The eastern streambank rises sharply and is dominated by tree cover, while the western streambank rises gradually and is characterized by shrubs and grasses.

### 2.4.6 Handheld Infrared Imaging

At Site 1, both the detailed winter and summer infrared imaging assessments (January 5, 2024, and August 14, 2024, respectively) supported the presence of groundwater discharge conditions identified during the summer reconnaissance in 2023. While groundwater discharge appeared to be occurring near the streambanks at various locations across the study reach, two primary areas seemed to exhibit the most pronounced groundwater discharge conditions, based on the infrared temperature contrasts. The first area is located along the eastern streambank, near the upstream edge of the study reach (Figures 2.8, 2.9a and 2.9b). This location is unique relative to the rest of the study reach in that there is no noticeable abrupt, raised streambank; instead, the bank area consists of a gradually rising, highly vegetated riparian zone. Groundwater discharge conditions appeared to exist at this location during both the winter and summer seasons (Figures 2.9c and 2.9d). The infrared temperature anomaly, however, was more noticeable in the winter with groundwater discharge extending over a larger area than that seen during the reconnaissance work or during the summer infrared imaging surveys. These findings appear to indicate that the infrared imaging in the winter is a more effective time for identifying groundwater discharge.

The second location exhibiting noticeable groundwater discharge conditions, based on the infrared imaging at Site 1, is located further downstream near the western streambank of the stream reach, near a point bar (Figures 2.8 and 2.10a). The infrared imaging results from the reconnaissance work (Figure 2.10b) were, once again, observed during the winter and summer of 2024 infrared assessments (Figures 2.10c and 2.10d), confirming the persistence during seasonal cycles. Like the upstream location, groundwater discharge was again more pronounced in the winter, including the presence of groundwater discharge further from the streambank than seen during the summer months.

The increased visibility of the groundwater discharge in the winter, based on the infrared imagery, is likely due to several reasons. This includes less vegetation being present in the winter due to plant abscission in the fall; this loss of vegetation would allow the infrared camera to have increased visibility of areas of groundwater discharge. Furthermore, due to the lower density of warm, ~10°C groundwater relative to the colder surface water, the warm water rises to the surface, making it easier for the infrared camera to capture.

At Site 2, the detailed winter and summer infrared imaging assessments (January 30, 2024, and August 15, 2024, respectively) again provided support for the presence of groundwater discharge

conditions. During the initial summer reconnaissance survey, technical issues with the infrared camera prevented its use along this stretch of stream. However, cold temperature point measurements within the streambed obtained during the reconnaissance survey, along with the presence of both visible bank seepage along the raised eastern streambank (Figures 2.11 and 2.12a) and a spring (Figures 2.11, 2.13a, 2.13b and 2.13c) just downstream of the study reach, led to the conclusion that groundwater discharge conditions were present along this segment of the stream.

The area of the Site 2 reach that exhibited visible bank seepage during the reconnaissance survey was verified as groundwater discharge in both the winter and summer, based on the infrared imaging, as seen in Figures 2.12b and 2.12c. As seen at Site 1, likely due to the lower density of the warm groundwater relative to the colder surface water in the winter, groundwater discharge was again more visible, as groundwater discharge appears within the stream, as indicated by the red colouration on the left side of Figure 2.12b. This groundwater discharge, however, was less pronounced than was observed at Site 1, based on the smaller stream/streambank surface area exhibiting groundwater discharge.

Further assessment of the downstream groundwater spring was also performed the following summer, where groundwater discharge conditions were confirmed (Figures 2.11, 2.13d, 2.13e, and 2.13f). Although the spring falls outside the instrumented Site 2 reach, such a significant source of groundwater discharge, in such close proximity to the study site and on the same side of the stream as the identified visible bank seepage, provides support to the likelihood of groundwater discharge conditions within the study area.

### 2.4.7 Aerial Infrared Imaging

No noticeable groundwater discharge conditions were visible in the infrared footage collected by the UAV at either site during the summer aerial infrared imaging (June 13, 2024). This is illustrated by the example snapshots of Site 1 in Figure 2.14. The lack of visible temperature contrasts is believed to be largely the result of the dense tree and vegetation cover, preventing the infrared camera from getting a clear view of the surface of the stream and bank regions, something that can be expected for a stream of this width and with the level of vegetation growth present during the summer months (Handcock et al., 2006). Also, due to the fact that this UAV footage was collected in the summer, the density contrast at this time of year would keep the relatively colder groundwater near the bottom of the stream, making it more difficult for cold groundwater discharge to be observed by the infrared

camera in the warmer surface water, including near the streambanks. UAV footage was not collected during the winter, making it impossible to assess the UAV's ability to detect groundwater discharge during a season where more ideal conditions would be expected. At this time of year, less vegetation would be present, while the temperature contrast between surface water and groundwater discharge would be favorable for groundwater discharge visibility, based on the previously discussed lower density of groundwater relative to surface water at this time of year.

### 2.4.8 Vertical Hydraulic Gradients

Surface water and groundwater level measurements of the piezometer and mini-piezometer installations located at Site 1 were performed on February 23, 2024, during the winter streambed temperature profiling campaign. The calculated vertical hydraulic gradients (Figure 2.15a) were all indicative of groundwater discharge conditions. The magnitude of the vertical hydraulic gradients, however, varied, with values ranging from 0.04 to 0.51. Areas identified as prominent groundwater discharge locations during the reconnaissance survey and the follow up detailed infrared imaging surveys were characterized by being in the areas of some of the highest vertical hydraulic gradients, illustrating the utility of the reconnaissance approaches (Figures 2.9 and 2.15a). From the data collected during the measurement period between November 2, 2023, and November 7, 2024, it was found that vertical hydraulic gradients were fairly consistent over time and remained largely upward, an indication of continuous groundwater discharge conditions. This was supported by differential stream gauging, performed upstream and downstream of Site 1 at or near baseflow conditions, as a net increase in streamflow was consistently measured, indicating groundwater discharge conditions over the reach of study.

Surface water and groundwater level measurements of the piezometers and mini-piezometer installations located at Site 2 were performed on February 8, 2024, during the winter streambed temperature profiling campaign. As observed at Site 1, the vertical hydraulic gradients (Figure 2.16a) were all indicative of upward groundwater flow or discharging conditions. However, the vertical hydraulic gradients appeared to show greater variability than that of Site 1, as values ranged from 0.03 to 0.66. The notably higher vertical hydraulic gradients measured in the downstream part of the study reach supports the reconnaissance surveys and detailed infrared imaging findings of the presence of groundwater discharge (Figures 2.12, 2.13 and 2.16a). As observed at Site 1, vertical hydraulic gradients generally remained upward and were fairly consistent over time between

December 1, 2023, and August 29, 2024, suggesting groundwater discharge conditions persisted across the study reach during the entire annual cycle. Differential stream gauging was, however, impractical due to limitations related to the short length of the study reach caused by land use restrictions.

### 2.4.9 Darcy Groundwater Fluxes

The vertical hydraulic gradient estimates from February 23, 2024 (Figure 2.15a), at Site 1, were used along with the corresponding hydraulic conductivity estimates made in May 2024 (Figure 2.15b; Zanatta et al., 2025), to estimate vertical fluxes based on Darcy's law (Figure 2.15c). As seen with the vertical hydraulic gradients, notable variability was also present in the vertical flux estimates, with values ranging over two orders of magnitude, from $1.0 \times 10^{-6}$ m/s to $1.5 \times 10^{-4}$ m/s. The highest Darcy flux values within the dataset were found where groundwater discharge conditions were observed during the reconnaissance, and through later infrared imaging verification, further supporting the reconnaissance work and the presence of groundwater discharge conditions in these areas (Figures 2.9, 2.10 and 2.15c).

The vertical hydraulic gradient estimates from February 8, 2024 (Figure 2.16a), at Site 2, were used with the corresponding hydraulic conductivity estimates made in May 2024 (Figure 2.16b; Zanatta et al., 2025), to calculate the Darcy fluxes at each monitoring point (Figure 2.16c). Significant variability in vertical flux was present at Site 2, with values ranging over two orders of magnitude, from $2.1 \times 10^{-6}$ m/s to $2.0 \times 10^{-4}$ m/s. The relatively higher Darcy fluxes found in the downstream part of the study reach correspond to the locations where groundwater discharge was identified during the reconnaissance survey, and later local infrared imaging, again providing support to the utility of the reconnaissance approaches in identifying locations of groundwater discharge. (Figures 2.12, 2.13 and 2.16c).

### 2.4.10 Temperature Profiling Groundwater Fluxes

During the winter streambed temperature profiling performed at Site 1 between February 21, 2024, and February 29, 2024, a total of 66 temperature profiles were measured. Upward vertical flux estimates were identified for 64 of the 66 temperature profiles, while data from the remaining 2 profiles yielded downward flux estimates based on the FLUX-LM spreadsheet tool (Kurylyk et al., 2017) (Figure 2.17a). These vertical fluxes ranged from $-4.3 \times 10^{-8}$ to $7.5 \times 10^{-6}$ m/s. For the summer

streambed temperature profiling performed at Site 1 between July 22, 2024, and July 24, 2024, a total of 88 temperature profiles were measured, with estimates based on the FLUX-LM tool yielding upward vertical fluxes for 80 of the 88 temperature profiles, while only 1 temperature profile yielded a downward vertical flux (Figure 2.17b). At the remaining 7 locations, temperature profiles could not be developed, as short term profiling did not exhibit the necessary concave up or down shape needed for a flux estimate. The vertical fluxes at this site were found to range from $-1.6 \times 10^{-6}$ to $1.4 \times 10^{-5}$ m/s.

The prevalence of groundwater discharge conditions across the Site 1 study reach was clear from the temperature profiling results collected both in the winter and summer, as indicated by the number of temperature profiles that yielded upward flux estimates. The vertical fluxes estimated during both temperature profiling campaigns appear to vary across the reach of study (Figures 2.17a and 2.17b). The temperature-derived vertical flux distributions correlate relatively well with the areas identified as locations of groundwater discharge based on the initial reconnaissance and further infrared imaging surveys. This is particularly noticeable in the vertical fluxes measured along the eastern streambank, near the upstream end of the study reach (Figures 2.9 and 2.17), where flux values appear higher than those measured near the opposite bank. These findings again emphasize the value of the reconnaissance methods in identifying areas of groundwater discharge.

During the winter streambed temperature profiling performed at Site 2 on February 8, 2024, a total of 53 temperature profiles were measured at this site, with estimates via the FLUX-LM tool yielding 45 upward fluxes (groundwater discharge) and 8 downward fluxes (groundwater recharge) (Figure 2.18a). The vertical fluxes were found to range from $-2.4 \times 10^{-6}$ to $6.9 \times 10^{-6}$ m/s. For the summer streambed temperature profiling performed at Site 2 on July 25, 2024, and July 26, 2024, a total of 53 temperature profiles were measured, with estimates via the FLUX-LM tool yielding upward vertical flux estimates at 44 of the 53 locations, and downward flux estimates at 6 locations (Figure 2.18b). The locations of where downward flux conditions were identified during the winter and summer campaigns were not identical. A reasonable flux estimate could not be obtained using FLUX-LM for 3 temperature profiles, as they did not exhibit the necessary concave up or down shape. The vertical fluxes at this site were found to range from $-4.6 \times 10^{-6}$ to $1.4 \times 10^{-5}$ m/s. For both cases, higher fluxes were found near the bottom of the study reach, an area where groundwater discharge conditions were identified during reconnaissance. These findings once again provide support to the value of the reconnaissance in identifying groundwater discharge (Figures 2.12, 2.13 and 2.18). However, the

groundwater recharge conditions identified in the middle of this study reach based on the notable zones of downward fluxes, were not identified during the reconnaissance, highlighting the limitations of this reconnaissance approach due to the apparent significant variability in groundwater flux at small spatial scales.

With regards to the absolute magnitude of the vertical flux estimates, values for the Darcy approach averaged approximately one order of magnitude greater than those for the temperature profiling approach. The Darcy fluxes were, however, determined by assuming isotropic conditions within the streambed through the application of hydraulic conductivities estimated through single well response tests to the vertical plane of study. For these reasons, the application of an anisotropy ratio would be of value to account for likely anisotropy in the system and to possibly yield flux estimates for the different techniques of a similar order of magnitude.

Several limitations exist pertaining to the temperature profiling groundwater flux estimation technique. One limitation relates to the assumption of vertical, one dimensional flow, which does not consider the potential of a lateral component of groundwater flow, which may alter the temperature profiles and, therefore, skew results (Lu & Ge, 1996). This is especially true for profiles developed away from the thalweg and closer to the streambanks, where the lateral component is of greater influence (Anibas et al. 2011; Ghysels et al., 2021; Kurylyk et al., 2017). The lateral groundwater flow may result in an overestimation of the temperature profiling vertical flux estimates, putting some doubt on vertical flux estimates near the streambanks and high groundwater discharge areas (Irvine et al., 2015; Lautz, 2010; Rau et al., 2010; Roshan et al., 2012).

In the current study, the alteration of the shape of the temperature profile due to horizontal groundwater flow may explain why it was not possible to estimate fluxes with the FLUX-LM tool for profiles located near areas of groundwater discharge, which were identified during the reconnaissance, and where cold streambed temperatures, notable infrared imaging contrasts, and high Darcy fluxes were found. This alteration is likely the result of the lateral component of groundwater flow from these spring/high groundwater discharge locations flushing out the expected shallow profile temperatures (e.g., cold lateral groundwater flow replacing warmer water in the shallow subsurface during the summer) and preventing the expected bend in the temperature profiles from developing. Therefore, instead of exhibiting the commonly concave up or concave down shape

temperature profiles for groundwater recharge and discharge locations, these profiles had fairly consistent temperatures with depth and lacked the profile curvature necessary to make flux estimates.

Another factor to consider is the significant spatial heterogeneity and anisotropy present within streambeds, and the complex nature of groundwater flow paths (Conant Jr., 2004; Irvine et al., 2015; Käser et al. 2009; Rosenberry et al. 2016), that may result in either high or low flux locations being missed. Equipment limitations also exist, as temperature probes capable of withstanding hammering to depths of 50 cm below an armored streambed require the use of durable material (i.e., steel) (Figure 2.3b). This material, however, is more susceptible to frictional heat generation then an aluminum design increasing the risk of higher temperatures readings due to possible heat transfer from the temperature probe to the thermistor which might impact the temperature measurements (Westberg, 2012).

## 2.5 Conclusions

Through this study, valuable insight was gained regarding the effectiveness of using small scale groundwater discharge identification techniques as part of reconnaissance work to identify stream reaches exhibiting groundwater discharge conditions within the main channel of a moderately sized watershed. The temperature techniques proved the most effective. Using visual observations and infrared imaging, groundwater discharge could be identified along the streambanks and shallow stream edges; however, they were limited in their ability to identify groundwater discharge from the streambed. The temperature probe, however, was capable of addressing this limitation, as it allowed for the identification of clusters of cold groundwater temperatures measurements within the streambed at ≥ 20 cm depth to identify possible signs of groundwater discharge. In addition, it was useful in verifying the groundwater discharge identified from visual observations and infrared imaging by measuring the temperature of the identified groundwater discharge. These techniques resulted in the identification of discrete higher flux zones of groundwater discharge across the watershed, which were used to identify gaining stream reaches. The measuring of hydraulic gradients using the Henry sampler device, however, proved ineffective due to the length of time needed to make measurements and the tools inability to penetrate the armored streambed, emphasizing the need for a more durable design for future work in such settings. The temperature techniques, while effective, remain limited to the summer and/or winter, during periods of notable surface water and groundwater temperature contrast, ultimately impacting when the reconnaissance can be performed.

Detailed field studies were completed along two reaches of study identified as displaying signs of groundwater discharge conditions, in order to verify the reconnaissance results. These studies included repeated infrared imaging observations, applying Darcy's law through routine monitoring of hydraulic gradients and estimating streambed hydraulic conductivities, intensive vertical streambed temperature profiling surveys, and differential stream gauging. These studies were largely successful in verifying the reconnaissance findings of the presence of groundwater discharge conditions along the identified study reaches. Aerial UAV infrared imaging in the summer, however, proved unsuccessful at identifying groundwater discharge conditions, indicative of the limitations that exist with these aerial techniques.

While these more detailed studies (e.g., Darcy fluxes, temperature profiling fluxes) provide support to the reconnaissance work's ability to identity overall gaining stream reaches and notable areas of groundwater discharge along the reach, they also emphasize its limitations. These more detailed investigations identify significant spatial variability in groundwater-surface water interactions across the study reaches, including zones of groundwater recharge, which the reconnaissance was unable to detect. Therefore, while the reconnaissance appears to be valuable in identifying specific zones of higher groundwater discharge and is helpful in identifying areas for more focused study, due to the complex nature of groundwater discharge, detailed investigations are likely needed to account for small scale variability in groundwater-surface water interactions that these reconnaissance techniques are not well suited to characterize. The findings of this research can assist in how future reconnaissance work is performed in identifying groundwater discharge conditions and can be used as a tool to assist in addressing concerns regarding water resource management and the transport and fate of nutrients and pollutants, though an improved understanding of groundwater surface water interactions.

## 2.6 Figures

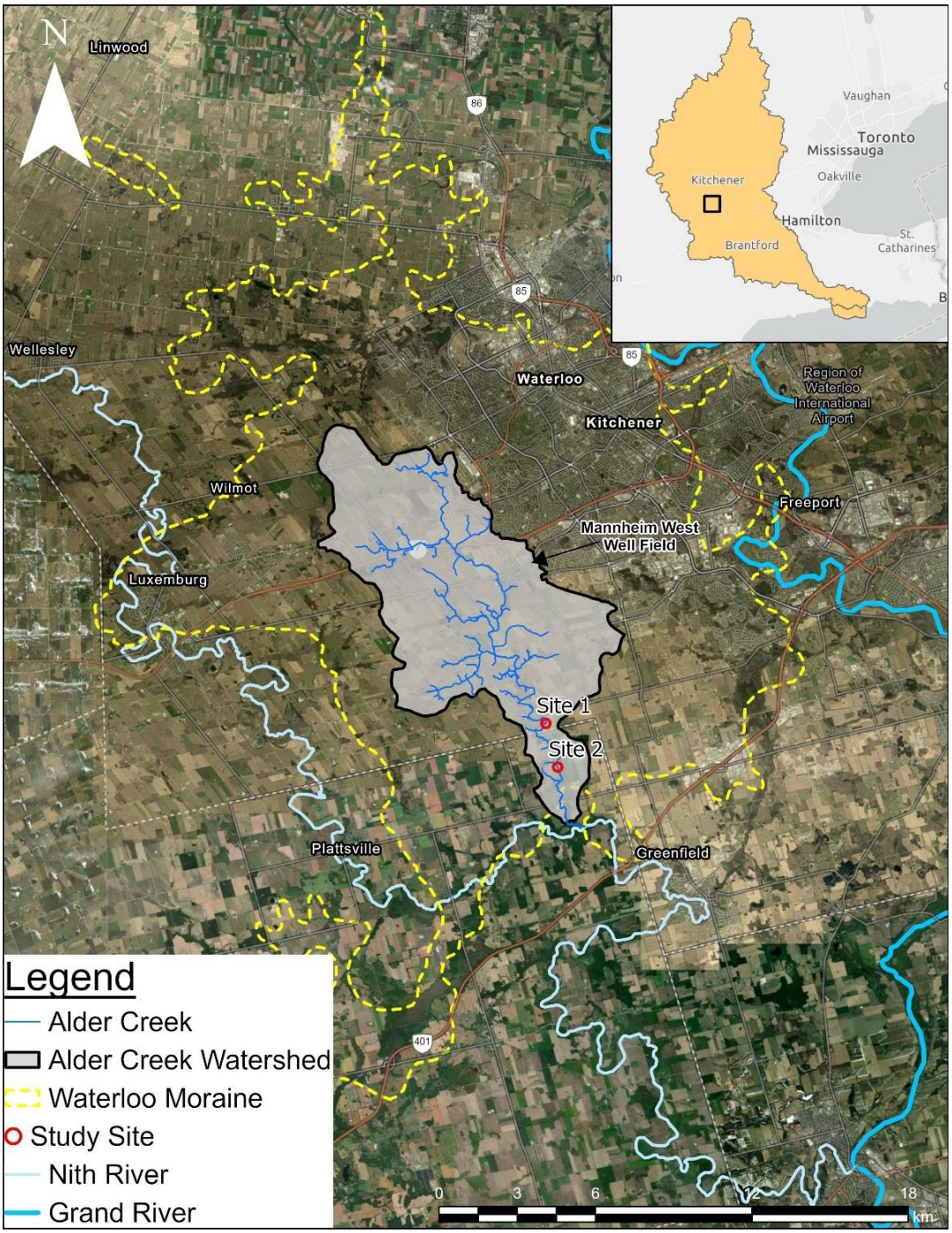



Figure 2.1: Alder Creek watershed (Esri et al., 2025a; Esri et al., 2025b; Government of Ontario, 2023; Grand River Conservation Authority, 2017; Grand River Conservation Authority, 2023; Sousa et al., 2014).

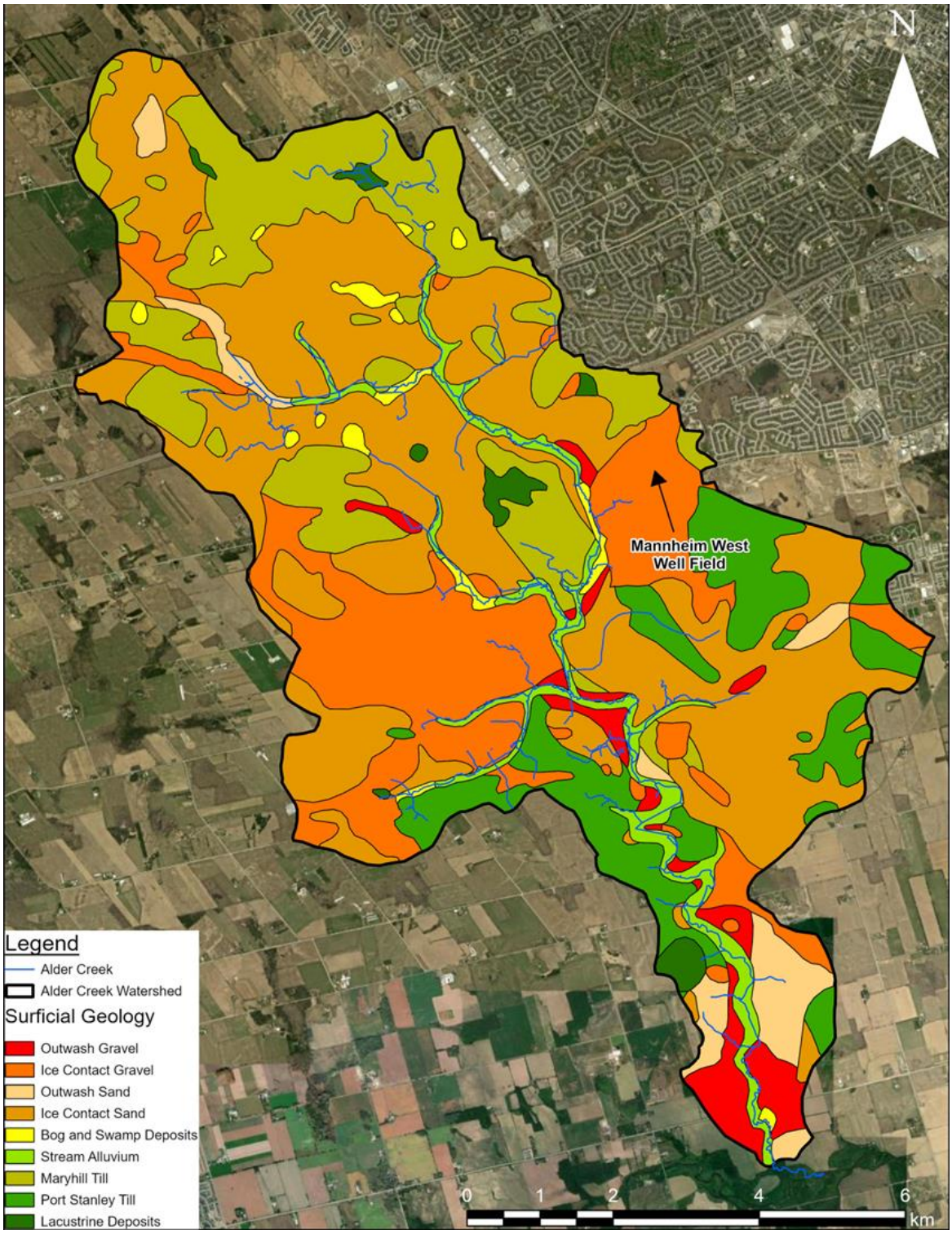



Figure 2.2: Surficial geology of the Alder Creek watershed (Esri et al., 2025a; Government of Ontario, 2023; Grand River Conservation Authority, 2017; Ontario Geological Survey, 2010).

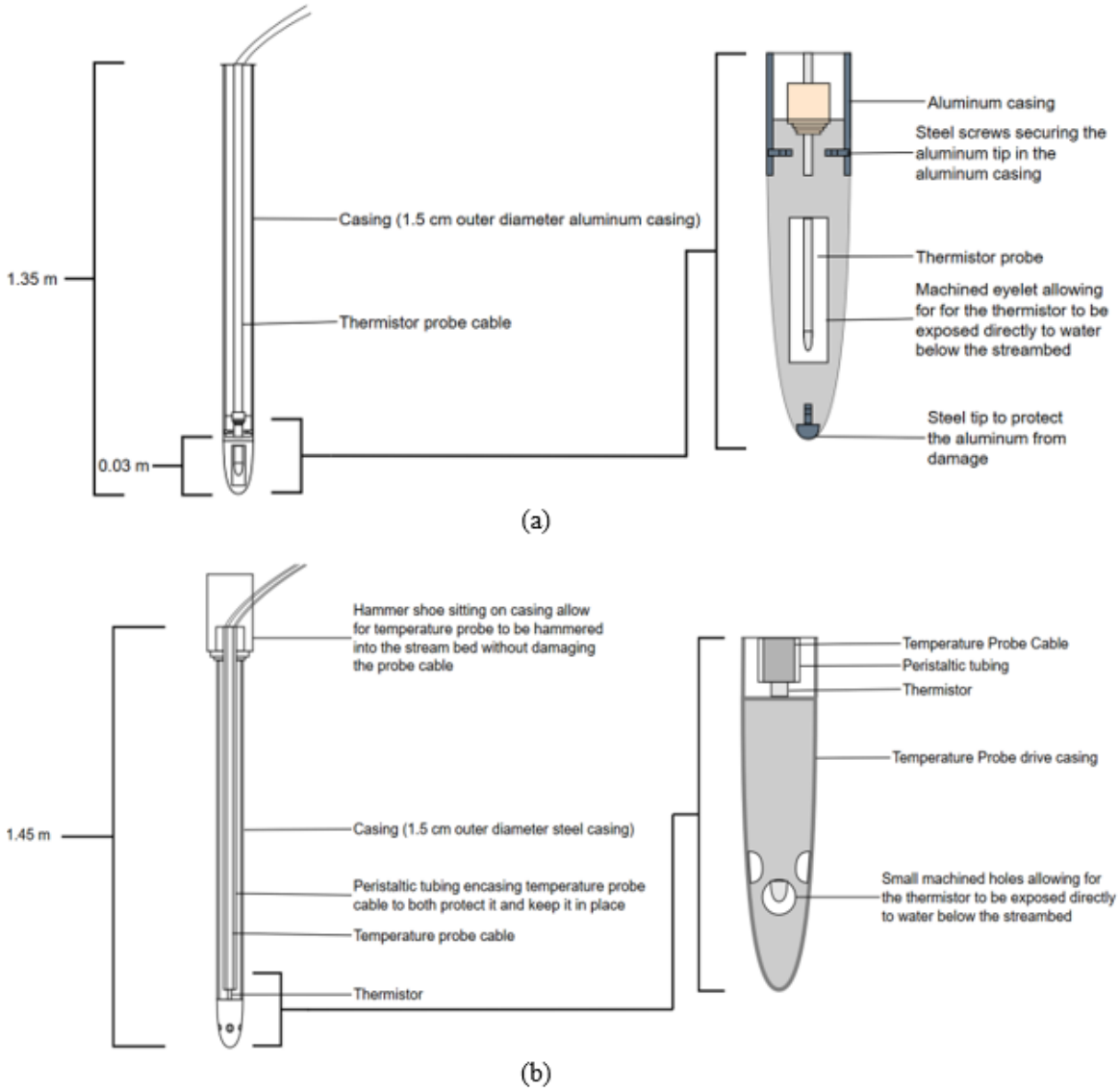


Figure 2.3: Temperature probes used during (a) reconnaissance and (b) temperature profiling.



Figure 2.4: Temporary extractable drive point piezometer known as a Henry Sampler (MHE Products Ltd.) used during reconnaissance.

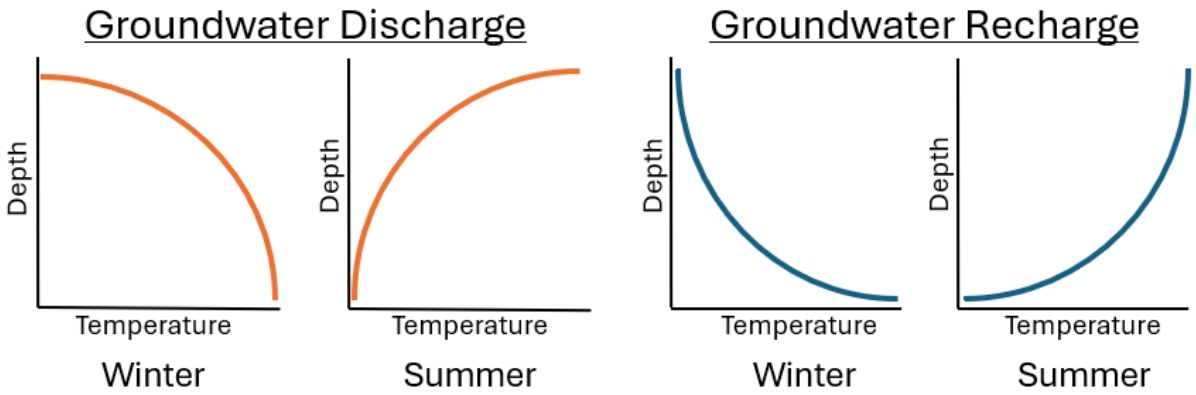


Figure 2.5: Shape of temperature profiles for both groundwater discharge and groundwater recharge conditions in the winter and summer months.

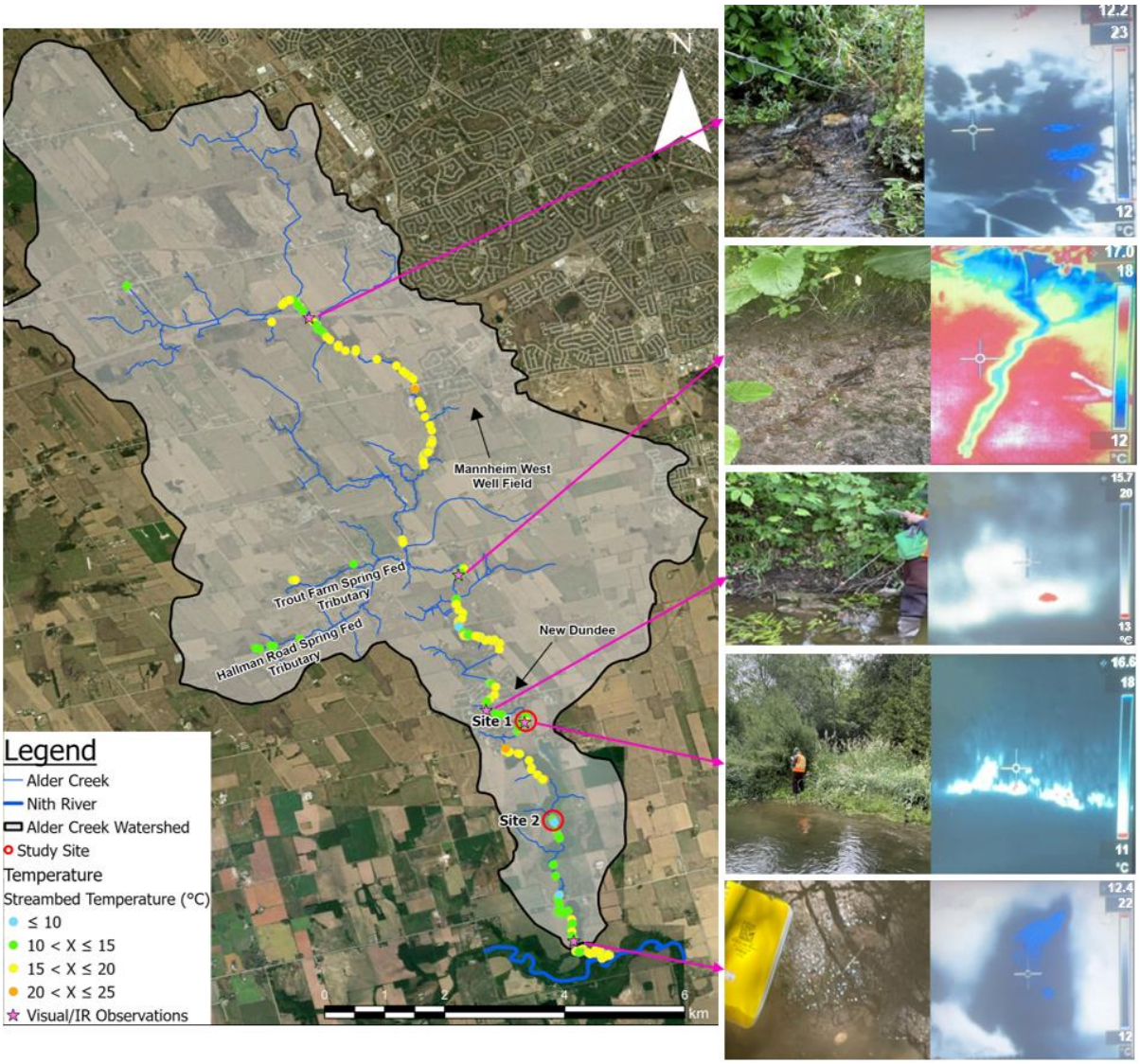



Figure 2.6: Map of streambed temperature data collected during reconnaissance, some areas of visual/infrared observations of groundwater discharge and identified study sites (Esri et al., 2025a; Government of Ontario, 2023; Grand Grand River Conservation Authority, 2017).



(a) (b)

Figure 2.7: Photos of the study reaches of interest (a) Site 1 and (b) Site 2.

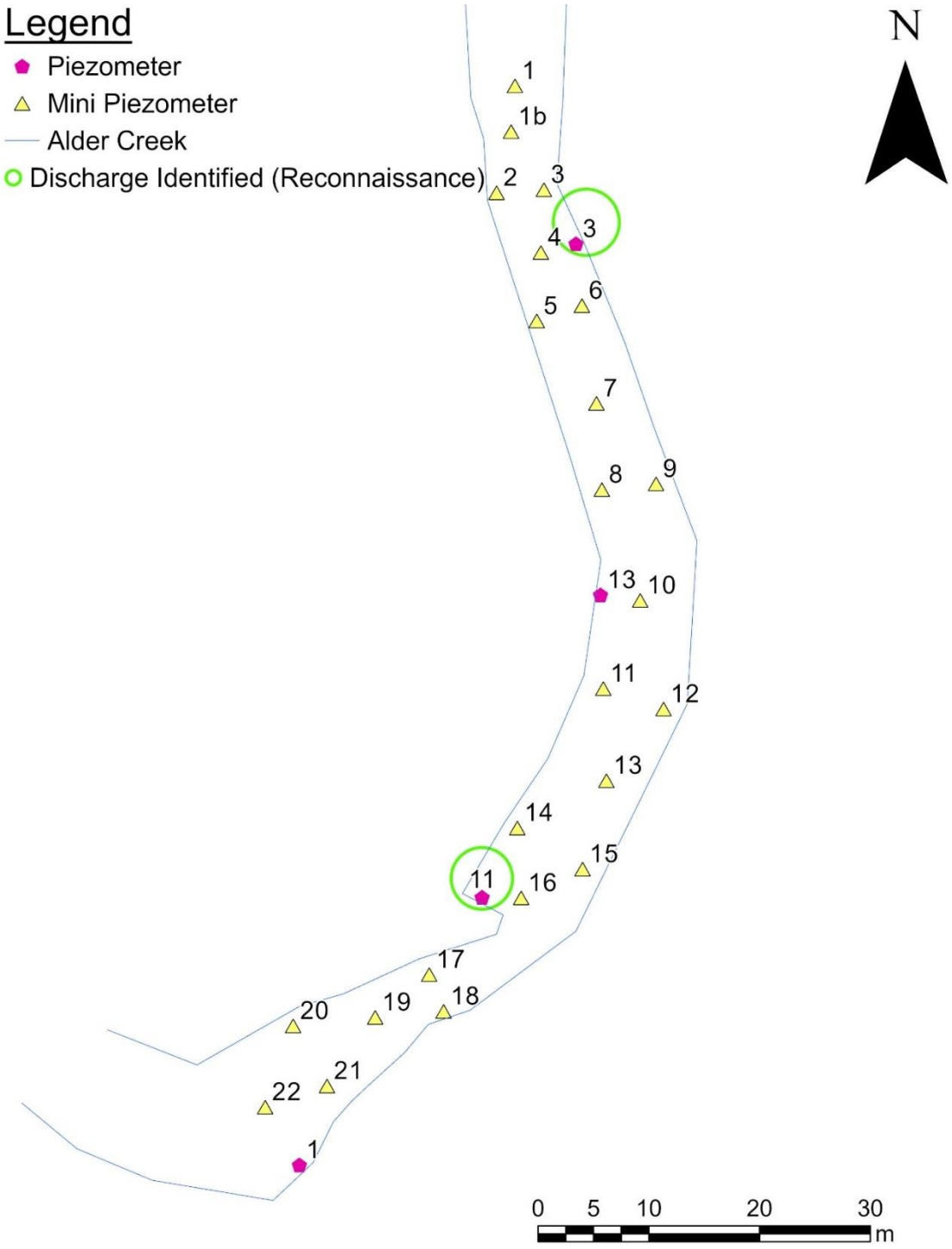
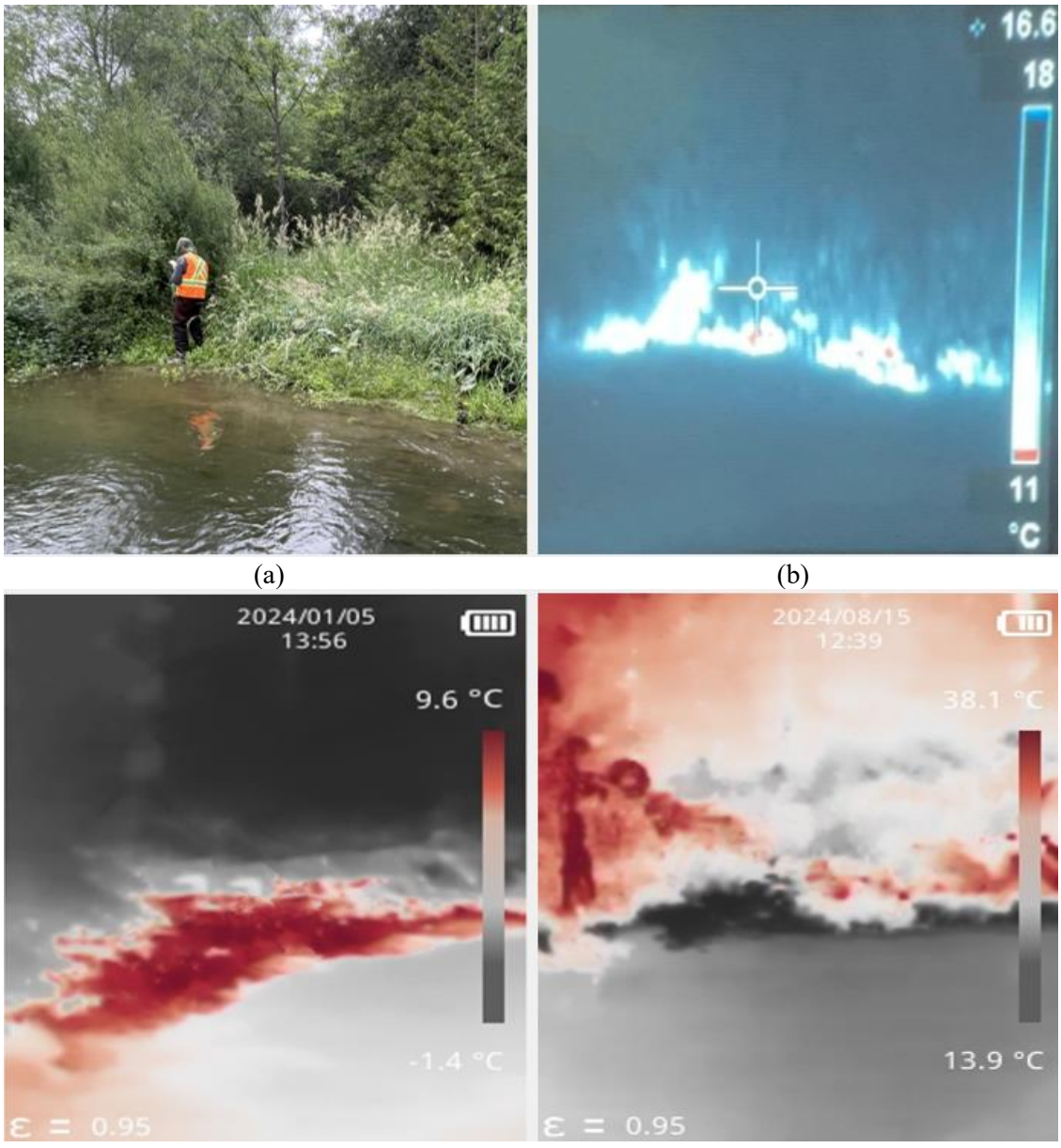


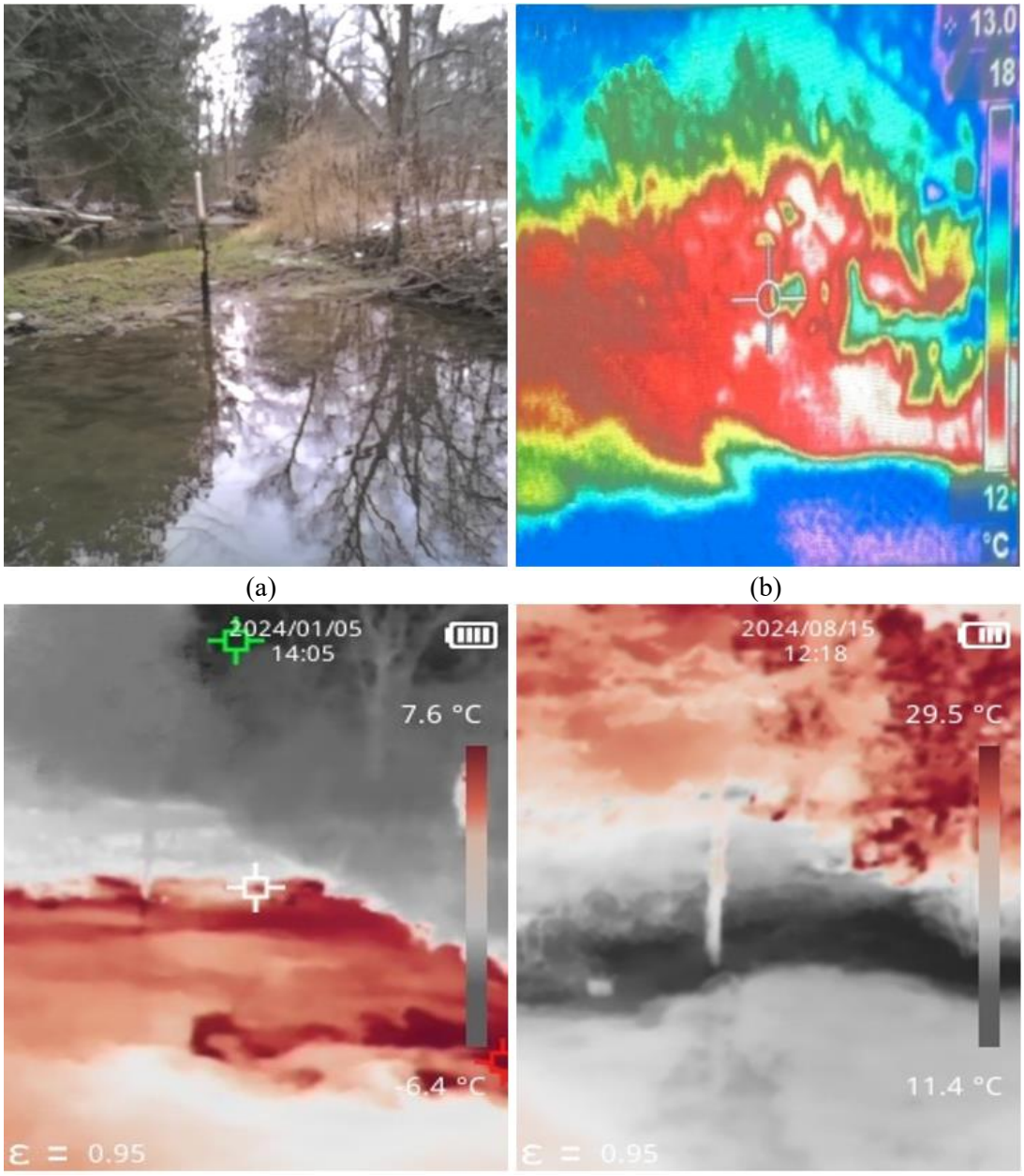

Figure 2.8: Map of piezometer installation locations and suspected areas of discharge based on reconnaissance findings at Site 1.




(a) (b)

(c) (d)

Figure 2.9: Discharge conditions identified at Site 1 near riparian zone. (a) Visual and (b) infrared images collected during reconnaissance. Images confirming the presence of groundwater discharge in (c) winter and (d) summer.




(a) (b)

(c) (d)

Figure 2.10: Discharge conditions identified at Site 1 near point bar. (a) Visual and (b) infrared images collected during reconnaissance. Images confirming the presence of groundwater discharge in (c) winter and (d) summer.

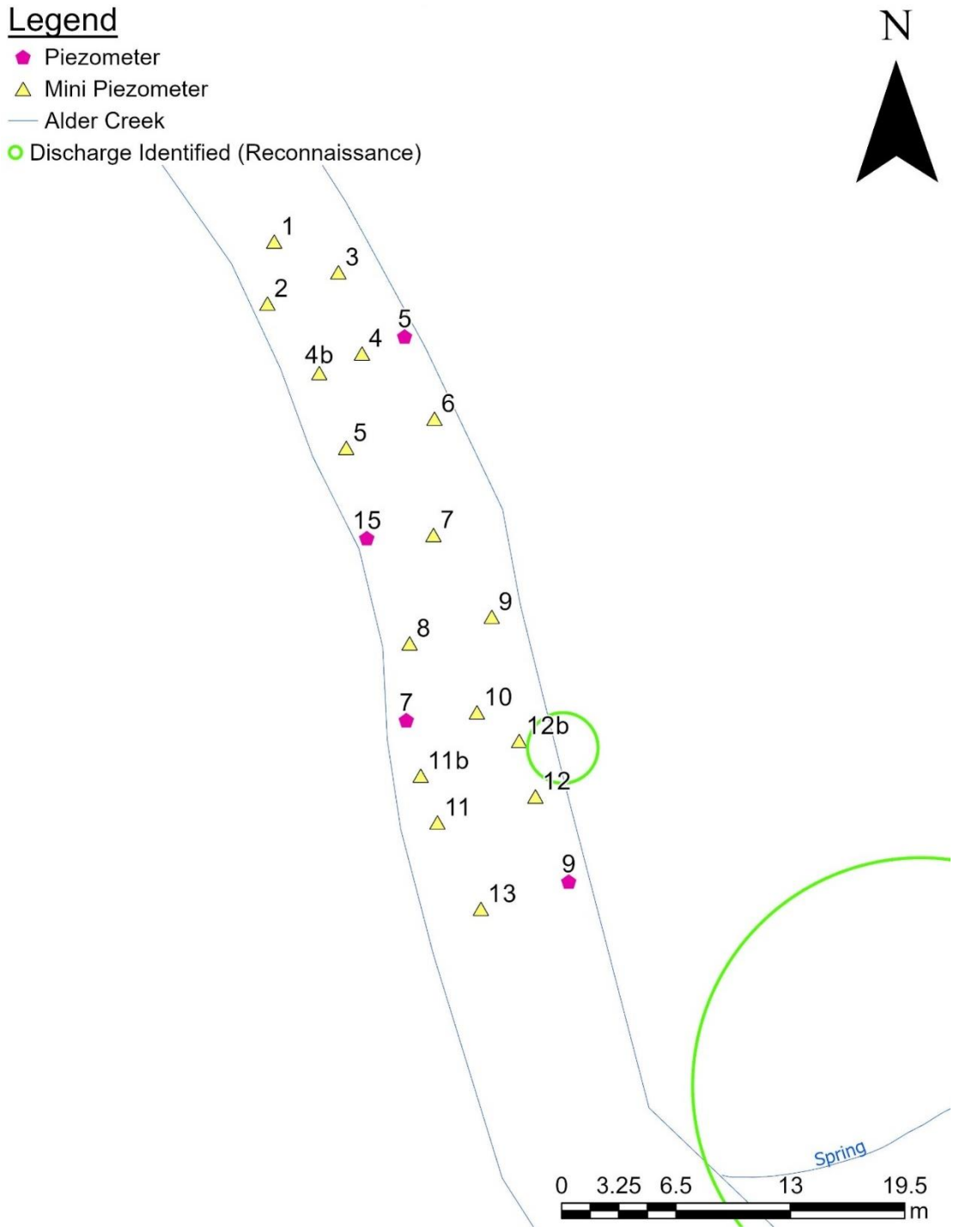
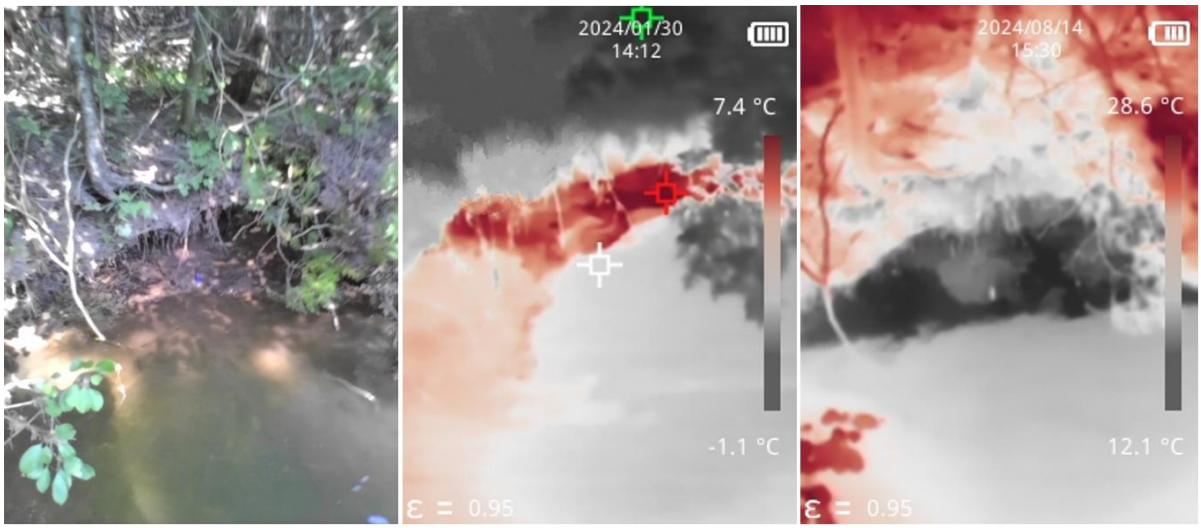



Figure 2.11: Map of piezometer installation locations and suspected areas of discharge based on reconnaissance findings at Site 2.




(a) (b) (c)

Figure 2.12: Discharge conditions identified at Site 2 through bank seepage near spring. (a) Visual and infrared images confirming the presence of groundwater discharge in (b) winter and (c) summer.

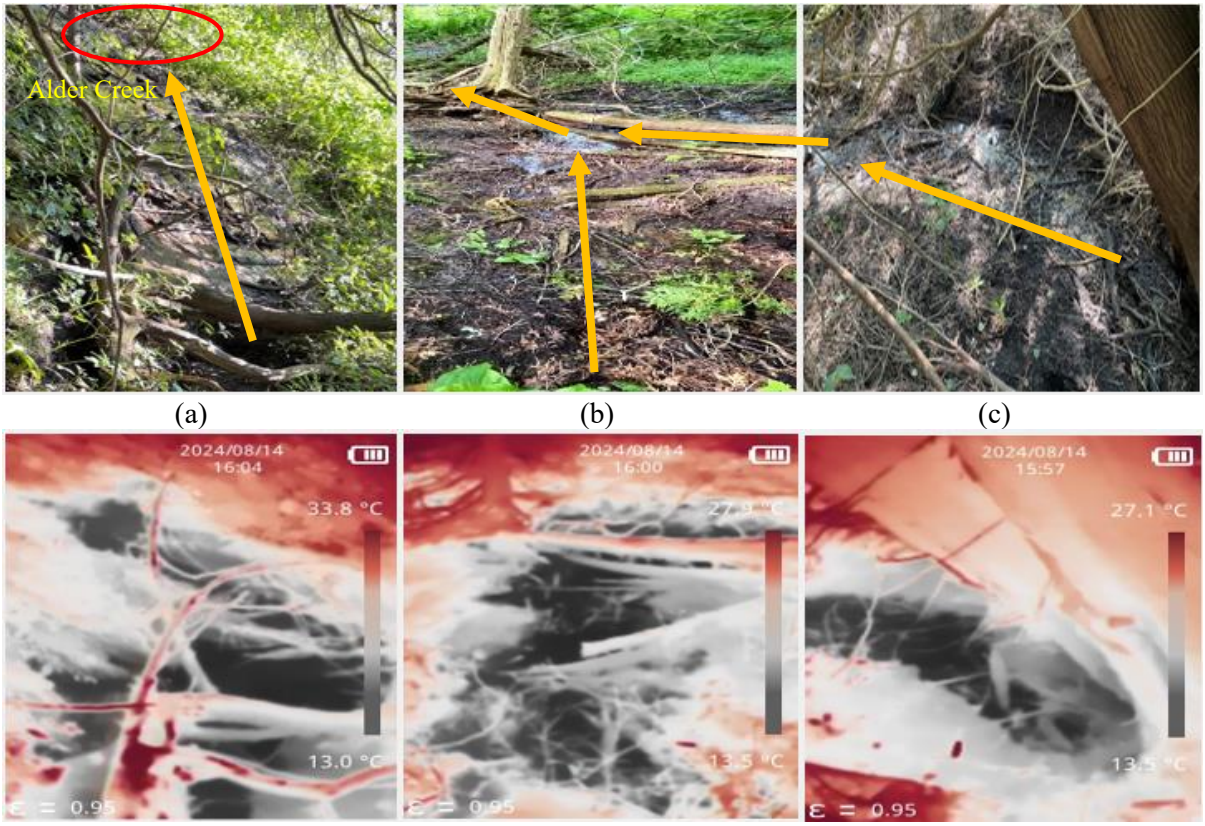
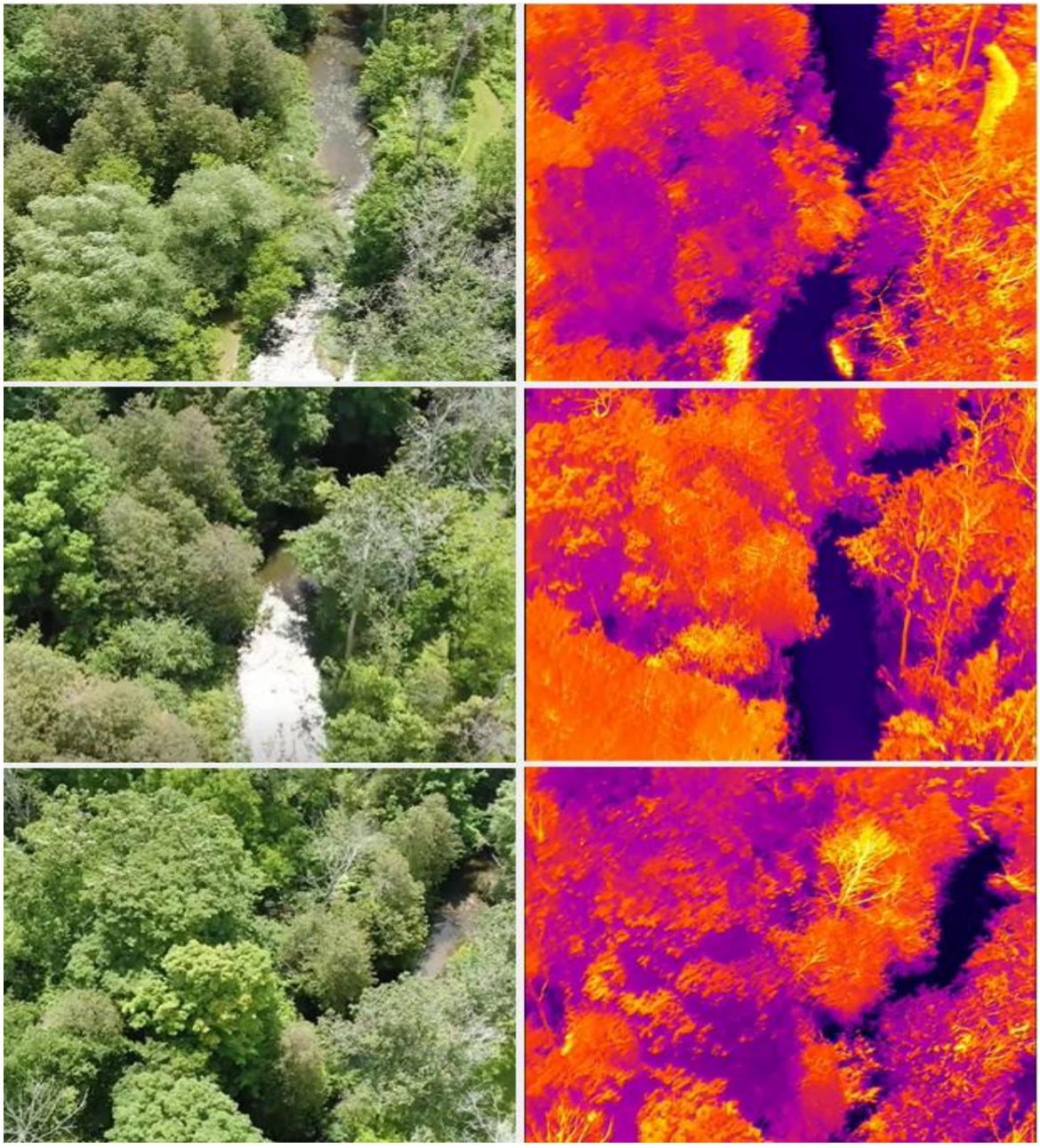
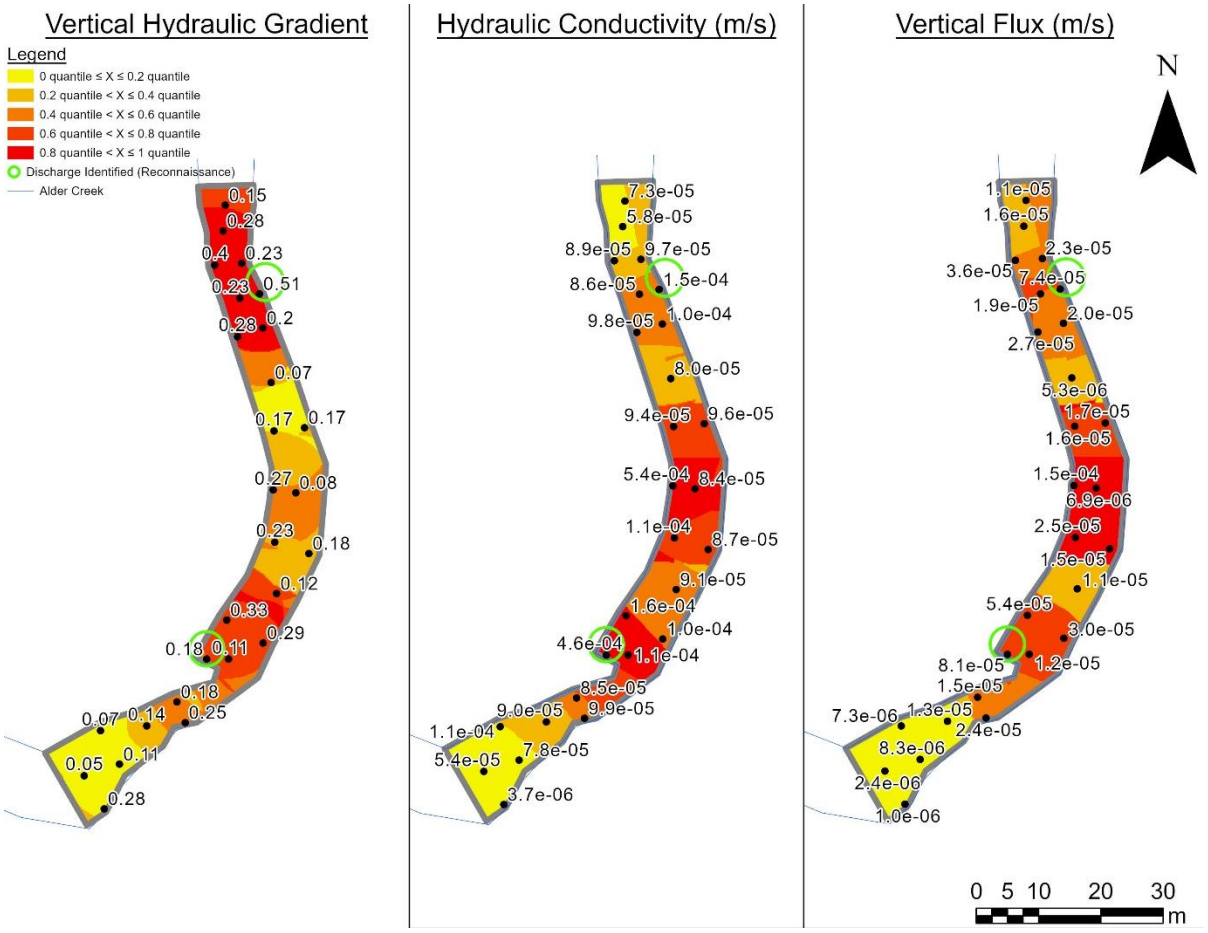



Figure 2.13: Spring found just downstream of Site 2 during reconnaissance that discharges into Alder Creek. The main branch of the spring (a) is fed by two converging smaller branches (b) and (c) discharging from the base of trees. Infrared images of the spring captured the following summer (d, e and f) correspond to the above images (Image (b) taken during reconnaissance, (a) and (c) taken the following summer.).



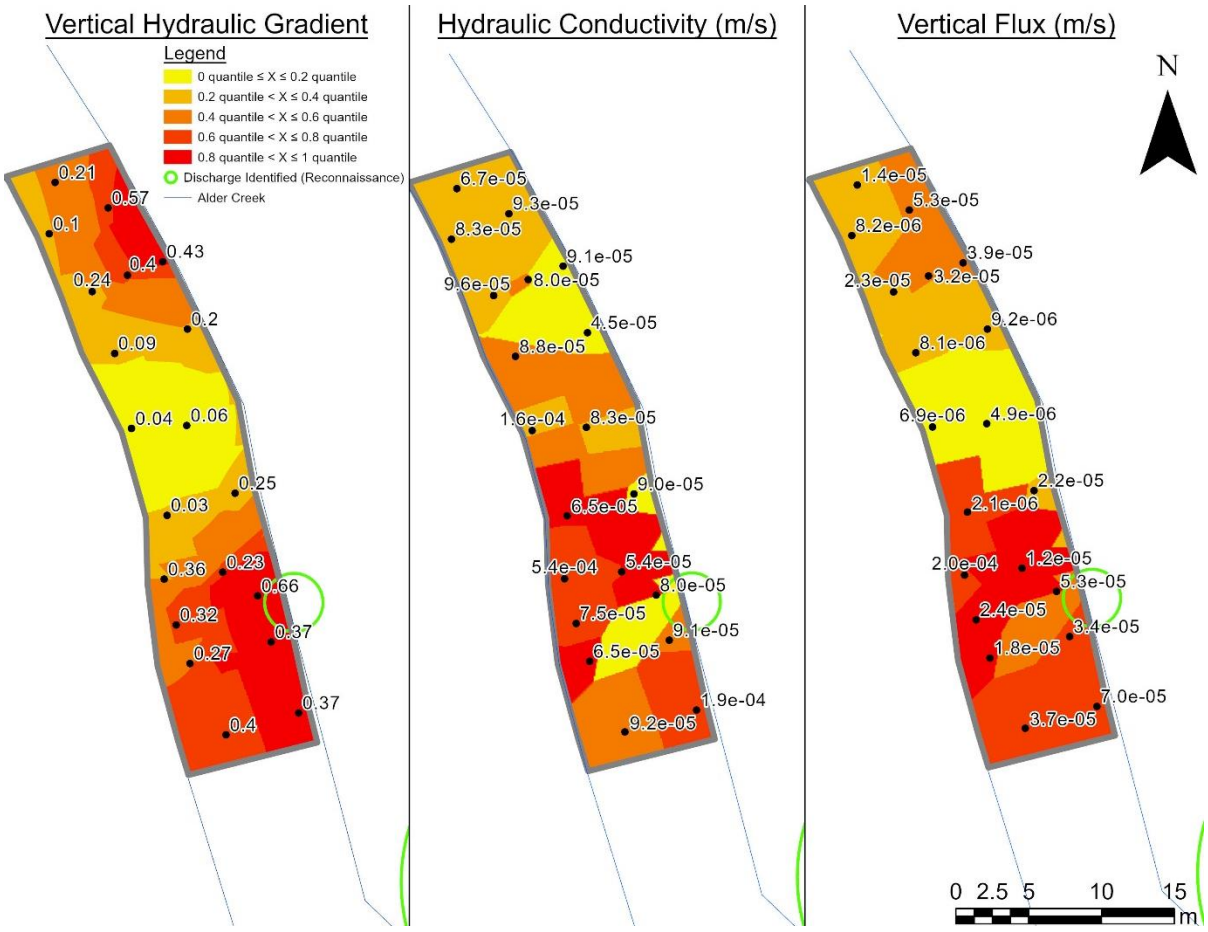
(a) (b)

Figure 2.14: (a) Visual and (b) infrared snapshots of aerial UAV survey over Site 1, performed in the summer of 2024.



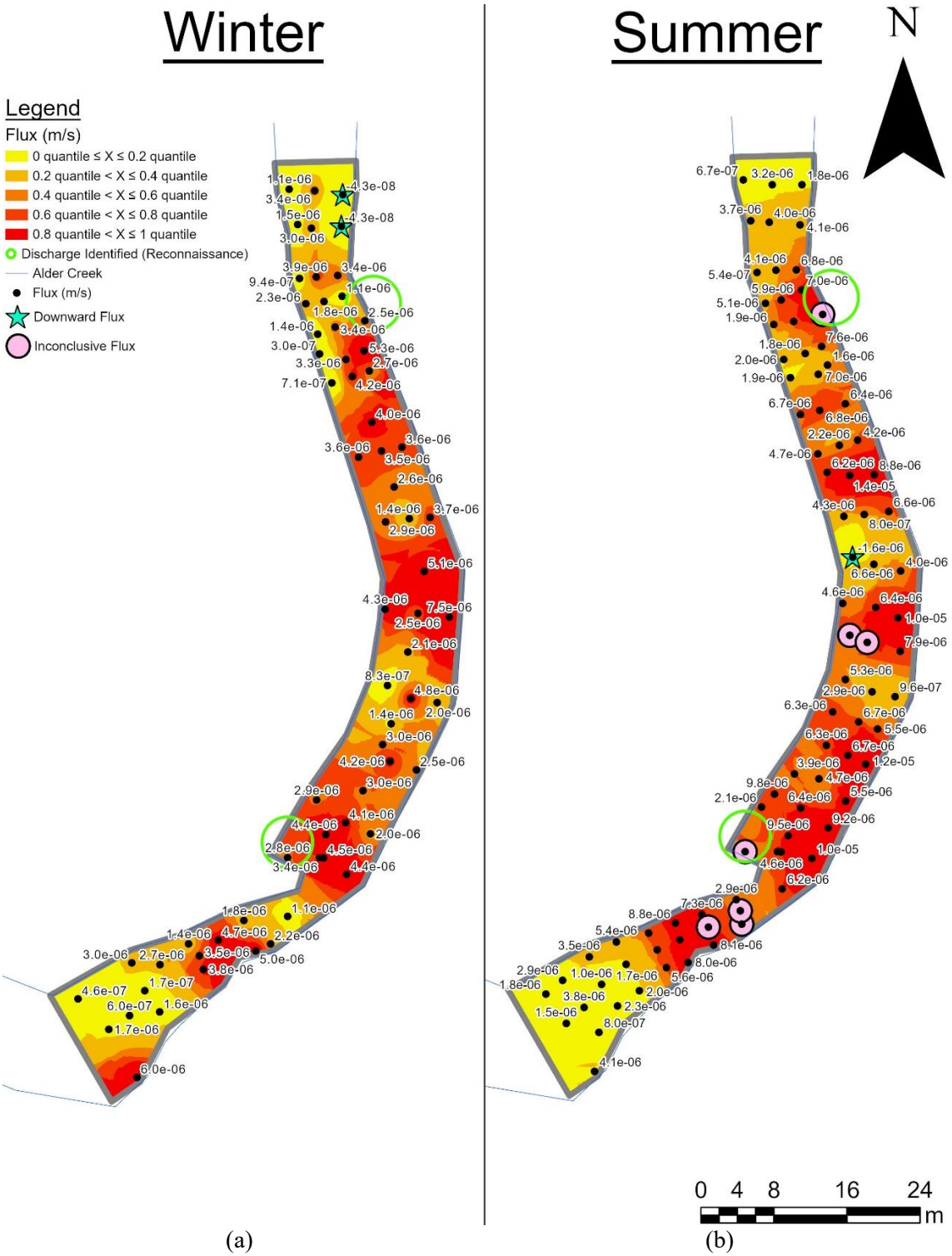

(a) (b) (c)

Figure 2.15: Site 1 (a) vertical hydraulic gradients measured on February 23, 2024, (b) hydraulic conductivities measured in May 2024 and (c) vertical fluxes estimated using Darcy's law.



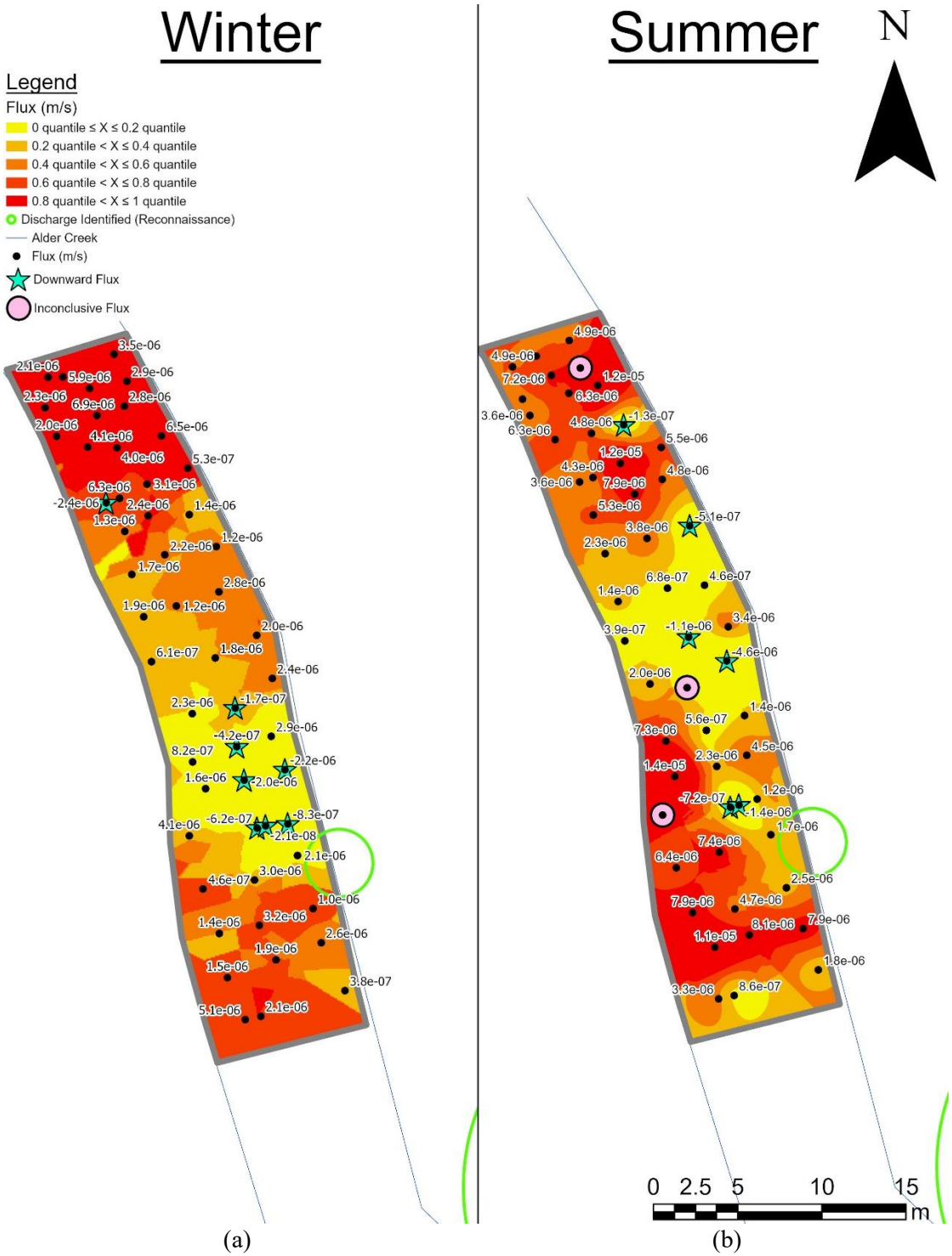

(a) (b) (c)

Figure 2.16: Site 2 (a) vertical hydraulic gradients measured on February 8, 2024, (b) hydraulic conductivities measured in May 2024 and (c) vertical fluxes estimated using Darcy's law.




(a) (b)

Figure 2.17: Vertical flux estimates based on streambed temperature profiles for Site 1 in (a) winter 2024 and (b) summer 2024.




(a) (b)

Figure 2.18: Vertical flux estimates based on streambed temperature profiles for Site 2 in (a) winter 2024 and (b) summer 2024.

# Chapter 3
# Quantifying Groundwater-Surface Water Exchange Within a Stream Through Field Monitoring

## 3.1 Introduction

As water quantity and quality issues become a greater concern in response to a multitude of external pressures including increased urbanization, poor agricultural practices and climate change, greater focus is required on how to better manage surface water features such as creeks and rivers. Groundwater-surface water exchange plays a crucial role in maintaining the health of surface water features, with groundwater discharge being the main contributor to streamflow during the annual cycle. This consistent source of streamflow helps sustain healthy aquatic ecosystems by supporting and protecting aquatic plant and animal populations. However, due to long-term groundwater extraction for municipal and industrial use, streamflow declines in response to decreasing baseflow has been documented (Barlow & Leake, 2012; Zipper et al., 2024). Furthermore, decreased confidence can be placed in forecasting expected groundwater recharge, storage, and subsequent discharge due to the potential impacts of climate change, which may significantly influence baseflow to surface water features (Dubois et al., 2022; Green et al., 2011; Taylor et al., 2013).

Quantifying groundwater-surface water exchange within creeks and rivers, and understanding its spatial variability, is challenging yet critical, considering the increasing external pressures on the groundwater reservoir, which sustains the baseflow. Insight gathered from studying baseflow dynamics can assist in the development of best management practices (BMP) designed to protect surface water features and support sustainable groundwater management plans. Advanced modeling tools, designed to simulate regional scale groundwater and surface water interactions, require accurate baseflow estimations to inform the modeling results, and assist in calibration. Much of the challenge regarding the quantification of groundwater-surface water exchange lies in the significant spatial variability that can exist due to the complex nature of streambeds, and their groundwater flow paths (Conant Jr., 2004; Käser et al., 2009; Rosenberry et al., 2016). While a wide range of approaches have been developed and applied to measure groundwater-surface water interactions, they all come with limitations related to accuracy and spatial variability.

Differential stream gauging is one of the more commonly used techniques (Becker et al., 2004; Cey et al., 1998; Harte & Kiah, 2009; McCallum et al., 2012). Using tools such as current flow meters and acoustic doppler current profilers (ADCP's), streamflow measurements can be made. If the measurements are made in quick succession, and no surface water sources are present, the difference in streamflow measured up and downstream of the reach of interest can provide an easily obtainable quantitative estimate of groundwater-surface water exchange. This technique is limited, however, due to uncertainty in streamflow measurements (Harte & Kiah, 2009), and the inability to identify discrete zones of groundwater discharge or account for small scale heterogeneity (Kalbus, 2006).

A variety of point measurement techniques exist that can better account for this small-scale variability. This includes the application of Darcy's law, where, through the measurement of vertical hydraulic gradients ($\Delta h/\Delta l$) and horizontal hydraulic conductivities (K) using streambed piezometers, Darcy fluxes can be estimated (Binley et al., 2013). Temperature is another technique (Conant Jr, 2004; Schmidt et al., 2007, Anibas et al., 2011; Ghysels et al., 2021), where, through the development of streambed temperature profiles, the data collected can be interpreted using heat transport models to provide quantitative estimates of the direction and magnitude of groundwater fluxes (Stonestrom & Constantz, 2003; Constantz, 2008). This technique, however, is largely limited to the winter and summer seasons, when temperature contrasts between surface water and groundwater are greatest, and the streambed temperature profiles are most pronounced (Coluccio & Morgan, 2019).

Arguably, the greatest limitation related to all of these point groundwater flux measurement techniques is the spatial restrictions inherent in representing large areas of a streambed with single point measurements. In stream reaches where there is significant spatial variability in the groundwater flux within the stream bed, measurements at multiple locations are needed to obtain data at a high enough spatial resolution to accurately represent the heterogeneity of GW-SW interactions within the streambed. However, at the same time in order to quantify a bulk value of groundwater-surface water exchange over a large area, such as stream reach, it requires the upscaling of the dataset in some way. To address these issues, numerous examples of densely monitored stream bed environments have been presented in the literature that account for spatial variability while also quantifying it over a reach scale. These include the application of contour mapping (Conant Jr, 2004; Schmidt et al., 2007), multiplying the median net flux by the surface area of the water body (Anibas et al., 2011), spatial kriging (Ghysels et al., 2021) and the Thiessen polygon approach (Lautz et al., 2012). Advantages

and disadvantages exist for all techniques, and while new techniques will continue to arise, limitations will likely continue to persist. Often, the best way to address the limitations of these and other techniques, is a multi-scale approach using various techniques, to reduce uncertainty and improve confidence in the results (Kalbus, 2006; Ma et al., 2024).

The goal of the current study was to evaluate the applicability of several conventional approaches for quantifying groundwater-surface water exchange, and to document spatial variability along stream reaches exhibiting groundwater discharge conditions. Additionally, this study sought to account for anisotropy, to improve on these conventional methods, in an attempt to more accurately quantify groundwater-surface water exchange. Differential stream gauging, intensive stream bed temperature profiling, Darcy's law and flow net analysis techniques were applied as part of quantifying and assessing the spatial variability of groundwater-surface water exchange. Using data collected from these Darcy's law and temperature profiling techniques (e.g., horizontal hydraulic conductivity, vertical hydraulic gradient, vertical flux), anisotropy ratios ($K_h/K_v$) were developed to account for anisotropy within the streambed at the identified study reaches. Through the evaluation of the results obtained from the field studies, insight into the comparable effectiveness of the different techniques under variable conditions will be derived, with the objective of providing informative advice for their effective application in other, similar settings, where there is a human influence.

## 3.2 Methodology

### 3.2.1 Field Site

Within the Grand River watershed of southwestern Ontario sits the 79 $km^2$ Alder Creek watershed, the field site for this study (Figure 3.1). In this area, annual air temperatures have been found to range from a minimum daily average of -10.2°C in January to a maximum daily average of 26.2°C in July (Government of Canada, 2025a). The average annual precipitation rate is approximately 900 mm per year, while the average groundwater recharge rate within the watershed is approximately 320 mm per year (Government of Canada, 2025a; Matrix and SSPA, 2014; Wiebe et al., 2022). The largest surface water feature within the watershed is the perennial stream Alder Creek, which is approximately 15 km in length from the headwaters to the confluence with the Nith River. The creek is predominantly groundwater fed, including by a number of smaller spring-fed tributaries, located

largely in the upper to middle reaches of the watershed. The surficial geology of the watershed is heterogeneous (Figure 3.2) as a result of its location within the south-central portion of the Waterloo Moraine, which is a significant topographic relief feature composed of numerous glacial till sheets deposited during the advance and retreat of glaciers in the region, and interlayered with glaciofluvial sand and gravel deposits (Bajc et al., 2014; CH2MHILL and SSPA, 2003; Karrow, 1993; Martin & Frind, 1998). These sand and gravel deposits form many of the major overburden aquifers that the Regional Municipality of Waterloo (RMOW) has relied on to provide much of its water supply.

Approximately 40% of the groundwater that is extracted from wellfields in the City of Kitchener, Ontario, is drawn from the Mannheim West wellfield, located within the Alder Creek watershed (Sousa et al., 2014; Matrix and SSPA, 2014; Wiebe et al., 2023). However, increased groundwater usage is expected as water demands increase in response to significant population growth in this expanding urban center. As land uses within the watershed change from historically agricultural, to increasingly urban (e.g., development of buildings, roads, etc.), and as weather patterns become increasingly unpredictable due to climate change, groundwater recharge rates are expected to change. As a result of these changes, interest is growing regarding their effect on the Waterloo Moraine's aquifer system, and the impact that it may have on baseflow to Alder Creek, and the aquatic ecosystems within it.

### 3.2.2 Study Sites

Site 1 is a 110 m long reach located in the mid to lower region of the Alder Creek watershed in New Dundee, Ontario (Figures 3.1 and 3.3a). Manual streamflow measurements ranged from 0.1 $m^3/s$ to 5.6 $m^3/s$ at the site. This reach of the stream is on average 8 m wide and is located at a meander bend. During low flow the average depth of the stream is approximately 0.4 m but reaches maximum depths of 1 m in pools. The streambed's surficial geology consists of cobbles and gravel, with the inner bank of the bend largely silt. The working conceptual model developed for this site indicates the presence of sand beneath the streambed interface, based on both qualitative observations made during instrument installation, along with streambed horizontal hydraulic conductivity estimates made through single well response tests. The streambanks at this site tend to rise sharply along much of the study reach, with trees, shrubs and grasses present, while more gradual slopes are present along small sections of the reach, where an increased presence of shrubs and grasses are found.

Site 2 is a 40 m long reach located in the lower region of the Alder Creek watershed, approximately 3 km downstream of Site 1 (Figures 3.1 and 3.3b). At this site, manual streamflow measurements ranged from between 0.3 $m^3/s$ and 4.2 $m^3/s$. This reach of stream is approximately 8.5 m wide and is relatively straight. The average depth of the stream in the summer during low flow conditions is approximately 0.6 m and reaches maximum depths of 0.7 m. At this site, while the surficial geology is still dominated by cobbles and gravels, an increased amount of sand is present relative to Site 1. When looking downstream, fine-grained materials have been deposited along the western streambank. Beneath the streambed interface, a sandy material is believed to be present, based on qualitative observations similar to those made at Site 1, and streambed horizontal hydraulic conductivity estimates. When looking downstream, the eastern streambank has a sharp rise, and is dominated by trees, while the western streambank rises much more gradually, and is characterized by shrubs and grasses. The field data collected at these study sites can be found in Zanatta et al. (2025).

### 3.2.3 Instrumentation at Study Sites

At the two field sites, conventional PVC piezometers (1” and 1 ½” ID) and mini-piezometers (1/4" ID) were installed in the streambed, and in the streambank, to measure hydraulic head and conduct single-well response tests. The piezometers were installed at numerous locations across and along the study site stream reaches. At Site 1 (Figure 3.4), 23 mini-piezometers and 4 conventional piezometers were installed in the streambed, while at Site 2 (Figure 3.5), 16 mini-piezometers and 4 conventional piezometers were installed in the streambed. Eight mini-piezometers and 4 conventional piezometers were installed on the banks at each site.

The mini-piezometer installations followed the procedure of Lee and Cherry (1979), which utilizes an extractable temporary drive casing. The streambed conventional piezometers were manually driven into the streambed with a sledgehammer, with the assumed natural collapse of streambed material around the piezometer screens sealing them and reducing the risk of unwanted vertical flow. For the streambank conventional piezometers, holes were initially hand augured until the water table was reached, followed by the piezometers being manually driven to their desired depths. Following installation, filter sand was added, followed by bentonite, to create a watertight seal to reduce the risk of once again, unwanted vertical flow. The midpoints of all piezometer screens were installed to depths ranging from 40 and 55 centimetres below the streambed. The screen length of the conventional piezometers was ~30 cm (slotted), while a screen length of ~15 cm (perforated and

Nitex® wrapped) was used for the mini-piezometers. To prevent the streambed mini-piezometer from being damaged or pulled out by the flowing stream water, a bolt was screwed into a metal plate, and gear clamped to a rubber stopper that ran through the mini-piezometer tubing. The plate was then installed to be flush with the streambed, with rocks placed on the plate in order to keep the piezometers in place. The piezometers were developed following installation and then surveyed using a Sokkia GCX3 GNSS receiver surveying device, a total station, and an automatic level to determine the instrument coordinates and elevations.

### 3.2.4 Groundwater Flux Estimates using Streambed Temperature Profiling

To yield flux estimates, temperature data were collected through manual measurements within the streambed over a multi-day period at both study sites, in the winter and summer of 2024, when large temperature contrasts were expected to exist between groundwater and surface water. Streambed temperature profiles were measured at dozens of locations along the streambed at each study site, to provide spatially distributed temperature data across the reaches of interest. These measurements were made along relatively evenly spaced transects, with temperature profiles normally measured along the thalweg, and to the left and right of the thalweg. Temperature profiles were measured near the piezometers and mini-piezometers, and at additional locations along the same cross-stream transects as the streambed piezometers installations, as well as along additional cross-stream transects in between.

Temperature measurements were made at seven streambed depths (0 cm, 10 cm, 20 cm, 25 cm, 30 cm, 40 cm, 50 cm), using a stainless steel Digi-Sense® Penetration Thermistor probe. To collect these readings at depth, the thermistor probe was encased within a more durable, 1.45 m long, 1.5 cm outer diameter, pointed steel pipe temperature probe. The thermistor probe's cable traversed the inside of the pipe, and was connected to a Digi-Sense® 91428-05 Temp-14 Single-Input Thermistor Thermometer, allowing for temperature readings to be made with an accuracy of ±0.2°C. The probe, which was progressively advanced to the 7 desired depth below the streambed, beginning at 0 cm, was held at these depths until the Digi-Sense® 91428-05 Temp-14 Single-Input Thermistor Thermometer produced a stable reading that held for at least 5 seconds.

In order to estimate the approximate depth with which steady state temperature conditions existed, continuously recording thermistor devices were installed as vertical series of 6 to 7 thermistors between the streambed and a maximum depth of 50 cm along the thalweg, where predominantly

vertical flow groundwater flow was expected. These recording thermistors allowed for the diel variability of groundwater temperatures to be monitored throughout the course of the winter and summer temperature profiling studies. Below 50 cm, it was deemed unnecessary to monitor the diel temperature variability, as at this depth the signal was expected to be fully dampened, following Kurylyk et al. (2019). Vertical fluxes were estimated using the spreadsheet solver "FLUX-LM", developed by Kurylyk et al. (2017), which was applied to the temperature and associated streambed depth data. This tool is based on the 1-D analytical solution of Shan & Bodvarsson (2004), which is an extension of the Bredehoeft and Papadopulos (1965) steady state solution. Four fundamental assumptions define this solution. These include: (1) heat transfer is restricted to one dimension, (2) the groundwater flux within each designated layer is constant and uniform, (3) temperature profiles are steady state, and (4) the soil properties are homogeneous within each layer. To address these assumptions, heat transfer in the non-vertical direction was considered to be minimal, while the stream was the only local point of discharge in which vertical fluxes were believed to be constant and uniform through the streambed material. Additionally, the temperature profiling data that was interpreted with the spreadsheet solver were those collected from depths below which the diel temperature amplitude was less than 1°C, following Kurylyk et al. (2017). This condition was achieved at a depth of 0.1 m at each monitoring location, which agrees well with the recommendations of Anibas et al. (2011) and Ghysels et al. (2021). The streambed material was assumed to be homogeneous, which limited the system to one layer. A thermal conductivity value of 2.2 W/(m °C) was obtained from the literature (Montieth & Unsworth, 2013), representative of a 100% saturated sandy soil, similar to what was encountered at the two study sites.

### 3.2.5 Hydraulic Head and Hydraulic Gradient Measurements

Surface water and groundwater hydraulic heads for each streambed piezometer were monitored through manual water level readings made approximately biweekly. For the conventional PVC piezometers, a water level tape was used, with measurements to the surface water and groundwater made with respect to the surveyed top of the piezometer casing. For the mini-piezometers, a ruler stick was placed on steel plates, bound to the base of the piezometers, and installed flush to the streambed. Following the purging of any air bubbles, surface water and groundwater levels were made using the surveyed plate as reference. The depths of the piezometers below the streambed were confirmed using the known piezometer lengths prior to installation. Using the measured surface water and groundwater hydraulic heads, and the known installation depths of the piezometers, vertical

hydraulic gradients were calculated to determine the direction of groundwater flow. The groundwater hydraulic heads for the streambank conventional piezometers were measured in the same manner as those of the streambed conventional piezometers. The streambank mini-piezometers' groundwater hydraulic heads were measured using a small diameter water level tape, where the stickup of the mini-piezometers was measured, and the elevation of the ground surface was surveyed.

### 3.2.6 Horizontal Hydraulic Conductivities ($K_h$)

Single well response tests were performed in May 2024/2025, to determine horizontal hydraulic conductivities ($K_h$) representative of the material around each piezometer screen. With regards to the conventional piezometers, slug tests (rising and falling head) were completed. Using a Solinst LevelLogger® installed just above the base of the piezometers, the change in head due to the displacement of water was monitored over time at 1 second intervals until water levels had recovered to near initial conditions. With regards to the mini-piezometers, falling head tests were performed. This technique involved connecting a Mityvac® handheld vacuum/pressure pump to the mini-piezometers using a piece of Tygon® tubing and removing the air through a suction process allowing for the head to rise above the initial static level. A video of the recovery was then recorded after the vacuum was released, with the mini-piezometer held beside a ruler. The videos were then reviewed in slow motion, with periodic readings of hydraulic head along the ruler recorded along with the associated elapsed time until the head returned to its original pre-test level. The Hvorslev (1951) approach was applied to calculate $K_h$, where the Butler (1996) recommendation was applied by matching the line of best fit to the data points within the $h/h_0$ interval of 0.15 to 0.25.

Constant head tests were performed for select conventional piezometers, where slug tests proved ineffective due to the piezometers being screened in highly permeable material. This test involved the use of an Iwaki® Magnetic Pump to pump the piezometers, with water levels monitored at 1 second intervals using a Solinst LevelLogger® to identify the displacement between the initial head and the final constant head. To generate estimates of the flow rate, a graduated cylinder and stopwatch were used. These parameters, along with the diameter and length of the piezometer screens and an assumed transformation ratio $\left(m = \sqrt{K_h/K_v}\right)$ value of 1, were applied to Hvorslev's (1951) Case G constant head equation to estimate the horizontal hydraulic conductivity ($K_h$).

### 3.2.7 Vertical Hydraulic Conductivity

Vertical hydraulic conductivities (K) at the study sites were estimated in the winter (February) and summer (July) of 2024 using the temperature profiling vertical flux estimates and associated vertical hydraulic gradients measurements, following a similar approach applied in Lapham (1989). The association of these two independent parameters was made because the vertical temperature profiles were measured on the same day, and near the same locations, where the vertical hydraulic gradients were measured at the streambed piezometers. Vertical hydraulic conductivity ($K_v$) values for the streambed at the location of each piezometer were determined by applying these fluxes and vertical hydraulic gradients to a rearranged form of Darcy's law (Equation 3.1) in order to solve for $K_v$ (Equation 3.2):

$$q = -K_v \times \left(\frac{dh}{dz}\right) \tag{3.1}$$

$$K_v = -\frac{q}{\left(\frac{dh}{dz}\right)} \tag{3.2}$$

### 3.2.8 Darcy's Groundwater Flux Estimates Assuming Isotropic Conditions

Using the single well response tests horizontal hydraulic conductivity values, along with the vertical hydraulic gradients measured on the dates of the winter and summer temperature profiling campaigns, vertical flux estimates were made using Darcy's law for these select days (Equation 3.1). While similar approaches have been applied in other studies (Binley et al., 2013; Cey et al., 1998; Käser et al., 2009), it was recognized that these hydraulic conductivities will be biased to the horizontal plane of study, and as a result, these hydraulic conductivities values may be overestimates if anisotropy is present within the streambed.

### 3.2.9 Spatial Distribution Analysis

The geostatistical method of ordinary kriging was applied to assess the spatial distribution of vertical hydraulic gradient, horizontal hydraulic conductivity, Darcy vertical flux, and temperature profiling vertical flux parameters. This technique uses spatial autocorrelation, in order to predict values, to

create continuous spatial maps from point measurement datasets. To present the kriging data a quantile distribution was used, dividing the datasets into five classes of equal size based on the ranked order of values. This allowed for the relative ranking of the datasets, which groups the data by their position within the larger dataset, instead of with regards to their overall magnitude. The resulting maps display zones corresponding to these quantile groups, providing a clear, relative understanding of spatial variation across the study area, and allowing for the identification of where on the study reaches high and low zones of vertical hydraulic gradients, horizontal hydraulic conductivity, and flux can be found with respect to each unique dataset.

### 3.2.10 Quantifying Groundwater-Surface Water Exchange using Point Measurement Fluxes

The groundwater fluxes measured and calculated through the Darcy's law, and the temperature profiling point-based estimation techniques, were then used to estimate groundwater-surface water exchange through the streambed across Site 1 (Figure 3.6) and Site 2 (Figure 3.7) using the ArcGIS "Thiessen Polygon" tool. This tool creates polygon shapes, based around the associated flux field measurement points, with the boundaries of the polygons defined by the area that is closest to the point, compared to all other points. Exchange values for each polygon were estimated by multiplying the individual fluxes by their respective polygon areas, and the total groundwater-surface water exchange into each reach was estimated by summing the values, allowing for the Darcian (Figures 3.6a and 3.7a) and temperature profiling (Figures 3.6b and 3.7b) related groundwater-surface water exchange to be compared with other techniques.

### 3.2.11 Stream Gauging

Stream gauging was performed at gauging locations just upstream and downstream of Site 1 (Figure 3.8). Streamflow measurements were collected between the late spring and summer months of 2024 and 2025 at the gauging stations using a StreamPRO® acoustic doppler current profiler (ADCP), with associated streamflow measurements made within a few hours of one another. To estimate the amount of net gain or loss in streamflow between the gauging locations, the difference in streamflow was calculated between gauging locations. If the difference in streamflow between upstream and downstream was positive, net gaining conditions (i.e. groundwater discharge) were estimated for the study reach; if the difference was negative, net losing conditions (i.e. groundwater recharge) were estimated over the study reach. Differential stream gauging was performed multiple times over the

course of the study in order to increase confidence, and to minimize the effect of measurement inaccuracy, because an increase in the number of streamflow measurements provides a more reliable statistical average (Harte & Kiah, 2009). To provide increased confidence that any measured increase or decrease in streamflow was a result of groundwater-surface water interactions, stream gauging was performed at or near baseflow conditions during periods of no precipitation, and where no overland flow into the stream was visible along the study reach. Stream gauging was not performed at Site 2 due to the short length of the study reach, which was limited by land access restrictions.

### 3.2.12 Flow Net

Two-dimensional plan view flow nets were developed for the study sites to provide an improved understanding of groundwater flow conditions in the vicinity of the instrumented stream reaches, and to quantify total groundwater discharge to the reaches. The flow nets were representative of hydraulic heads measured for a single day during low flow conditions in the late summer of 2024. The hydraulic head data used in the construction of the flow nets were obtained from the piezometer installations in the stream, and on the streambanks, as previously discussed. Using the flow nets, quantitative estimates of the total groundwater-surface water exchange into the stream were made using the following equation (modified from Porter & Hsieh, 2020):

$$Q = \frac{m}{n} KHb \tag{3.3}$$

where:
Q is the flow rate per unit thickness of cross section ($m^3/s$)
m is the number of flow tubes (-)
n is the number of head or equipotential intervals (-)
H is the total head drop over the flow domain (m)
K is the hydraulic conductivity (m/s)
b is the thickness of the aquifer (m)

For each site, two approaches were applied to estimate hydraulic conductivity values for the flow net equation. The first was the arithmetic mean horizontal hydraulic conductivity for all of the streambed piezometers, and the four streambank conventional PVC piezometers. The second approach employed only the horizontal hydraulic conductivity values for the streambank piezometers, using the arithmetic means of the two conventional PVC piezometers for each bank of the stream. The arithmetic mean was applied because it considers all hydraulic conductivity values as equal in

weight, making it sensitive to extreme values rather than minimizing their influence, as flow is biased within the higher hydraulic conductivity layers (Fuchs et al., 2009, Heeren et al., 2010). This was important, as spatial variability in hydraulic conductivity can be expected at the reaches of study. In both of these approaches, the aquifer thickness (b) was approximated using geologic cross sections developed within the Alder Creek watershed (CH2MHILL, 2003) along with historical well records (Ontario Ministry of the Environment, Conservation and Parks [MECP], 2024) from around the study sites.

## 3.3 Results

### 3.3.1 Differential Stream Gauging

Differential stream gauging was performed up and downstream of Site 1 (Figure 3.8) ten times under presumed baseflow conditions. The net increase in streamflow along the reach due to groundwater discharge ranged from between 17 L/s and 55 L/s, with an average net increase in streamflow due to groundwater discharge of approximately 40 L/s (Figure 3.9), about 10% of the total streamflow measured downstream of the site. The error bars seen in Figure 3.9 were calculated by combining the assumed individual 5% error for each of the upstream and downstream measurements' (Rehmel, 2006). As previously mentioned, differential stream gauging was not performed at Site 2 due to the short length of the study reach.

### 3.3.2 Horizontal Hydraulic Conductivities

At Site 1, streambed horizontal hydraulic conductivities were found to range from $3.7 \times 10^{-6}$ m/s to $5.4 \times 10^{-4}$ m/s, with an arithmetic average of $1.2 \times 10^{-4}$ m/s (Zanatta et al., 2025). Using the complete dataset for this site, including the conventional streambank piezometers, horizontal hydraulic conductivities were found to range from $3.7 \times 10^{-6}$ m/s to $3.1 \times 10^{-3}$ m/s, with an arithmetic average of $2.3 \times 10^{-4}$ m/s. At Site 2, the streambed horizontal hydraulic conductivities were found to range from $4.5 \times 10^{-5}$ m/s to $5.4 \times 10^{-4}$ m/s, with an arithmetic average of $1.1 \times 10^{-4}$ m/s. While for the complete dataset for this site, horizontal hydraulic conductivities were found to range from $4.4 \times 10^{-6}$ m/s to $5.4 \times 10^{-4}$ m/s, with an arithmetic average of $9.9 \times 10^{-5}$ m/s.

### 3.3.3 Vertical Hydraulic Gradients

At Site 1, the vertical hydraulic gradients measured on the dates of temperature profiling in the winter (February 2024) (Figure 3.10a), and summer (July 2024) (Figure 3.11a) were found to be upward, indicative of groundwater discharge conditions. In the case of the winter measurements, the vertical hydraulic gradients were found to range from 0.04 to 0.51, while for the summer measurements, vertical hydraulic gradients ranged from 0.04 to 0.52. Although the vertical hydraulic gradients vary across the study reach, spatial patterns appear to exist, as in both cases the hydraulic gradient appears to be the highest near the upstream part of the study reach, and the lowest in the downstream region.

In the case of Site 2, groundwater discharge conditions once again appeared to be present based on the winter (Figure 3.12a) and summer (Figure 3.13a) vertical hydraulic gradients, which were also found to be upward. The winter vertical hydraulic gradients ranged from 0.03 to 0.66, while those measured in the summer ranged from 0.02 to 0.60, indicative of once again spatial variability. For both the winter and summer, the spatial distribution appears similar, with lower hydraulic gradients in the middle of the reach relative to those measured upstream and downstream.

### 3.3.4 Groundwater Flux and Discharge Estimates using Darcy's Law

At Site 1, the winter and summer vertical hydraulic gradients (Figures 3.10a and 3.11a) along with the single well response test horizontal hydraulic conductivities (Figures 3.10b and 3.11b) were applied to Darcy's law to estimate vertical fluxes. These vertical groundwater fluxes calculated for the winter (February 2024) (Figure 3.10c), and summer (July 2024) (Figure 3.11c), were found to be positive, indicative of groundwater discharge. For the Darcy fluxes measured during the winter, they were variable across the study reach, with values that ranged over two orders of magnitude from $1.0 \times 10^{-6}$ m/s to $1.5 \times 10^{-4}$ m/s. In the case of the summer, Darcy fluxes were found to also range over two orders of magnitude, from $1.0 \times 10^{-6}$ m/s to $1.3 \times 10^{-4}$ m/s. Spatially, during the both the winter and summer study periods, relatively lower Darcy fluxes were found at the downstream segment of the reach, similar to the vertical hydraulic gradient findings, while higher Darcy fluxes values found along the middle, and to a slightly lesser degree, the upper parts of the study reach. In the case of Site 1, the cumulative groundwater discharge over the reach of study was estimated to be 19.3 L/s and 19.5 L/s for the winter and summer, respectively, suggesting a slight increase in discharge conditions.

Groundwater flux maps were also developed for the winter (February 2024) (Figure 3.12c), and summer (July 2024) (Figure 3.13c), at Site 2 using the associated vertical hydraulic gradient (Figures

3.12a and 3.13a), and horizontal hydraulic conductivity estimates (Figures 3.12b and 3.13b) data. These results indicated groundwater discharge conditions once again appeared to be present based on the positive vertical Darcy fluxes found in both the winter and summer. The fluxes for the winter were found to range over two orders of magnitude, from $2.1 \times 10^{-6}$ m/s to $2.0 \times 10^{-4}$ m/s. The summer fluxes ranged over two orders of magnitude, from $1.5 \times 10^{-6}$ m/s to $1.8 \times 10^{-4}$ m/s. Spatially, the Darcy fluxes appeared similar to the vertical gradients, as the Darcy fluxes were lower in the middle of the reach compared to those upstream and downstream. The cumulative groundwater discharge over the reach of study was estimated to be 10.5 L/s and 8.3 L/s, respectively, when applying the vertical hydraulic gradients measured during the winter and summer temperature profiling campaigns, assuming isotropic conditions, indicating a percent decrease in groundwater discharge of approximately 20% between seasons.

### 3.3.5 Groundwater Flux and Discharge Estimates using Streambed Temperature Profiling

Point measurement streambed groundwater flux estimates were made across both study reaches by interpreting the temperature profiling data collected in the winter (February 2024), and summer (July 2024), using the FLUX-LM spreadsheet method described above. In the case of Site 1, a total of 66 temperature profiles were measured over three closely spaced days in the winter (Figure 3.14a). For 64 of the 66 temperature profiles, upward vertical flux was estimated, with the remaining two estimating downward flux. These fluxes ranged from $-4.3 \times 10^{-8}$ to $7.5 \times 10^{-6}$ m/s. In the summer (Figure 3.14b), a total of 88 temperature profiles were measured over three consecutive days. Of these, 80 were upward vertical fluxes, 1 was downward, and flux estimates could not be estimated for the remaining 7 locations due to the lack of a concave up or down shape in these short term profiles. The vertical fluxes ranged from $-1.6 \times 10^{-6}$ to $1.4 \times 10^{-5}$ m/s. The vertical fluxes measured in the winter and summer clearly show spatial variability across the study reaches (Figure 3.14), and although differences exist in the absolute magnitudes of the flux estimates, the spatial distribution of fluxes between seasons appears fairly similar. This was seen in the lower upward flux estimates measured in the upstream and downstream sections of the study reach, while within the middle of the reach, higher upward flux estimates were found.

Although the temperature profile flux datasets are much larger, and although the Darcy flux estimates were higher by on average, an order of magnitude, the spatial distribution appears to be

fairly similar between datasets (Figures 3.10c, 3.11c and 3.14). Lower upward flux estimates were measured in the downstream, and to some degree, upstream sections of the study reach, while higher upward flux estimates were found in the middle. Unlike the Darcy flux approach, however, signs of possible groundwater recharge were found. Using the Thiessen polygon approach, the individual point measurements were used to estimate the cumulative groundwater-surface water exchange during the winter and summer study periods along the study reach. As a result, the groundwater discharge over the 110 m long study reach was estimated to be 2.7 L/s and 4.7 L/s, respectively, during the winter and summer temperature profiling campaigns. These results indicate an approximately 1.7 times increase in groundwater discharge from the winter to the summer temperature profiling campaign.

With regards to Site 2, a total of 53 temperature profiles were measured over a day in the winter (Figures 3.15a), yielding 45 upward fluxes (groundwater discharge) and 8 downward fluxes (groundwater recharge), with the fluxes ranging from $-2.4 \times 10^{-6}$ to $6.9 \times 10^{-6}$ m/s. Over two concurrent days in the summer (Figure 3.15b), 53 temperature profiles were measured, resulting in upward vertical flux estimates at 44 locations and downward flux estimates at 6 locations. A reasonable flux estimate could not be obtained for 3 temperature profiles that did not exhibit the required concave up or down shape. The vertical fluxes were found to range from $-4.6 \times 10^{-6}$ to $1.4 \times 10^{-5}$ m/s. Both in the winter and summer seasons, the spatial distribution was similar, as higher upward vertical fluxes values (groundwater discharge) were observed at the upstream and downstream ends of the study reach, while the middle of the reach exhibited relatively lower upward fluxes, to some downward fluxes (recharge) (Figure 3.15).

Once again, while the temperature profile vertical flux datasets are much larger, and while the Darcy vertical fluxes are nearly an order of magnitude greater, on average, than the temperature profile vertical fluxes, the spatial distribution of vertical fluxes correlate well between datasets (Figures 3.12c, 3.13c and 3.15). However, the notable presence of downward fluxes, indicative of recharge conditions, identified in the middle of this study reach based on the temperature profile data were not detected for the Darcy flux approach. The groundwater discharge over the approximately 40 m long study reach was estimated to be 0.7 L/s and 1.5 L/s, respectively, during the winter and summer temperature profiling campaigns. These results indicated an increase in groundwater discharge from the winter to the summer by a factor of 2.1 at this site.

### 3.3.6 Groundwater Flux and Discharge Estimates assuming Anisotropy

To improve the accuracy of the Darcy flux and groundwater discharge estimates, anisotropy ratios for the winter and summer at each study site were estimated. Through the application of the vertical hydraulic gradients and associated temperature profiling vertical fluxes to Equation 3.2, vertical streambed hydraulic conductivities were estimated at each site for the winter and summer seasons (Table 3.1). At Site 1, arithmetic average winter and summer streambed vertical hydraulic conductivities of $1.9 \times 10^{-5}$ m/s and $2.9 \times 10^{-5}$ m/s were estimated (Table 3.1). When the arithmetic average streambed horizontal hydraulic conductivity of $1.2 \times 10^{-4}$ m/s, determined through single well response tests, was divided by the average streambed vertical hydraulic conductivities, anisotropy ratios of approximately 6 and 4 were estimated with respect to the winter and summer seasons (Table 3.2). After applying these anisotropy ratios to the Darcy fluxes, groundwater discharges for the winter and summer were 3.2 L/s and 4.9 L/s respectively. At Site 2, average streambed vertical hydraulic conductivities of $1.1 \times 10^{-5}$ m/s and $3.7 \times 10^{-5}$ m/s were estimated for the winter and summer, respectively (Table 3.1). When used in association with the average streambed horizontal hydraulic conductivity of $1.1 \times 10^{-4}$ m/s, anisotropy ratios of approximately 10 and 3 were estimated for the winter and summer (Table 3.2). When applying these anisotropy ratios to the Darcy fluxes, the respective groundwater discharges for the winter and summer were 1.1 L/s and 2.8 L/s. Through the application of these anisotropy ratios, a significant decrease in groundwater discharge was estimated for both sites and for both seasons, relative to the initial Darcy groundwater discharge estimates that assumed isotropic conditions.

### 3.3.7 Groundwater Discharge using Flow Nets

Using hydraulic head data collected on August 20, 2024, from piezometers within the stream and on the streambanks, and using equipotential lines with a 0.1 metre spacing, a flow net was developed for Site 1 (Figure 3.16). As seen in the flow net, groundwater flows towards the stream from both streambanks as hydraulic heads largely decrease towards the stream, indicating groundwater discharge. Based on the close spacing of the equipotential lines on the eastern streambank, relative to that of the western streambank, the eastern streambank exhibits a greater horizontal hydraulic gradient. The greater horizontal hydraulic gradient, and the increased elevation of this streambank, indicate likely lower hydraulic conductivity and groundwater discharge. Quantitatively, the eastern streambank of the flow net contains 33 flow tubes, 3.31 equipotential intervals, and a total head drop

over the flow domain of 0.3 m. The western streambank of the flow net contains 7 flow tubes, 3.18 equipotential intervals, and a total head drop over the flow domain of 0.5 m. These equipotential interval values were the average of the equipotential intervals estimated for each flow tube. Groundwater discharge was quantified by applying the aforementioned parameters for each streambank to Equation 3.3, along with an estimated aquifer thickness of 5 m, deemed representative of the study site based on geologic cross sections and historical well records for the area, and hydraulic conductivity values representative of the study site.

Two different approaches were used to estimate the hydraulic conductivity of each study site. The first approach applied an arithmetic mean horizontal hydraulic conductivity value of $2.3 \times 10^{-4}$ m/s at Site 1, which incorporated the 27 streambed piezometers and 4 conventional streambank piezometers at the study site. The second approach used the arithmetic mean horizontal hydraulic conductivity for each streambank's two conventional piezometers, with the eastern and western streambanks having hydraulic conductivities of $1.8 \times 10^{-4}$ m/s and $1.7 \times 10^{-3}$ m/s, respectively. For this first approach at Site 1, the flow net derived groundwater discharge estimates from the eastern and western streambanks of 3.4 L/s and 1.3 L/s, respectively, for a total groundwater discharge of 4.7 L/s. For the second approach, the groundwater discharge was found to be 2.6 L/s from the eastern streambank and 9.5 L/s from the western streambank, for a total groundwater discharge of 12.1 L/s.

The flow net for Site 2 (Figure 3.17) used hydraulic head data collected on August 23, 2024. As seen in the flow net, groundwater flows towards the stream from both streambanks, as hydraulic heads largely decrease towards the stream, indicating gaining conditions. Based on the proximity of the equipotential lines to one another, the horizontal hydraulic gradient on the eastern streambank appears to be greater than that seen on the western streambank. This greater horizontal hydraulic gradient, and higher elevation of this streambank, were expected to be associated with lower hydraulic conductivity and groundwater discharge estimates. The eastern streambank of the flow net contains 37 flow tubes, 6.73 equipotential intervals, and a total head drop over the flow domain of 0.8 m. The western streambank of the flow net contains 3 flow tubes, 0.71 equipotential intervals, and a total head drop over the flow domain of 0.1 m. For this site, an estimated aquifer thickness of 3.5 m was applied, while the same two approaches applied at Site 1 were used to estimate the hydraulic conductivity of this study site. The first approach applied an arithmetic mean horizontal hydraulic conductivity of $9.9 \times 10^{-5}$ m/s, for the 20 streambed piezometers and 4 conventional streambank piezometers at the study site. The second approach once again used the arithmetic mean horizontal

hydraulic conductivity for each streambank's two conventional piezometers, with the eastern and western streambanks having hydraulic conductivities of $7.6 \times 10^{-6}$ m/s and $6.9 \times 10^{-5}$ m/s, respectively. When applying the first approach, groundwater discharge from the eastern and western streambank were 1.5 L/s and 0.2 L/s, respectively, for a total groundwater discharge of 1.7 L/s. For this second approach, the groundwater discharge was found to be 0.12 L/s from the eastern streambank and 0.1 L/s from the western streambank, for a total groundwater discharge of 0.2 L/s. The groundwater discharge estimates for all techniques are presented in Table 3.3.

## 3.4 Discussion

Based on differential stream gauging, it was estimated that, on average, an approximately 40 L/s net increase in streamflow due to groundwater discharge occurs over the Site 1 study reach. As a result of the repetitive nature of the differential stream gauging measurements, performed 10 times under anticipated baseflow conditions, the estimate improved as random error decreased, ultimately leading to a groundwater discharge value of higher confidence. The other quantification techniques applied in this study involved the use of point measurement techniques. These techniques were applied only once or twice over the course of the study, resulting in increased uncertainty in the results. Furthermore, these point measurements were often extrapolated over larger areas through the use of the Thiessen polygon tool, in what is a heterogeneous setting, ultimately leading to further uncertainty. Also, the flow net approaches not only relied on limited, point scale measurements of hydraulic parameters, but numerous assumptions were required, increasing the uncertainty in the results. Therefore, the groundwater discharge value acquired through differential stream gauging was believed to be the most representative of groundwater-surface water exchange along the study reach and was the benchmark for comparison.

At Site 1 approximately 48% of the groundwater discharge measured through differential stream gauging was accounted for using the Darcy's law technique in the winter and summer, assuming isotropic conditions. It should be noted that differential stream gauging was performed under late spring to summer conditions and, therefore, may not ideally represent winter conditions. Darcy's law also produced groundwater discharge estimates that were 7.2 and 4.1 times larger than the vertical temperature profiling techniques related groundwater discharges. At Site 2, while differential stream gauging at the study site was not performed, the Darcy's law point measurement technique again produced much larger groundwater discharge estimates, assuming isotropic conditions, as these

values were approximately 15.0 and 5.5 times larger than the vertical temperature profiling techniques groundwater discharges.

These Darcy fluxes assumed isotropic conditions through the application of horizontal hydraulic conductivities within Darcy's law. This approach, however, is limited when attempting to accurately understand vertical groundwater flow. This is especially true with regards to study sites located in streams with highly variable floodplain sediment complexes, where anisotropy in the streambed material is highly likely. As a result, accounting for anisotropy is important in producing flux estimates more representative of the study sites. Anisotropy ratios for each season were therefore applied to the Darcy flux estimates at both Site 1 and Site 2. For Site 1, these anisotropy ratios resulted in declines in groundwater discharge that were very similar to the temperature profiling groundwater discharge estimates, as they were now larger by just 1.2 and 1.04 times. However, now only approximately 7% and 12% of the benchmark groundwater discharge is accounted for. At Site 2, these anisotropy ratios also resulted in declines in groundwater discharge, making them also very similar to the temperature profiling groundwater discharge estimates, at 0.6 and 0.5 times smaller. These results show the significant variability that exists when anisotropy is, and is not, considered in hydraulic conductivity estimates. Should the temperature profiling groundwater discharge estimates be accurate representations of groundwater discharge, it also highlights the value of accounting for anisotropy with regards to accurately estimating groundwater discharge.

As it pertains to the summer and winter temperature profiling data for Site 1, only approximately 7% and 12%, respectively, of the benchmark groundwater discharge measured through differential stream gauging was accounted for. Based on the assumption that differential stream gauging is the most representative of groundwater-surface water exchange, these results indicate that a significant amount of groundwater discharge is unaccounted for. This underestimation of groundwater discharge using these point measurement techniques may be due to a number of reasons. This includes significant spatial heterogeneity and anisotropy present within streambeds, and the complex nature of groundwater flow paths (Conant Jr., 2004; Irvine et al., 2015; Käser et al. 2009; Rosenberry et al. 2016), which results in high flux locations possibly being missed during temperature profiling. The issue of not accounting for high flux locations is then exacerbated by the multiplication of these flux estimates by their associated Thiessen polygon areas, yielding groundwater discharge estimates that may significantly underestimate the actual groundwater discharge in the area.

Additional reasons for this underestimation of groundwater discharge include the possible generation of frictional heat due to the hammering of the temperature probe into the streambed that could possibly alter and lead to erroneous temperatures readings (Westberg, 2012), that may affect the temperature profiles shape and, therefore, impact flux estimates, including possible underestimating fluxes. Also, this temperature profiling technique was designed around the assumption of only vertical groundwater flow, meaning lateral groundwater flow contributions would not be accounted for (Ghysels et al., 2021). While this technique does not account for lateral groundwater flow, the vertical one dimensional temperature profiles were likely influenced by it (Lu & Ge, 1996). This influence, however, comes in the form of overestimating the vertical flux estimates as a result of increased error, especially when the vertical flow component is dominated by the lateral flow component (Irvine et al., 2015; Lautz, 2010; Rau et al., 2010; Roshan et al., 2012). This is an issue that appears to be more pronounced for temperature profiles measured away from the thalweg, and towards the streambanks, where deviation from exclusively vertical flow is greater, as a result of the increased influence of the lateral component of flow (Anibas et al. 2011; Ghysels et al., 2021; Kurylyk et al., 2017). This greater lateral groundwater flow component from around the streambank alters the upper part of the temperature profile, and therefore, the shape of the temperature profile. This may explain why a number of profiles measured at the study sites lacked the profile curvature necessary to make a flux estimate using the FLUX-LM tool, due to their fairly consistent temperatures with depth.

Due to the fact that numerous temperature profiles lacking this curvature were measured in areas of suspected high groundwater discharge, based on nearby high vertical hydraulic gradient measurements, locations of high vertical groundwater fluxes were possibly not accounted for because of missing values within the Thiessen polygon approach, leading to the underestimation of groundwater discharge overall. Another factor to consider is the accuracy of the thermal conductivity value used in the FLUX-LM tool to estimate the fluxes. The thermal conductivity value varies based on the material and is directly proportional to the flux, assuming the temperature gradient remains the same. Therefore, this underestimation of groundwater discharge using the temperature profiling approach may partially be the result of using a thermal conductivity value that does not accurately represent that of the streambed material. Although all of these sources of uncertainty discussed may have contributed to the underestimation of the differential stream gauging estimate of groundwater discharge, the most probable cause is that these vertical flux approaches are only quantifying the

vertical groundwater discharge through the streambed at the measurement locations. This means that vertical groundwater discharge only contributes a small amount of the total groundwater discharge to the stream, and that a significant component of the total groundwater discharge entering the stream is coming from an alternative source that is not being accounted for. Based on the notable groundwater discharge identified entering the stream along the streambank, as discussed in Chapter 2, it is believed that a majority of the groundwater discharge enters the stream near the streambank, emphasizing the importance of applying techniques that can account for groundwater discharge near the streambank.

As previously mentioned, the groundwater discharge during the winter and summer temperature profiling campaigns were found to differ, with increased groundwater discharge measured in the summer at both study sites. This increase in groundwater discharge measured in the summer was also found at a study site of similar length in the work of Conant Jr. (2004). In his work, lower groundwater discharge measured in the winter was attributed to the increase in the viscosity of the water due to the colder water temperatures at this time of year. To verify this explanation and its applicability to this study, the temperature profiles developed in the winter and summer at each study site were compared. The combined average temperature at a depth of 10 cm for both sites in the winter and summer were approximately 7°C and 14°C, respectively. When applied to a water temperature vs dynamic viscosity relationship, this increase in temperature resulted in an approximately 20% increase in hydraulic conductivity between seasons. However, due to the variability in temperature difference measured across the study site, it is expected that the increase in hydraulic conductivity will vary from location to location. Furthermore, at shallower depths (i.e., < 10 cm), these temperature contrasts would be expected to be even greater, resulting in an even greater increase in hydraulic conductivity, making a 20% increase a likely underestimate. This 20% increase in hydraulic conductivity, and therefore groundwater discharge, due to variability in water viscosity, however, only appears to account for a portion of the 74% and 114% increase in discharge seen at Sites 1 and 2, respectively, meaning a significant component of seasonal change in groundwater discharge is still unaccounted for. The density of water can also change with temperature; however, an increase from 7°C to 14°C results in a 0.1% decrease in hydraulic conductivity, making its influence negligible.

Another factor to consider is the role of colmation and decolmation. Colmation, or more specifically external colmation, is the decrease in hydraulic conductivity due to the clogging of the top layer of channel sediments as a result of extended periods of low stream velocity, commonly

found during periods of low flow (Brunke, 1999). Decolmation, on the other hand, refers to processes that increase hydraulic conductivity due to the breaking up of the streambed sediment, in response to high discharge events (Brunke, 1999). While the temperature profiling was performed under low flow conditions, the summer temperature profiling campaign was preceded by the largest discharge event of the entire study period, by just six days. Through visual observations of the streambed following the event, it was found that much of the stream bed vegetation had been washed away, while the streambed morphology had been altered, with much of the fine-grained sediments having also been washed away. With regards to the winter temperature profiling, over 2 weeks passed since a notable discharge event occurred, with that event being much smaller than the later summer event. This significant summer event, and the observed changes in the streambed thereafter, indicate likely decolmation, which would have increased hydraulic conductivity and induced greater groundwater discharge. This decolmation may, therefore, also account for the increased groundwater discharge measured in the summer at the study sites.

The influence of the hydraulic gradient is a parameter that also needs to be considered to better understand why groundwater discharge was found to be higher in the summer, relative to the winter. In the case of Site 1, the average vertical hydraulic gradients on the days of temperature profiling were 0.20 in the winter, and 0.23 in the summer (Table 1). This increase in the average vertical hydraulic gradient, while small, was higher in the summer, supporting the increased groundwater discharge found in the summer at Site 1. In the case of Site 2, the average vertical hydraulic gradients on the days of temperature profiling were 0.28 in the winter, and 0.27 in the summer (Table 1). At this site, the average vertical hydraulic gradients, while very similar, show a slight decrease from the winter to the summer. This would indicate a slight decrease in groundwater discharge, contradictory to what was seen at Site 1, and would mean that change in hydraulic conductivity is what is responsible for the increased groundwater discharge measured in the summer. This seasonal variability in groundwater discharge, due to changes in hydraulic conductivity and hydraulic gradients with time, brings to light another significant issue with regards to quantifying groundwater discharge, which is the influence of temporal variability. With seasonality in water budget parameters (e.g., precipitation, recharge, and evapotranspiration), and the growing influence of climate change on weather patterns, accounting for temporal variability will be crucial in better understanding groundwater-surface water interactions.

Unlike the previously discussed point measurement techniques, which only quantified vertical discharge through the streambed, the 2-D plan view flow net approach attempted to account for the total groundwater discharge, like the differential stream gauging approach. With regards to Site 1, the total groundwater discharge determined using the flow nets varies, as the hydraulic conductivity differs between approaches. Based on the eastern streambank's higher elevation and greater horizontal hydraulic gradient, lower hydraulic conductivity and likely lower groundwater discharge relative to the western streambank were expected, which was the case when applying the second approach of using just each streambank's piezometers average horizontal hydraulic conductivity. The first approach, which uses the bulk arithmetic average horizontal hydraulic conductivity of all 31 piezometers, shows notably more groundwater discharge from the eastern streambank, contradicting what would be expected. These findings appear to provide support to the streambank hydraulic conductivity approach being a more effective method to represent natural hydrogeological flow conditions.

When applying the bulk arithmetic mean horizontal hydraulic conductivity approach to the flow net groundwater discharge equation, approximately 12% of the groundwater discharge was accounted for, with respect to the differential stream gauging groundwater discharge estimate. The second approach, using the arithmetic mean horizontal hydraulic conductivity values for each individual streambank, accounted for 30% of the groundwater discharge measured through differential stream gauging. The greater groundwater discharge estimated using just the streambank piezometer data appears to emphasize the influence of the streambank with regards to groundwater contributions to streamflow, based on the generally higher average hydraulic conductivities relative to those measured in the streambed. This total groundwater discharge was also closer to the value of 40 L/s estimated through differential stream gauging and notably higher than that of the temperature profiling and Darcy approaches (assuming anisotropy), which measured exclusively vertical groundwater discharge. Therefore, the flow net approach appears to account for some groundwater discharge contributions near the streambank.

However, neither version of the flow net approach was able to account for the total groundwater discharge of 40 L/s estimated through differential stream gauging, indicating possible limitations in the flow net conceptual model's parameters. These include the possible underestimation of the aquifer thickness (b), due to reliance on historical data not collected directly at the study sites, and more importantly the underestimation of hydraulic conductivity within the aquifer that intercepts the

streambanks, as this parameter can exhibit significant spatial variability. The first possible explanation for this underestimation is heterogeneity, because relying on so few piezometers, especially for the two streambanks, can result in estimates of hydraulic conductivity that are not representative of the study site. Another possible explanation is that the hydraulic conductivities estimated, specifically those of the streambank piezometers, were screened too deep at half a metre below the elevation of the streambed. At this depth, the hydraulic conductivity of material near the streambank may not have been measured. Based on the notable groundwater discharge identified entering near the streambanks, as discussed in Chapter 2, and the expected less consolidated, more biologically active nature of this shallower zone, the area near the streambank is believed to be a highly permeable zone of preferential flow.

Therefore, if the hydraulic conductivity for the flow net equation was modified, for instance, using a value of $2 \times 10^{-3}$ m/s, then an estimate similar to the benchmark would be obtained. This value is representative of a sandy material, which is common around the study site based on qualitative observations, and similar to the highest measured hydraulic conductivity value for this site of $3 \times 10^{-3}$ m/s. Using the flow net equation, the total groundwater discharge would be estimated to be 41 L/s, much greater than the vertical discharge estimates and very similar to the differential stream gauging total groundwater discharge estimate of 40 L/s. These results highlight the influence of groundwater discharge near the streambank and appear to explain the unaccounted groundwater discharge when applying the vertical point measurement techniques.

At Site 2, where the eastern streambank was also of a higher elevation and larger horizontal hydraulic gradient, lower hydraulic conductivities were also measured for the streambank using the second approach of average streambank horizontal hydraulic conductivity, while groundwater discharge was similar to that estimated through the western streambank. This was in great contrast to the results for the first approach, using the bulk arithmetic mean of all 24 piezometers, where groundwater discharge from the eastern streambank was much higher than that of the western streambank. Once again, this provides support to the streambank hydraulic conductivity approach, being a more effective method to represent natural hydrogeologic conditions.

For the flow net approach using the arithmetic mean horizontal hydraulic conductivity of the 24 piezometers at Site 2, groundwater discharge was relatively similar to the vertical flux approaches of temperature profiling and anisotropic Darcy's law. For the approach using the average horizontal

hydraulic conductivity values for each individual streambank, the discharge just slightly underestimates these vertical flux approaches. This similarity of the flow net derived total groundwater discharge estimates to that of the vertical groundwater discharge approach estimates appear to indicate that groundwater discharge near the streambank is minimal to nonexistent. However, due to the inability to perform differential stream gauging at this site to calculate a benchmark, the ability to assess the effectiveness of the other techniques is limited at Site 2.

Based on the findings at Site 1, greater emphasis should be put into increasing understanding of streambank hydraulic conductivities, specifically near the streambank. This should be done through the increase in streambank piezometers installations, including the use of multilevel piezometers with screens set at different elevations, and the assessment of each streambank separately. This will result in a larger dataset of hydraulic conductivities and allow for differences in the streambank morphology to be considered. These multilevel streambank piezometers should be screened at shallower depths, closer to where most of the visible groundwater discharge was found, in order to get more representative estimates of hydraulic conductivity in these zones of groundwater discharge. Numerical groundwater modelling of the study sites should also be considered using collected field data, as it may be valuable in providing greater insight into the expected proportion of groundwater discharge occurring near the streambank.

## 3.5 Conclusions

Numerous conventional approaches were applied to quantify and assess the spatial variability of groundwater-surface water exchange. The point measurement techniques of Darcy's law and temperature profiling identified notable spatial variability in groundwater-surface water exchange, with similar spatial patterns observed for both approaches, supporting their utility. However, the groundwater discharge that was quantified differed greatly between techniques, with the Darcy law approach producing noticeably greater estimates of groundwater discharge relative to the temperature profiling technique. The Darcy's law approach, however, is limited by its assumption of isotropic conditions. Therefore, anisotropy ratios were developed for both sites in the winter and summer, to produce improved estimates of groundwater discharge. These estimates were found to be more similar to the temperature profiling related estimates, emphasizing the value of accounting for anisotropy within the streambed. Additionally, the groundwater discharge estimates for both

techniques were found to be higher in the summer relative to the winter, indicating temporal differences likely driven by seasonal changes in hydraulic conductivity and hydraulic gradients. These findings highlight the importance of taking temporal variability into account when attempting to better understand groundwater-surface water interactions. Such approaches, however, are limited, as they only account for vertical groundwater discharge into the stream.

Differential stream gauging was an alternative technique applied at Site 1, which, while limited in its ability to assess spatial variability, was easily repeatable and capable of quantifying the total groundwater-surface water exchange. Through repeated measurements, a consistent increase in streamflow (indicative of groundwater discharge conditions) was observed, allowing for improved confidence in the average groundwater discharge over the study reach, and making it the benchmark for comparison of all other techniques. The Darcy's law and temperature profiling vertical groundwater discharge estimates, however, were found to greatly underestimate the differential stream gauging estimate. Therefore, it was concluded that only a relatively small component of groundwater discharge flows vertically upward below the streambed, and that a significant source of groundwater discharge was unaccounted for. This unaccounted groundwater discharge was presumed to be entering near the streambanks, where visible groundwater discharge had been previously identified. A 2-D plan view flow net model was developed using historical data and data collected from the field, but it proved unsuccessful in accounting for the missing groundwater discharge. It was presumed that the hydraulic conductivity was being underestimated and was not representative of the aquifer adjacent to the stream. Using a higher hydraulic conductivity value, still deemed representative of Site 1, the flow net estimates were capable of accounting for the missing groundwater discharge near the streambank. This fact highlights the significant influence of groundwater discharge near the streambank, and the importance of being able to accurately quantify it.

At Site 2, the 2-D plan view flow net model produced groundwater discharge estimates very similar to the vertical groundwater discharge techniques. These findings appear to indicate that groundwater discharge near the streambank is minimal to nonexistent. However, due to differential stream gauging not being performed at the site, a more detailed assessment was not possible, due to the lack of what might be considered a benchmark for comparison of total groundwater discharge estimates.

The approaches applied as part of this study related to groundwater-surface water exchange are all very different, with their applicability largely dependent on the goal of the study and the type of question being asked. This includes, but is not limited to, the scale of study, the time of year of the study, and whether quantifying groundwater-surface water exchange or assessing spatial variability is greater importance. Using field data, in association with numerical groundwater models, further insight into groundwater-surface water exchange within a stream could be gained.

## 3.6 Figures

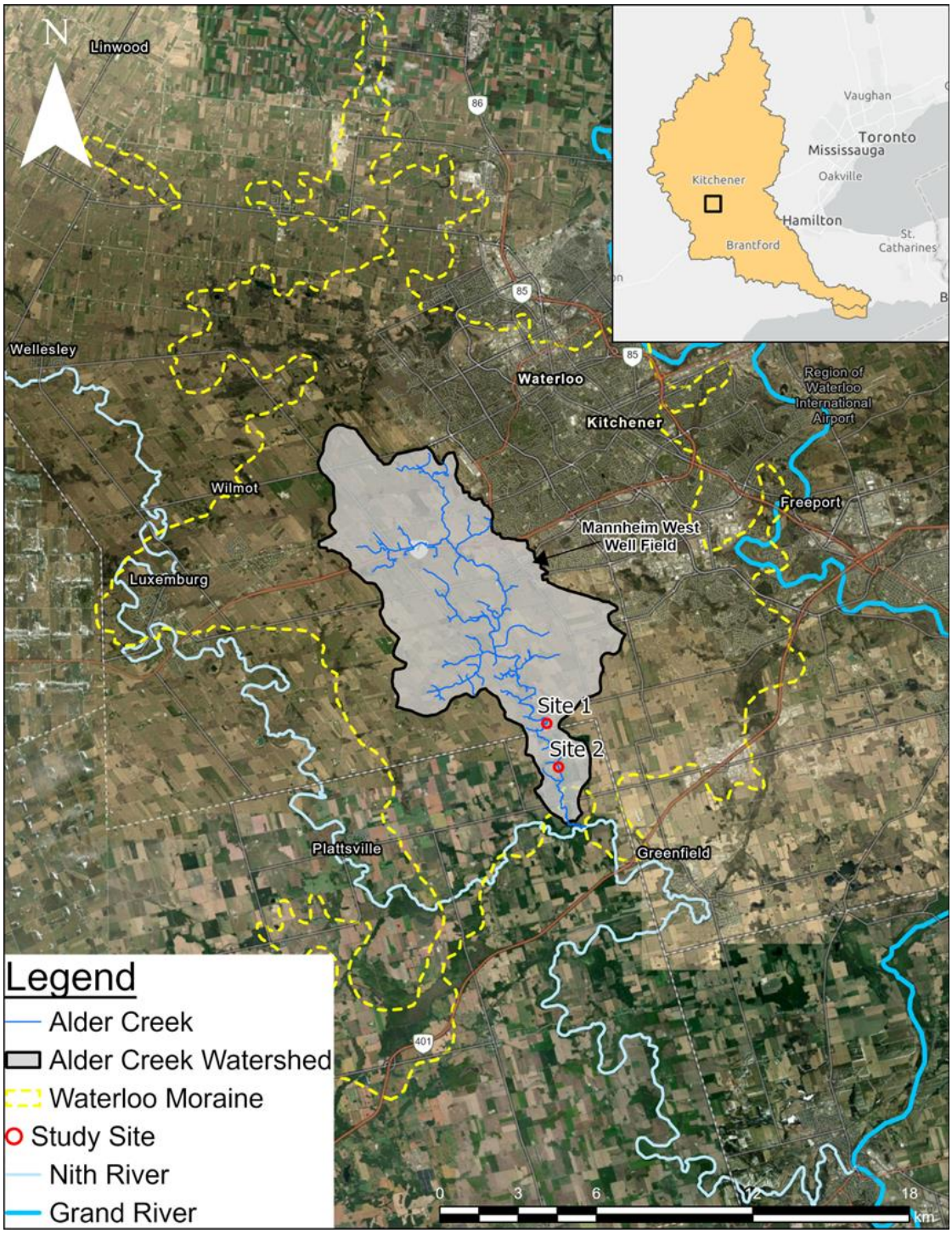



Figure 3.1: Alder Creek watershed and study site locations (Esri et al., 2025a; Esri et al., 2025b; Government of Ontario, 2017; Grand River Conservation Authority, 2023; Sousa et al., 2014).

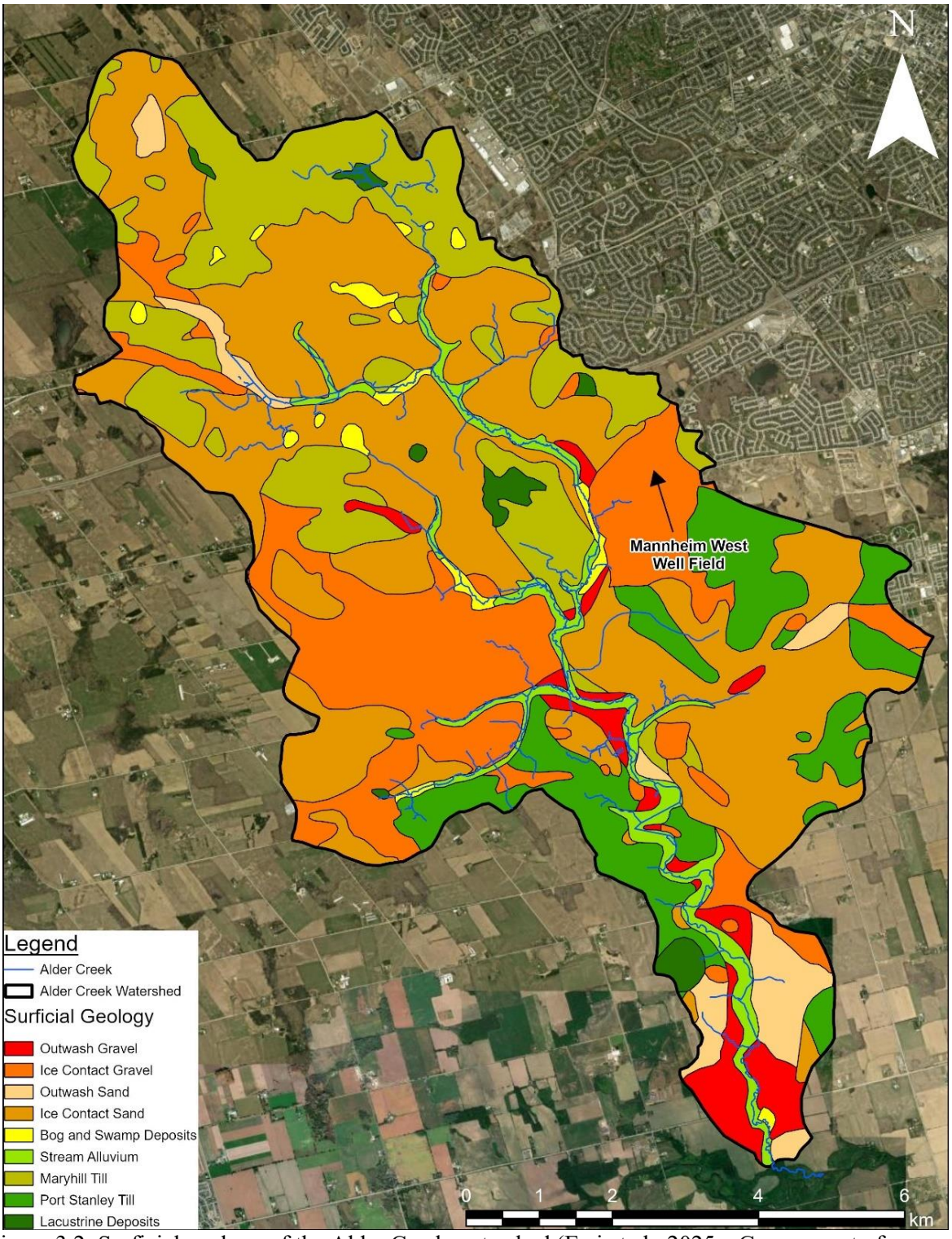



Figure 3.2: Surficial geology of the Alder Creek watershed (Esri et al., 2025a; Government of Ontario, 2023; Grand River Conservation Authority, 2017; Ontario Geological Survey, 2010).



(a) (b)

Figure 3.3: Photos of (a) Site 1 and (b) Site 2.

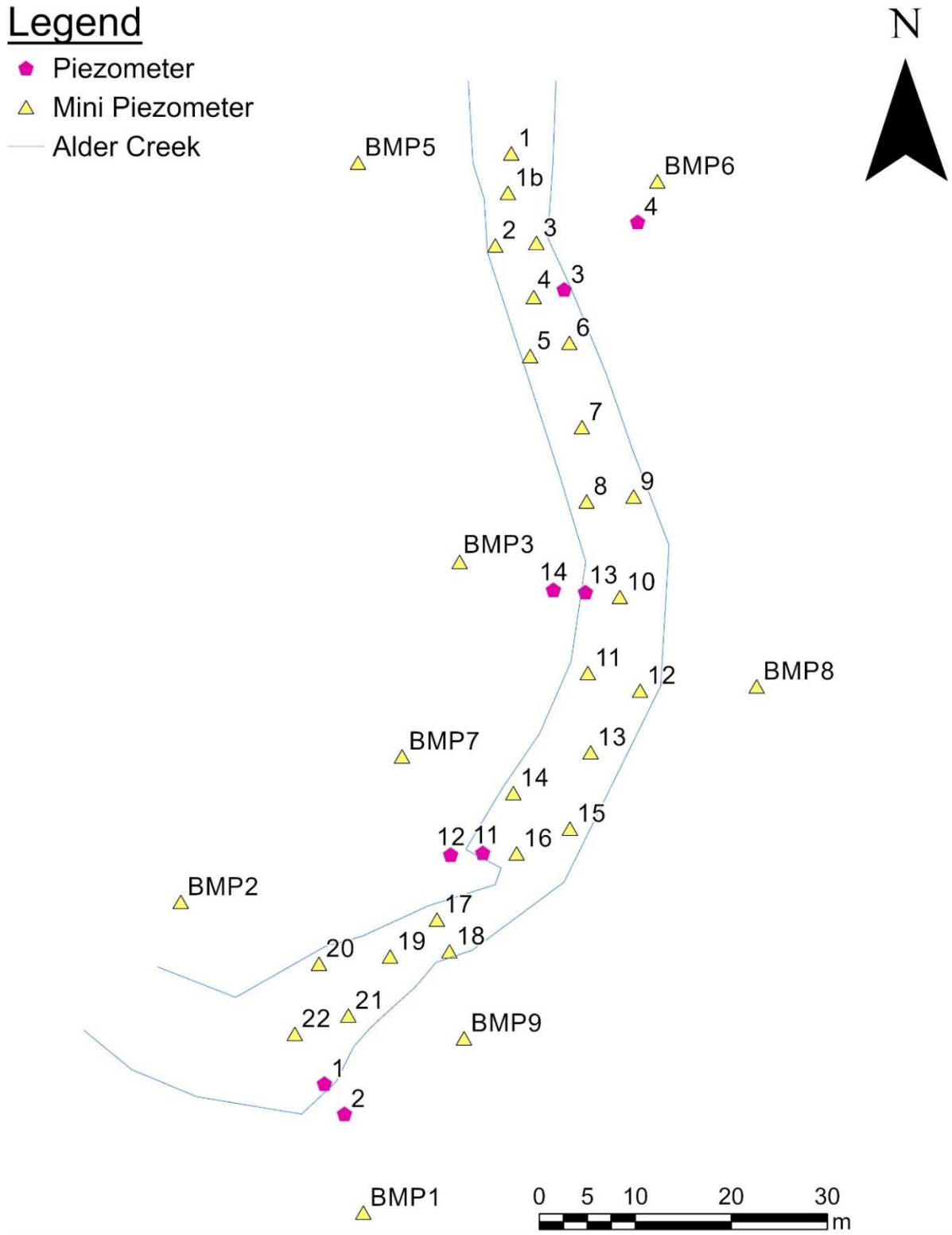



Figure 3.4: Map of Site 1 and piezometer installations. 'BMP' indicates 'bank mini-piezometer.'

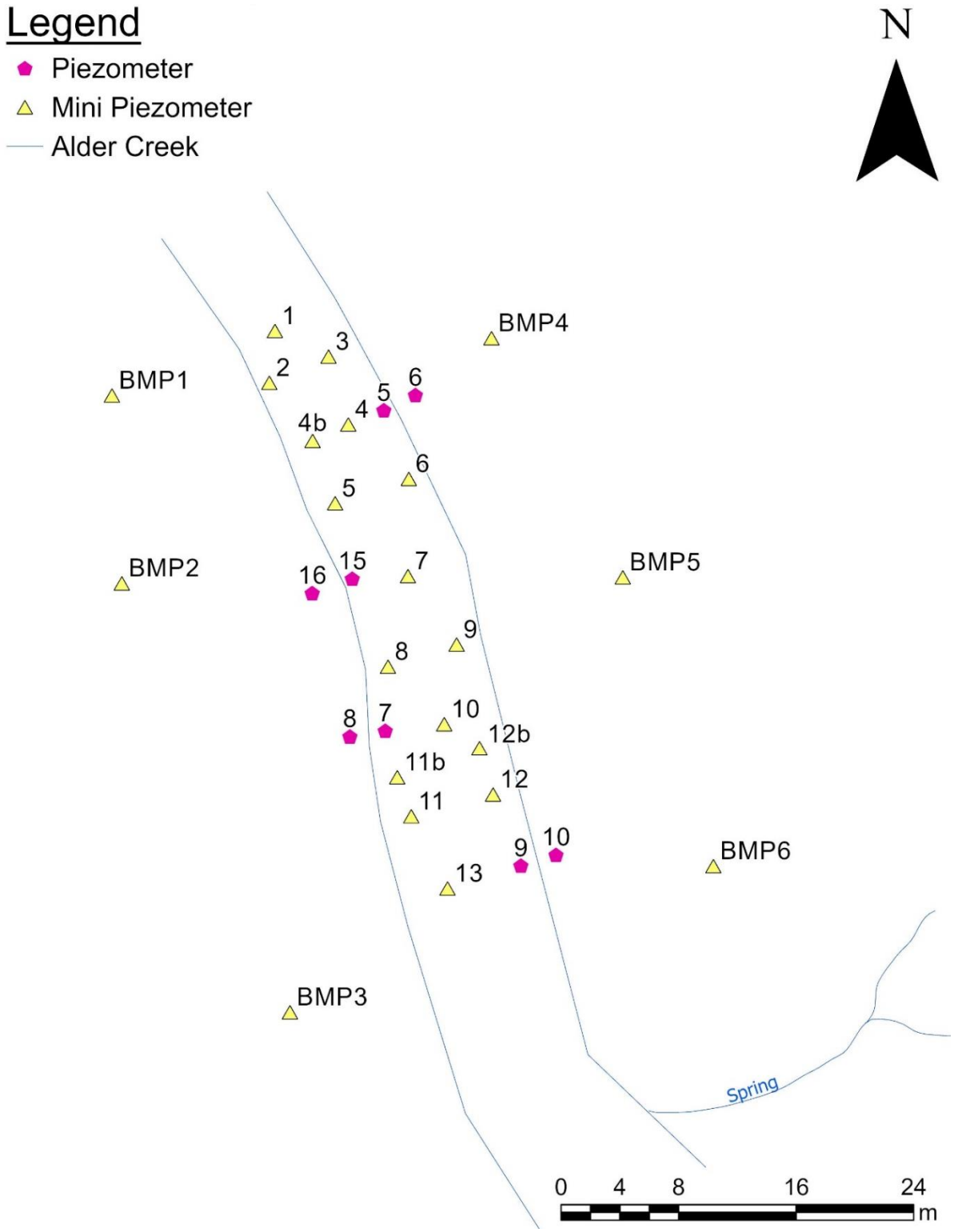
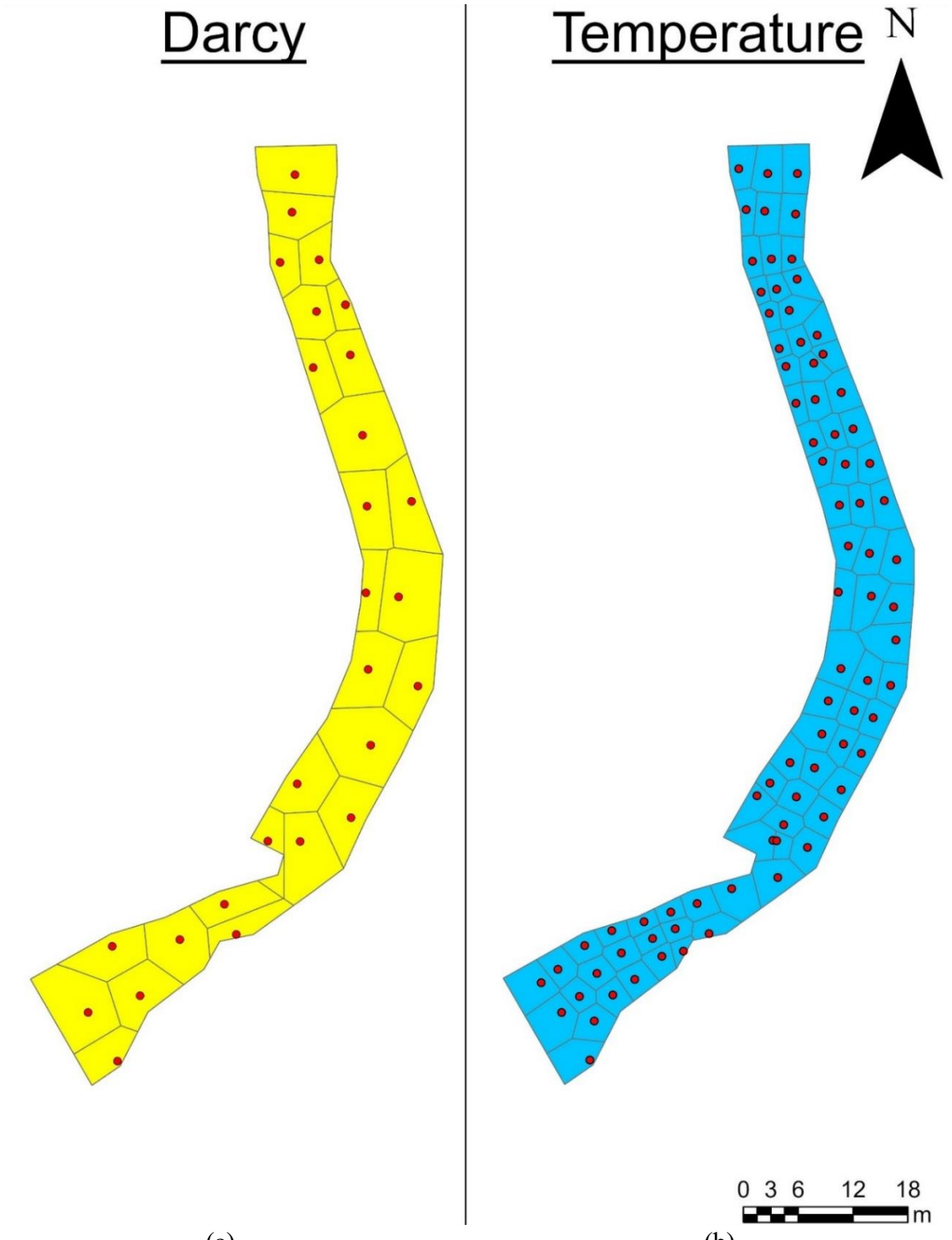
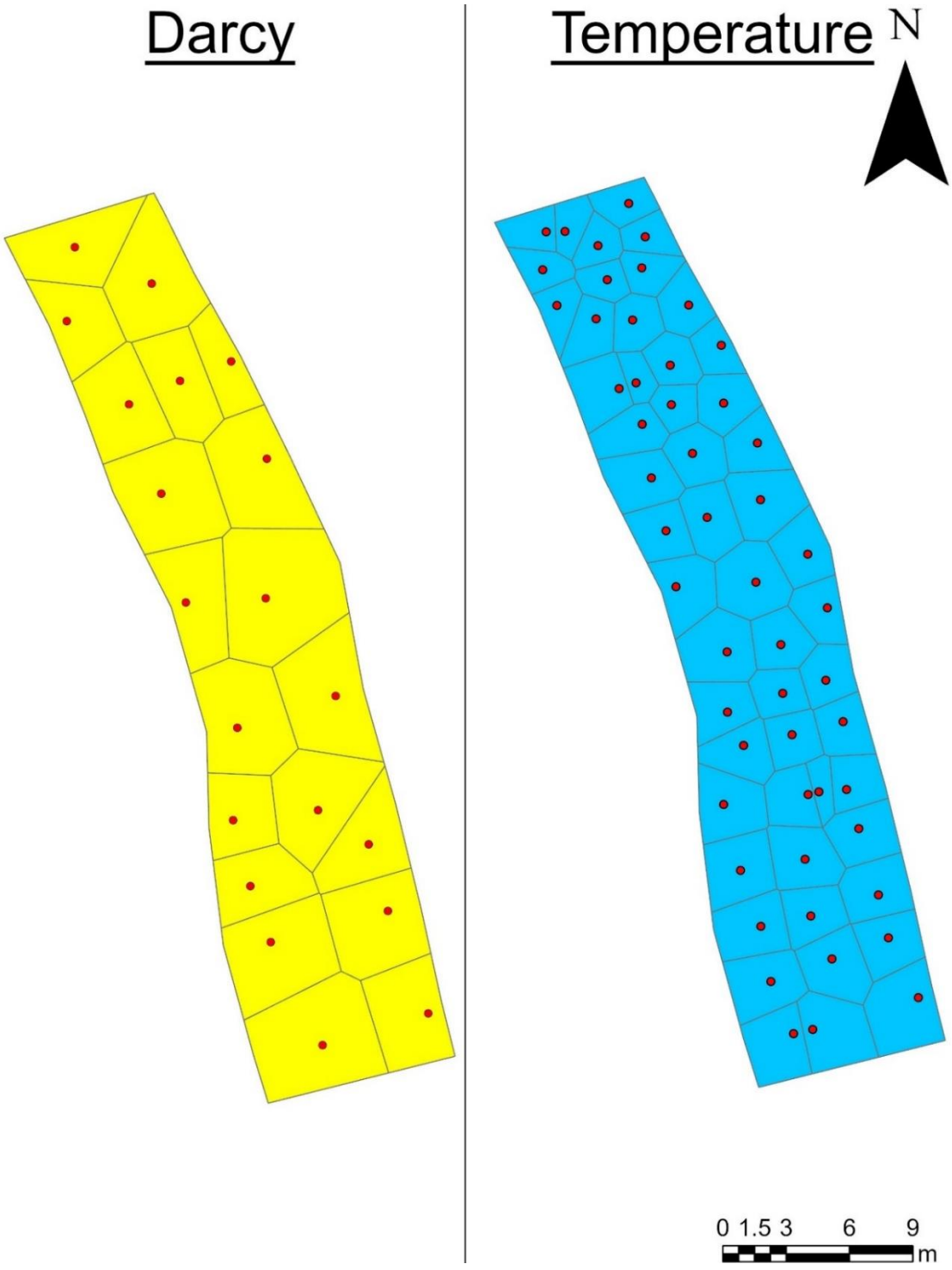



Figure 3.5: Map of Site 2 and piezometer installations. 'BMP' indicates 'bank mini-piezometer.'




(a) (b)

Figure 3.6: Examples of Thiessen polygon approach applied at Site 1 for (a) Darcy fluxes and (b) temperature profile fluxes.




(a) (b)

Figure 3.7: Examples of Thiessen polygon approach applied at Site 2 for (a) Darcy fluxes and (b) temperature profile fluxes.

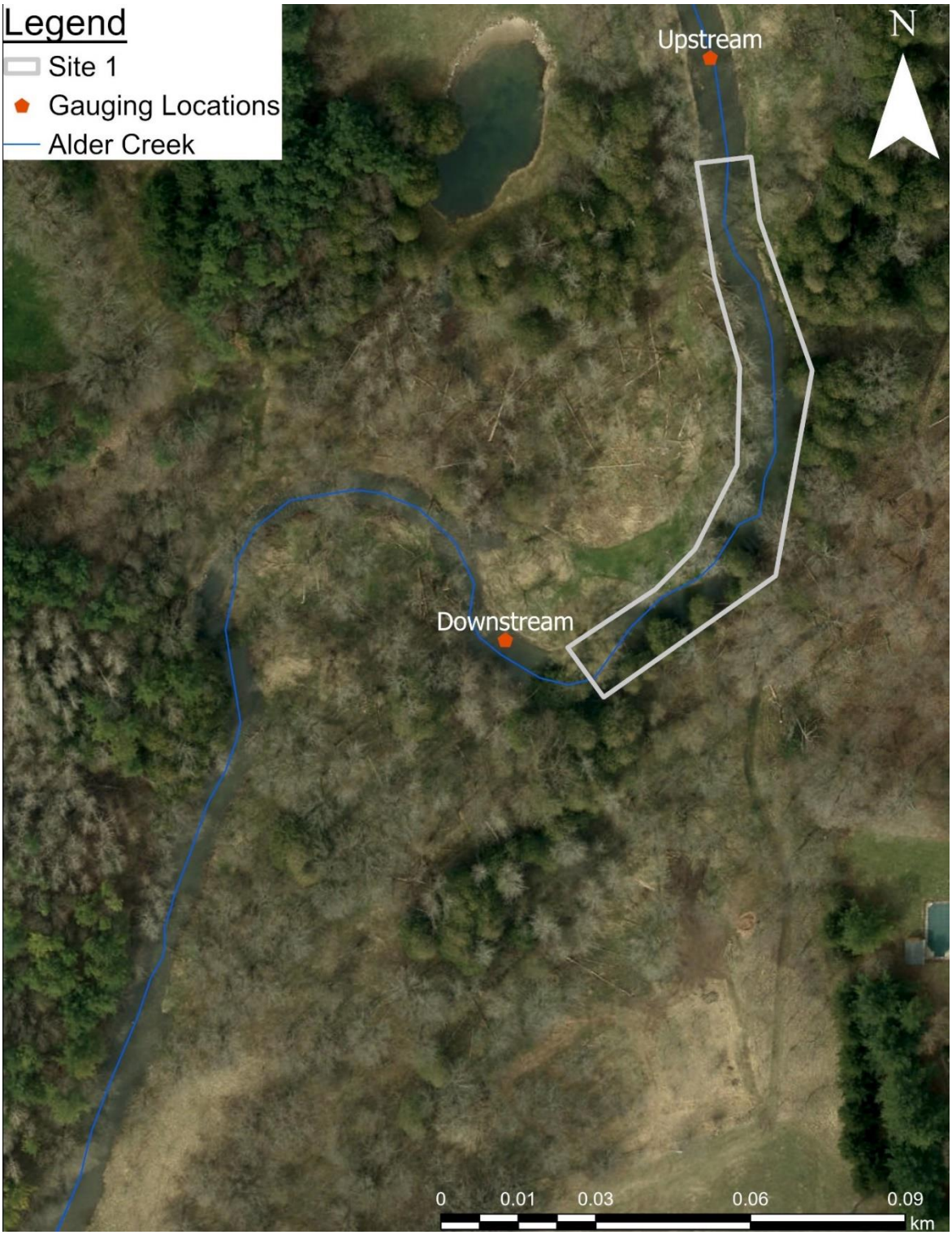


Figure 3.8: Stream gauging locations at Site 1 (Esri et al., 2025a).

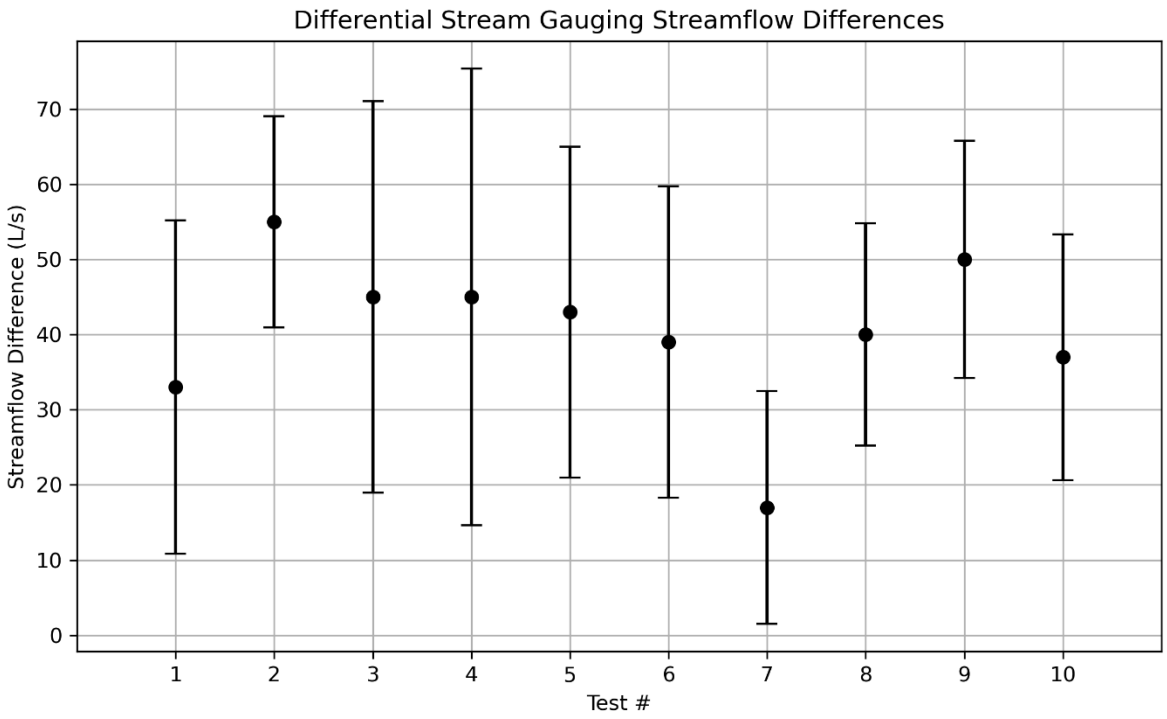
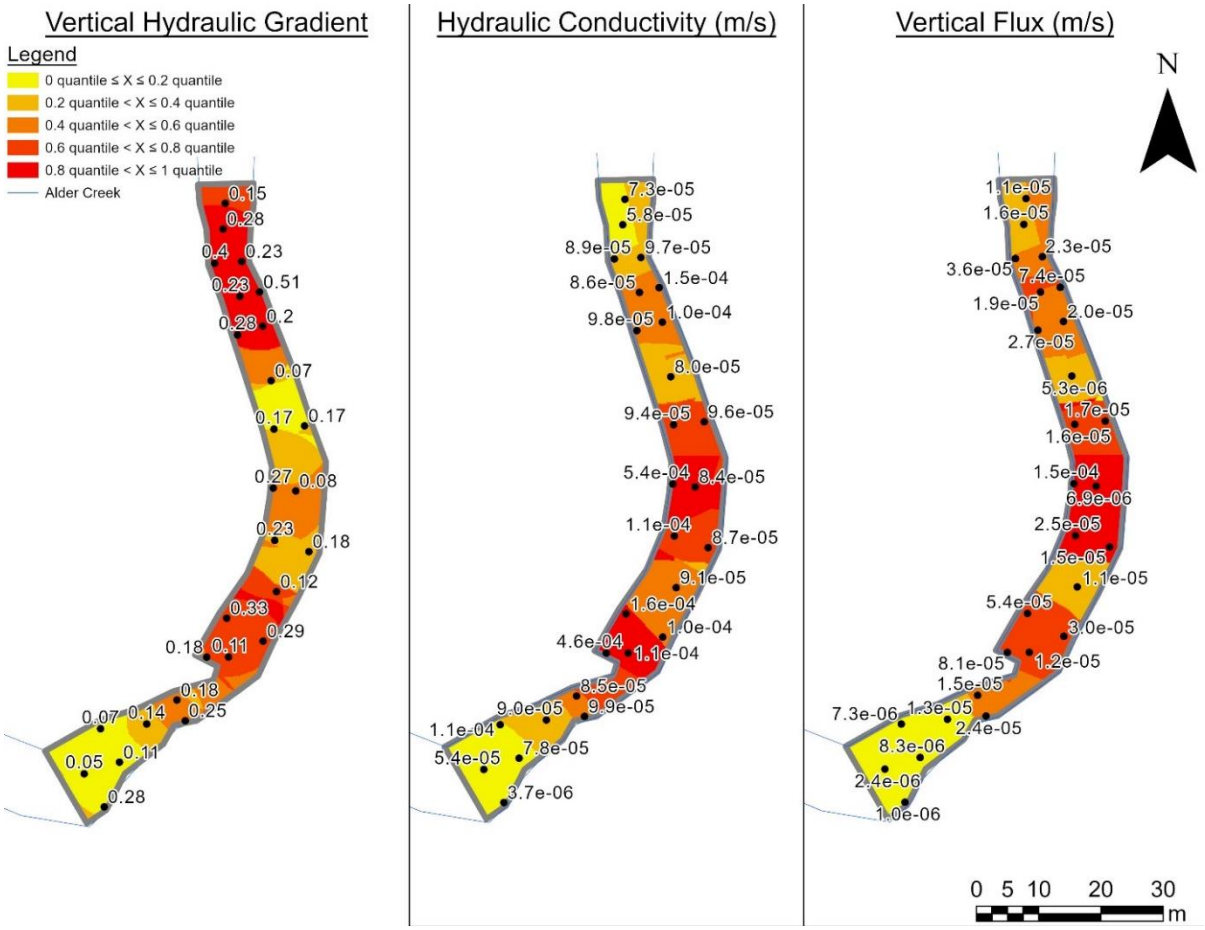
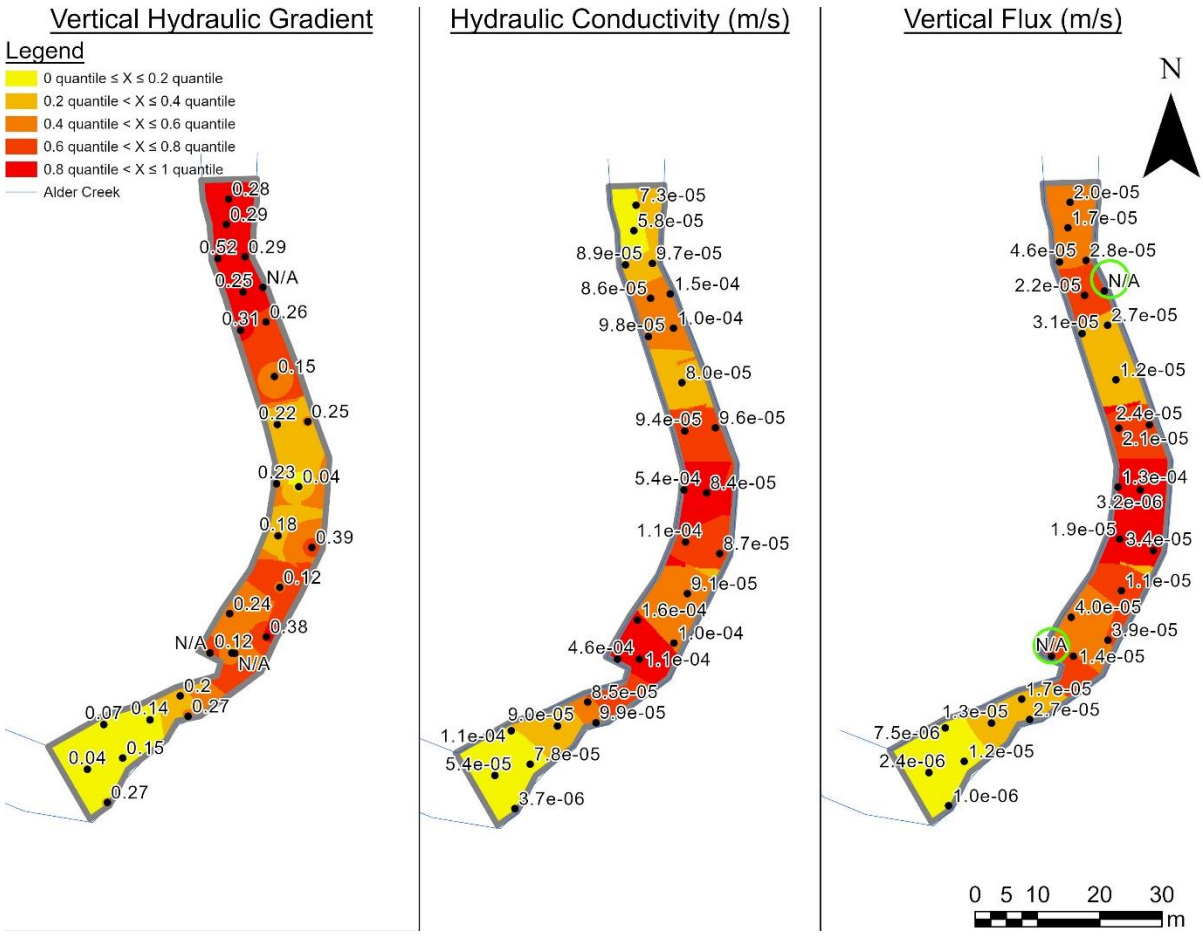



Figure 3.9: Differential stream gauging estimates of net increase in streamflow due to groundwater discharge. The error bars show the combined error resulting from the individual measurements, assuming 5% error for both upstream and downstream streamflow measurements.



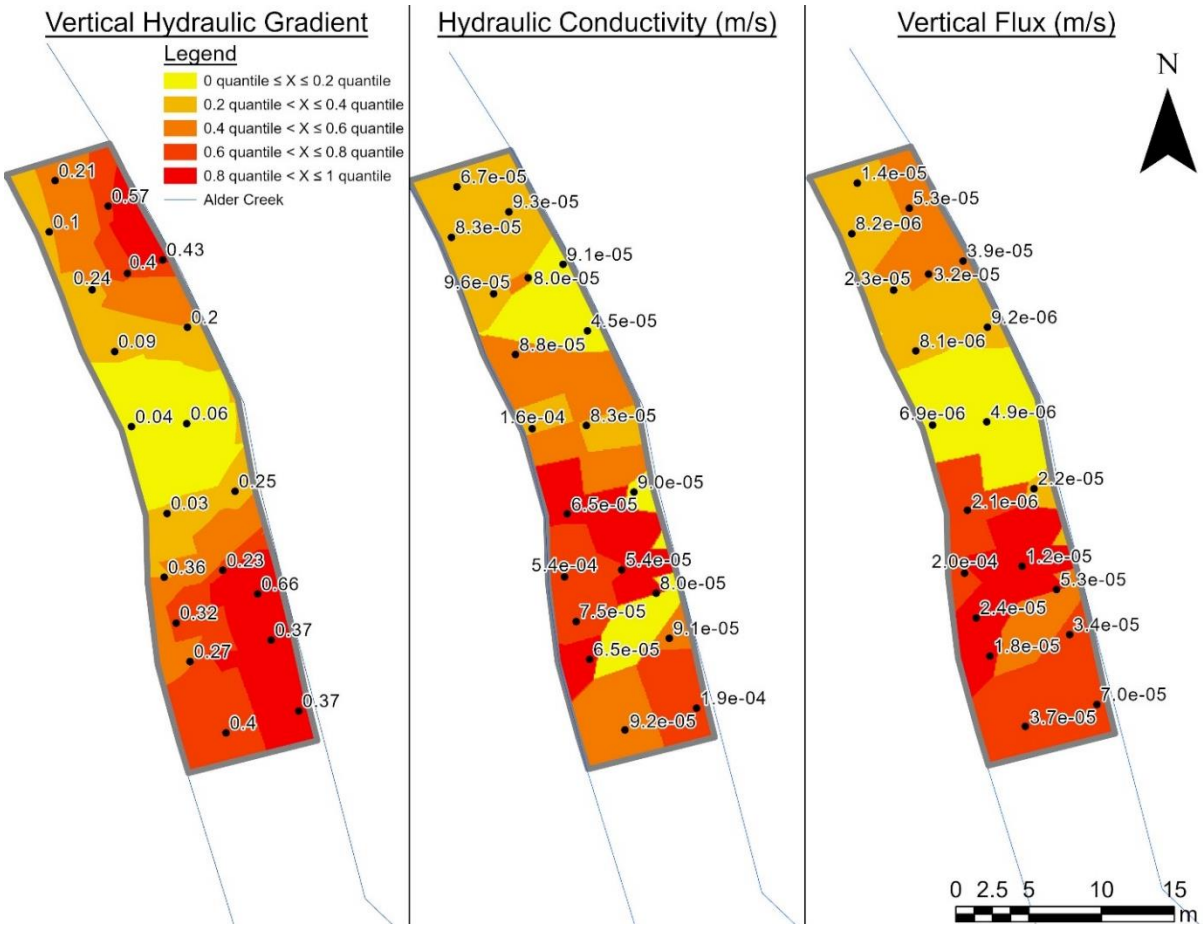

(a) (b) (c)

Figure 3.10: Site 1 (a) winter vertical hydraulic gradients, (b) horizontal hydraulic conductivities measured in May 2024, and (c) vertical fluxes estimated using Darcy's law.



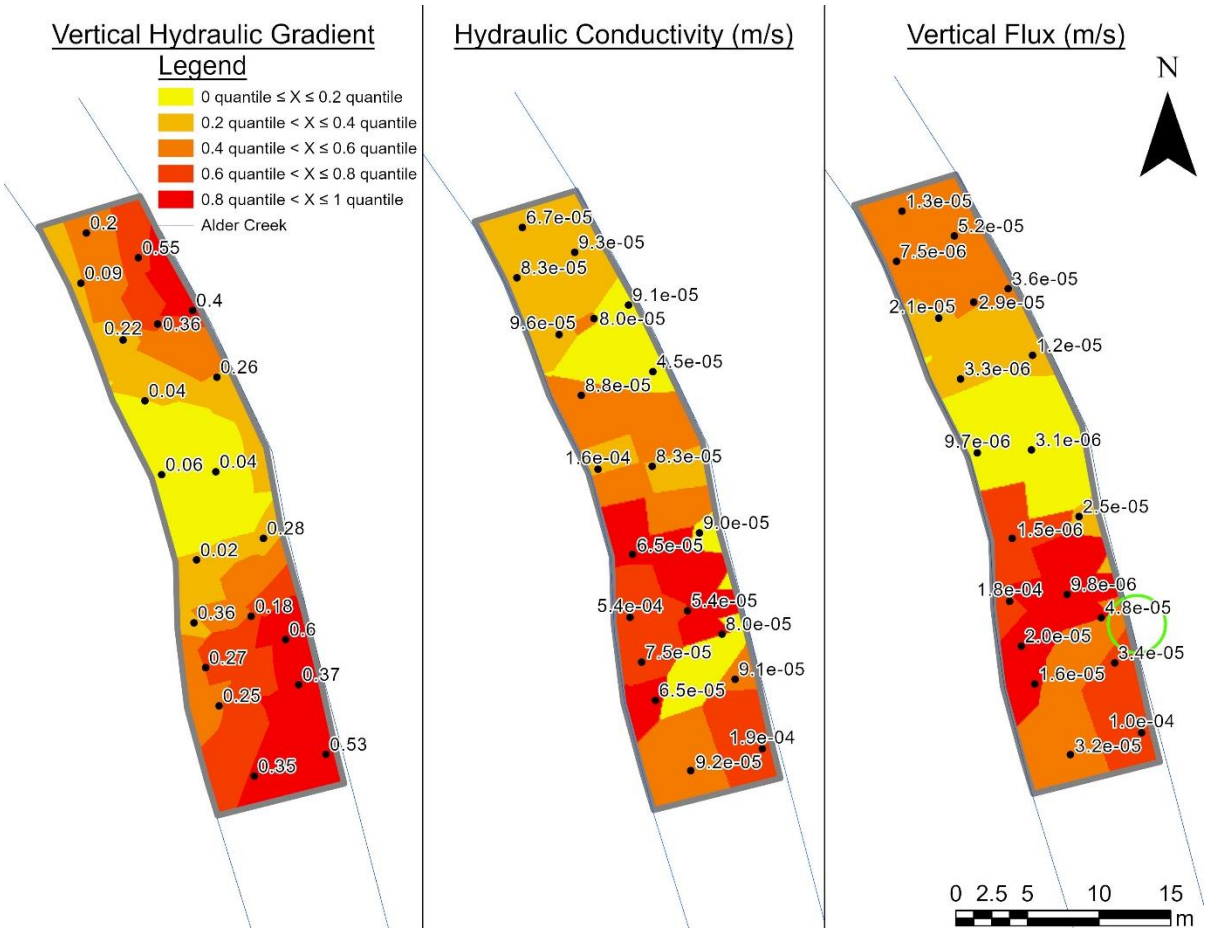

(a) (b) (c)

Figure 3.11: Site 1 (a) summer vertical hydraulic gradients, (b) horizontal hydraulic conductivities measured in May 2024, and (c) vertical fluxes estimated using Darcy's law.



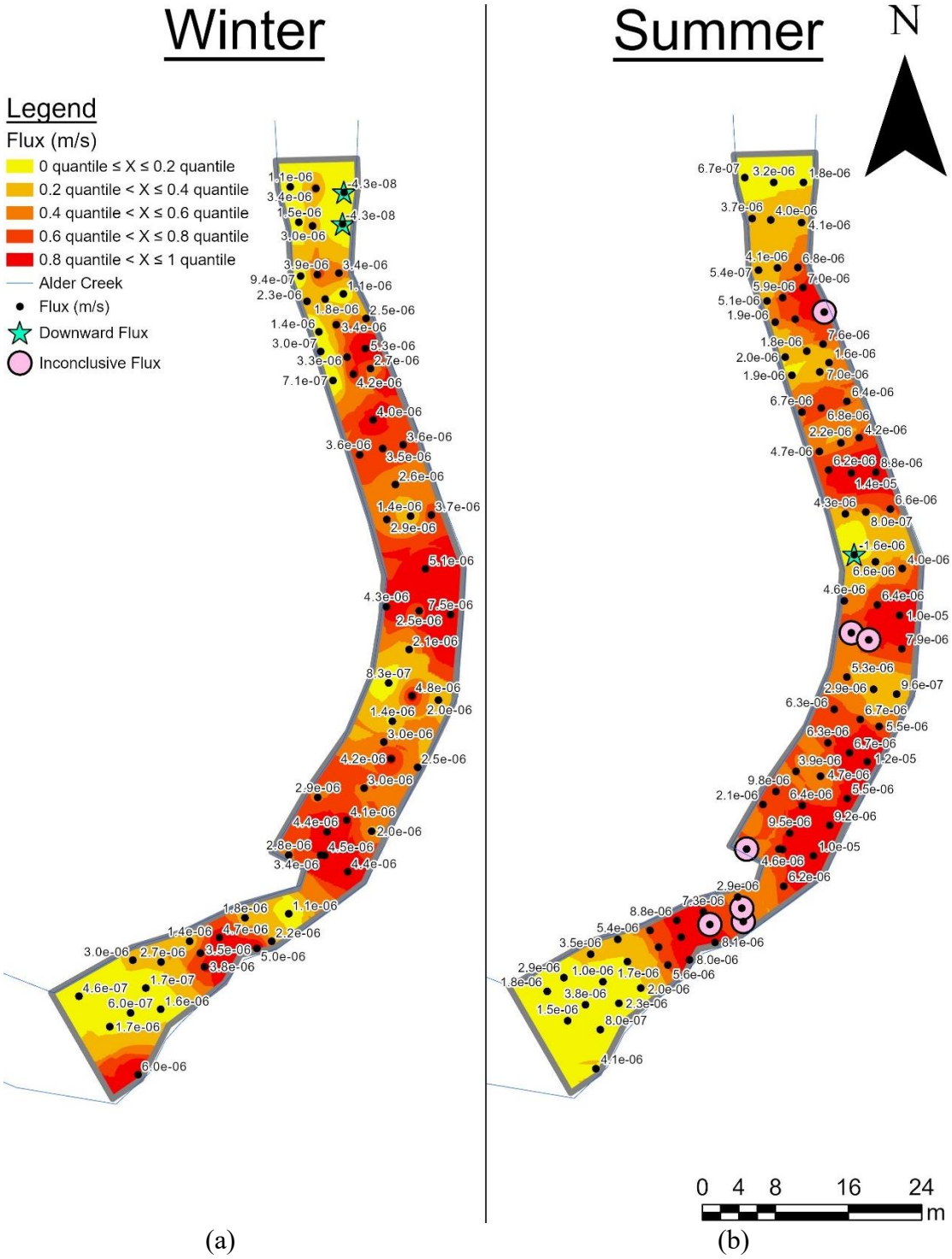

(a) (b) (c)

Figure 3.12: Site 2 (a) winter vertical hydraulic gradients, (b) horizontal hydraulic conductivities measured in May 2024, and (c) vertical fluxes estimated using Darcy's law.



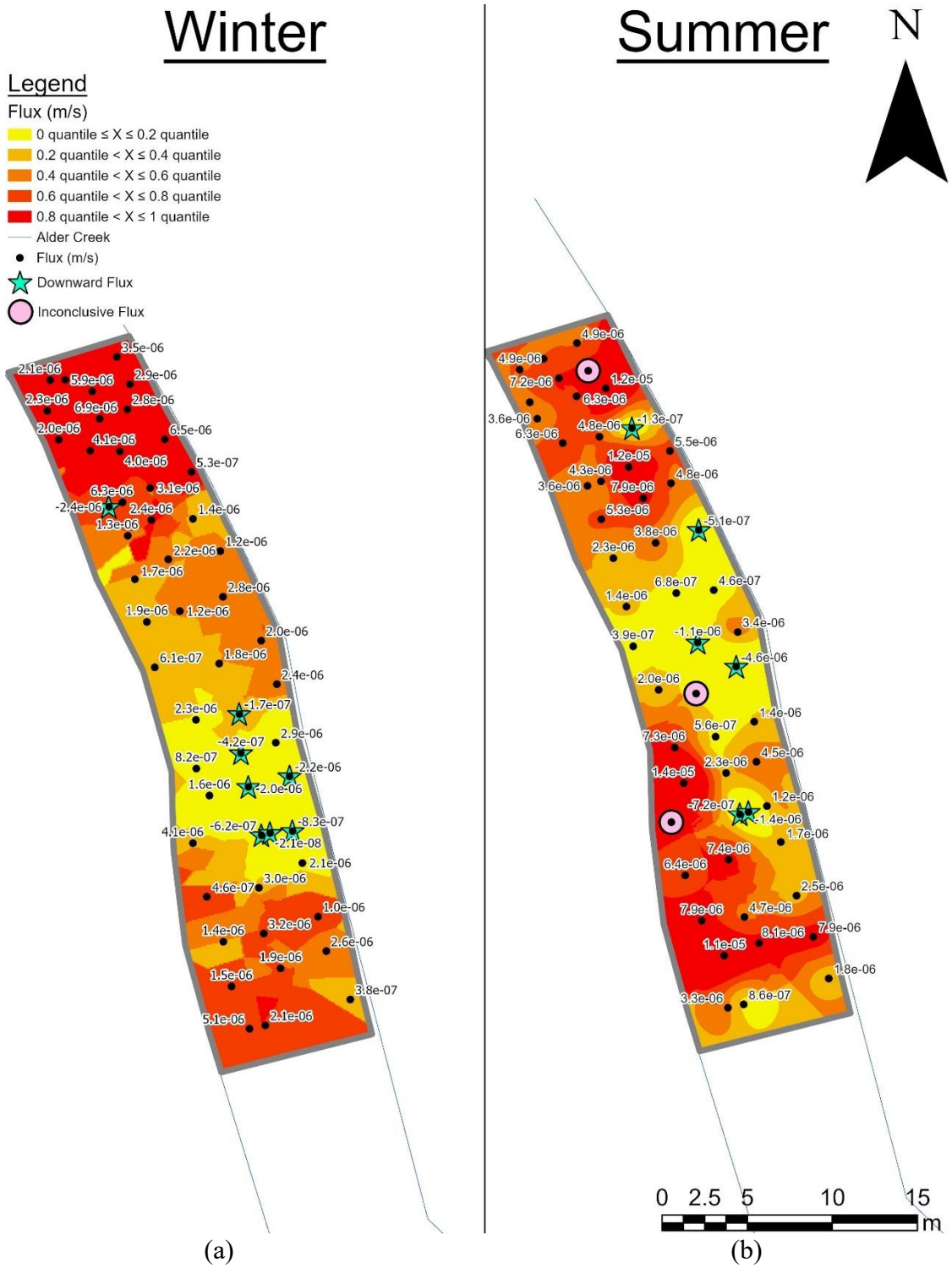

(a) (b) (c)

Figure 3.13: Site 2 (a) summer vertical hydraulic gradients, (b) horizontal hydraulic conductivities measured in May 2024, and (c) vertical fluxes estimated using Darcy's law.




(a) (b)

Figure 3.14: Vertical flux estimates based on streambed temperature profiles for Site 1 in (a) winter 2024 and (b) summer 2024.




(a) (b)

Figure 3.15: Vertical flux estimates based on streambed temperature profiles for Site 2 in (a) winter 2024 and (b) summer 2024.

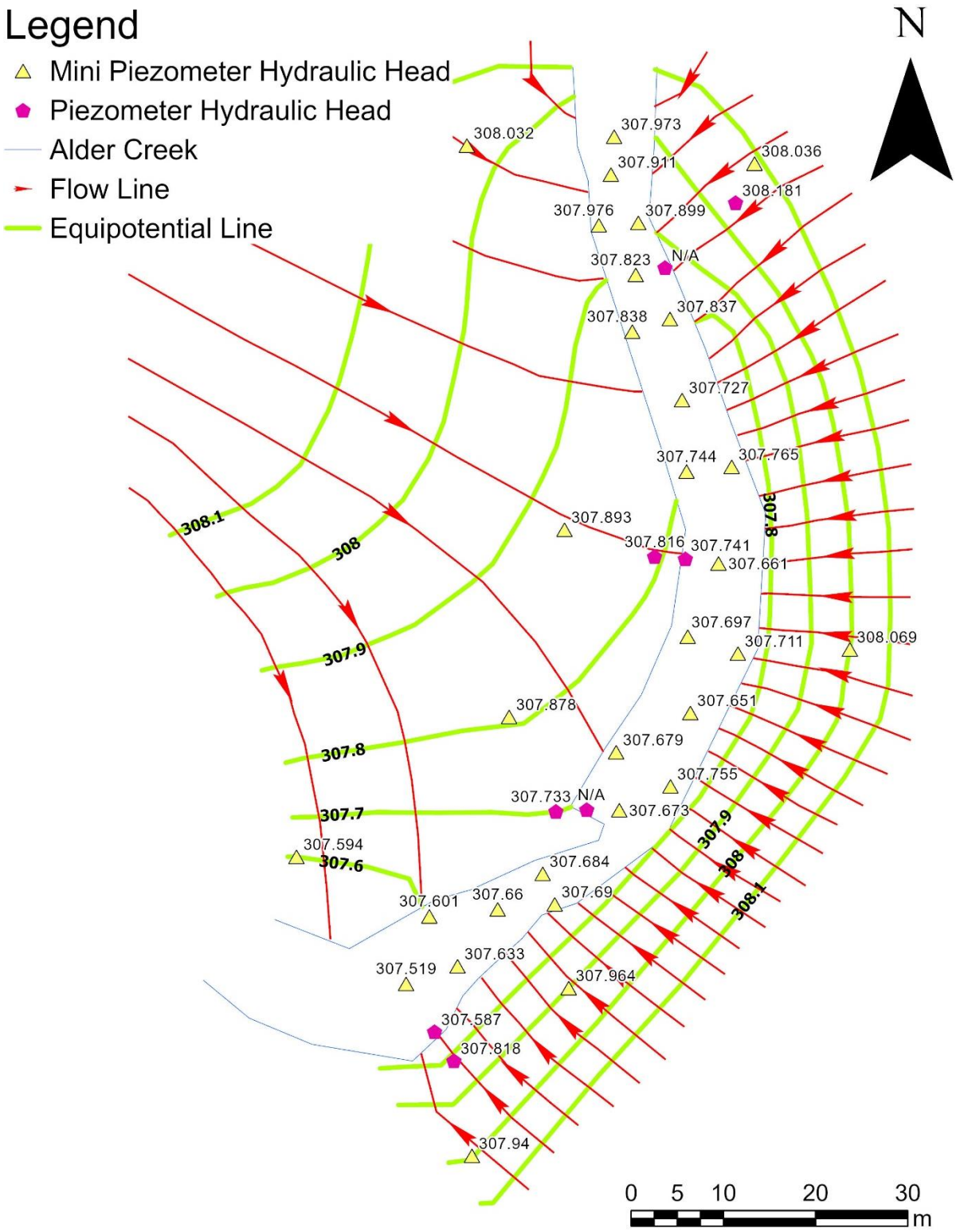



Figure 3.16: Groundwater flow net for Site 1 on August 20, 2024.

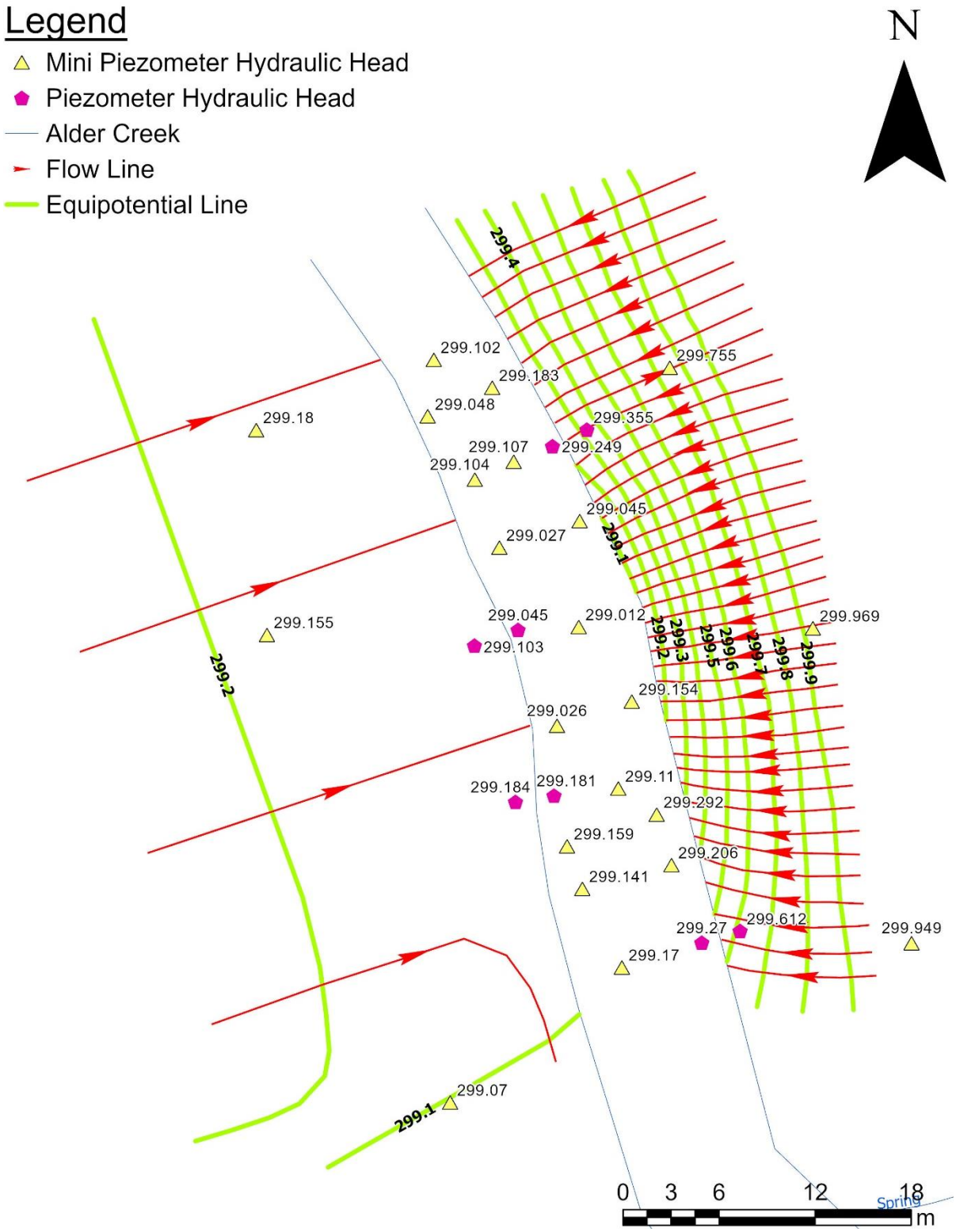



Figure 3.17: Groundwater flow net for Site 2 on August 23, 2024.

## 3.7 Tables

Table 3.1: Average vertical hydraulic gradient and vertical flux values from temperature profiling, determined from data collected at each streambed piezometer and resulting average vertical hydraulic conductivity.

| Site | Average Vertical Hydraulic Gradient | Average Vertical Flux (m/s) | Average Vertical Hydraulic Conductivity ($K_v$) (m/s) |
|---|---|---|---|
| **Site 1 - Winter** | 0.20 | $2.9 \times 10^{-6}$ | $1.9 \times 10^{-5}$ |
| **Site 1 - Summer** | 0.23 | $4.4 \times 10^{-6}$ | $2.9 \times 10^{-5}$ |
| **Site 2 - Winter** | 0.28 | $1.5 \times 10^{-6}$ | $1.1 \times 10^{-5}$ |
| **Site 2 - Summer** | 0.27 | $3.8 \times 10^{-6}$ | $3.7 \times 10^{-5}$ |

Table 3.2: Anisotropy ratios determined for both sites in the winter and summer using average horizontal hydraulic conductivity values determined from single well response test results and average vertical hydraulic conductivity values determined using temperature profiling related vertical flux estimates and vertical hydraulic gradient measurements applied to a rearranged form of Darcy's law.

| Site | Average Horizontal Hydraulic Conductivity (m/s) ($K_h$) | Average Vertical Hydraulic Conductivity (m/s) ($K_v$) | Anisotropy Ratio ($K_h/K_v$) |
|---|---|---|---|
| **Site 1 - Winter** | $1.2 \times 10^{-4}$ | $1.9 \times 10^{-5}$ | 6 |
| **Site 1 - Summer** | $1.2 \times 10^{-4}$ | $2.9 \times 10^{-5}$ | 4 |
| **Site 2 - Winter** | $1.1 \times 10^{-4}$ | $1.1 \times 10^{-5}$ | 10 |
| **Site 2 - Summer** | $1.1 \times 10^{-4}$ | $3.7 \times 10^{-5}$ | 3 |

Table 3.3: Summary of groundwater discharge estimates.

| **Study Site** | **Site 1** | | **Site 2** | |
|---|---|---|---|---|
| **Differential Stream Gauging** | 40 L/s | | N/A | |
| **Season** | **Winter** | **Summer** | **Winter** | **Summer** |
| **Temperature** | 2.7 L/s | 4.7 L/s | 0.7 L/s | 1.5 L/s |
| **Darcy (Isotropy)** | 19.3 L/s | 19.5 L/s | 10.5 L/s | 8.3 L/s |
| **Darcy (Anisotropy)** | 3.2 L/s | 4.9 L/s | 1.1 L/s | 2.8 L/s |
| **Average Horizontal Hydraulic Conductivity** | **All Piezometers** | **Each Bank's Piezometers** | **All Piezometers** | **Each Bank's Piezometers** |
| **Flow Net** | 4.7 L/s | 12.1 L/s | 1.7 L/s | 0.2 L/s |

# Chapter 4
# Assessing Temporal Variability in Groundwater-Surface Water Exchange Within a Stream Through Continuous Monitoring

## 4.1 Introduction

As a major contributor to streamflow throughout the year, groundwater-surface water exchange is crucial in maintaining surface water features and safeguarding the plant and animal species that depend on these aquatic ecosystems. This is especially true when precipitation is low, as baseflow becomes the primary contributor to streamflow. However, because of external pressures, such as urbanization, groundwater pumping, extensive agricultural practices and climate change, concern is growing with regards to the impact these threats may have on water quantity and quality of surface water features, such as creeks and rivers.

Decreases in baseflow rates have been documented at both local and regional scales in response to increasing long-term groundwater extraction, as a result of growing populations and subsequent increased demand for water (Barlow & Leake, 2012; Zipper et al., 2024). These decreases in baseflow have led to declines in streamflow, ultimately putting creeks and rivers at risk (Barlow & Leake, 2012; Zipper et al., 2024). As a result of the increased unpredictability of the timing and volume of annual precipitation and snowmelt brought on by climate change, uncertainty has grown with regards to the ability to accurately forecast expected groundwater recharge, storage, and discharge (Dubois et al., 2022; Green et al., 2011; Taylor et al., 2013).

The growing influence of climate change on groundwater-surface water exchange emphasizes the importance of better understanding its temporal variability. Through an improved understanding of how groundwater-surface water interactions respond to weather events and seasonality, knowledge can be gained, and data can be collected to help support the next generation of integrated hydrogeologic modelling tools, which will assist in developing water management strategies at multiple scales. With these tools, Best Management Practices (BMPs) can be designed and implemented to support sustainable groundwater management, while at the same time preserving surface water features.

The temporal variability of groundwater-surface water interactions has been assessed in a variety of ways. A commonly used technique is baseflow separation, which uses graphical methods (Sloto

and Crouse, 1996) or digital filter methods (Aksoy et al., 2009; Chapman and Maxwell, 1996; Eckhardt, 2005; Furey and Gupta, 2001) to distinguish between the baseflow component and the quick flow component of a streamflow dataset. Graphical methods apply differing criteria, while digital filter methods are more complex approaches that apply numerical algorithms (Cheng et al., 2022). Through the association of long-term water level data with streamflow rating curves, streamflow datasets can be generated and subsequently used for baseflow separation. While a useful approach to quantify groundwater discharge (gaining conditions) over time, this technique is limited in its ability to assess groundwater recharge (losing conditions).

Differential stream gauging is a technique that involves measuring streamflow at two locations and finding the difference, to quantify groundwater-surface water exchange over a reach of study (Becker et al., 2004; Cey et al., 1998; Harte & Kiah, 2009; McCallum et al., 2012). However, this approach is normally used for snapshot measurements and is not commonly applied to assess temporal variability in groundwater-surface water exchange. Another technique that is more applicable to assessing groundwater discharge and recharge conditions is the monitoring of hydraulic gradients over time. This technique allows for the magnitude and direction of groundwater flow over time to be assessed. Upward vertical hydraulic gradients in surface water features, and horizontal hydraulic gradients in the direction of surface water features, are likely signs of groundwater discharge conditions, while under groundwater recharge conditions the opposite would be expected. The monitoring of hydraulic gradients over time has been done in previous studies through both manual readings and continuous monitoring using data loggers (Käser et al. 2009; Malcolm et al. 2006; Puckett et al., 2008).

The goal of the current study is to gain an improved understanding of the temporal variability of groundwater-surface water exchange within a perennial stream system throughout the annual seasonal cycle, through the application of several different techniques. This was supported through insight provided by historical surface water level data previously collected within the Alder Creek watershed, combined with recent surface water and groundwater level data that was collected over an annual cycle at two study sites along Alder Creek. This new water level data not only provided valuable info on water level temporal variability but also allowed for the development of continuous hydraulic gradient and differential stream gauging datasets, providing deeper insight into groundwater-surface water exchange over time.

## 4.2 Methodology

### 4.2.1 Field Site

Alder Creek is a perennial stream that is approximately 15 km in length from the headwaters to the confluence with the Nith River, and is located within the 79 $km^2$ Alder Creek watershed, a sub watershed of the greater Grand River watershed located in southwestern Ontario (Figure 4.1). The creek is largely groundwater fed, including by a number of smaller, spring-fed tributaries found within the upper to middle reaches of the watershed. Air temperatures in this area range significantly, with a minimum daily average of -10.2°C measured in January, to a maximum daily average of 26.2°C in July (Government of Canada, 2025a). The rate of average annual precipitation is approximately 900 mm per year, while the rate of average groundwater recharge is approximately 320 mm per year (Government of Canada, 2025a; Matrix and SSPA, 2014; Wiebe et al., 2022). Due to its location within the south-central portion of the Waterloo Moraine, which is a significant topographic relief feature in the area, the surficial geology of the watershed is heterogeneous (Figure 4.2), and composed of a number of glacial till sheets that were deposited during the advance and retreat of glaciers in the region, that are interlayered with glaciofluvial sand and gravel deposits (Bajc et al., 2014; CH2MHILL and SSPA, 2003; Karrow, 1993; Martin & Frind, 1998). Many wells in the Regional Municipality of Waterloo are screened within these glaciofluvial sand and gravel deposits, which supply much of the area's water.

Some of the wells screened within these glaciofluvial sand and gravel deposit can be found in the Mannheim West wellfield (Figure 4.2), which is located within the Alder Creek watershed, and supplies approximately 40% of the total groundwater extracted within the City of Kitchener, Ontario (Sousa et al., 2014; Matrix and SSPA, 2014; Wiebe et al., 2023). However, as water demands increase in response to significant population growth in this expanding urban center, increased demand for groundwater is expected. As urbanization within the watershed expands (e.g., development of buildings, roads, etc.), and the influence of climate change increases (through for example increasingly unpredictable weather patterns), groundwater recharge rates are expected to change. Due to this multitude of factors, concerns regarding their effects within the Waterloo Moraine's aquifer system, and their impact on baseflow to Alder Creek and the aquatic ecosystems within it, are increasing.

### 4.2.2 Study Sites

Site 1 is a 110 m long reach located in the mid to lower region of the Alder Creek watershed, within the community of New Dundee, Ontario (Figures 4.1 and 4.3a). This study reach is located at a meander bend and is on average 8 m in width. The average depth of the stream in the summer, during low flow conditions, is on average approximately 0.4 m but reaches maximum depths of 1 m in pools. Streamflow measurements ranged from 0.1 $m^3/s$ to 5.6 $m^3/s$ at the site. The streambanks at this site tend to have a steep rise, and contain a mixture of trees, shrubs, and grasses. Along select sections of the reach, an increased presence of shrubs and grasses are found where more gradual sloping streambanks are present. The surficial geology of the streambed consists of largely cobbles and gravel, with the inner bank of the bend largely silt. Based on streambed horizontal hydraulic conductivity estimates made through single well response tests and qualitative observations made during instrument installation, the working conceptual model of the study site indicates predominantly sand beneath the streambed interface.

Site 2 is a 40 m long reach located in the lower regions of the Alder Creek watershed, approximately 3 km downstream of Site 1 (Figures 4.1 and 4.3b). This study reach is relatively straight, and approximately 8.5 m wide. The stream depth in the summer, during low flow conditions, is on average approximately 0.6 m and reaches depths as great as 0.7 m. Streamflow at the site was found to range from 0.3 $m^3/s$ to 4.2 $m^3/s$. The eastern streambank is dominated by trees, and has a sharply rising topography, while the western streambank, which is vegetated predominantly by shrubs and grasses, rises much more gradually. The surficial geology is predominantly gravels and cobbles, with fine-grained deposits along the western streambank, looking downstream. Beneath the streambed interface, a sandy material is presumed to be present based on qualitative observations similar to those made at Site 1, and streambed horizontal hydraulic conductivity estimates. These streambed hydraulic conductivities, and all other field data collected over the course of this study can be found in Zanatta et al. (2025).

### 4.2.3 Instrumentation at Study Sites

Conventional PVC piezometers (1” and 1 ½” ID) and mini-piezometers (1/4" ID) were installed in the streambed and in the streambank at both study sites, to collect water level data and conduct single-well response tests. These piezometers installations were spatially distributed relatively evenly across the reaches of study. Site 1 (Figure 4.4) had 23 mini-piezometers and 4 conventional piezometers

installed in the streambed, while Site 2 (Figure 4.5) had 16 mini-piezometers and 4 conventional piezometers installed in the streambed. On the streambank of both sites, 4 conventional piezometers were installed, with 2 on each streambank.

The Lee and Cherry (1979) approach was applied as part of the mini-piezometer installation, using an extractable temporary drive casing. The streambed conventional piezometers were manually driven into the streambed using a sledgehammer. During installation, the natural collapse of streambed material around the piezometer screens was assumed, sealing them, and ultimately reducing the risk of unwanted vertical flow. Auguring by hand was performed for each piezometer installation on the streambank until the water table was reached; this was then followed by the manual driving of the piezometers into the streambank until the desired depths were reached. After installation was complete, filter sand was added, followed by bentonite, to produce a watertight seal in order to minimize the risk of unwanted vertical flow. For each conventional PVC streambed piezometer, stilling wells were attached just above the streambed, allowing for data loggers to be installed in order to collect continuous surface water level data. These stilling wells were designed using screens from 1" ID conventional PVC piezometers that were capped at the bottom to keep the installed data loggers in place. The piezometers were installed so that the midpoints of all of their screens ranged from depths of between 40 and 55 centimetres below the streambed. The screen lengths of the mini-piezometers were approximately 15 cm (perforated and Nitex® wrapped), while those of the conventional piezometers were approximately 30 cm (slotted). After installation was completed, the piezometers were developed, and the elevations and coordinates were surveyed using a Sokkia GCX3 GNSS receiver surveying device, a total station, and an automatic level.

### 4.2.4 Surface Water Level, Groundwater Level and Hydraulic Gradient Measurements

Manual surface water and groundwater level readings were made approximately bi-weekly in each streambed mini-piezometer and each streambed/streambank conventional piezometer. For the conventional piezometers, readings were made using a water level tape, with respect to the top of the piezometer casing, whose elevations were surveyed. For the mini-piezometers, a ruler stick was placed on steel plates that were fastened to the piezometer and installed flush to the streambed. Using the plate as reference, surface water and groundwater levels were made following purging of any air bubbles. To measure continuous surface water and groundwater levels, data loggers, recording at 15 minute intervals were installed in all of the conventional PVC piezometers and in associated stilling

wells. The consistency of the mini-piezometer screen depths below the streambed was verified using the known piezometer length.

Using the known installation depths of the piezometers, along with the manual and continuous surface water and groundwater levels, vertical hydraulic gradients were calculated. To measure the horizontal hydraulic gradients, the conventional piezometers installed on the streambanks at the study sites were used in conjunction with an associated conventional streambed piezometer, with two sets installed on each side of the stream at the study sites (Figures 4.4 and 4.5). Using the distance between the sets of conventional piezometers and the groundwater levels measured in each piezometer, horizontal hydraulic gradients were calculated. These periodic and continuous long-term datasets provided valuable information on the temporal variability of both the vertical and horizontal hydraulic gradients at each study reach.

This study also incorporated a historical surface water level dataset, managed by the National Hydrological Service (NHS) of Canada, to assist in the evaluation of temporal groundwater-surface water exchange. Surface water level data were collected daily from January 2002 to December 24, 2025, at the Huron Road hydrometric station. This station (02GA030) is located in the middle of the watershed and upstream of the study sites (Government of Canada, 2025b) (Figure 4.1).

### 4.2.5 Trend Analysis

To assess trends in the hydraulic gradient time series data, in support of visual observations, the modified Mann-Kendall test (Hamed & Rao, 1998) was used. This is a non-parametric test that identifies trends in time series data. Unlike the standard Mann-Kendall test, this test accounts for autocorrelation in which current values are statistically influenced by previous values, a common occurrence in hydrologic data (Hamed & Rao, 1998). This trend analysis test was applied over three-month intervals for both the vertical and horizontal hydraulic gradient datasets. The trend analysis coincided with the start of the Site 1 dataset, and the time intervals also correlating relatively well with the four seasons.

### 4.2.6 Stream Gauging

Stream gauging was performed just upstream, and about 200 metres downstream of Site 1 (Figure 4.6). At these gauging stations, water levels were continuously recorded over the course of the study, from November 7, 2023, to August 31, 2024, using streambed brackets fixed to the streambed, with

Solinst Leveloggers® installed inside. Streamflow measurements were collected between early October 2023 and early June 2025 at the gauging stations. A Sontek FlowTracker Handheld ADV® was applied from October 5, 2023, to January 30, 2024, with streamflow values determined using the six-tenths-depth method, where the velocity measured at 0.6 of the depth below the surface is used as the mean velocity. From March 12, 2024, to June 11, 2025, a StreamPRO® acoustic doppler current profiler (ADCP) was used to determine streamflow values. Following each streamflow measurement, manual stream water level readings were taken relative to the streambed logger brackets installed flush with the streambed, to correlate the streamflow values with a stream stage.

Streamflow values were collected over a wide range of stream stages, including baseflow conditions, allowing for detailed rating curves to be developed for each gauging station. The rating curves were then applied to the water level data collected, producing a long-term continuous streamflow dataset at each gauging station. To estimate the net gain or loss in streamflow between the gauging locations, the difference in streamflow was calculated between the gauging locations. If the net difference between these gauging locations was positive, groundwater discharge conditions (i.e., gaining) were assumed over the reach of study; if the net difference was negative, groundwater recharge conditions (i.e., losing) were estimated over the reach of study. Using these continuous datasets, insight into the variability in groundwater-surface water exchange over time could be assessed. With respect to Site 2, due to the short length of the study reach caused by land access limitations, stream gauging was not performed.

## 4.3 Results

### 4.3.1 Continuous Surface Water and Groundwater Levels

The long-term continuous surface water and groundwater level data collected at each study site shows a general trend at both study sites, as seen in Figures 4.7a and 4.7b. Beginning in November 2023, both study sites had groundwater and surface water levels that appeared to slowly rise until approximately February, where they remained relatively constant throughout much of the wet season, until approximately May. Beginning around May, a slow decline in water level began, and continued throughout the remainder of each site's study period, which ended in August and November, respectively. In support of these findings, a very similar trend was visible for this same time interval

in the long-term daily surface water level data collected at the upstream hydrometric data station (02GA030) (Figure 4.7c).Within this dataset, water levels appeared to reach their low during the summer period, between approximately July and September; this was then followed by a rise until approximately February/March, where water levels remained relatively high until around May, which was then followed by a decline into the summer months once again. This ongoing dataset, which dates back to January 1, 2002, also appeared to exhibit this same sinusoidal pattern year after year (Figure 4.8).

### 4.3.2 Periodic Vertical Hydraulic Gradients

Long-term, bi-weekly monitoring of vertical hydraulic gradients using the mini-piezometers installations in the streambed took place between November 2, 2023, and October 29, 2024, at Site 1, and from December 1, 2023, to August 23, 2024, at Site 2. Consistent upward vertical hydraulic gradients were measured in each mini-piezometer at both sites over the course of the study. While the data appears to show some variability over time, the degree of variability differs between mini-piezometers. The change in vertical hydraulic gradients over time (i.e. when hydraulic gradients were rising/falling) does not seem to be consistent throughout the mini-piezometer networks, making it difficult to identify any possible seasonal trends related to the vertical hydraulic gradients. In addition, no noticeable trends pertaining to changes in stream stage, following high flow events, were visible within the dataset. The manual reading datasets were limited, as readings were made only approximately bi-weekly, leaving significant periods of time when no data was collected. This limitation ultimately made it challenging to identify the effect of seasonal and stream stage variation on vertical hydraulic gradients, even if they did exist, and emphasizes the need for increased frequency of measurement in order to gain greater insight from manual readings.

### 4.3.3 Continuous Vertical Hydraulic Gradients

Continuous surface water and groundwater level data were collected between November 7, 2023, and November 7, 2024, at Site 1, in order to capture a much clearer temporal record of vertical hydraulic gradient variation (Figure 4.9). As seen in Figure 4.9, each conventional piezometer at Site 1 has a consistently upward vertical gradient present, matching with the manual readings. The increased resolution of this dataset lends greater confidence to the interpretation of groundwater discharge conditions being continuously present throughout the year at these piezometer locations, and likely for the rest of the study site. Rapid stream stage increases (i.e., hydrograph peaks), during high flow

events (e.g., rainfall and snow melt), resulted in a decline in the hydraulic gradient; as the stream stage declined following the event, the hydraulic gradient then temporarily increased, followed by a decline to a more stable hydraulic gradient. This is likely a result of the groundwater having a delayed response to the event, relative to changes in stream stage. The declines in the vertical hydraulic gradient largely appeared to be more pronounced following more significant changes in stream stage, associated with the larger flow events. Reversals of the hydraulic gradients were rare and short lived and only appear to have occurred for select piezometers in response to the most extreme flow event in July of 2024.

Unlike the bi-weekly vertical hydraulic gradient readings, the greater resolution of these continuous datasets allowed for improved visual interpretation, and the use of the modified Mann-Kendall trend test (Hamed & Rao, 1998), which was applied over 3 month intervals to assess temporal variability. Notable seasonal trends appeared to exist in the datasets, but were not consistent between all piezometers, and not all the trends were statistically significant. With regards to piezometers 1 and 13, changes in vertical hydraulic gradients over time appeared to be similar (Figure 4.9) (Table 4.1). Initially, between early November 2023 and early February 2024, vertical hydraulic gradients appeared to differ as piezometer 13 showed a slight increase in hydraulic gradient, while piezometer 1 showed a slight decrease. This was, however, followed by a consistent trend over the next 3-time intervals of the trend analysis. Between early February 2024 and early May 2024, both piezometers showed a noticeable decrease in vertical hydraulic gradient, while between early May 2024 and early August 2024, both piezometers once again showed a clear increasing trend in the hydraulic gradient. Finally, between early August 2024 and early November 2024, a decrease in the vertical hydraulic gradient was visible. With respect to piezometers 3 and 11, while the datasets stopped in mid July 2024 due to equipment damage following a major storm event, for the initial 9 1/2 months this seasonal pattern was not visible, with hydraulic gradients appearing relatively consistent over time (Figure 4.9).

Using data collected at Site 2 between December 1, 2023, and August 29, 2024, Figure 4.10 shows a pattern very similar to Site 1 with regards to the effect of high flow events on vertical hydraulic gradient. With regards to the effect of seasonality on vertical hydraulic gradient variability, noticeable seasonal trends appear to exist based on visual interpretation, and with the assistance of the modified Mann-Kendall trend test but were once again not consistent between all piezometers. Changes in vertical hydraulic gradients over time appeared to be similar at piezometers 5, 7 and to a lesser degree

9 (Figure 4.10) (Table 4.2). Beginning in early December 2023, vertical hydraulic gradients rise until late January/early February, followed by a decline in hydraulic gradients until around May/June. This was then followed by a rise in vertical hydraulic gradients until mid-August, followed by a possible decline as seen in piezometer 5, although interpretation over this interval was limited as the datasets at this site ended in late August. Variability in the vertical hydraulic gradient appeared to be less pronounced for piezometer 9. The vertical hydraulic gradient at piezometer 15 appeared to be consistently upward but was low in comparison to the other piezometers and showed little similarity to the other data sets with regards to seasonal variability (Figure 4.10) (Table 4.2). Unlike the limited bi-weekly vertical hydraulic gradients, the continuous hydraulic gradient data allowed for temporal trends to be identified, providing insight into the seasonality of groundwater-surface water exchange. In addition, it also provided an improved understanding of how groundwater-surface water exchange responds during high flow events.

### 4.3.4 Continuous Horizontal Hydraulic Gradients

Horizontal hydraulic gradients measured across the Site 1 study reach (Figure 4.11), between November 7, 2023, and November 7, 2024, were positive throughout the study, indicating groundwater flow in the direction of the stream. A similar pattern to the vertical hydraulic gradient data was observed during high flow events. These events often appeared to result in a rapid drop in the hydraulic gradient, followed by a temporary increase, before returning to a more stable hydraulic gradient. Some of the more extreme flow events appeared to result in the reversal of the hydraulic gradient, indicating temporary groundwater flow away from the stream for a brief period of time. Variability in the horizontal hydraulic gradients over the course of the study was small for most of the piezometer pairs. With regards to temporal trends, while not highly variable, piezometer sets 11-12 and 13-14 appeared to exhibit an increasing hydraulic gradient, while piezometer sets 1-2 and 3-4 had relatively consistent, if not declining, horizontal hydraulic gradients over time (Figure 4.11) (Table 4.3). These results indicate possible differences in how these two streambanks horizontal hydraulic gradient respond to temporal trends.

The horizontal hydraulic gradients measured between December 1, 2023, and August 29, 2024, across the Site 2 study reach (Figure 4.12) were only consistently positive for 3 sets of piezometers, piezometer set 7 and 8 exhibited a negative hydraulic gradient for part of the year, until May 2024, indicating flow away from the stream. High positive hydraulic gradients were observed between

piezometer set 9 and 10, where hydraulic gradients hovered between 0.15 and 0.2, indicating notable spatial variability across the study site. Again, the response of the horizontal hydraulic gradients during high flow events were similar to those previously noted for Site 1. Long-term temporal variability also appeared to be relatively high in comparison to Site 1, even when ignoring the high flow event response noise (Figure 4.12). One noticeable trend was that for the piezometer sets 5-6 and 7-8, horizontal hydraulic gradients appeared to peak around early June through early August (Figure 4.12). Otherwise, temporal trends in the horizontal hydraulic gradient were unclear (Table 4.4).

### 4.3.5 Continuous Differential Stream Gauging Estimates

To estimate streamflow over time at the upstream and downstream gauging stations, water level data was collected, and streamflow rating curves were developed. At the gauging stations, water level data was collected from November 7, 2023, to August 31, 2024, although significant portions of the dataset were lost due to either the loss of data loggers or data recording issues. A segmented approach was applied to develop the streamflow rating curves. At low stream stages, the exponential law was applied, while at higher stream stages, the power law was applied. In the case of the upstream rating curve (Figure 4.13), at stages less than or equal to 0.6459 m, an exponential equation $\mathrm{Q} = e^{(Stage(m)-0.4493)/0.1721}$ was applied, while at stages greater than 0.6459 m, the power law equation $\mathrm{Q} = 8.8199\ (\mathrm{stage(m)} - 0.046)^{2.0249}$ was applied. In the case of the downstream rating curve (Figure 4.14), at stages less than or equal to 0.7033 m, the exponential equation $\mathrm{Q} = e^{(Stage(m)-0.5638)/0.1669}$ was applied, while at stages greater than 0.7033 m, the power law equation $\mathrm{Q} = 8.0171\ (\mathrm{stage(m)} - 0.254)^{1.5572}$ was applied. The power law equation was used at these high stages as a result of the logarithmic equation producing unrealistically high streamflow estimates at high stream stages.

The net gain or loss in streamflow measured between the gauging stations was used to assess groundwater contributions over time, as seen in Figure 4.15b. From these results, gaining conditions as a result of groundwater discharge appear to be fairly consistent over the gauging reach, although variability does occur over time. A decline in groundwater discharges appeared from November until late January, when a loss of data occurred. This was then followed by groundwater discharge, appearing to have remained relatively stable up until June, at which point data was unfortunately lost. Losing conditions do appear to have occurred but were rare and temporary. These losing conditions appear often in response to extreme flow events (Figure 4.15c) and were likely a result of rapid rises

in stream stage, in exceedance of groundwater levels, resulting in a temporary reversal of the hydraulic gradient and the inducing of recharge conditions. While it assumed that the net gain in streamflow is a result of groundwater discharge, it is also recognized that around the time of high flow events, non-groundwater contributions of precipitation and overland flow may result in additional contributions to streamflow over the gauged reach, challenging that assumption.

## 4.4 Discussion

The consistently upward vertical hydraulic gradients, along with the horizontal hydraulic gradients being largely in the direction of the stream across both study reaches, indicate that groundwater baseflow was likely persistent throughout the year along these stretches of the stream. This means that the aquifer system provides a consistent source of groundwater to augment streamflow in these areas of study, despite seasonal variability. The deviation from this occurs during extreme flow events, when short term gradient reversals occurred as a result of rapid rises in the stream stage.

Vertical and horizontal hydraulic gradients do appear to vary over time, with the vertical hydraulic gradients often reaching their peak during the summer and winter seasons, when baseflow was expected to be the dominant contributor to streamflow, and declining though the spring and fall, a pattern also seen in Fraser & Williams (1998). Due to the dry, hot conditions of summer, precipitation in the early fall replenishes moisture deficits in the vadose zone. As time progresses and precipitation events continue throughout the fall, in which cooler temperatures and lower evaporation rates persist, soil saturation and the likelihood of surface water runoff increases, while water percolates through the vadose zone and reaches the water table. This results in rising groundwater levels, and an even greater rise in surface water levels, ultimately leading to a decline in the vertical hydraulic gradient in the fall. In the winter, much of the precipitation is stored as solid snow or ice at the ground surface; however, water retained in the vadose zone during the fall continues to percolate downward and recharge the water table, resulting in a rise in groundwater levels, and ultimately leading to an increasing vertical hydraulic gradient during this period of the year. Advancing into the spring, groundwater levels continue to rise, but not to the same degree as surface water, which receives contributions from both winter melt events and more frequent rainfall. This greater rise in surface water levels relative to groundwater levels results in a decline in the vertical hydraulic gradient. However, as the summer season begins, temperatures and evaporation rates rise, while rainfall rates decrease, resulting in

surface water levels declining faster than groundwater levels, leading once again to a rise in the vertical hydraulic gradient. Based on the larger vertical gradients often found during the winter and summer months, and assuming relatively constant hydraulic conductivity, it is expected that groundwater flux, and therefore groundwater discharge, was greater at these times of the year.

Although each study site exhibits gaining conditions over time, based on the horizontal hydraulic gradients largely towards the stream, these study sites seem to differ with regards to the variability in these gradients. Site 2, which exhibited hydraulic gradients away from the stream for part of the year in piezometer set 7-8, also has, on the opposite streambank just downstream, piezometer set 9-10, where gradients consistently exceeded 0.15, possibly a result of the nearby spring and the likely elevated groundwater levels. These results seem to indicate a more heterogeneous setting than was present at Site 1 further upstream, where much less variability in horizontal hydraulic gradients was present.

Regarding the effect of rapid stream stage rises during high-flow events on the hydraulic gradient, a pattern previously reported in the literature by Käser et al. (2009) and Malcolm et al. (2006) persisted. Due to a delayed response of groundwater levels to surface water level changes, a decline in the hydraulic gradient occurs during the initial rise in stream stage; then, as the stream stage declines, a rise in the hydraulic gradient occurred before the hydraulic gradient returned to a steady level. During more extreme rises in the stream stage, the hydraulic gradient was shown to have reversed, as previously reported by Puckett et al. (2008). These short-term reversals are likely the result of the stream stage rising above the water table and were often the only times when losing conditions were found to be present with regards to some of the vertical hydraulic gradients, and for a majority of the horizontal hydraulic gradients.

The collection of continuous water level and hydraulic gradient datasets have provided valuable insight into how hydraulic gradients behave in response to high flow events and seasonal cycles. Periodic bi-weekly readings, which were useful in correcting the continouous water level datasets, also proved effective in identifying gaining conditions and seasonality variability. The continuous datasets, however, provided all the capabilities of the biweekly readings, while also enabling the monitoring of short term high flow event responses, and the identification of seasonal trends through visual and/or analytical techniques. Therefore, further emphasis should be put into continuous

monitoring of water levels and hydraulic gradients in order to gain a greater understanding of groundwater-surface water exchange.

As it relates to the long-term differential stream gauging dataset developed at Site 1 (Figure 4.15b), in addition to the notable consistent presence of gaining conditions as a result of groundwater discharge, there does appear to be some temporal trends that correlate to the vertical hydraulic gradient data (Figure 4.15a). During late fall and into the early winter when the groundwater discharge appears to be higher, the vertical hydraulic gradients were higher. Furthermore, the relatively lower groundwater discharge seen through the spring correlates well with a period of lower vertical hydraulic gradients. These findings support the influence of hydraulic gradient on the expected groundwater discharge over the reach of study.

## 4.5 Conclusions

Through the monitoring of surface water levels, groundwater levels, hydraulic gradients, and streamflow datasets an improved understanding of how groundwater-surface water exchange behaves temporally, both in response to seasonal changes and high flow events was gained. Consistently upward vertical hydraulic gradients were measured at the study sites through both bi-weekly and continuous monitoring, indicating that groundwater discharge conditions prevail throughout the year. This conclusion is further supported by the continuous horizontal hydraulic gradient measurements, which indicated flow predominantly towards the stream over the course of this study. The exception to this appears to be during, and/or immediately after, high flow events, where a significant increase in the stream stage results in a rapid decline, if not reversal, in the vertical and horizontal hydraulic gradient, as a result of surface water levels exceeding groundwater levels due to delayed responses in the groundwater system. This finding was, however, not identified in the manual, bi-weekly readings, emphasizing the importance of collecting continuous data in order to gain a better understanding of groundwater-surface water exchange.

This need for continuous data was further supported when assessing for seasonal trends that were unidentifiable with just bi-weekly readings. These high resolution continuous vertical hydraulic gradients datasets could be both visually interpreted and assessed using trend analysis techniques such as the modified Mann Kendall test, which provided an analytical perspective for data interpretation that could capture trends not easily identifiable by eye. As a result, notable increases in the winter and

summer were identified. The higher vertical hydraulic gradients measured in the summer were believed to relate to lower surface water levels due to increased evaporation at this time of year, combined with a slower decline in groundwater levels. Higher vertical gradients in the winter reflect the delayed influence of higher infiltration rates in the fall, that result in increasing groundwater levels, while the surface water levels are low due to the precipitation freezing on the ground surface.

The long-term differential stream gauging dataset also exhibited variability in groundwater-surface water exchange. These results indicated consistently gaining conditions throughout most of the year, with the exception being during extreme flow events, as rapid increases in stream stage resulted in losing conditions, as the stream water levels temporarily exceeded groundwater levels. From the results of differential stream gauging, as well as the results for the various other techniques, it is clear that groundwater-surface water exchange exhibits temporal variability across the annual cycle within a perennial stream system. Therefore, accounting for temporal variability is essential when evaluating groundwater–surface water interactions.

## 4.6 Figures

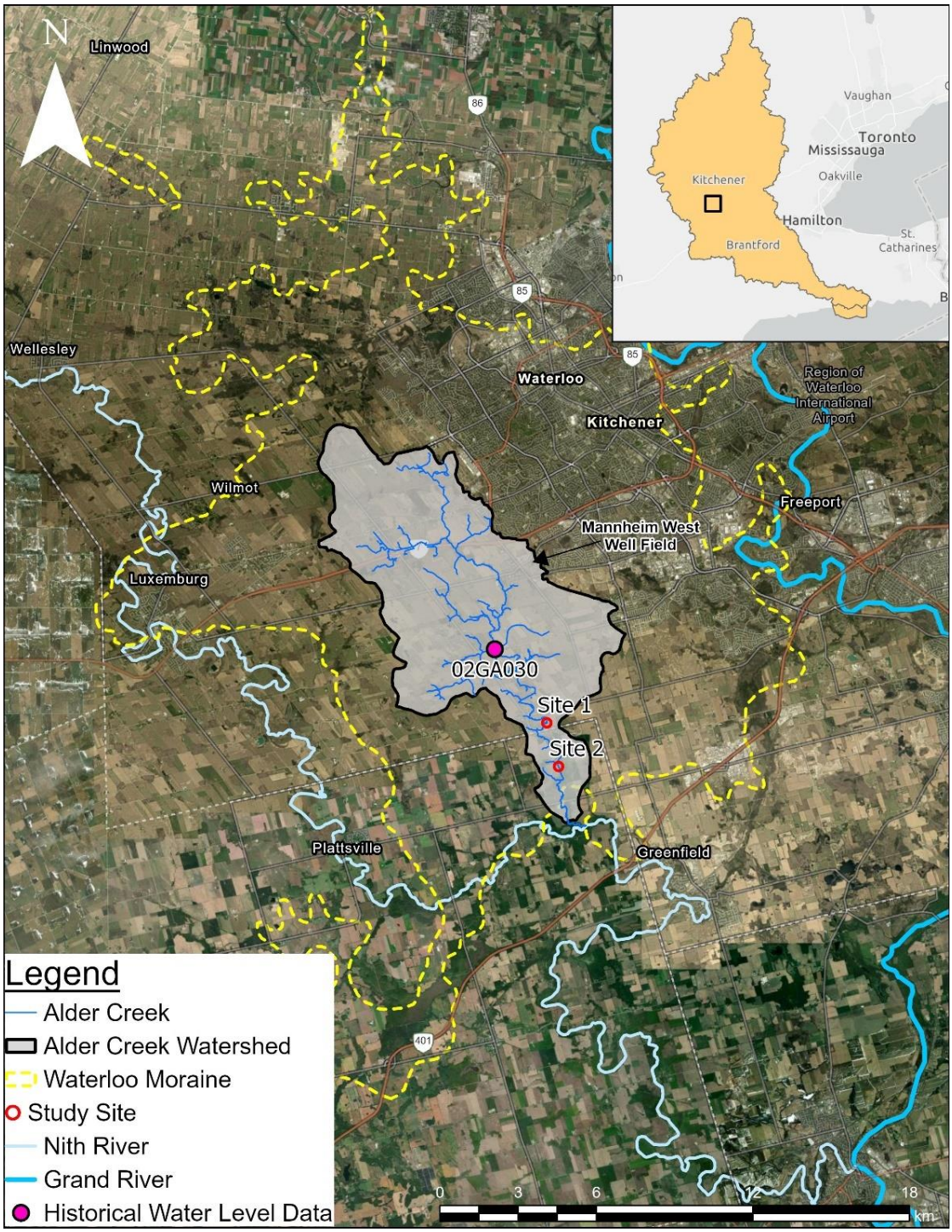



Figure 4.1: Alder Creek watershed and study site locations (Esri et al., 2025a; Esri et al., 2025b; Government of Ontario, 2023; Grand River Conservation Authority, 2017; Sousa et al., 2014).

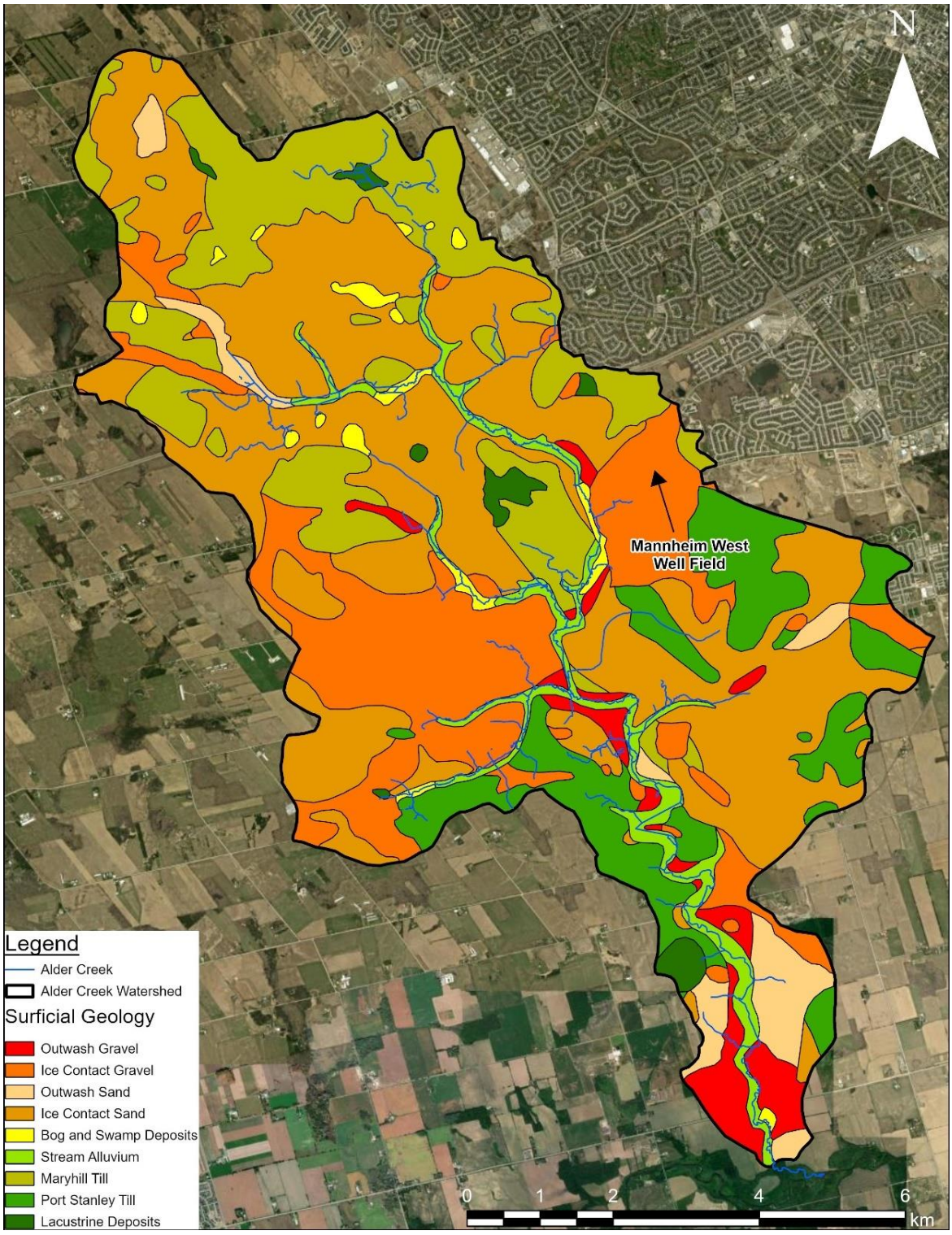



Figure 4.2: Surficial geology of the Alder Creek watershed (Esri et al., 2025a; Government of Ontario, 2023; Grand River Conservation Authority, 2017; Ontario Geological Survey, 2010).



(a) (b)

Figure 4.3: Photos of (a) Site 1 and (b) Site 2.

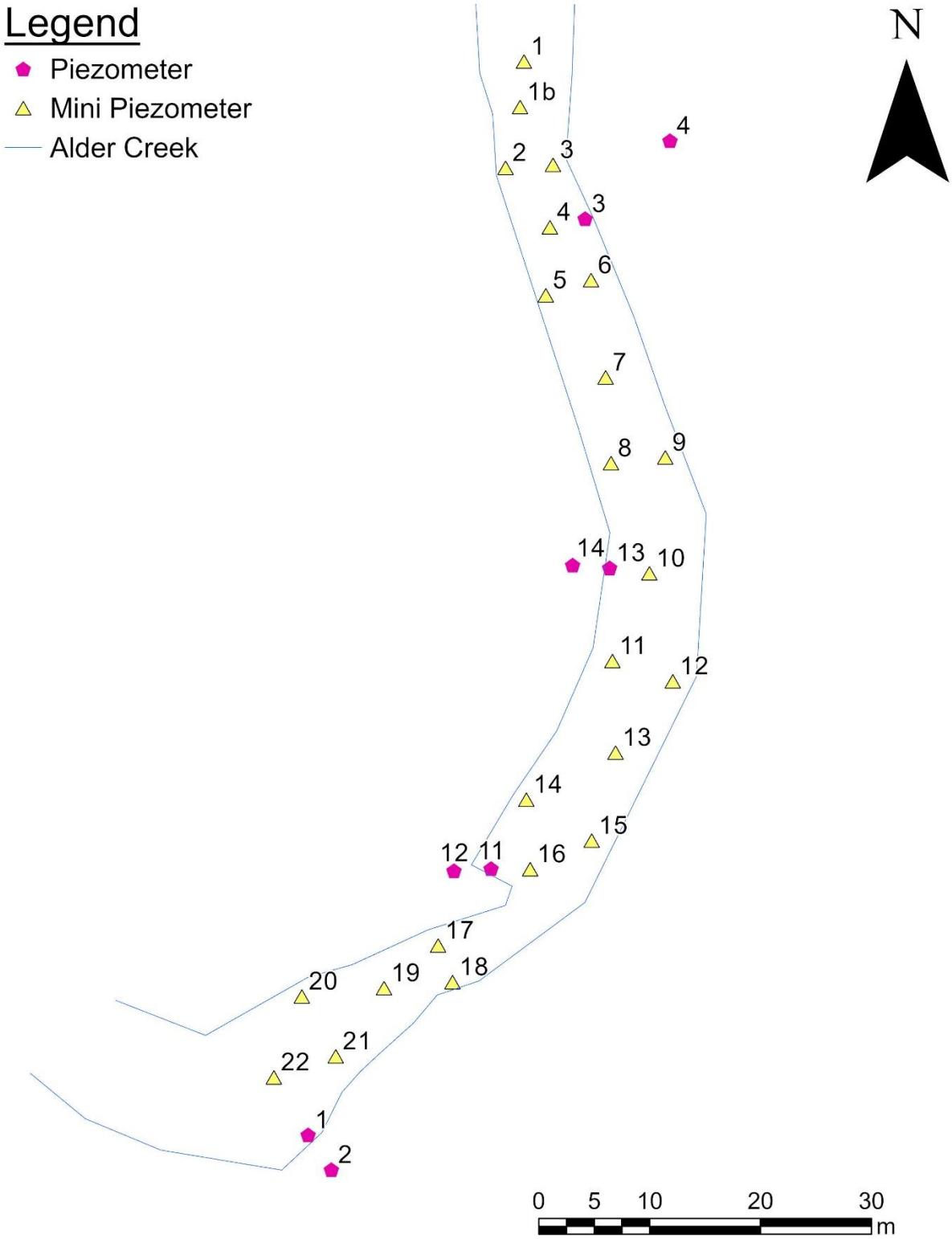



Figure 4.4: Map of piezometer installation locations at Site 1.

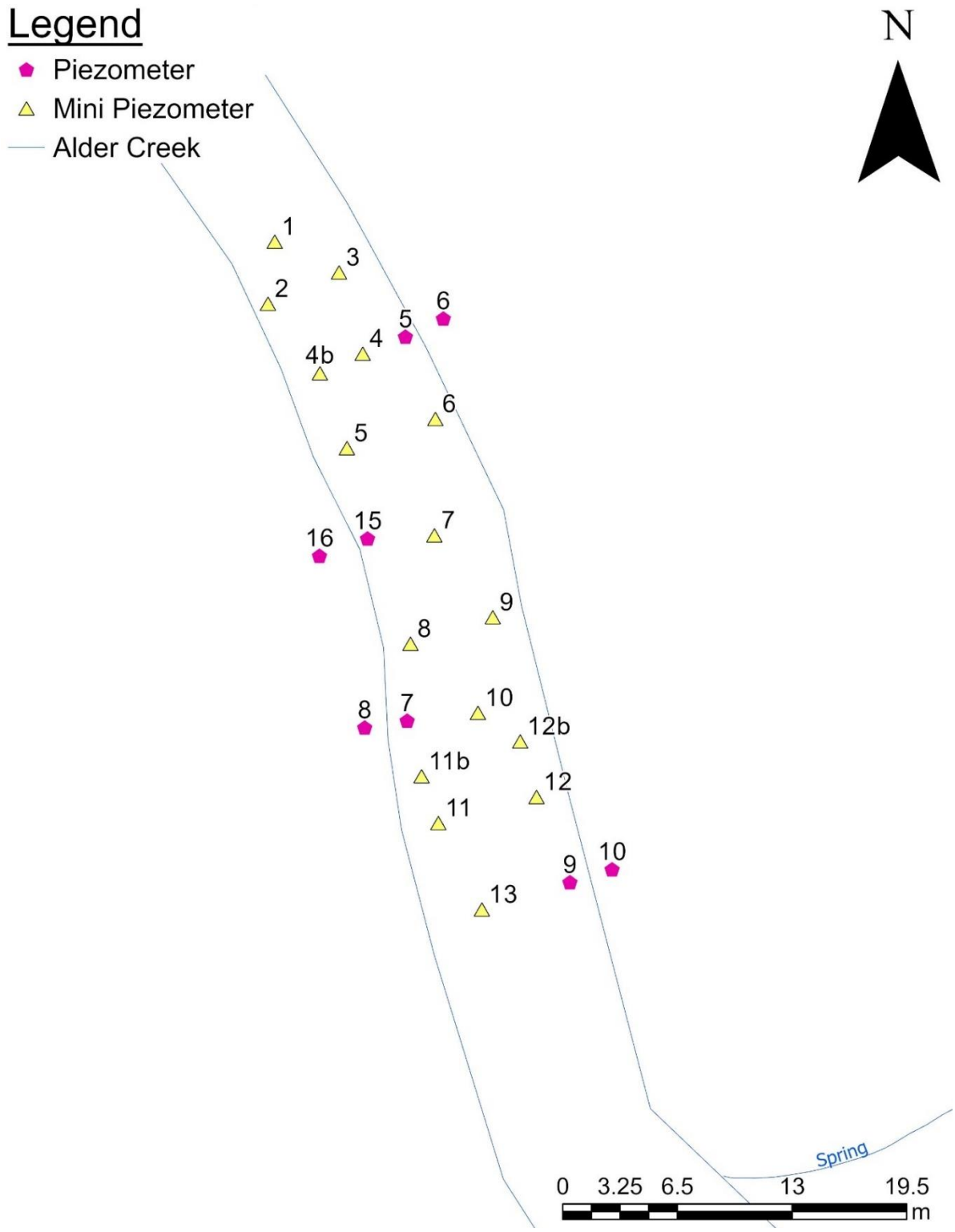



Figure 4.5: Map of piezometer installation locations at Site 2.



Figure 4.6: Stream gauging locations at Site 1 (Esri et al., 2025a).

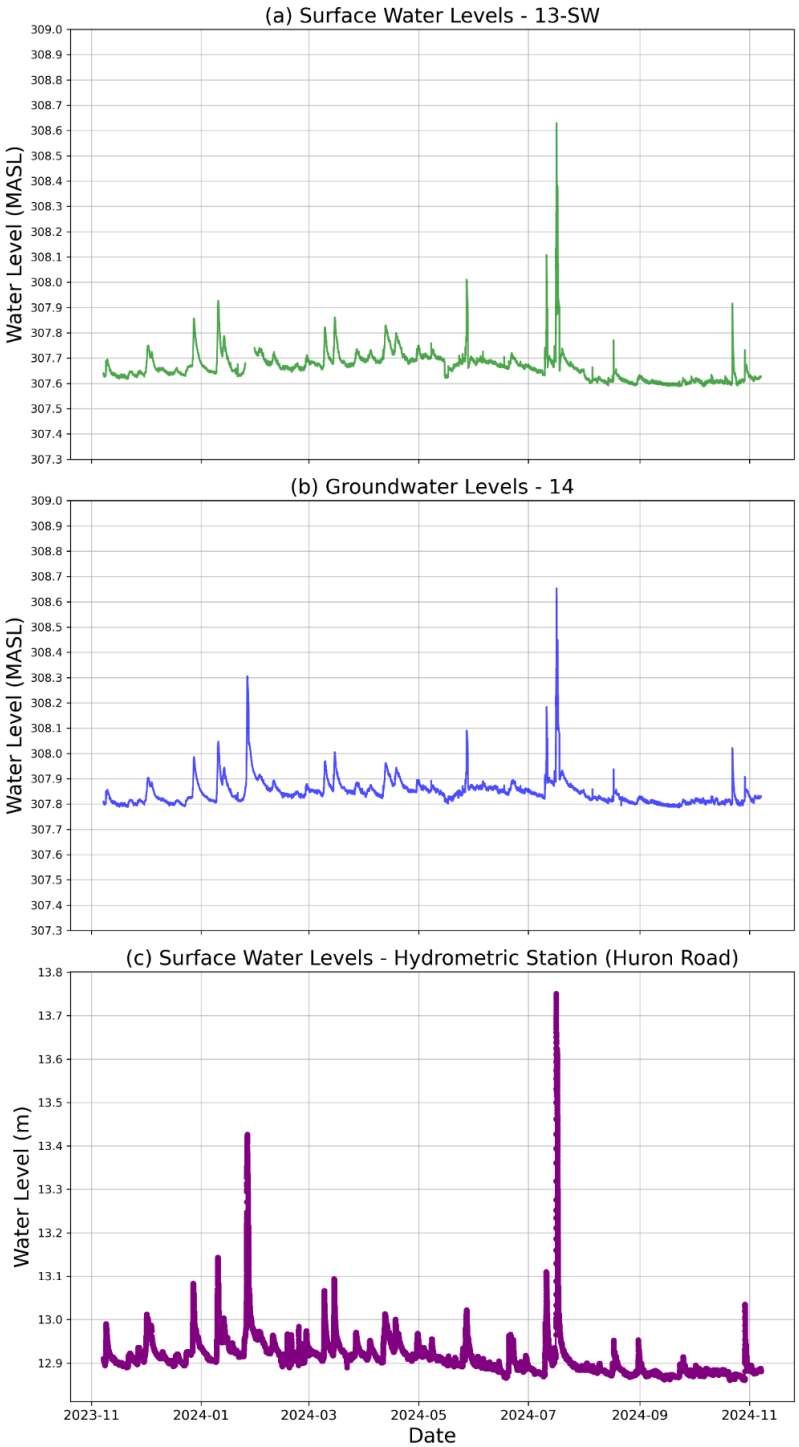



Figure 4.7: (a) Surface water levels measured at Site 1's piezometer 13, (b) streambank groundwater levels measured at Site 1's piezometer 14 and (c) surface water levels measured at the Huron Road Hydrometric Station from November 7, 2023, to November 7, 2024 (Government of Canada, 2025b).

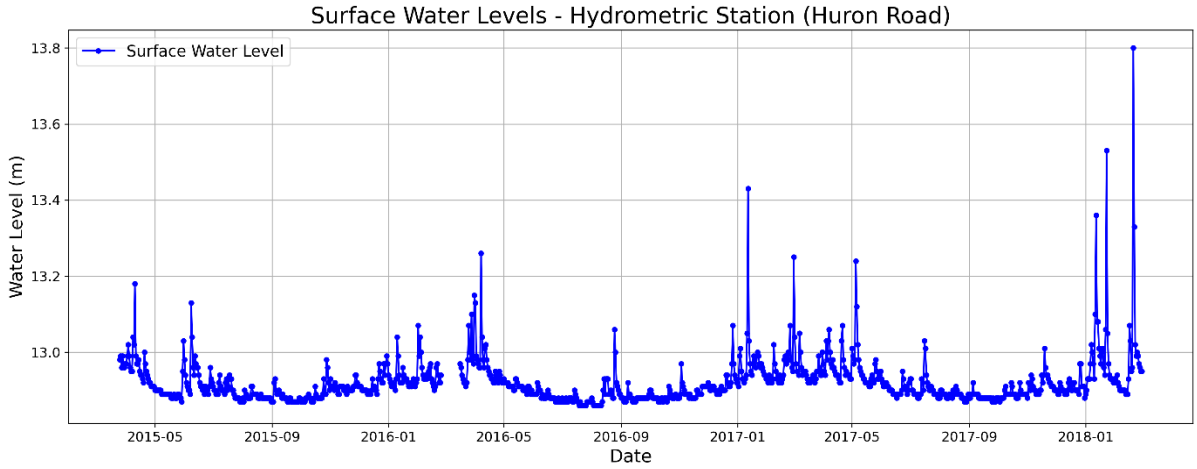



Figure 4.8: Historical surface water levels measured at the Huron Road Hydrometric Station between March 1, 2015, and March 1, 2018 (Government of Canada, 2025b).

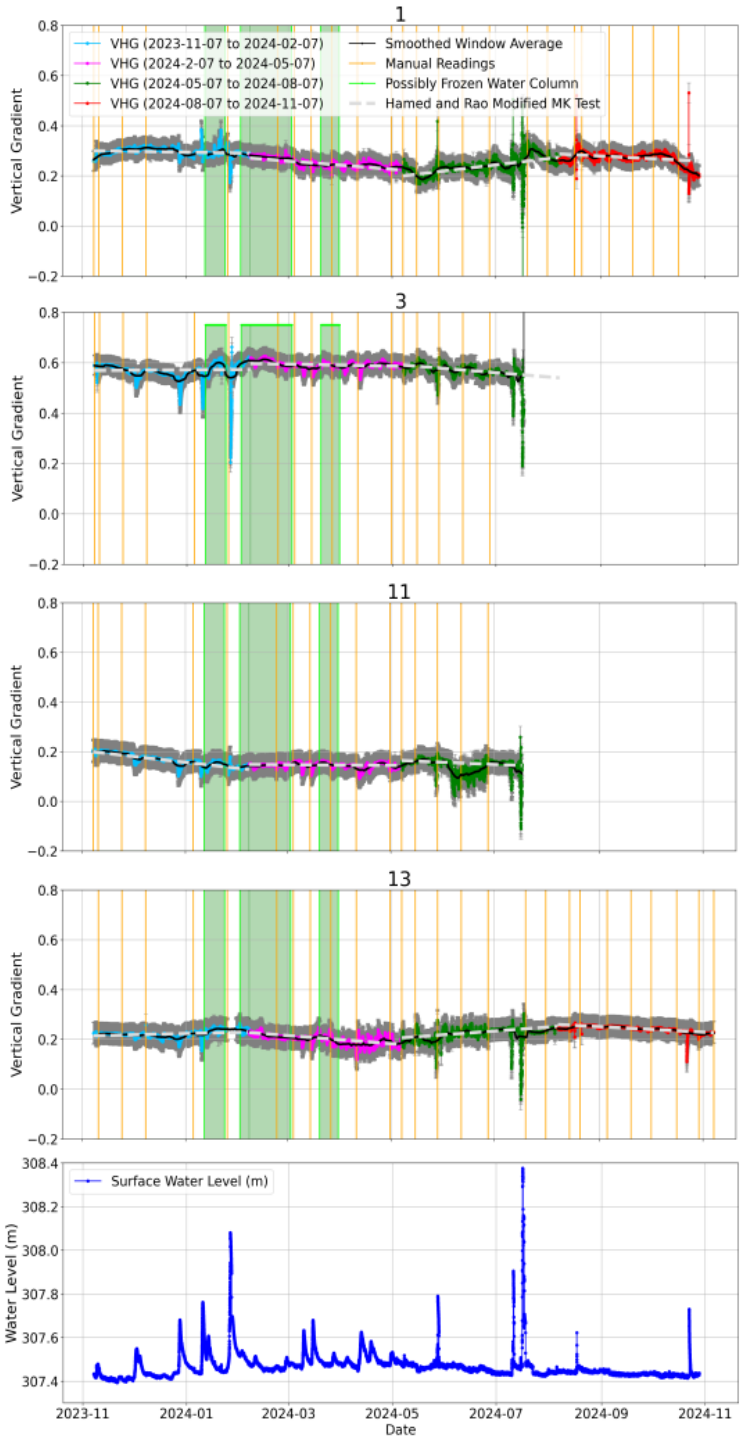



Figure 4.9: Continuous vertical hydraulic gradients (VHG) for Site 1 piezometers from November 7, 2023, to November 7, 2024 (data lost for piezometer 3 and 11 due to piezometer damage following storm event on July 17, 2024). Surface water levels at Piezometer 1 are shown in bottom panel.

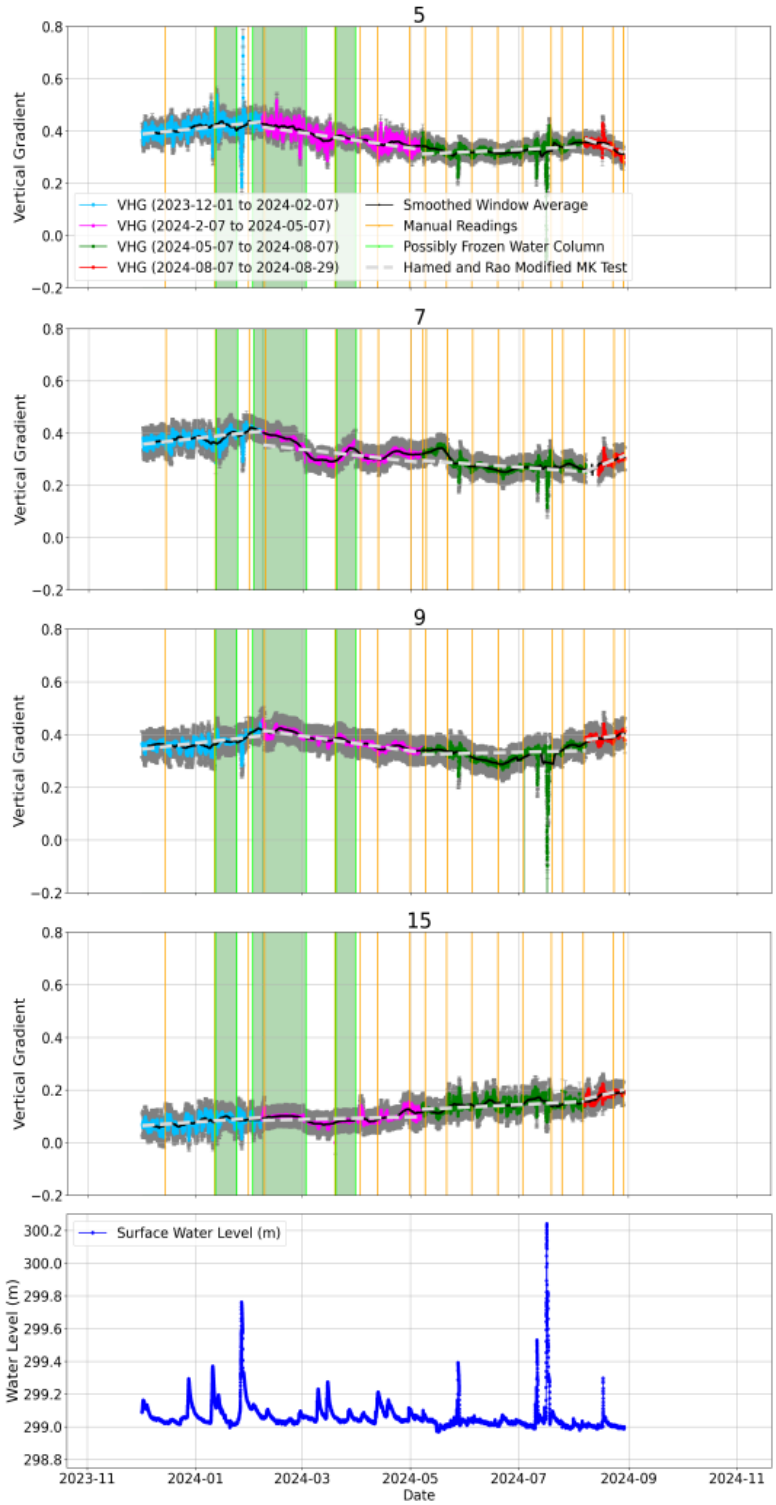



Figure 4.10: Continuous vertical hydraulic gradients (VHG) for Site 2 piezometers from December 1, 2023, to August 29, 2024. Surface water levels at Piezometer 15 are shown in bottom panel.

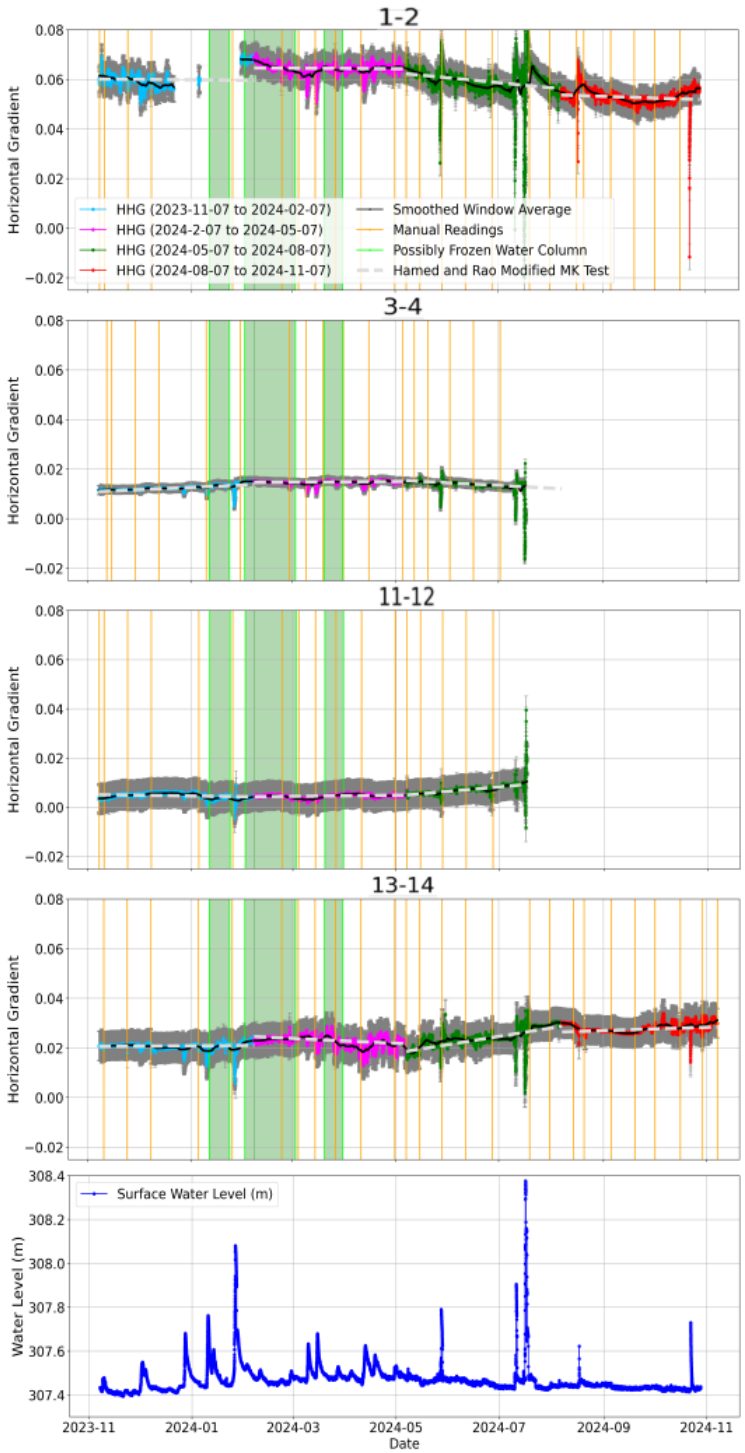



Figure 4.11: Continuous horizontal hydraulic gradients (HHG) for Site 1 piezometers from November 7, 2023, to November 7, 2024 (data lost for piezometer 3 and 11 due to piezometer damage following storm event on July 17, 2024). Surface water levels at Piezometer 1 are shown in bottom panel.

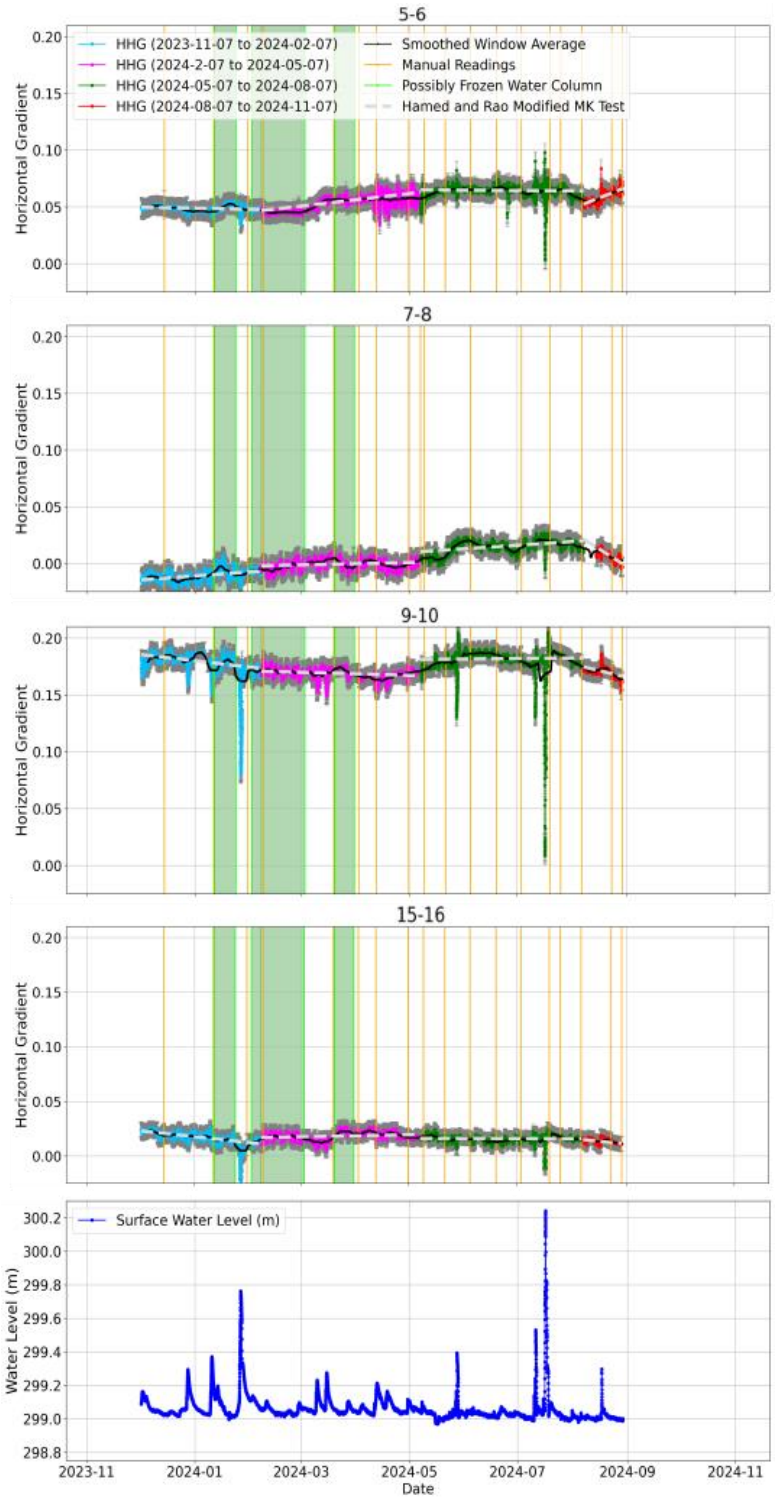



Figure 4.12: Continuous horizontal hydraulic gradients (HHG) for Site 2 piezometers from December 1, 2023, to August 29, 2024. Surface water levels at Piezometer 15 are shown in bottom panel.

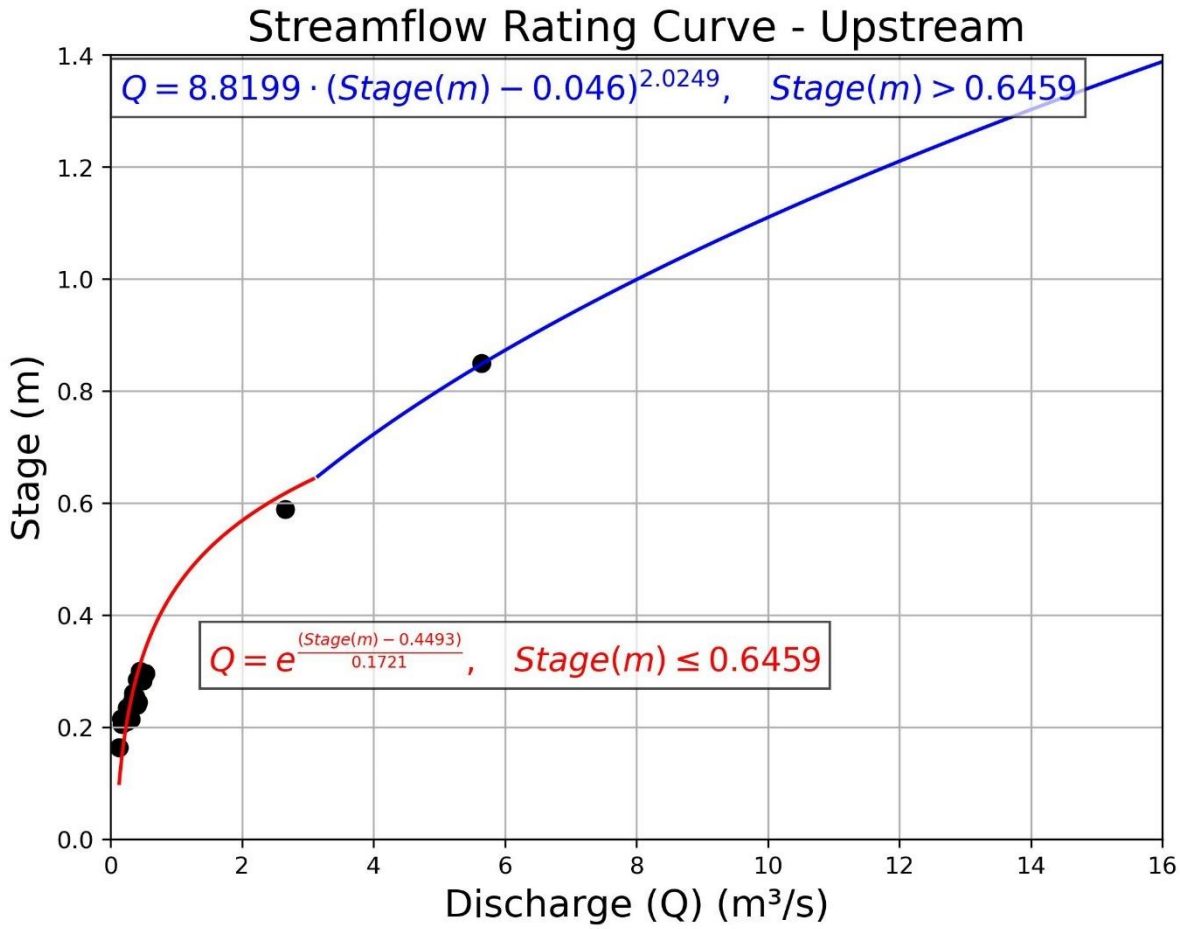



Figure 4.13: Streamflow rating curve for Site 1 upstream gauging station.

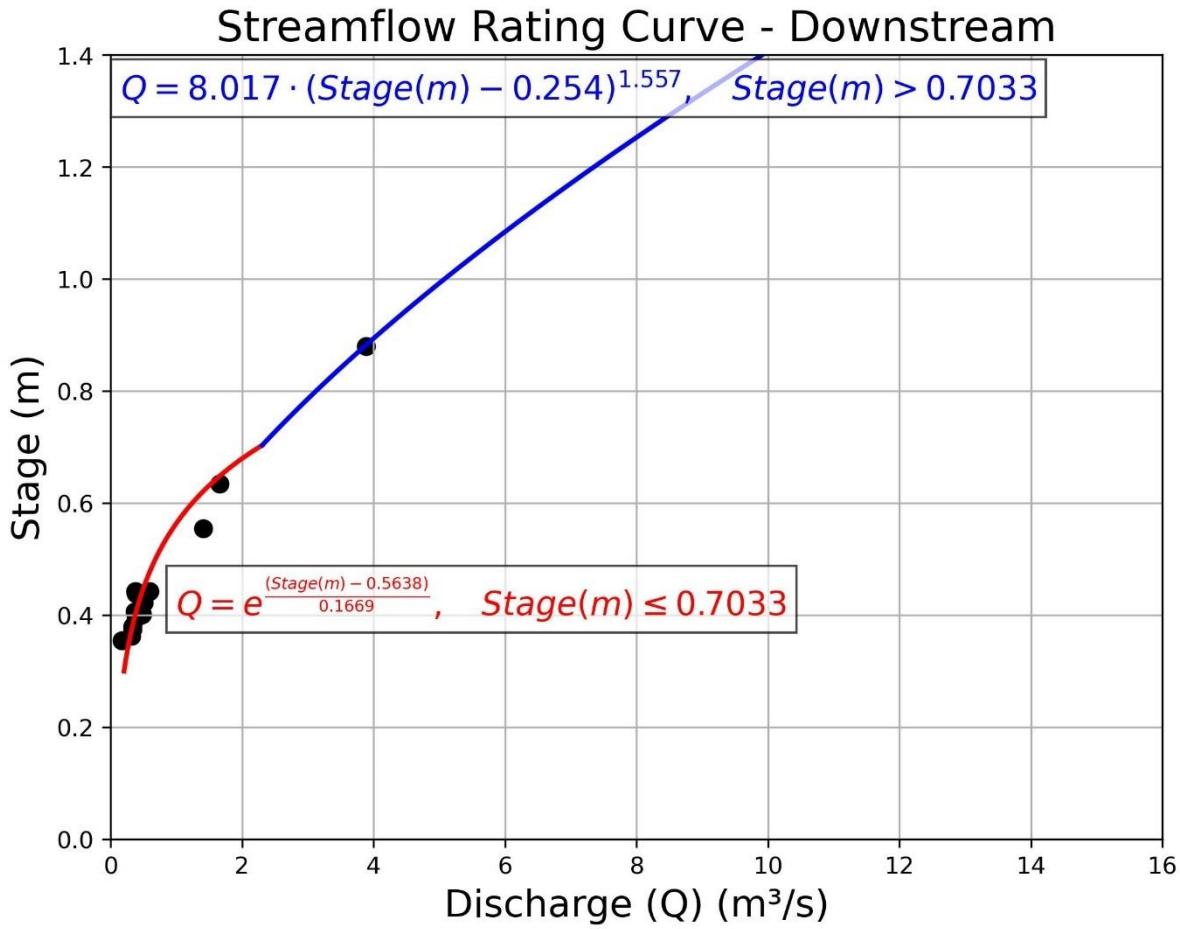



Figure 4.14: Streamflow rating curve for Site 1 downstream gauging station.

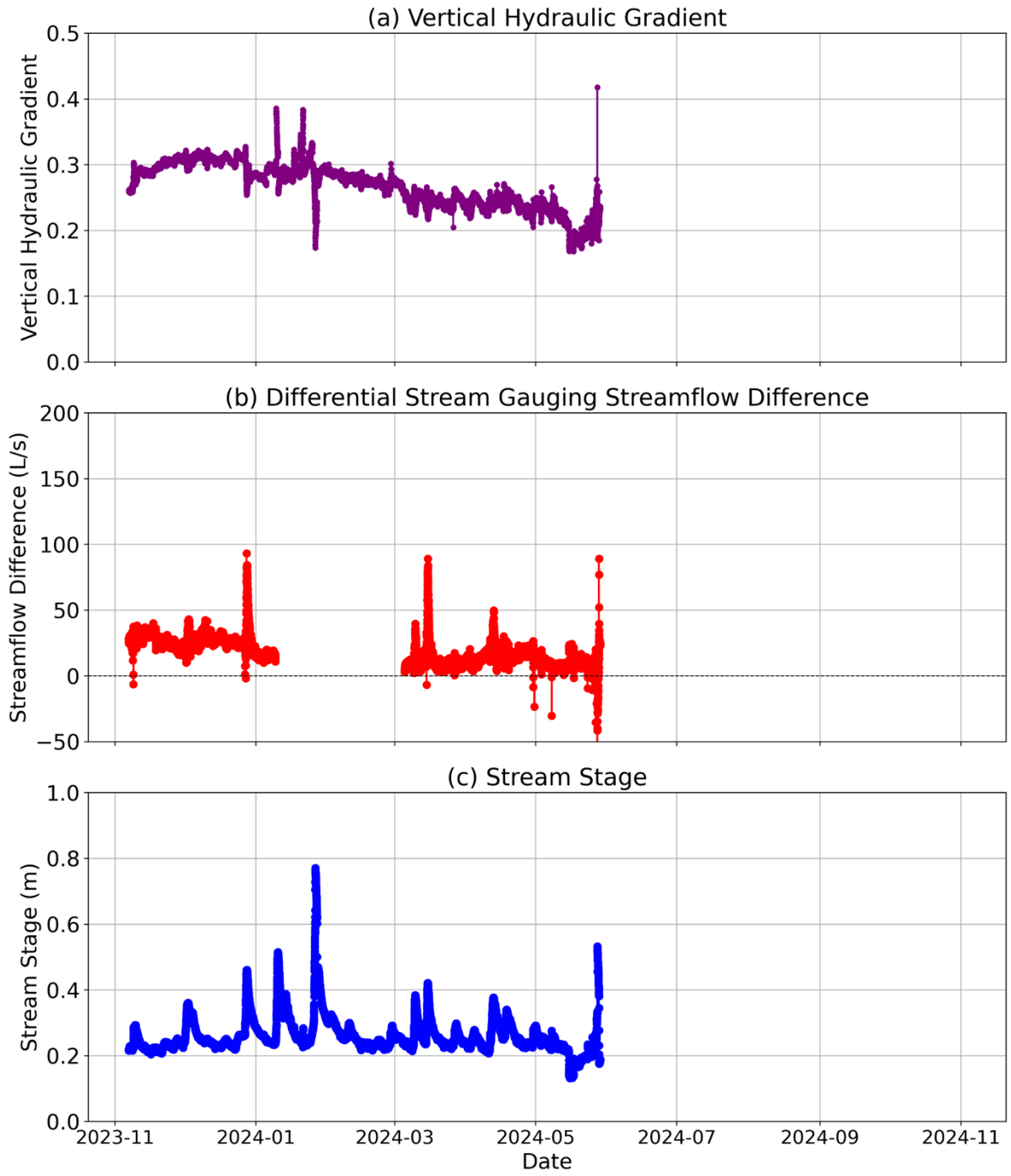



Figure 4.15: The (a) vertical hydraulic gradient measured at Piezometer 1, the (b) difference in streamflow measured through differential stream gauging where positive is assumed to be groundwater discharge (L/s), and the (c) stream stage (m) data measured at Piezometer 1 from November 7, 2023, to May 29, 2024, at Site 1.

## 4.7 Tables

Table 4.1: Modified Mann Kendall trend test results for Site 1 vertical hydraulic gradients.

| Piezometer | 2023-11-07 to 2024-02-07 | 2024-2-07 to 2024-05-07 | 2024-05-07 to 2024-08-07 | 2024-08-07 to 2024-11-07 |
|---|---|---|---|---|
| 1 | **Trend:** Decreasing<br>**p-value:** 0.3817<br>**h:** False<br>**Tau:** -0.1210<br>**Slope:** -1.1486e-06 | **Trend:** Decreasing<br>**p-value:** 6.3825e-05<br>**h:** True<br>**Tau:** -0.5774<br>**Slope:** -5.5582e-06 | **Trend:** Increasing<br>**p-value:** 6.7386e-12<br>**h:** True<br>**Tau:** 0.4938<br>**Slope:** 8.4074e-06 | **Trend:** Decreasing<br>**p-value:** 0.1751<br>**h:** False<br>**Tau:** -0.1943<br>**Slope:** -3.5716e-06 |
| 3 | **Trend:** Increasing<br>**p-value:** 0.8747<br>**h:** False<br>**Tau:** 0.02731<br>**Slope:** 4.7707e-07 | **Trend:** Decreasing<br>**p-value:** 0.2495<br>**h:** False<br>**Tau:** -0.1519<br>**Slope:** -1.2188e-06 | **Trend:** Decreasing<br>**p-value:** 1.5543e-15<br>**h:** True<br>**Tau:** -0.3864<br>**Slope:** -5.7321e-06 | N/A |
| 11 | **Trend:** Decreasing<br>**p-value:** 8.3915e-10<br>**h:** True<br>**Tau:** -0.7134<br>**Slope:** -8.0485e-06 | **Trend:** Decreasing<br>**p-value:** 0.3669<br>**h:** False<br>Tau: -0.0784<br>**Slope:** -4.9286e-07 | **Trend:** Decreasing<br>**p-value:** 0.06571<br>**h:** False<br>**Tau:** -0.2297<br>**Slope:** -3.02986e-06 | N/A |
| 13 | **Trend:** Increasing<br>**p-value:** 0.3070<br>**h:** False<br>**Tau:** 0.2025<br>**Slope:** 1.7476e-06 | **Trend:** Decreasing<br>**p-value:** 1.4279e-10<br>**h:** True<br>**Tau:** -0.4734<br>**Slope:** -5.5349e-06 | **Trend:** Increasing<br>**p-value:** 0.0011<br>**h:** True<br>**Tau:** 0.4064<br>**Slope:** 5.1889e-06 | **Trend:** Decreasing<br>**p-value:** 1.0758e-05<br>**h:** True<br>**Tau:** -0.6152<br>**Slope:** -3.7262e-06 |

Table 4.2: Modified Mann Kendall trend test results for Site 2 vertical hydraulic gradients.

| Piezometer | 2023-12-01 to 2024-02-07 | 2024-2-07 to 2024-05-07 | 2024-05-07 to 2024-08-07 | 2024-08-07 to 2024-08-29 |
|---|---|---|---|---|
| 5 | **Trend:** Increasing<br>**p-value:** 1.5543e-15<br>**h:** True<br>**Tau:** 0.3974<br>**Slope:** 7.2014e-06 | **Trend:** Decreasing<br>**p-value:** 1.1324e-14<br>**h:** True<br>**Tau:** -0.6035<br>**Slope:** -1.0032e-05 | **Trend:** Increasing<br>**p-value:** 0.04874<br>**h:** True<br>**Tau:** 0.2918<br>**Slope:** 3.2489e-06 | **Trend:** Decreasing<br>**p-value:** 9.0998e-05<br>**h:** True<br>**Tau:** -0.5749<br>**Slope:** -2.4392e-05 |
| 7 | **Trend:** Increasing<br>**p-value:** 6.1431e-07<br>**h:** True<br>**Tau:** 0.3887<br>**Slope**: 7.8109e-06 | **Trend:** Decreasing<br>**p-value:** 0.1352<br>**h:** False<br>**Tau:** -0.2755<br>**Slope:** -7.8094e-06 | **Trend:** Decreasing<br>**p-value:** 0.0934<br>**h:** False<br>**Tau: -**0.3142<br>**Slope:** -4.8519e-06 | **Trend:** Increasing<br>**p-value:** 2.5464e-05<br>**h:** True<br>**Tau:** 0.4111<br>**Slope:** 2.8779e-05 |
| 9 | **Trend:** Increasing<br>**p-value:** 0.0017<br>**h:** True<br>**Tau:** 0.4119<br>**Slope:** 7.7724e-06 | **Trend:** Decreasing<br>**p-value**: 0.0<br>**h:** True<br>**Tau:** -0.7423<br>**Slope:** -9.6419e-06 | **Trend:** Increasing<br>**p-value:** 0.5621<br>**h:** False<br>**Tau:** 0.1095<br>**Slope:** 1.5843e-06 | **Trend:** Increasing<br>**p-value:** 0.05209<br>**h:** False<br>**Tau:** 0.2469<br>**Slope:** 9.2173e-06 |
| 15 | **Trend:** Increasing<br>**p-value:** 1.4744e-05<br>**h:** True<br>**Tau:** 0.2774<br>**Slope:** 4.7426e-06 | **Trend:** Increasing<br>**p-value:** 0.5218<br>**h:** False<br>**Tau:** 0.1159<br>**Slope:** 1.5787e-06 | **Trend:** Increasing<br>**p-value:** 0.0007<br>**h:** True<br>**Tau:** 0.2931<br>**Slope:** 3.3731e-06 | **Trend:** Increasing<br>**p-value:** 2.4299e-05<br>**h:** True<br>**Tau:** 0.4391<br>**Slope:** 1.7098e-05 |

Table 4.3: Modified Mann Kendall trend test results for Site 1 horizontal hydraulic gradients.

| Piezometers | 2023-11-07 to 2024-02-07 | 2024-2-07 to 2024-05-07 | 2024-05-07 to 2024-08-07 | 2024-08-07 to 2024-11-07 |
|---|---|---|---|---|
| 1-2 | **Trend:** Decreasing<br>**p-value:** 0.9213<br>**h:** False<br>**Tau:** -0.0137<br>**Slope:** -6.1016e-08 | **Trend:** Decreasing<br>**p-value:** 0.7233<br>**h:** False<br>**Tau:** -0.0419<br>**Slope:** -3.9408e-08 | **Trend:** Decreasing<br>**p-value:** 0.0223<br>**h:** True<br>**Tau:** -0.3100<br>**Slope:** -6.8561e-07 | **Trend:** Decreasing<br>**p-value:** 0.4739<br>**h:** False<br>**Tau:** -0.1207<br>**Slope:** -2.3453e-07 |
| 3-4 | **Trend:** Increasing<br>**p-value:** 4.5623e-06<br>**h:** True<br>**Tau:** 0.6775<br>**Slope:** 3.1645e-07 | **Trend:** Increasing<br>**p-value:** 0.1259<br>**h:** False<br>**Tau:** 0.1478<br>**Slope:** 4.5875e-08 | **Trend:** Decreasing<br>**p-value:**3.7245e-07<br>**h:** True<br>**Tau:** -0.5586<br>**Slope:** -3.6964e-07 | N/A |
| 11-12 | **Trend:** Decreasing<br>**p-value:** 0.4685<br>**h:** False<br>**Tau:** -0.1366<br>**Slope:** -9.7259e-08 | **Trend:** Increasing<br>**p-value:** 0.1956<br>**h:** False<br>**Tau:** 0.1785<br>**Slope:** 7.29995e-08 | **Trend:** Increasing<br>**p-value:** 0.0<br>**h:** True<br>**Tau:** 0.6901<br>**Slope:** 6.3232e-07 | N/A |
| 13-14 | **Trend:** Increasing<br>**p-value:** 0.5609<br>**h:** False<br>**Tau:** 0.08446<br>**Slope:** 5.1883e-08 | **Trend:** Decreasing<br>**p-value:** 0.01587<br>**h:** True<br>**Tau:** -0.2240<br>**Slope:** -3.3716e-07 | **Trend:** Increasing<br>**p-value:** 3.3928e-07<br>**h:** True<br>**Tau:** 0.5739<br>**Slope:** 1.1448e-06 | **Trend:** Increasing<br>**p-value:** 0.1376<br>**h:** False<br>**Tau:** 0.2058<br>**Slope:** 2.2622e-07 |

Table 4.4: Modified Mann Kendall trend test results for Site 2 horizontal hydraulic gradients.

| Piezometers | 2023-12-01 to 2024-02-07 | 2024-2-07 to 2024-05-07 | 2024-05-07 to 2024-08-07 | 2024-08-07 to 2024-08-29 |
|---|---|---|---|---|
| 5-6 | **Trend:** Decreasing<br>**p-value:**0.3794<br>**h:** False<br>**Tau:** -0.1268<br>**Slope:** -2.9691e-07 | **Trend:** Increasing<br>**p-value:** 0.0002<br>**h:** True<br>**Tau:** 0.5440<br>**Slope:**1.8747e-06 | **Trend:** Decreasing<br>**p-value:**0.67780<br>**h:** False<br>**Tau:** -0.04507<br>**Slope:** -9.6845e-08 | **Trend:** Increasing<br>**p-value:** 9.5974e-10<br>**h:** True<br>**Tau:** 0.5906<br>**Slope:** 6.4352e-06 |
| 7-8 | **Trend:** Increasing<br>**p-value:** 3.968e-05<br>**h:** True<br>**Tau:** 0.3290<br>**Slope:** 1.1768e-06 | **Trend:** Increasing<br>**p-value:**0.2122<br>**h:** False<br>**Tau:** 0.1189<br>**Slope:** 3.5057e-07 | **Trend:** Increasing<br>**p-value:**0.0200<br>**h:** True<br>**Tau:** 0.2766<br>**Slope:** 1.08489e-06 | **Trend:** Decreasing<br>**p-value:** 3.7446e-11<br>**h:** True<br>**Tau:** -0.6005<br>**Slope:** -1.0288e-05 |
| 9-10 | **Trend:** Decreasing<br>**p-value:** 0.0016<br>**h:** True<br>**Tau:** -0.3278<br>**Slope:** -1.8625e-06 | **Trend:** Decreasing<br>**p-value:** 0.0423<br>**h:** True<br>**Tau:** -0.1711<br>**Slope:** -4.557e-07 | **Trend:** Increasing<br>**p-value:** 0.7757<br>**h:** False<br>**Tau:** 0.03763<br>**Slope:** 1.4687e-07 | **Trend:** Decreasing<br>**p-value:** 0.05778<br>**h:** False<br>**Tau:** -0.3549<br>**Slope:** -3.8949e-06 |
| 15-16 | **Trend:** Decreasing<br>**p-value:** 0.0<br>**h:** True<br>**Tau:** -0.5612<br>**Slope:** -1.8356e-06 | **Trend:** Increasing<br>**p-value:**0.2543<br>**h:** False<br>**Tau:** 0.1308<br>**Slope:** 3.2719e-07 | **Trend:** Decreasing<br>**p-value:** 0.8522<br>**h:** False<br>**Tau:** -0.0198<br>**Slope:** -2.9315e-08 | **Trend:** Decreasing<br>**p-value:** 0.02372<br>**h:** True<br>**Tau:** -0.3105<br>**Slope:** -1.6795e-06 |

# Chapter 5
# Final Conclusions and Recommendations

## 5.1 Conclusions

This study focused on improving the understanding of groundwater-surface water interactions within a small, perennial stream in southern Ontario (Alder Creek), through the identification and quantification of groundwater-surface water exchange and how it varied spatially and temporally over a seasonal cycle. Field reconnaissance of Alder Creek was initially performed to identify areas exhibiting groundwater discharge conditions. This was then followed by detailed, longer term studies using a variety of techniques that verified the reconnaissance findings, addressed challenges pertaining to quantifying groundwater-surface water exchange, and identified spatial and temporal variability.

Chapter 2 presented a novel reconnaissance approach that involved applying small scale temperature probe readings, visual and infrared imaging observations, and hydraulic gradient techniques throughout a watershed to identify signs of groundwater discharge. Visual observations and infrared imaging proved valuable in identifying groundwater discharge along the streambanks and shallow edges of the stream but was not applicable when assessing the streambed. The temperature probe addressed this issue, as it allowed for cold streambed temperatures to be measured to identify discharge in addition to verify the infrared findings. The measuring of hydraulic gradients proved ineffective, as the tool applied struggled to penetrate the armoured streambed and was inefficient in terms of operator time. Overall, the reconnaissance proved successful at identifying higher flux groundwater discharge conditions, and based on the reconnaissance survey data, two suspected gaining stream reaches, referred to as Site 1 and Site 2, were identified for more detail study. Longer-term studies at the two sites proved successful in verifying the reconnaissance findings. This verification was based on the consistently upward vertical hydraulic gradients and Darcy fluxes within the dense network of conventional and mini-piezometers installed along and within the stream at each site, the predominantly upward temperature profiling fluxes, the confirmation of temperature contrast between surface water and groundwater discharge features through additional, focused infrared imaging, and the consistent increase in streamflow due to groundwater discharge measured through differential stream gauging. These detailed, long-term investigations (e.g. Darcy and temperature fluxes) commonly showed that groundwater discharge was greater where the

reconnaissance had identified groundwater discharge along the study reaches. These more detailed studies also emphasized potential limitations of the reconnaissance scale monitoring, as significant spatial variability in groundwater exchange phenomena was detected throughout the dense monitoring network that may not have been captured with the coarse spatial reconnaissance measurements. While understanding the complexity and variability in groundwater-surface water interactions requires more detailed studies, this reconnaissance approach appears to be a valuable technique for identifying overall gaining stream reaches and can be a valuable approach for finding where to focus future groundwater discharge studies.

Chapter 3 evaluated the applicability of different field monitoring techniques to quantify groundwater-surface water exchange and assess its spatial variability. This involved differential stream gauging, upscaling point measurements of streambed groundwater flux using the Thiessen polygon tool and developing flow nets. The point measurement vertical flux techniques of temperature profiling and Darcy's law produced similar spatial patterns of groundwater-surface water exchange across the study reaches, supporting their effectiveness for assessing spatial variability. However, the Darcy's law technique, with the assumption of isotropic conditions, greatly overestimated the temperature profiling groundwater discharge. Through the application of anisotropy ratios, the discharge estimates were greatly reduced and became similar to the temperature profiling groundwater discharge estimates, highlighting the importance of accounting for anisotropy. These techniques also provided insight into temporal variability in discharge, as the groundwater discharge estimates were higher in the summer than in the winter, indicative of the variability in hydraulic conductivity and hydraulic gradients with time and emphasizing the importance of seasonality in groundwater-surface water interactions. These point scale groundwater discharge estimates, however, greatly underestimated the differential stream gauging total groundwater discharge estimate at Site 1; this was interpreted as being related to their inability to account for non-vertical groundwater discharge. It was therefore concluded that vertical groundwater discharge contributes relatively little to total groundwater discharge at Site 1, and that another source must exist that is not being accounted for. Based on visible discharge near the streambanks, it was presumed that a majority of the discharge was entering near the streambanks. To quantify this, 2-D plan view flow nets were developed, but the field and historical data used were unable to account for the missing component of discharge. This was attributed to underestimating the hydraulic conductivity representative of the aquifer that intercepts the stream. After applying a higher hydraulic conductivity, still considered reasonable for

the sites, a more representative estimate of the total groundwater discharge was produced. These findings suggest substantial contributions of groundwater discharge near the streambank to total groundwater discharge may exist at some sites, and the importance of being able to account for it. Future application of numerical groundwater models using the collected field data would be valuable in gaining a better understanding of the relative importance of streambank discharge and the conditions under which this should be considered.

Chapter 4 assessed the temporal variability of groundwater-surface water exchange at Sites 1 and 2 using groundwater level, surface water level, hydraulic gradient and stream flow data. Bi-weekly hydraulic head monitoring, used to calculate vertical hydraulic gradients, in addition to helping correct the continuous water level datasets, identified the presence of consistently upward groundwater flow and temporal variability in groundwater exchange during the course of a seasonal cycle. Continuously recorded hydraulic head data and associated hydraulic gradient estimates, however, provided additional insight relative to the bi-weekly readings. These more temporally dense datasets were also able to identify seasonal trends, such as increasing vertical hydraulic gradients in the summer and winter at both study sites, through the use of visual interpretations and analytical techniques. Additionally, the continuous data captured rapid changes in hydraulic gradients, including reversals in response to short-term high flow events. The horizontal hydraulic gradient data behaved similarly during high flow events, but otherwise indicated consistent groundwater flow toward the stream, in support of gaining conditions. These hydraulic gradient results supported the long-term differential stream gauging dataset at Site 1, which exhibited groundwater discharge conditions during most of the year outside of the extreme flow events. Through the application of these various techniques across the annual cycle of a perennial stream system, it was clear that temporal variability of groundwater-surface water exchange takes place. These findings highlight the importance of accounting for temporal variability in groundwater-surface water exchange in order to better understand the complex dynamics of groundwater surface water interactions.

## 5.2 Recommendations

Recommendations for future work to build on the findings of this study include:

1) Attempt to collect data for the various groundwater discharge quantification techniques concurrently, in order to minimize the impact of the temporal variability of groundwater-surface water exchange.

2) Apply the data collected as part of this study to numerical groundwater models, in order to gain an improved understanding of groundwater-surface water exchange, especially near the streambanks at the study sites, throughout the Alder Creek watershed, and at a greater regional scale.

3) Assess surface water and groundwater quality parameters such as nitrate, chloride and/or phosphorus within the watershed, including at the identified study sites, in order to better understand the role that groundwater discharge has on surface water quality within the watershed.

4) Perform a similar study upstream of the identified study sites, closer to the headwaters of Alder Creek, where more seasonal variability in groundwater levels can be expected, in order to better assess how hydraulic gradients and groundwater flux vary over time in that context.

5) Perform a similar study in an unarmoured streambed, where more techniques can be applied to better understand groundwater-surface water interactions – techniques such as, but not limited to, the installation of seepage meters, and the collection of cores for grain size analysis.

6) Apply environmental tracer techniques (e.g., 2H, 18O, radon, chloride, and/or chlorofluorocarbons) in order to identify and quantify groundwater discharge.

7) Apply hydrograph separation techniques to both existing and new long term streamflow datasets.

8) Develop techniques to better quantify groundwater discharge entering near the streambank.

# References


Aksoy, H., Kurt, I., & Eris, E. (2009). Filtered smoothed minima baseflow separation method. *Journal of Hydrology (Amsterdam)*, *372*(1), 94–101. https://doi.org/10.1016/j.jhydrol.2009.03.037.

Anibas, C., Fleckenstein, J. H., Volze, N., Buis, K., Verhoeven, R., Meire, P., & Batelaan, O. (2009). Transient or steady-state? Using vertical temperature profiles to quantify groundwater-surface water exchange. *Hydrological Processes*, *23*(15), 2165–2177. https://doi.org/10.1002/hyp.7289.

Anibas, C., Buis, K., Verhoeven, R., Meire, P., & Batelaan, O. (2011). A simple thermal mapping method for seasonal spatial patterns of groundwater–surface water interaction. Journal of Hydrology (Amsterdam), 397(1), 93–104. https://doi.org/10.1016/j.jhydrol.2010.11.036.

Aldous A. R., & Gannett M. W. (2021). Groundwater, biodiversity, and the role of flow system scale. *Ecohydrology*, *14*(8). doi:10.1002/eco.2342.

Bardini, L., Boano, F., Cardenas, M. B., Revelli, R., & Ridolfi, L. (2012). Nutrient cycling in bedform induced hyporheic zones. *Geochimica et Cosmochimica Acta, 84*, 47–61. https://doi.org/10.1016/j.gca.2012.01.025.

Barlow, P. M., & Leake, S. A. (2012). *Streamflow depletion by wells: Understanding and managing the effects of groundwater pumping on streamflow* (U.S. Geological Survey Circular 1376, 84 pp.). U.S. Geological Survey. https://pubs.usgs.gov/circ/1376/.

Bajc, A. F., Russell, H. A. J., & Sharpe, D. R. (2014). A three-dimensional hydrostratigraphic model of the Waterloo Moraine area, southern Ontario, Canada. *Canadian Water Resources Journal*, *39*(2), 95–119. https://doi.org/10.1080/07011784.2014.914794.

Becker, M. W., Georgian, T., Ambrose, H., Siniscalchi, J., & Fredrick, K. (2004). Estimating flow and flux of ground water discharge using water temperature and velocity. *Journal of Hydrology (Amsterdam)*, *296*(1), 221–233. https://doi.org/10.1016/j.jhydrol.2004.03.025.

Binley, A., Ullah, S., Heathwaite, A. L., Heppell, C., Byrne, P., Lansdown, K., Trimmer, M., & Zhang, H. (2013). Revealing the spatial variability of water fluxes at the groundwater-surface water interface. *Water Resources Research*, *49*(7), 3978–3992. https://doi.org/10.1002/wrcr.20214.

Bredehoeft, J. D., & Papadopoulos, I. S. (1965). Rates of vertical groundwater movement estimated from the Earth's thermal profile. *Water Resources Research*, *1*(2), 325–328. https://doi.org/10.1029/WR001i002p00325.

Briggs, M. A., Lautz, L. K., & McKenzie, J. M. (2012). A comparison of fibre-optic distributed temperature sensing to traditional methods of evaluating groundwater inflow to streams. *Hydrological Processes*, *26*(9), 1277–1290. https://doi.org/10.1002/hyp.8200.

Brodie, R., Sundaram, B., Tottenham, R., Hostetler, S., & Ransley, T. (2007). *An overview of tools for assessing groundwater-surface water connectivity* (133 pp.). Bureau of Rural Sciences.

Brunke, M. (1999). Colmation and Depth Filtration within Streambeds: Retention of Particles in Hyporheic Interstices. *International Review of Hydrobiology*, *84*(2): 99–117. https://doi.org/10.1002/iroh.199900014.

Butler, J. J., Jr. (1996). Slug tests in situ characterization: Some practical considerations. Environmental Geosciences, 3(4), 154–163. https://doi.org/10.1306/eg.04189601153.

Cey, E. E., Rudolph, D. L., Parkin, G. W., & Aravena, R. (1998). Quantifying groundwater discharge to a small perennial stream in southern Ontario, Canada. *Journal of Hydrology (Amsterdam)*, *210*(1), 21–37. https://doi.org/10.1016/S0022-1694(98)00172-3.

Cheng, S., Tong, X., & Illman, W. A. (2022). Evaluation of baseflow separation methods with real and synthetic streamflow data from a watershed. *Journal of Hydrology (Amsterdam), 613,* Article 128279. https://doi.org/10.1016/j.jhydrol.2022.128279.

Chapman, T.G., Maxwell, A.I. (1996). Baseflow Separation-comparison of Numerical Methods With Tracer Experiments. In: Hydrology and Water Resources Symposium 1996: Water and the Environment; Preprints of Papers. *Institution of Engineers, Australia*, p. 539.

CH2MHILL, S.S. Papadopulos & Associates Inc. (SSPA). (2003). Alder Creek Groundwater Study: Final Report. Prepared for The Regional Municipality of Waterloo, Kitchener, ON.

Coluccio, K., & Morgan, L. K. (2019). A review of methods for measuring groundwater-surface water exchange in braided rivers. *Hydrology and Earth System Sciences, 23*(10), 4397–4417. https://doi.org/10.5194/hess-23-4397-2019.

Conant, B. J. (2004). Delineating and quantifying ground water discharge zones using streambed temperatures. *Ground Water*, *42*(2), 243–257. https://doi.org/10.1111/j.1745-6584.2004.tb02671.x.

Constantz, J. (2008). Heat as a tracer to determine streambed water exchanges. *Water Resources Research*, *44*(4), W00D10-n/a. https://doi.org/10.1029/2008WR006996.

Cook, P. G., Favreau, G., Dighton, J. C., & Tickell, S. (2003). Determining natural groundwater influx to a tropical river using radon, chlorofluorocarbons and ionic environmental tracers. *Journal of Hydrology (Amsterdam)*, *277*(1), 74–88. https://doi.org/10.1016/S0022-1694(03)00087-8.

Crites, H., Kokelj, S. V., & Lacelle, D. (2020). Icings and groundwater conditions in permafrost catchments of northwestern Canada. *Scientific Reports, 10*(1), 3283–3283. https://doi.org/10.1038/s41598-020-60322-w.

Deitchman, R. S., & Loheide II, S. P. (2009). Ground-based thermal imaging of groundwater flow processes at the seepage face. *Geophysical Research Letters*, *36*(14), L14401-n/a. https://doi.org/10.1029/2009GL038103.

Dubois, E., Larocque, M., Gagné, S., & Braun, M. (2022). Climate Change Impacts on Groundwater Recharge in Cold and Humid Climates: Controlling Processes and Thresholds. *Climate, 10*(1), 6. https://doi.org/10.3390/cli10010006.

Eaton, J. W., Bateman, D., Hauberg, S., & Wehbring, R. (2024). GNU Octave: A high-level interactive language for numerical computations (9th ed., for Octave Version 9.2.0). https://octave.org/support.

Eckhardt, K. (2005). How to construct recursive digital filters for baseflow separation. *Hydrological Processes, 19*(2), 507–515. https://doi.org/10.1002/hyp.5675.

Esri, Maxar, Earthstar Geographics, TomTom, Garmin, FAO, NOAA, USGS, © OpenStreetMap contributors, and the GIS User Community. (2025a). World Imagery Hybrid, Esri [data set], https://www.arcgis.com/home/item.html?id=28f49811a6974659988fd279de5ce39f. (Accessed 2025).

Esri, TomTom, Garmin, FAO, NOAA, USGS, © OpenStreetMap contributors, and the GIS User Community. (2025b). World Light Gray Base, Esri [data set], https://www.arcgis.com/home/item.html?id=291da5eab3a0412593b66d384379f89f. (Accessed 2025).

Fraser, B. G., & Williams, D. D. (1998). Seasonal Boundary Dynamics of a Groundwater/Surface-Water Ecotone. *Ecology (Durham), 79*(6), 2019–2031. https://doi.org/10.1890/0012-9658(1998)079[2019:SBDOAG]2.0.CO;2.

Fuchs, J. W., Fox, G. A., Storm, D. E., Penn, C. J., & Brown, G. O. (2009). Subsurface transport of phosphorus in riparian floodplains: Influence of preferential flow paths. *Journal of Environmental Quality, 38*(2), 473–484. https://doi.org/10.2134/jeq2008.0201

Furey, P. R., & Gupta, V. K. (2001). A physically based filter for separating base flow from streamflow time series. *Water Resources Research, 37*(11), 2709–2722. https://doi.org/10.1029/2001WR000243.

Ghysels, G., Anibas, C., Awol, H., Tolche, A., Schneidewind, U., & Huysmans, M. (2021). The Significance of Vertical and Lateral Groundwater–Surface Water Exchange Fluxes in Riverbeds and Riverbanks: Comparing 1D Analytical Flux Estimates with 3D Groundwater Modelling. *Water (Basel), 13*(3), 306-. https://doi.org/10.3390/w13030306.

Glass, B. K., Rudolph, D. L., Duguay, C., & Wicke, A. (2021). Identifying groundwater discharge zones in the central Mackenzie Valley using remotely sensed optical and thermal imagery. *Canadian Journal of Earth Sciences, 58*(2), 105–121. https://doi.org/10.1139/cjes-2019-0169.

Government of Canada. (2025a). Canadian Climate Normals 1981-2010 Station Data for the Roseville, ON, weather station, Government of Canada [data set]. Extracted from the Environment and Climate Change Canada Historical Climate Data web site, https://climate.weather.gc.ca/climate_normals/results_1981_2010_e.html?stnID=4816&autofwd=1. (Accessed 2025).

Government of Canada. (2025b). Historical daily water-level data for station 02GA030 [data set]. Environment and Climate Change Canada, Water Office. Extracted from the Environment and Climate Change Canada Historical Hydrometric Data web site, https://wateroffice.ec.gc.ca/report/historical_e.html?stn=02GA030&dataType=Daily&parameterType=Level&first_year=2024&last_year=2024&mode=Table&page=historical&year=2024&start_year=1850&end_year=2025. (Accessed 2025).

Government of Ontario. (2023). service02 (n/a) [data set], https://ws.lioservices.lrc.gov.on.ca/arcgis1071a/rest/services/LIO_OPEN_DATA/LIO_Open02/MapServer.

Grand River Conservation Authority (GRCA). (2017). Subcatchment basins [data set]. Contains Information made available under Grand River Conservation Authority's Open Data Licence v2.0. (https://data.grandriver.ca/about-licensing.html). https://data.grandriver.ca/downloads-geospatial.html. (Accessed 2025).

Grand River Conservation Authority (GRCA). (2023). Watershed Boundary - Jurisdiction Polygon [data set]. Contains Information made available under Grand River Conservation Authority's Open Data Licence v2.0. (https://data.grandriver.ca/about-licensing.html). https://data.grandriver.ca/downloads-geospatial.html. (Accessed 2025).

Green, T. R., Taniguchi, M., Kooi, H., Gurdak, J. J., Allen, D. M., Hiscock, K. M., Treidel, H., & Aureli, A. (2011). Beneath the surface of global change: Impacts of climate change on groundwater. *Journal of Hydrology (Amsterdam), 405*(3), 532–560. https://doi.org/10.1016/j.jhydrol.2011.05.002.

Hamed, K. H., & Ramachandra Rao, A. (1998). A modified Mann-Kendall trend test for autocorrelated data. *Journal of Hydrology (Amsterdam), 204*(1), 182–196. https://doi.org/10.1016/S0022-1694(97)00125-X.

Handcock, R. N., Gillespie, A. R., Cherkauer, K. A., Kay, J. E., Burges, S. J., & Kampf, S. K. (2006). Accuracy and uncertainty of thermal-infrared remote sensing of stream temperatures at multiple spatial scales. *Remote Sensing of Environment*, *100*(4), 427–440. https://doi.org/10.1016/j.rse.2005.07.007.

Harris, P. J. (1995). Water quality impacts from on-site waste disposal systems to coastal areas through groundwater discharge. *Environmental Geology (Berlin), 26*(4), 262–268. https://doi.org/10.1007/BF00770477.

Harte, P. T., & Kiah, R. G. (2009). Measured river leakages using conventional streamflow techniques: the case of Souhegan River, New Hampshire, USA. *Hydrogeology Journal, 17*(2), 409–424. https://doi.org/10.1007/s10040-008-0359-.

Hatch, C. E., Fisher, A. T., Revenaugh, J. S., Constantz, J., & Ruehl, C. (2006). Quantifying surface water–groundwater interactions using time series analysis of streambed thermal records: Method development. *Water Resources Research*, *42*(10), W10410-n/a. https://doi.org/10.1029/2005WR004787.

Heeren, D. M., Miller, R. B., Fox, G. A., Storm, D. E., Halihan, T., & Penn, C. J. (2010). Preferential flow effects on subsurface contaminant transport in alluvial floodplains. *Transactions of the ASABE, 53*(1), 127–136. https://doi.org/10.13031/2013.29511

Hodson, T. O., Doore, K. J., Kenney, T. A., Over, T. M., & Yeheyis, M. B. (2024). Ratingcurve: A Python Package for Fitting Streamflow Rating Curves. Hydrology, 11(2), Article 14. https://doi.org/10.3390/hydrology11020014.

Holman, I. P., Whelan, M. J., Howden, N. J. K., Bellamy, P. H., Willby, N. J., Rivas-Casado, M., & McConvey, P. (2008). Phosphorus in groundwater--an overlooked contributor to eutrophication? *Hydrological Processes, 22*(26), 5121–5127. https://doi.org/10.1002/hyp.7198.

Howard, K. W. F., & Livingstone, S. (2000). Transport of urban contaminants into Lake Ontario via sub-surface flow. *Urban Water, 2*(3), 183–195. https://doi.org/10.1016/S1462-0758(00)00058-3.

Hvorslev, M. J. (1951). *Time lag and soil permeability in ground-water observations* (Bulletin No. 36). U.S. Army Corps of Engineers, Waterways Experiment Station.

Irvine, D. J., Cranswick, R. H., Simmons, C. T., Shanafield, M. A., & Lautz, L. K. (2015). The effect of streambed heterogeneity on groundwater-surface water exchange fluxes inferred from temperature time series. *Water Resources Research, 51*(1), 198–212. https://doi.org/10.1002/2014WR015769.

Irvine, D. J., Cartwright, I., Post, V. E. A., Simmons, C. T., & Banks, E. W. (2016). Uncertainties in vertical groundwater fluxes from 1-D steady state heat transport analyses caused by heterogeneity, multidimensional flow, and climate change. *Water Resources Research*, *52*(2), 813–826. https://doi.org/10.1002/2015WR01770.

Jensen, J. K., & Engesgaard, P. (2011). Nonuniform groundwater discharge across a streambed; heat as a tracer. *Vadose Zone Journal*, *10*(1), 98–109. https://doi.org/10.2136/vzj2010.0005.

Karrow, P. F. (1993). *Quaternary geology of the Stratford-Conestogo area, Ontario* (Ontario Geological Survey Open File Report 283). Ontario Geological Survey.

Kalbus, E., Reinstorf, F., & Schirmer, M. (2006). Measuring methods for groundwater - surface water interactions: a review. *Hydrology and Earth System Sciences*, *10*(6), 873–887. https://doi.org/10.5194/hess-10-873-2006.

Käser, D. H., Binley, A., Heathwaite, A. L., & Krause, S. (2009). Spatio-temporal variations of hyporheic flow in a riffle-step-pool sequence. *Hydrological Processes, 23*(15), 2138–2149. https://doi.org/10.1002/hyp.7317.

Keery, J., Binley, A., Crook, N., & Smith, J. W. N. (2007). Temporal and spatial variability of groundwater–surface water fluxes: Development and application of an analytical method using temperature time series. *Journal of Hydrology (Amsterdam)*, *336*(1), 1–16. https://doi.org/10.1016/j.jhydrol.2006.12.003.

Kendy, E., & Bredehoeft, J. D. (2006). Transient effects of groundwater pumping and surface-water-irrigation returns on streamflow. *Water Resources Research, 42*(8), W08415-n/a. https://doi.org/10.1029/2005WR004792.

Kluge, T., Ilmberger, J., von Rohden, C., and Aeschbach-Hertig, W. (2007). Tracing and quantifying groundwater inflow into lakes using a simple method for radon-222 analysis. *Hydrology and Earth System Sciences, 11*(5), 1621–1631. https://doi.org/10.5194/hess-11-1621-2007.

Krause, S., Blume, T., & Cassidy, N. J. (2012). Investigating patterns and controls of groundwater up-welling in a lowland river by combining Fibre-optic Distributed Temperature Sensing with observations of vertical hydraulic gradients. *Hydrology and Earth System Sciences*, *16*(6), 1775–1792. https://doi.org/10.5194/hess-16-1775-2012.

Kurylyk, B. L., Irvine, D. J., Carey, S. K., Briggs, M. A., Werkema, D. D., & Bonham, M. (2017). Heat as a groundwater tracer in shallow and deep heterogeneous media: Analytical solution, spreadsheet tool, and field applications. *Hydrological Processes*, *31*(14), 2648–2661. https://doi.org/10.1002/hyp.11216.

Kurylyk, B. L., Irvine, D. J., & Bense, V. F. (2019). Theory, tools, and multidisciplinary applications for tracing groundwater fluxes from temperature profiles. *Wiley Interdisciplinary Reviews. Water*, *6*(1), e1329-n/a. https://doi.org/10.1002/wat2.1329.

Laursen, A., & Seitzinger, S. (2005). Limitations to measuring riverine denitrification at the whole reach scale: Effects of channel geometry, wind velocity, sampling interval, and temperature inputs of N 2-enriched groundwater. *Hydrobiologia*, *545*(1), 225–236. https://doi.org/10.1007/s10750-005-2743-3.

Lapham, W. W. (1989). *Use of temperature profiles beneath streams to determine rates of vertical ground-water flow and vertical hydraulic conductivity* (U.S. Geological Survey Water-Supply Paper 2337). U.S. Government Publishing Office.

Lautz, L. K. (2010). Impacts of nonideal field conditions on vertical water velocity estimates from streambed temperature time series. *Water Resources Research, 46*(1). https://doi.org/10.1029/2009WR007917.

Lautz, L. K., & Ribaudo, R. E. (2012). Scaling up point-in-space heat tracing of seepage flux using bed temperatures as a quantitative proxy. *Hydrogeology journal*, *20*(7), 1223–1238. https://doi.org/10.1007/s10040-012-0870-2.

Lee, D.R., & Cherry, J.A. (1979). A Field Exercise on Groundwater Flow Using Seepage Meters and Mini-piezometers. *Journal of Geological Education, 27*, 6-10.

Liu, C., Liu, J., Hu, Y., Wang, H., & Zheng, C. (2016). Airborne Thermal Remote Sensing for Estimation of Groundwater Discharge to a River. *Ground Water*, *54*(3), 363–373. https://doi.org/10.1111/gwat.12362.

Lowry, C. S., Walker, J. F., Hunt, R. J., & Anderson, M. P. (2007). Identifying spatial variability of groundwater discharge in a wetland stream using a distributed temperature sensor. *Water Resources Research*, *43*(10), W10408-n/a. https://doi.org/10.1029/2007WR006145.

Lu, N., & Ge, S. (1996). Effect of Horizontal Heat and Fluid Flow on the Vertical Temperature Distribution in a Semiconfining Layer. *Water Resources Research*, *32*(5), 1449–1453. https://doi.org/10.1029/95WR03095.

Luce, C. H., Tonina, D., Gariglio, F., & Applebee, R. (2013). Solutions for the diurnally forced advection-diffusion equation to estimate bulk fluid velocity and diffusivity in streambeds from temperature time series. *Water Resources Research, 49*(1), 488–506. https://doi.org/10.1029/2012WR012380.

Ma, R., Chen, K., Andrews, C. B., Loheide, S. P., Sawyer, A. H., Jiang, X., Briggs, M. A., Cook, P. G., Gorelick, S. M., Prommer, H., Scanlon, B. R., Guo, Z., & Zheng, C. (2024). Methods for Quantifying Interactions Between Groundwater and Surface Water. *Annual Review of Environment and Resources, 49*(1), 623–653. https://doi.org/10.1146/annurev-environ-111522-104534.

Malcolm, I. A., Soulsby, C., & Youngson, A. F. (2006). High-frequency logging technologies reveal state-dependent hyporheic process dynamics: implications for hydroecological studies. *Hydrological Processes, 20*(3), 615–622. https://doi.org/10.1002/hyp.6107.

Martin, P. J., & Frind, E. O. (1998). Modeling a complex multi-aquifer system: the Waterloo Moraine. *Ground Water, 36*(4), 679–690. https://doi.org/10.1111/j.1745-6584.1998.tb02843.x.

Matrix Solutions Inc. (Matrix), & S.S. Papadopulos and Associates Inc. (SSPA). (2014). Region of Waterloo tier three water budget and local area risk assessment, model calibration and water budget report. Prepared for: The Regional Municipality of Waterloo. Waterloo, ON; August 2014.

McCallum, J. L., Cook, P. G., Berhane, D., Rumpf, C., & McMahon, G. A. (2012). Quantifying groundwater flows to streams using differential flow gaugings and water chemistry. *Journal of Hydrology (Amsterdam)*, *416*, 118–132. https://doi.org/10.1016/j.jhydrol.2011.11.040.

Mohamed, R. A. M., Gabrielli, C., Selker, J. S., Selker, F., Brooks, S. C., Ahmed, T., & Carroll, K. C. (2021). Comparison of fiber-optic distributed temperature sensing and high-sensitivity sensor spatial surveying of stream temperature. *Journal of Hydrology (Amsterdam), 603*(PB), 127015-. https://doi.org/10.1016/j.jhydrol.2021.127015.

Monteith, J. L. & Unsworth, M. H. (2013). *Principles of environmental physics: plants, animals, and the atmosphere* (4th ed.). Elsevier/Academic Press.

Moore, E. M., Barclay, J. R., Haynes, A. B., Jackson, K. E., Bisson, A. M., Briggs, M. A., & Helton, A. M. (2023). Where the past meets the present: connecting nitrogen from watersheds to streams through groundwater flowpaths. *Environmental Research Letters*, *18*(12), 124039-. https://doi.org/10.1088/1748-9326/ad0c86.

Ontario Geological Survey. (2010). *Surficial Geology of Southern Ontario* [data set]. Ontario Ministry of Mines. https://www.geologyontario.mines.gov.on.ca/persistent-linking?publication=MRD128-REV.

Ontario Ministry of the Environment, Conservation and Parks (MECP). (2024). Map: Well records. Retrieved from https://www.ontario.ca/page/map-well-records: 18 February 2025.

Poeter, E., & Hsieh, P. (2020). Graphical construction of groundwater flow nets. The Groundwater Project.

Puckett, L. J., Zamora, C., Essaid, H., Wilson, J. T., Johnson, H. M., Brayton, M. J., & Vogel, J. R. (2008). Transport and Fate of Nitrate at the Ground-Water/Surface-Water Interface. J*ournal of Environmental Quality, 37*(3), 1034–1050. https://doi.org/10.2134/jeq2006.0550.

Rau, G. C., Andersen, M. S., McCallum, A. M., & Acworth, R. I. (2010). Analytical methods that use natural heat as a tracer to quantify surface water–groundwater exchange, evaluated using field temperature records. *Hydrogeology Journal, 18*(5), 1093–1110. https://doi.org/10.1007/s10040-010-0586-0.

Rau, G. C., Post, V. E. A., Shanafield, M., Krekeler, T., Banks, E. W., & Blum, P. (2019). Error in hydraulic head and gradient time-series measurements: A quantitative appraisal. *Hydrology and Earth System Sciences, 23*(9), 3603–3629. https://doi.org/10.5194/hess-23-3603-2019.

Rehmel, M. S. (2006). Field Evaluation of Shallow-Water Acoustic Doppler Current Profiler Discharge Measurements. *Examining the Confluence of Environmental and Water Concerns - Proceedings of the World Environmental and Water Resources Congress 2006*, Article 162. https://doi.org/10.1061/40856(200)162.

Rosenberry, D. O., Striegl, R. G., & Hudson, D. C. (2000). Plants As Indicators of Focused Ground Water Discharge to a Northern Minnesota Lake. *Ground Water*, *38*(2), 296–303. https://doi.org/10.1111/j.1745-6584.2000.tb00340.x.

Rosenberry, D. O., Briggs, M. A., Delin, G., & Hare, D. K. (2016). Combined use of thermal methods and seepage meters to efficiently locate, quantify, and monitor focused groundwater discharge to a sand-bed stream. *Water Resources Research*, *52*(6), 4486–4503. https://doi.org/10.1002/2016WR018808.

Roshan, H., Rau, G. C., Andersen, M. S., & Acworth, I. R. (2012). Use of heat as tracer to quantify vertical streambed flow in a two-dimensional flow field. *Water Resources Research, 48*(10). https://doi.org/10.1029/2012WR011918.

Schmidt, C., Bayer-Raich, M., & Schirmer, M. (2006). Characterization of spatial heterogeneity of groundwater-stream water interactions using multiple depth streambed temperature measurements at the reach scale. *Hydrology and Earth System Sciences*, *10*(6), 849–859. https://doi.org/10.5194/hess-10-849-2006.

Schmidt, C., Conant, B., Bayer-Raich, M., & Schirmer, M. (2007). Evaluation and field-scale application of an analytical method to quantify groundwater discharge using mapped streambed temperatures. *Journal of Hydrology (Amsterdam)*, *347*(3), 292–307. https://doi.org/10.1016/j.jhydrol.2007.08.022.

Schuetz, T., & Weiler, M. (2011). Quantification of localized groundwater inflow into streams using ground-based infrared thermography. *Geophysical Research Letters*, *38*(3), np-n/a. https://doi.org/10.1029/2010GL046198.

Selker, J., van de Giesen, N., Westhoff, M., Luxemburg, W., & Parlange, M. B. (2006). Fiber optics opens window on stream dynamics. *Geophysical Research Letters*, *33*(24), L24401-n/a. https://doi.org/10.1029/2006GL027979.

Shan, C., & Bodvarsson, G. (2004). An analytical solution for estimating percolation rate by fitting temperature profiles in the vadose zone. *Journal of Contaminant Hydrology*, *68*(1), 83–95. https://doi.org/10.1016/S0169-7722(03)00126-8.

Sloto, R. A., & Crouse, M. Y. (1996). *HYSEP: A computer program for streamflow hydrograph separation and analysis* (U.S. Geological Survey Water-Resources Investigations Report 1996–4040, 46 p.). U.S. Geological Survey. https://pubs.er.usgs.gov/publication/wri964040.

Sörengård, M., & Di Baldassarre, G. (2017). Simple vs complex rating curves: accounting for measurement uncertainty, slope ratio and sample size. *Hydrological Sciences Journal, 62*(13), 2072–2082. https://doi.org/10.1080/02626667.2017.1367397.

Sousa, M. R., Rudolph, D. L., & Frind, E. O. (2014). Threats to groundwater resources in urbanizing watersheds: The Waterloo Moraine and beyond. *Canadian Water Resources Journal, 39*(2), 193–208. https://doi.org/10.1080/07011784.2014.914801.

Stallman, S. (1965). Steady one-dimensional fluid flow in a semi-infinite porous medium with sinusoidal surface temperature. *Journal of Geophysical Research 70*(12), 2821–2827.

Stonestrom, D., & Constantz, J. (2003). *Heat as a tool for studying the movement of ground water near streams* (U.S. Geological Survey Circular 1260). U.S. Geological Survey.

Taylor, R. G., Scanlon, B., Döll, P., Rodell, M., van Beek, R., Wada, Y., Longuevergne, L., Leblanc, M., Famiglietti, J. S., Edmunds, M., Konikow, L., Green, T. R., Chen, J., Taniguchi, M., Bierkens, M. F. P., MacDonald, A., Fan, Y., Maxwell, R. M., Yechieli, Y., … Treidel, H. (2013). Ground water and climate change. *Nature Climate Change, 3*(4), 322–329. https://doi.org/10.1038/nclimate1744.

Taylor, C. A., & Stefan, H. G. (2009). Shallow groundwater temperature response to climate change and urbanization. *Journal of Hydrology (Amsterdam), 375*(3), 601–612. https://doi.org/10.1016/j.jhydrol.2009.07.009.

Tecklenburg, C., & Blume, T. (2017). Identifying, characterizing and predicting spatial patterns of lacustrine groundwater discharge. *Hydrology and Earth System Sciences*, *21*(10), 5043–5063. https://doi.org/10.5194/hess-21-5043-2017.

Wallis, I., Prommer, H., Berg, M., Siade, A. J., Sun, J., & Kipfer, R. (2020). The river–groundwater interface as a hotspot for arsenic release. *Nature Geoscience, 13*(4), 288–295. https://doi.org/10.1038/s41561-020-0557-6.

Watts, C. L., Hatch, C. E., & Wicks, R. (2023). Mapping groundwater discharge seeps by thermal UAS imaging on a wetland restoration site. *Frontiers in Environmental Science, 10*. https://doi.org/10.3389/fenvs.2022.946565.

Westberg, R. (2012). *The use of temperature and environmental isotopes as tools to characterize groundwater discharge to the Grand River, Ontario, Canada*. [MSc. Thesis, University of Waterloo]. http://hdl.handle.net/10012/7280.

Wiebe, A. J., & Rudolph, D. L. (2022). Meteorological and hydrological data from the Alder Creek watershed, SW Ontario. *Earth System Science Data, 14*(7), 3229–3248. https://doi.org/10.5194/essd-14-3229-2022.

Wiebe, A. J., Menkveld, P. G., & Rudolph, D. L. (2023). Quantifying seasonal, depression focused recharge in the context of public supply well vulnerability. *Hydrological Processes, 37*(7), Article e14938. https://doi.org/10.1002/hyp.14938.

Winter, T. C. (1999). Relation of streams, lakes, and wetlands to groundwater flow systems. Hydrogeology Journal, 7(1), 28–45. https://doi.org/10.1007/s100400050178.

Zipper, S., Brookfield, A., Ajami, H., Ayers, J. R., Beightel, C., Fienen, M. N., Gleeson, T., Hammond, J., Hill, M., Kendall, A. D., Kerr, B., Lapides, D., Porter, M., Parimalarenganayaki, S., Rohde, M. M., & Wardropper, C. (2024). Streamflow Depletion Caused by Groundwater Pumping: Fundamental Research Priorities for Management-Relevant Science. *Water Resources Research, 60*(5). https://doi.org/10.1029/2023WR035727.

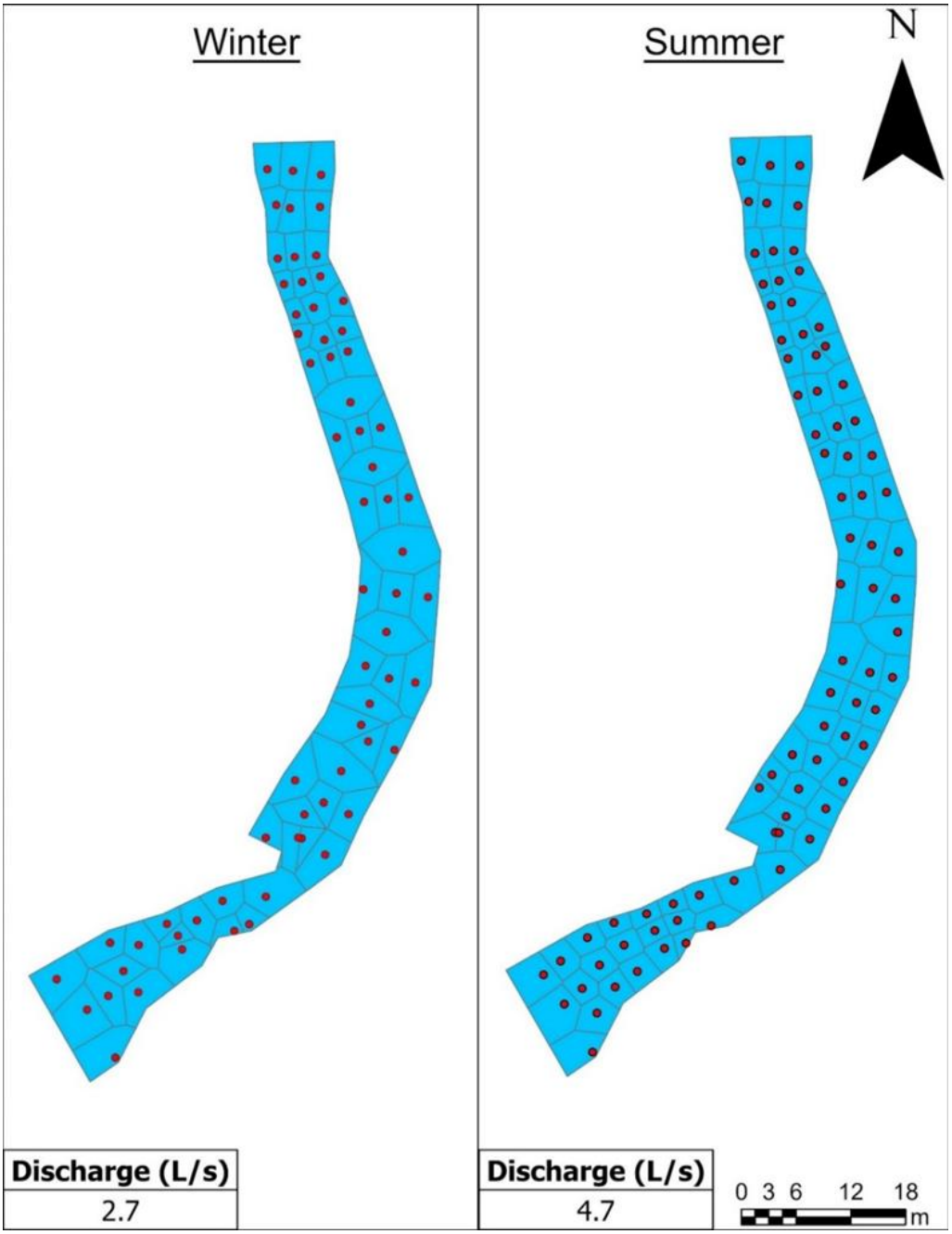
Zanatta, C., Wiebe, A., Rudolph, D. (2025). Groundwater Surface Water Exchange Data for Alder Creek Watershed, Grand River Basin, Ontario. https://doi.org/10.20383/103.01224

# Data Availability Statement

The data that supports the findings of this MSc study are openly available in Federated Research Data Repository at http://doi.org/10.20383/103.01224.

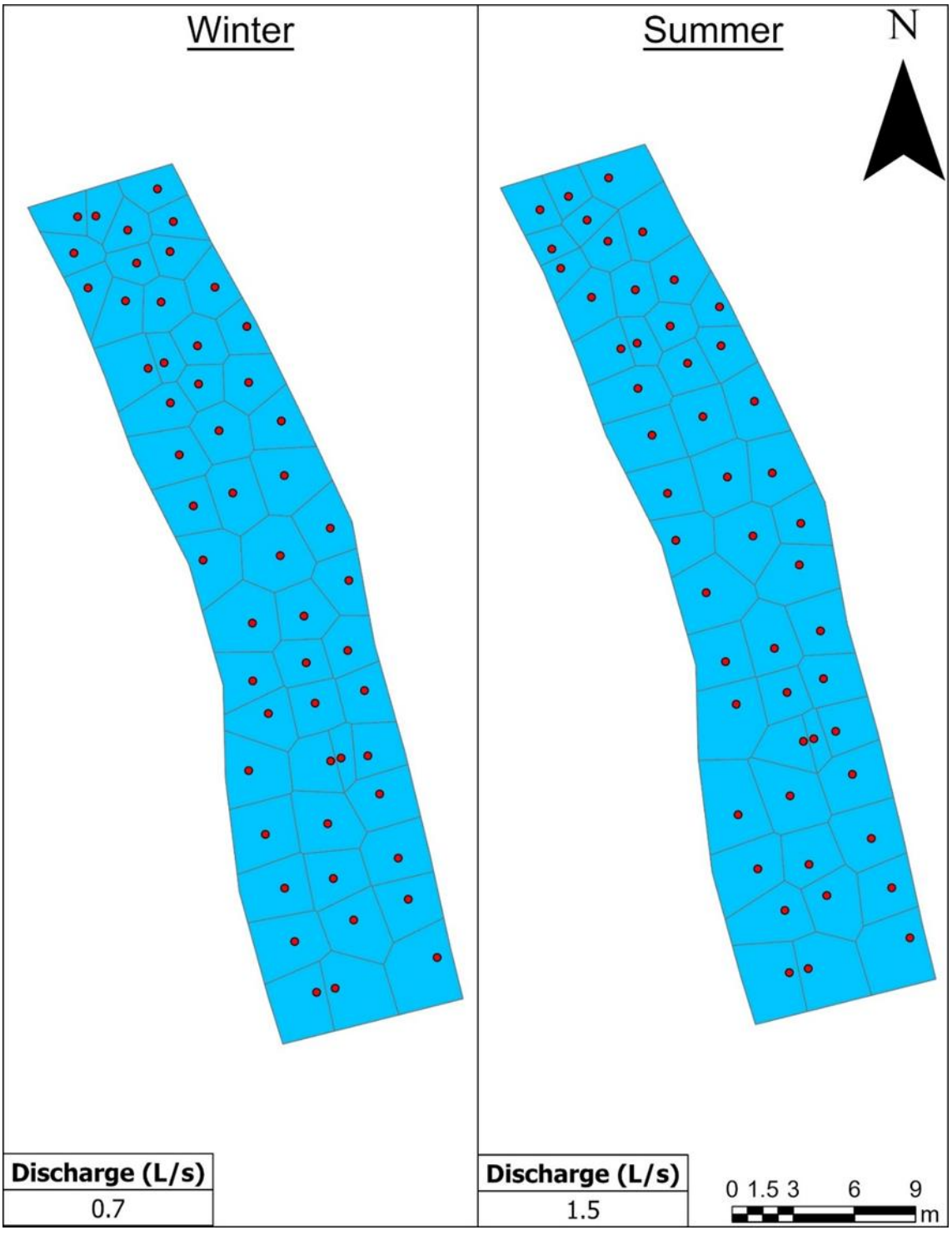
# Appendix A

## Thiessen Polygons



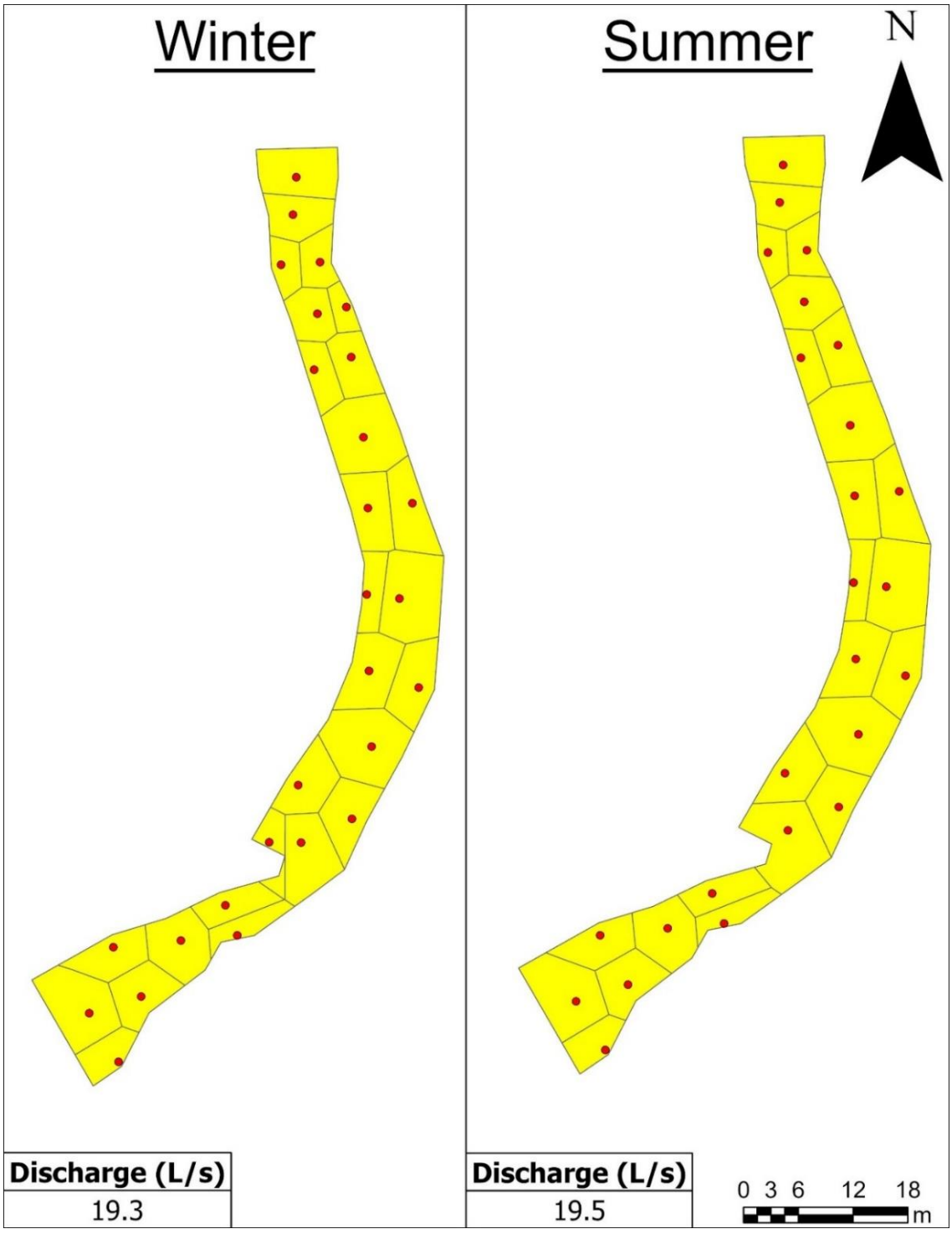

(a) (b)

Figure A.1: Temperature profiling discharge estimates using Thiessen polygon approach for Site 1 in (a) winter 2024 and (b) summer 2024.



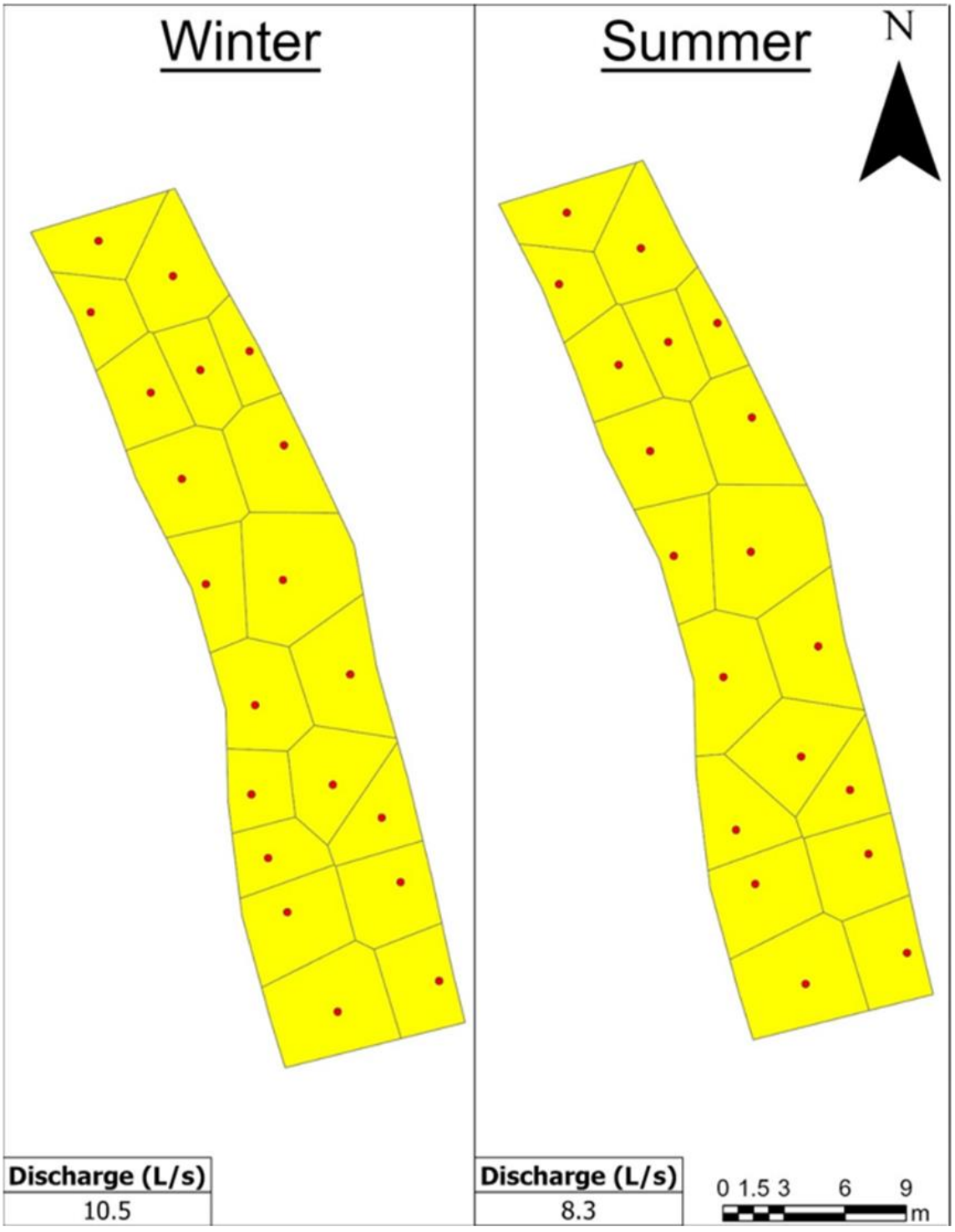

(a) (b)

Figure A.2: Temperature profiling discharges estimate using Thiessen polygon approach for Site 2 in (a) winter 2024 and (b) summer 2024.




(a) (b)

Figure A 3: Darcy's law discharge estimates using Thiessen polygon approach for Site 1 in (a) winter 2024 and (b) summer 2024.

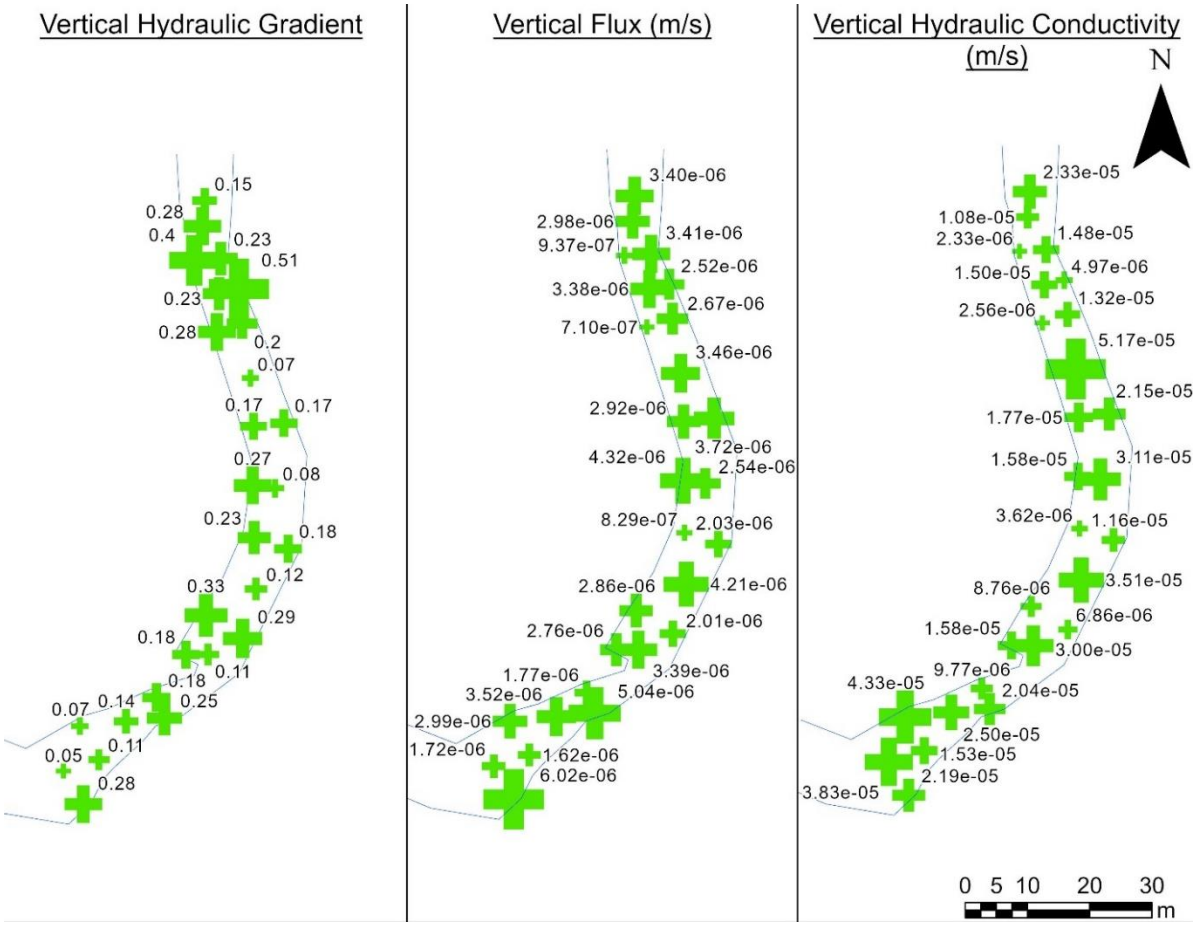



(a) (b)

Figure A.4: Darcy's law discharge estimates using Thiessen polygon approach for Site 2 in (a) winter 2024 and (b) summer 2024.

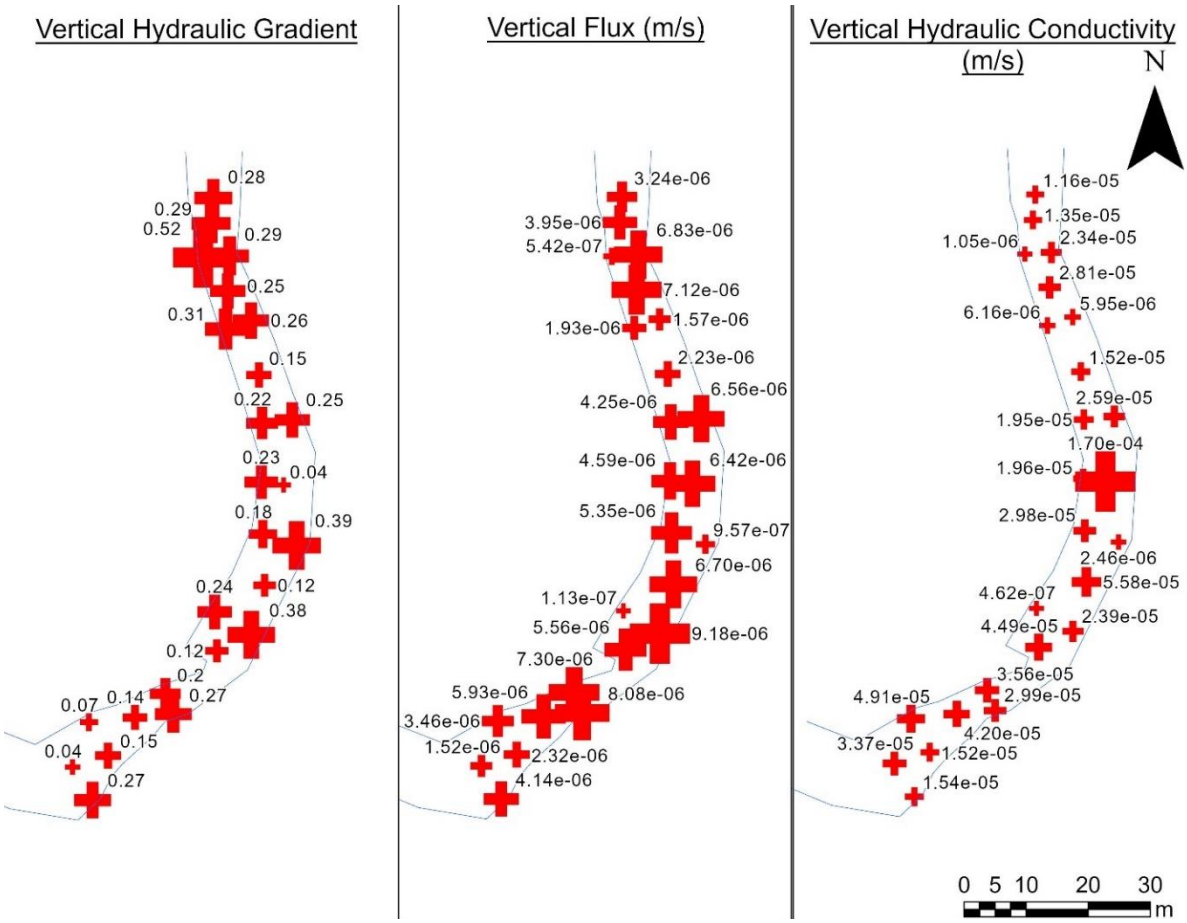
# Appendix B

# Vertical Hydraulic Conductivity



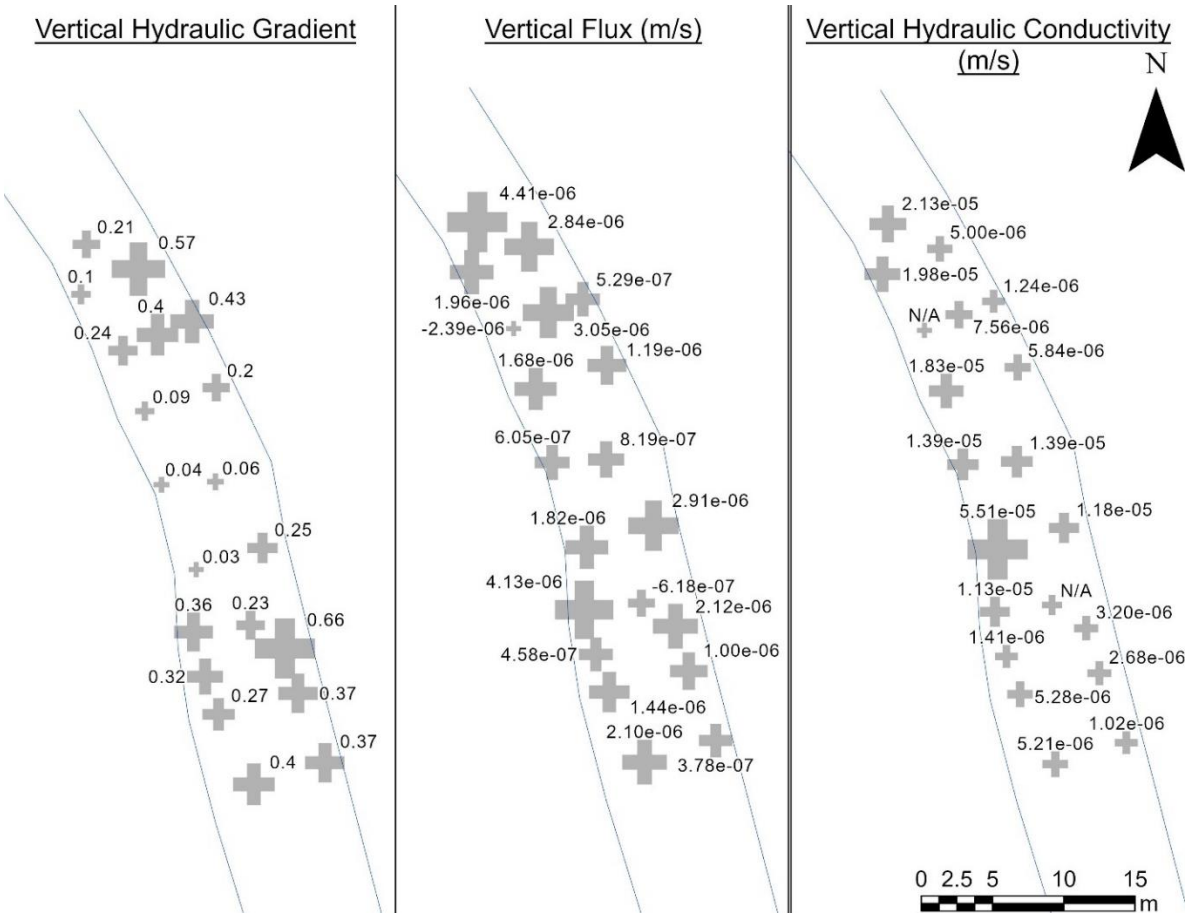

(a) (b) (c)

Figure B.1: (a) Vertical hydraulic gradients and (b) vertical fluxes measured in winter 2024 that were used to estimate (c) vertical hydraulic conductivity at Site 1.



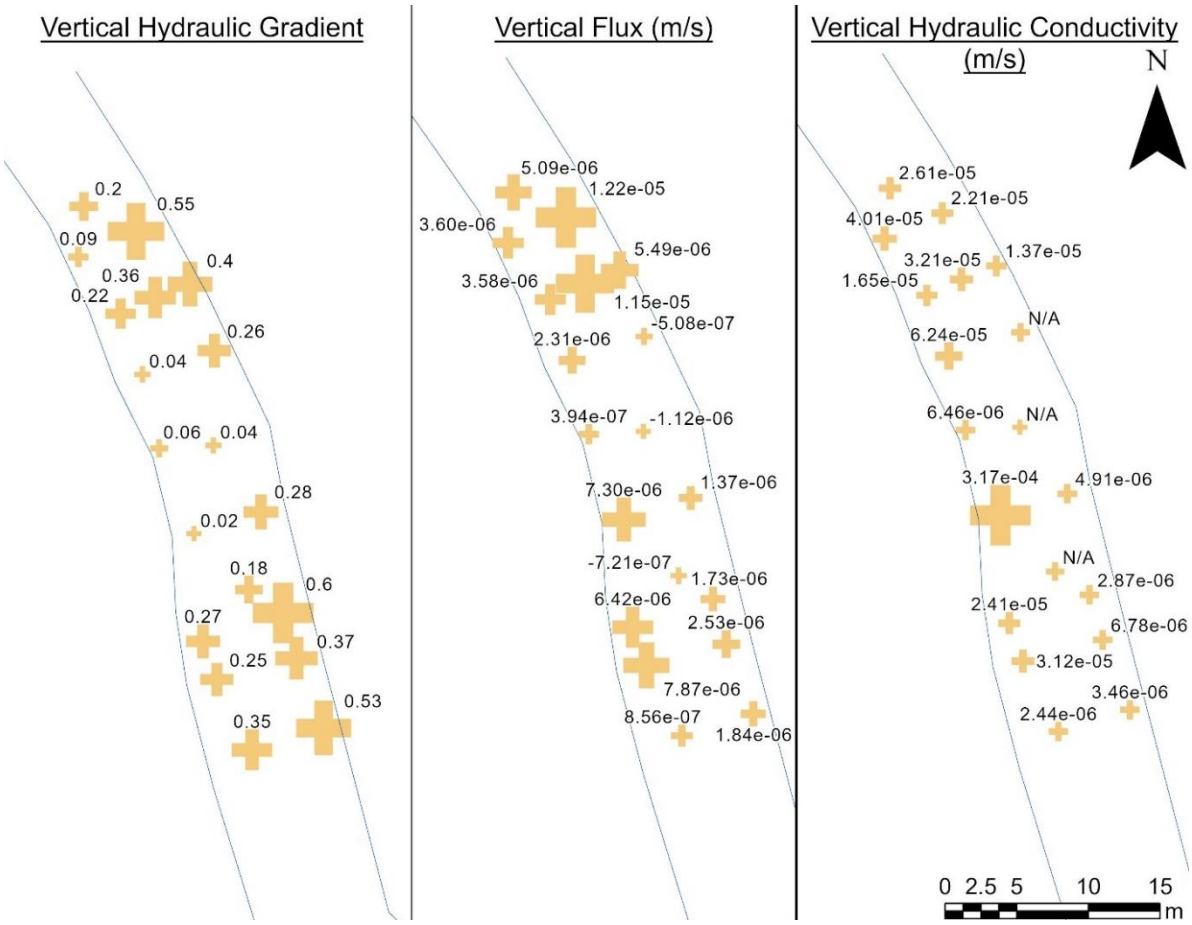

(a) (b) (c)

Figure B.2: (a) Vertical hydraulic gradients and (b) vertical fluxes measured in summer 2024 that were used to estimate (c) vertical hydraulic conductivity at Site 1.




(a) (b) (c)

Figure B.3: (a) Vertical hydraulic gradients and (b) vertical fluxes measured in winter 2024 that were used to estimate (c) vertical hydraulic conductivity at Site 2. If the flux direction and vertical gradient direction contradicted one another, no hydraulic conductivity value was estimated and is therefore denoted as “N/A”.




(a) (b) (c)

Figure B.4: Vertical hydraulic gradients and (b) vertical fluxes measured in summer 2024 that were used to estimate (c) vertical hydraulic conductivity at Site 2. If the flux direction and vertical gradient direction contradicted one another, no hydraulic conductivity value was estimated and is therefore denoted as "N/A".

# Appendix C

## Temperature Profiles

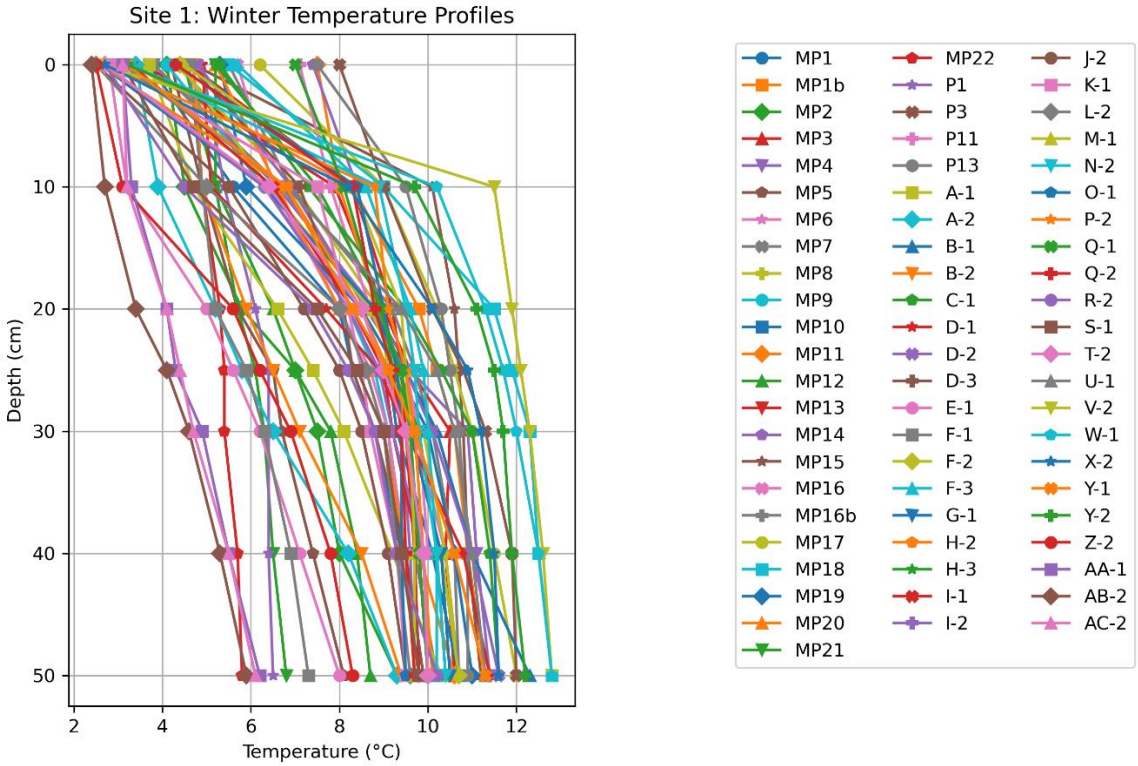



Figure C.1: Temperature profiles collected at Site 1 in the winter of 2024.

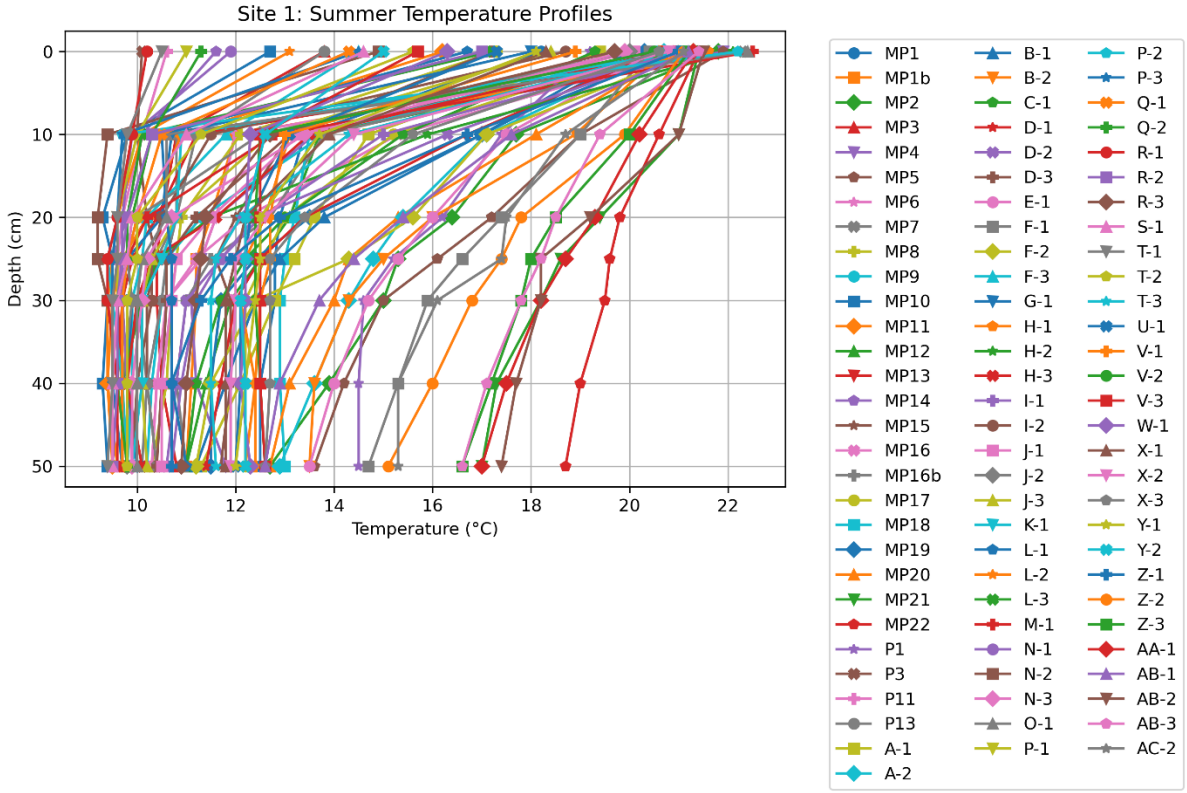



Figure C.2: Temperature profiles collected at Site 1 in the summer of 2024.

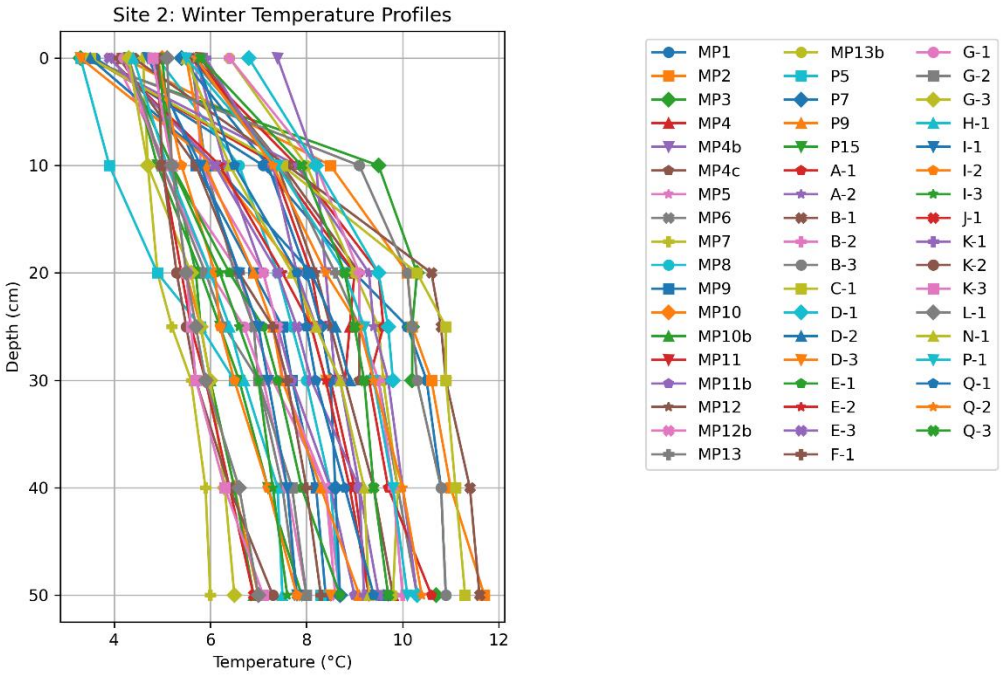



Figure C.3: Temperature profiles collected at Site 2 in the winter of 2024.

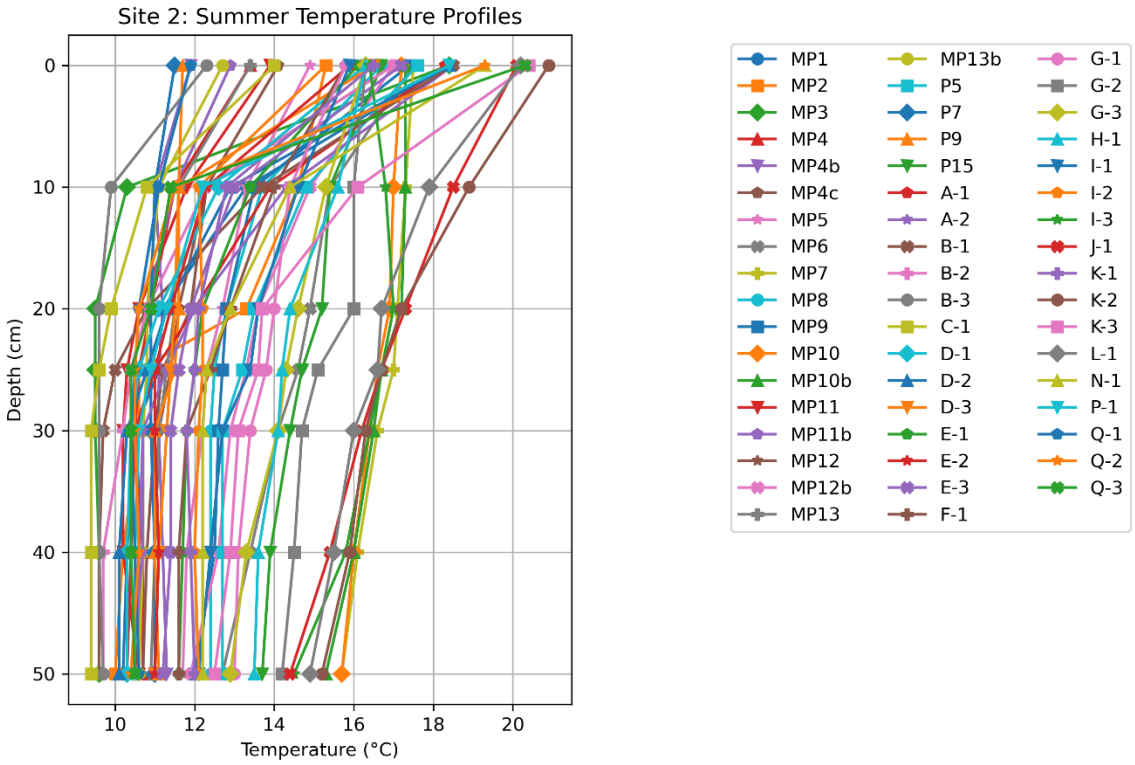



Figure C.4: Temperature profiles collected at Site 2 in the summer of 2024.

# Appendix D

# Hydraulic Gradient Error Calculations

**Vertical Hydraulic Gradient – Piezometer 13/13-SW Example**

$\delta z_g$ = Total Station error = 1.9 mm $km^{-1}$ = 0.19 mm per 100 m = 0.019 cm (Rau et al., 2019)
$\delta d_{gw}$ = Water level meter error = 8.4 mm = 0.84 cm (Rau et al., 2019)
$\delta d_{sw}$ = Surface Water level meter error = 10 mm = 1 cm (Sörengård, M. & Di Baldassarre, G, 2017)
$\delta h_{pt}$ = Non vented transducer with barometric compensation = 3 mm = 0.3 cm (Rau et al., 2019)

$$\delta\Delta h = 2\sqrt{(\delta z_g)^2 + (\delta d_w)^2 + (\delta h_{pt})^2} \qquad 2 = \text{surface water error and groundwater error}$$

$$\delta\Delta h = \sqrt{(\delta z_g)^2 + (\delta d_{gw})^2 + (\delta h_{pt})^2} + \sqrt{(\delta z_g)^2 + (\delta d_{sw})^2 + (\delta h_{pt})^2}$$

$$\delta\Delta h = \sqrt{(0.019\text{ cm})^2 + (0.84\text{ cm})^2 + (0.3\text{ cm})^2} + \sqrt{(0.019\text{ cm})^2 + (1\text{ cm})^2 + (0.3\text{ cm})^2}$$

$$\delta\Delta h = 1.9731\text{ cm}$$

$\delta s_g^v = \delta z_g$ = Total Station error (vertical) = 1.9 mm $km^{-1}$ = 0.19 mm per 100 m = 0.019 cm

$$\delta\Delta s_h^v = 2\sqrt{(\delta s_g^v)^2}$$

$$\delta\Delta s_h^v = 2\sqrt{(0.019\text{ cm})^2}$$

$$\delta\Delta s_h^v = 0.38\text{ cm}$$

**Relative error of the head - vertical gradient**

$\delta\Delta h = 1.9731$ cm
$\delta\Delta s_h^v = 0.38$ cm
$\Delta h$ = difference in head (cm) = 307.7406931 m − 307.6303654 = 0.110327631 m × 100 = 1.103 cm
$\Delta s_h^v$ = depth of piezometer (cm) = 60.3 cm

$$\frac{\delta\nabla h^v}{|\nabla h^v|} = \sqrt{\left(\frac{\delta\Delta h}{\Delta h}\right)^2 + \left(\frac{\delta\Delta s_h^v}{\Delta s_h^v}\right)^2}$$

$$\frac{\delta\nabla h^v}{|\nabla h^v|} = \sqrt{\left(\frac{1.9731\text{ cm}}{1.103\text{ cm}}\right)^2 + \left(\frac{0.38\text{ cm}}{60.3\text{ cm}}\right)^2}$$

$$\text{Relative Error} = \frac{\delta\nabla h^v}{|\nabla h^v|} = 0.178955987$$

$$\text{Error} = \frac{\delta\nabla h^v}{|\nabla h^v|} \times \text{Vertical Gradient}$$

$$\text{Error} = 0.178955987 \times 0.245992489$$

$$\text{Error} = 0.044021829$$

## Horizontal Hydraulic Gradient - Piezometer 13/14 Example

$\delta s_g^h = \delta z_g =$ Total Station error (horizontal) $= 1$ mm $= 0.1$ cm (Rau et al., 2019)

$$\delta \Delta s_h^h = 2\sqrt{\left(\delta s_g^h\right)^2}$$

$$\delta \Delta s_h^v = 2\sqrt{(0.1 \text{ cm})^2}$$

$$\delta \Delta s_h^v = 0.2 \text{ cm}$$

**Relative error of the head – horizontal gradient**

$$\frac{\delta \nabla h^h}{|\nabla h^h|} = \sqrt{\left(\frac{\delta \Delta h}{\Delta h}\right)^2 + \left(\frac{\delta \Delta s_h^h}{\Delta s_h^h}\right)^2}$$

$\delta \Delta h = 1.9731$ cm

$\delta \Delta s_h^v = 0.2$ cm

$\Delta h =$ difference in head (cm) $= 307.7406931 \text{ m} - 307.8070692 \text{ m} = -0.066376146 \text{ m} \times 100$

$= -6.637$ cm

$\Delta s_h^v =$ depth of piezometer (cm) $= 60.3$ cm

$$\frac{\delta \nabla h^h}{|\nabla h^h|} = \sqrt{\left(\frac{1.9731 \text{ cm}}{-6.637 \text{ cm}}\right)^2 + \left(\frac{0.2 \text{ cm}}{60.3 \text{ cm}}\right)^2}$$

$$\text{Relative Error} = \frac{\delta \nabla h^h}{|\nabla h^h|} = 0.297335399$$

$$\text{Error} = \frac{\delta \nabla h^v}{|\nabla h^v|} \times \text{Horizontal Gradient}$$

$$\text{Error} = 0.297335399 \times 0.019839961$$

$$\text{Error} = 0.005899123$$

*All systematic errors are assumed to have been eliminated. Therefore, the only error remaining is the random error.

# Appendix E
# Rating Curve Procedure

- An exponential equation was generated for the streamflow-stage data rating curve using Excel; however, at high stream stages, this rating curve produced unrealistically high estimates of streamflow.
- To address this issue, a segmented rating curve was adopted using an exponential equation at low stream stages and a power law equation at high stream stages to produce more representative estimates of streamflow.
- A power law equation rating curve was fit to the streamflow-stage data using a Python script by Hodson et al. (2024) to determine $h_0$ (stage of zero flow).
- A nonlinear solver (sequential quadratic programming, SQP) was used in GNU Octave (Eaton et al., 2024) to fit a power law rating curve to the streamflow-stage dataset by minimizing the root mean squared error between observed and fitted values; this incorporated the $h_0$ value and determined the C and b parameters for a common power law equation: $Q = C(H-h_0)^b$; this fitting was performed because the Hodson et al. (2024) script did not output the parameters of this form of the equation.
- The exponential and power law equations were spliced by using "Goal Seek" in Excel to determine the point where the two rating curve segments intersect, so that the power law could assess high stream stage streamflow (for stages above the intersection point) and the exponential equation could assess low stream stage streamflow (for stages below the intersection point).